Water absorbing polymer (WAP)-soil interaction study for drought stress management

Thesis

Submitted in the Partial Fulfilment of the Requirement for the Degree of

DOCTOR OF PHILOSOPHY

by

Abhisekh Saha

[Roll no. 166104034]

Department of Civil Engineering

Indian Institute of Technology Guwahati

Guwahati - 781039, India

November 2021

TH-2777_166104034

Dedicated to my beloved family and teachers

TH-2777_166104034

CERTIFICATE

This is to certify that the thesis entitled "**Water absorbing polymer (WAP)-soil interaction study for drought stress management**" submitted by Abhisekh Saha to the Indian Institute of Technology Guwahati, for the award of the degree of Doctor of Philosophy (PhD) in Civil Engineering is a record of bonafide research work carried out by him under our supervision and guidance. The thesis work, in our opinion, has reached the requisite standard fulfilling the requirement for the degree of Doctor of Philosophy.

The results contained in this thesis have not been submitted in part or full to any other University or Institute for award of any degree or diploma.

IIT Guwahati
Date:

Dr. Sreedeep S
Professor
Department of Civil Engineering
Indian Institute of Technology Guwahati
Guwahati-781039
India

IIT Guwahati
Date:

Dr. Uttam Manna
Associate Professor
Department of Chemistry and Center for Nanotechnology
Indian Institute of Technology Guwahati
Guwahati-781039
India

TH-2777_166104034

STATEMENT

I do hereby declare that the matter embodied in this thesis is the result of investigations carried out by me in the Department of Civil Engineering, Indian Institute of Technology Guwahati (IITG), Assam, India.

In keeping with the general practice of reporting scientific observations, due acknowledgements have been made wherever the work described is based on the findings of other investigators.

IIT Guwahati

Date: ***Abhisekh Saha***

TH-2777_166104034

ACKNOWLEDGEMENTS

The major work of completing this research work was made possible with continuous guidance and support of my supervisor Dr. Sreedeep S. His insight, motivation and direction have helped me navigate the doctoral tenure with ease. Special thanks are given to my co-supervisor Dr. Uttam Manna for the freedom that he had given me for working comfortably throughout this research work and all his valuable time that he had spent for discussion. I am grateful to my doctoral committee members Dr. Anil Kumar Mishra, Dr. Bulu Pradhan, and Dr. Arindam Dey for their constructive comments and suggestions that helped me immensely to carry out my study. I would also like to thank my former doctoral committee member Dr. A. Murali Krishna during his tenure at IIT Guwahati for his valuable suggestions and encouragement at the initial stage of this research work.

Special thanks need to be mentioned for my research colleague, Mr. Bharat Rattan, who have worked with me in the present research work. I would like to acknowledge the friendship and support of my colleagues in Indian Institute of Technology Guwahati. They are: Dr. Sudheer, Dr. Janarul, Dr. Sanandam, Dr. Vinay, Mr. Chandra bhanu, Mr. Suman, Mrs. Soumi, Mr. Tapas, Mr. Rojimul, Mr. Ankit, Mr. Deepak, Mr. Anant, Mr. Sidharth, Mr. Arnab. I am really thankful to Mr. Hariram Upadhay, Mr. Samarjyoti Kalita, and Mrs. Syeda Reshima Begum, for their help in carrying out laboratory experiments.

I am also filled with gratitude to all the faculty members, staff members of Civil engineering department, IIT Guwahati and to all those who have been related to this study, either directly or indirectly, in smooth completion of the project work. I am thankful to Central Instruments Facility (CIF) and Department of Chemistry of IIT Guwahati for providing research facility which helped in the study.

I am indebted to my family members, father Uttam Kumar Saha, mother Aparna Saha, brother Arka for their support and encouragement during my PhD tenure. I would like to thank my wife, Mandira, who has stood by me through all my travails, my absences and impatience.

Abhisekh Saha

TH-2777_166104034

Table of content

Abstract v

List of Figures vii

List of Tables xi

Notations xii

Abbreviation xiii

Chapter 1

Introduction 1

1.1 General 1

1.2 Motivation for the study 3

1.3 Organization of the thesis 4

Chapter 2

Literature review 6

2.1 General 6

2.2 Drought 6

2.3 Water absorbing Polymer (WAP) 8

2.4 Influence of WAP amendment on soil and plant properties 15

2.4.1 Influence on water retention characteristics of soil 15

2.4.2 Influence on plant available water content 19

2.4.3 Influence on hydraulic conductivity and infiltration characteristics 22

2.4.4. Influence of WAP on plant parameter 26

2.4.5. WAP amended soil under drought condition 29

2.4.6. Effect of soil salinity on WAP amended soil 31

2.4.7. Eco-compatibility and biodegradability of WAP 32

2.5 Current scenario of FA production and utilization 34

2.5.1 Physicochemical properties of FA 35

2.5.2 Potential hazards of FA to environment 38

2.5.3 Utilization of FA as soil amendment 39

TH-2777_166104034

2.6 Critical appraisal of the reviewed literature 40

2.7 Objective and scopes of the proposed work 42

Chapter 3

Materials and Methodology 43

3.1 General 43

3.2 Materials selection 43

3.3 Characterization of the used soils 44

3.4 Characterization of the used FA 47

3.5 Characterization of Commercial WAP 47

3.6 Measurement of soil suction 51

3.6.1 T5 tensiometer 52

3.6.2 Capacitance sensor (TEROS21) 53

3.6.3 Dew point potentiameter (WP4) 54

3.7 Measurement of soil moisture content 55

Chapter 4

Transformation of fly ash to water absorbing polymer 58

4.1 General 58

4.2 Methodology 58

4.2.1 Used reagents 58

4.2.2 Preparation of FA-WAP 58

4.2.3 Characterization of FA-WAP 61

4.2.4 Measurement of swelling characteristics 62

4.2.5 Toxicity assessment of FA and FA-WAP 64

4.3 Observations and discussion 65

4.3.1 Characterization of FA-WAP 66

4.3.2 Optimizing the synthesis of FA-WAP for maximum WAC 70

4.3.3 Swelling characteristics 72

4.3.4 Toxicity assessment of FA and FA-WAP 86

TH-2777_166104034

4.4 Summary 87

Chapter 5

Moisture movement in WAP-soil system 88

5.1 General 88

5.2 Horizontal absorption test for moisture diffusion 88

5.3 Theory 89

5.3.1 Sorption kinetics of WAP 89

5.3.2 Moisture movement through soil 90

5.4 Test Setup and Procedures 92

5.5 Sorption mechanism of WAP 93

5.7 Moisture desorption from swollen WAP 107

5.8 Summary 110

Chapter 6

Performance evaluation of suction and moisture sensors 111

6.1 General 111

6.2 Performance evaluation of TEROS21 111

6.2.1 Test plan and procedure 111

6.2.2 Observations and Discussion 114

6.3 Performance evaluation of moisture sensor 118

6.3.1 Background 118

6.3.2 Test procedure 120

6.3.3 Observations and Discussion 122

6.4 Summary 132

Chapter 7

Water retention characteristics of WAP amended soil 134

7.1 General 134

7.2 Measurement methodology of WRCC 134

7.3 Drying WRCC of commercial WAP (Com-WAP) amended soil 136

TH-2777_166104034

7.4 Drying WRCC of FA-WAP amended soil 142

7.4.1 Saturated VWC of Com-WAP and FA-WAP amended soil 142

7.4.2 Plant available water content (PAWC) in Com-WAP and FA-WAP amended soil 144

7.4.3 Plant wilting time in Com-WAP and FA-WAP amended soil 145

7.5 Prediction of drying WRCC of WAP amended soil 150

7.5.1 Development of WRCC model 152

7.5.2 Validation of the proposed WRCC model 154

7.6 Hysteresis in WRCC of WAP amended soil 160

7.7 Hysteresis model for WAP amended soil 165

7.7.1 Theoretical background of hysteresis model 165

7.7.2 Proposed model 167

7.7.3 Validation of the proposed model 170

7.8 Degree of hysteresis in WAP amended soil 171

7.9 Degradation of WAP in soil 183

7.9.1 Test plan and procedure 183

7.9.2 Observations and discussion 185

7.10 Summary 189

Chapter 8

Conclusions and Future scope 192

8.1 General 192

8.2 Conclusions from this study 192

8.3 Statement of Novelty 194

8.4 Major contributions from the study 194

8.5 Limitations and future scope 195

References 196

List of publications from this study 220

TH-2777_166104034

Abstract

Drought is one of the worst natural disasters that affect the economic, social, and environmental status of any country. The long-term drought affects the soil ecosystem and can initiate desertification and deterioration of soil health. This leads to severe water distress, which is further aggravated by improper water management, poor irrigation practice, degradation of soil quality, and low water holding capacity of soil. Effective land management is the most feasible solution during drought. One of the ways for handling water stress conditions is the use of water absorbing polymer (WAP) that can absorb and store water within its polymer network and transfer the stored water to plant roots under the water stress condition. Encouraging the utility of WAP for drought management would necessitate clarity in the understanding of WAP-soil interaction. Therefore, objective of this study is to evaluate the performance of WAP for drought stress management considering WAP-soil interaction.

To begin with, a novel, eco-friendly WAP was synthesized by transforming an industrial solid waste, fly ash (FA). The synthesis process was optimized to achieve maximum water-absorbing capacity (WAC). The transformed FA-WAP exhibited high WAC (310 g/g and 230 g/g in distilled and tap water, respectively), very much comparable with the commercially available WAP. The study quantified the swelling kinetics and characterized the re-swelling behavior of the FA-WAP under alternate wetting-drying cycles and compared with the commercial WAP. The performance of the synthesized FA-WAP and commercial WAP was evaluated as a soil amendment for improving the drought tolerance of soil. The water transport mechanism from swollen WAP to soil particles was characterized in a diffusion cell by placing the swollen WAP and dry soil in contact with each other. The water retention characteristics curve (WRCC) of the WAP amended soils (both drying and wetting curve) at three different concentrations (0.1%, 0.2%, and 0.4% on weight by weight basis) were evaluated with both the WAPs to assess the efficacy of WAP for the effective management of water resources during drought. For an accurate measurement of WRCC of WAP amended soils, the performance assessment of two different capacitance-based sensors, including suction (TEROS21) and moisture (ECH_2O 5TM) sensor, was carried out. Predictive models were proposed to estimate the drying WRCC of WAP amended soils and the hysteresis in WRCC of WAP amended soils with multiple drying-wetting cycles. The study not only demonstrated the usefulness of FA-WAP for increasing the irrigation intervals and thereby saving water during drought conditions but also offering an eco-friendly solution to mass utilization of industrial solid waste, FA for a meaningful application in drought management.

TH-2777_166104034

Keywords: Drought; water absorbing polymer; soil management; waste valorization; fly ash; water retention characteristic curve; hysteresis; diffusion.

TH-2777_166104034

List of Figures

Fig. 2.1 Classification and long-term effects of drought 7
Fig. 2.2 Conceptual diagram to represent the effectiveness of soil amendment for drought 8
Fig. 2.3 (a) The chemical structure of commercial acrylate WAP (modified after Huttermann et al. 2009), (b) SEM image of acrylate WAP and (c) Swelling mechanism of acrylate WAP 9
Fig. 2.4 Mechanism involved in the graft polymerization reaction (modified after Feng et al. 2014) . 11
Fig. 2.5 Various criteria for classification of WAP 14
Fig. 2.6 Idealized water retention characteristic curve (WRCC) and important parameters 17
Fig. 2.7 Identifying the important zone of WRCC for vegetation growth 20
Fig. 2.8 Variation in PAWC improvement factor in different soil texture 21
Fig. 2.9 Variation in survival time improvement factor for different soil texture 30
Fig. 2.10 Different sources of electricity generation in India (adapted from CEA, 2019a) 35
Fig. 2.11 FA production and utilization rate in India for the past 10 years (adapted from CEA, 2018b) 36
Fig. 2.12 Modes of utilization of FA in India (adapted from CEA, 2018b) 37

Fig. 3.1 Elemental compositions (EDX analysis) of (a) fine sand (FS), (b) Brahmaputra silt (BS), and (c) Red soil (RS) 46
Fig. 3.2 Commercial WAP at (a) dry state, (b) swollen state, (c) FTIR spectrum, and surface morphology at (d) 500X and (e) 100X magnification. 49
Fig. 3.3 Elemental composition (EDX spectrum) of the used WAP 50
Fig. 3.4 Chemical Structure of the used WAP 50
Fig. 3.5 Details of (a) T5 tensiometer and (b) capacitance sensor (TEROS21) 52
Fig. 3.6 Details of (a) WP4C and (b) block chamber 55
Fig. 3.7 Details of 5TM sensor 56

Fig. 4.1 Collection of FA and polymerization setup for the preparation of FA-WAP 60
Fig. 4.2 Synthesis scheme of FA-WAP production process 61
Fig. 4.3 Methodology adopted for the measurement of WAC 63
Fig. 4.4 FTIR Spectrum of FA, PAA and FA-WAP 67
Fig. 4.5 XRD analysis of FA, PAA and FA-WAP 67
Fig. 4.6 FESEM image of (a) raw FA, (b) PAA, (c) FA-WAP at 3000X and (d) FA-WAP at 1000X magnification 68

TH-2777_166104034

Fig. 4.7 BET N_2 adsorption-desorption isotherm of (a) FA, and (c) FA-WAP, and pore size distribution of (b) FA and (d) FA-WAP 69
Fig. 4.8 Effect of (a) FA content, (b) Crosslinker content (c) initiator content and (d) neutralization degree of AA on WAC of the synthesized FA-WAP 71
Fig. 4.9 Swelling and deswelling mechanism of FA-WAP 72
Fig. 4.10 Swelling kinetics of (a) FA-WAP and (b) Com-WAP in distilled and tap water 74
Fig. 4.11 Deswelling kinetics of com-WAP and FA-WAP at two different temperatures 75
Fig. 4.12 Variation in the moisture evaporation rate from WAP at different temperature 76
Fig. 4.13 Re-swelling characteristics of (a) FA-WAP and (b) Com-WAP 77
Fig. 4.14 Effect of various (a) cations and (b) anions on WAC of FA-WAP 80
Fig. 4.15 Effect of various (a) cations and (b) anions on WAC of Com-WAP 81
Fig. 4.16 Sensitivity factor of different WAPs in different salt solutions 82
Fig. 4.17 Effect of pH on WAC of (a) FA-WAP and (b) Com-WAP 84
Fig. 4.18 Relationship between WAC of WAP and EC of swelling medium 85

Fig. 5.1 Experimental setup for the measurement of moisture movement from swollen WAP to soil. 93
Fig. 5.2 Advancement of wetting front at different time intervals in BS for commercial WAP 94
Fig. 5.3 Sorption kinetic of (a) Com-WAP, (c) FA-WAP, and moisture diffusion behavior (b) Com-WAP, (d) FA-WAP 95
Fig. 5.4 Variation of wetting front distance with time for FS 97
Fig. 5.5 Variation of wetting front distance with time for BS 98
Fig. 5.6 Variation of wetting front distance with time for RS 98
Fig. 5.7 Measured moisture profiles through (a) FS, (b) BS, and (c) RS at different time intervals with Com-WAP 100
Fig. 5.8 Measured moisture profiles through (a) FS, (b) BS, and (c) RS at different time intervals with FA-WAP 101
Fig. 5.9 Comparison of degree of saturation achieved by soil at different locations from the WAP-soil interface 102
Fig. 5.10 Difference in the moisture flow path in different textured soils 103
Fig. 5.11 Boltzmann constant variation with VWC for the used soils with Com-WAP 104
Fig. 5.12 Boltzmann constant variation with VWC for the used soils with FA-WAP 105
Fig. 5.13 Soil moisture diffusivity as a function of VWC obtained in the present study 107
Fig. 5.14 Comparison of the obtained soil moisture diffusion value with the literature data 107
Fig. 5.15 Moisture desorption kinetics of the used WAPs in different soils 109

TH-2777_166104034

Fig. 6.1 Osmotic suction of soil-pore solution (RS) after soil washing and standard NaCl solution . 113
Fig. 6.2 Methodology adopted for the measurement of WRCC of the soil 114
Fig. 6.3 Measured SWRC of (a) BS and (b) RS using T5, TEROS21, and WP4C 115
Fig. 6.4 Sensitivity of TEROS21 to ambient relative humidity (RH)..... 116
Fig. 6.5 Relationship between TEROS21 measured suction (kPa) and raw data 117
Fig. 6.6 Schematic diagram to represent the motivation of the study..... 120
Fig. 6.7 Experimental methodology adopted to evaluate the performance of 5TM sensor 122
Fig. 6.8 Comparison between 5TM sensor measured VWC and accurate VWC at different concentrations of WAP 124
Fig. 6.9 Polynomial calibration procedure for accurate measurement of VWC of WAP amended soils 125
Fig. 6.10 Illustrations of different parameters contributing to the permittivity (ε_a) of bare soil and WAP amended soil 126
Fig. 6.11 Linear calibration procedure for accurate measurement of VWC 128
Fig. 6.12 Correlation of correction factor (k) with (a) clay content and (b) WAP concentrations 130
Fig. 6.13 Comparison between corrected VWC (using LC) and accurate VWC at different concentrations of FA-WAP..... 131

Fig. 7.1 Methodology adopted for measurement of drying-wetting WRCC of the WAP amended soil 135
Fig. 7.2 Measured DWRCC of (a) Fine sand (FS), (b) Brahmaputra silt (BS) and (c) Red soil (RS) with different Com-WAP concentration 137
Fig. 7.3 FESEM images of FS with (a) C0, (b) C1, (c) C2, (d) C3 WAP concentrations 139
Fig. 7.4 FESEM images of BS with (a) C0, (b) C1, (c) C2, (d) C3 WAP concentrations..... 139
Fig. 7.5 FESEM images of RS with (a) C0, (b) C1, (c) C2, (d) C3 WAP concentrations..... 140
Fig. 7.6 Comparison of WRCC of the different texture soils with varying WAP concentration..... 141
Fig. 7.7 Measured DWRCC of (a) Fine sand (FS), (b) Brahmaputra silt (BS) and (c) Red soil (RS) with different FA-WAP concentration..... 143
Fig. 7.8 Comparison of saturated VWC of the used soils with different WAP concentrations 144
Fig. 7.9 FC, PWP of (a) Fine sand (FS), (b) Brahmaputra silt (BS) and (c) Red soil (RS) with different WAP concentrations 146
Fig. 7.10 Suction-time variation time for (a) FS, (b) BS, and (c) RS with varying Com-WAP concentration..... 148
Fig. 7.11 Suction-time variation time for (a) FS, (b) BS, and (c) RS with varying FA-WAP concentration..... 149

TH-2777_166104034

Fig. 7.12 Requirement of irrigation water in different textured soils 151
Fig. 7.13 Phase diagram of unsaturated soil amended with WAP 153
Fig. 7.14 Experimental methodology to measure WRCC of WAP 155
Fig. 7.15 Measured gravimetric-WRCC of (a) Com-WAP and (b) FA-WAP using T5 tensiometer . 156
Fig. 7.16 Measured and predicted WRCC of Com-WAP amended soils 158
Fig. 7.17 Measured and predicted WRCC of FA-WAP amended soils 159
Fig. 7.18 Measured (Leciejewski, 2009) and predicted WRCC of WAP amended soil (Loamy sand) 160
Fig. 7.19 Measured 1st drying-wetting WRCC of Com-WAP amended (a) FS, (b) BS and (c) RS .. 162
Fig. 7.20 Measured 1st drying-wetting WRCC of FA-WAP amended (a) FS, (b) BS and (c) RS 163
Fig. 7.21 Illustration of swelling mechanism and water molecule attraction inside FA-WAP..... 164
Fig. 7.22 Hysteresis in WRCC for bare soil 166
Fig. 7.23 Hysteresis in WRCC for WAP amended soil 168
Fig. 7.24 Measured and predicted hysteresis in WRCC for two alternate cycles for Com-WAP amended FS..... 175
Fig. 7.25 Measured and predicted hysteresis in WRCC for two alternate cycles for FA-WAP amended FS 176
Fig. 7.26 Measured and predicted hysteresis in WRCC for two alternate cycles for Com-WAP amended BS 177
Fig. 7.27 Measured and predicted hysteresis in WRCC for two alternate cycles for FA-WAP amended BS..... 178
Fig. 7.28 Measured and predicted hysteresis in WRCC for two alternate cycles for Com-WAP amended RS 179
Fig. 7.29 Measured and predicted hysteresis in WRCC for two alternate cycles for FA-WAP amended RS..... 180
Fig. 7.30 Quantification of degree of hysteresis (modified after Lu and Khorsidi 2015)..... 181
Fig. 7.31 Pictorial view of the dry and water-swollen FA-WAP amended soils 184
Fig. 7.32 Variation of gravimetric water content (GWC) of WAP amended FS and water absorbency of WAP in FS with the number of alternate cycle 186
Fig. 7.33 Variation of gravimetric water content (GWC) of WAP amended BS and water absorbency of WAP in BS with the number of alternate cycle..... 187
Fig. 7.34 Variation of gravimetric water content (GWC) of WAP amended RS and water absorbency of WAP in RS with the number of alternate cycle..... 188
Fig. 7.35 Degradation kinetics of the used WAPs in different textured soils 190

TH-2777_166104034

List of Tables

Table 2.1 Details of various hybrid WAP prepared by graft polymerization 13
Table 2.2 Summary of relevant literatures related to WAP influence on soil properties 24
Table 2.3 Brief overview of the parameter consider for soil-WAP-plant interaction 27
Table 2.4 Cost comparison of commercial WAP with fertilizer 34
Table 2.5 Summary of basic physical properties of FA 38
Table 3.1 Details of various materials used in the study 43
Table 3.2 Details of the references used for basic characterization of the soils 44
Table 3.3 Basic geotechnical properties of the used soils 45
Table 3.4 Basic physical properties of the used FA 47
Table 3.5 Chemical composition of the used FA 48
Table 3.6 Technical specifications of T5 tensiometer 53
Table 3.7 Technical specifications of TEROS21 54
Table 3.8 Technical specifications of WP4C 55
Table 3.9 Technical specifications of ECH$_2$O 5TM 57
Table 4.1 Important combinations of reagent quantity for the preparation of FA-WAP 59
Table 4.2 BET surface area and average pore diameter of FA and FA-WAP 69
Table 4.3 Comparison of WAC of FA-WAP with other available WAP 73
Table 4.4 Rate constant of FA-WAP and Com-WAP in distilled and tap water 73
Table 4.5 Leachability of various metals from FA, FA-WAP and FA-WAP amended FS 86
Table 5.1 Details of the parameters for moisture diffusion into WAP particles 96
Table 5.2 Details of the compaction properties of the used soils 96
Table 5.3 Summary of the parameters related to moisture diffusion through soil 106
Table 5.4 Details of the desorption kinetic model parameters 108
Table 6.1 Details of soil washing with deionized water 112
Table 6.2 Details of the calibration parameters (PC) for WAP amended soils 127
Table 6.3 Obtained k parameter for linear calibration (LC) of WAP amended soils 127
Table 7.1 Calculated irrigation frequency (IF) for the used soils 150
Table 7.2 Polymer based parameters for the used WAPs 155
Table 7.3 Summary of the WRCC parameters [Eq. (7.3)] for different textured bare soil 157
Table 7.4 Predicted curve-fitting parameters for wetting WRCC of WAP amended FS 172
Table 7.5 Predicted curve-fitting parameters for wetting WRCC of WAP amended BS 173
Table 7.6 Predicted curve-fitting parameters for wetting WRCC of WAP amended RS 174
Table 7.7 Obtained degree of hysteresis in WAP amended soils 182

TH-2777_166104034

Notations

ψ	soil suction
θ	Volumetric water content
ε_a	Dielectric constant
λ	Boltzmann transformation variable
D(θ)	Moisture diffusivity function
M_{ss}	Mass of soil particle
V_{ss}	Volume of soil particle
M_{sp}	Mass of WAP particle
V_{sp}	Volume of WAP particle
M_{wp}	Mass of water absorbed by WAP
V_{wp}	Volume of water absorbed by WAP
M_{ws}	Mass of water in soil pores
V_{ws}	Volume of water in soil pores
V_{as}	Volume of air voids in soil
V_{vs}	Volume of voids in soil
V_{sa}	Volume of solid in amended soil
V_{va}	Volume of void in amended soil
G_s	Specific gravity of soil
G_p	Specific gravity of WAP
$w_{p(\psi)}$	Gravimetric water content of WAP at any suction, ψ
m	Mass ratio of WAP and soil = $\frac{M_{sp}}{M_{ss}}$
θ_s	Saturated volumetric water content
θ_r	Volumetric water content at residual state
S_r	Degree of saturation
D_h	Average degree of hysteresis

TH-2777_166104034

Abbreviation

WAP	Water absorbing polymer
SAH	Superabsorbent hydrogel
WAC	Water absorbing capacity
USDA	United States Department of Agriculture
FA	Fly ash
FS	Fine sand
BS	Brahmaputra silt
RS	Red soil
Com-WAP	Commercial water absorbing polymer
FA-WAP	Fly ash water absorbing polymer
XRD	X-Ray diffraction
EDX	Energy dispersive X-Ray
FESEM	Field emission scanning electron microscope
FTIR	Fourier transform infrared
BET	Brunauer–Emmett–Teller
AA	Acrylic acid
APS	Ammonium per sulfate
MBA	N, N’ methylene bisacrylamide
PAA	Poly acrylic acid
TCLP	Toxicity characteristic leaching procedure
USEPA	United States Environment Protection Agency
WHO	World Health Organization
VWC	Volumetric water content
WRCC	Water retention characteristic curve
FC	Field capacity
PWP	Permanent wilting point
PAWC	Plant available water content
PC	Polynomial calibration
LC	Linear calibration
DWRCC	Drying water retention characteristic curve
WWRCC	Wetting water retention characteristic curve
GWC	Gravimetric water content

TH-2777_166104034

Chapter 1

Introduction

1.1 General

Optimizing the use of rain and irrigation water by crop and non-crop species is not only important in the semi-arid regions but also for frequently occurring drought in tropical climate (impact of climate change), where water becomes a limited resource for vegetation growth and development. Any mismanagement in water use can lead to excessive drought stress in the plants and crops, affecting food security. India is one of the world's most drought-prone countries, where more than 60% of the cropped area is in the semi-arid region (Kalhapure et al. 2016; Zhang et al. 2017). The lack of adequate surface water is also a major concern in various civil engineering infrastructures, such as vegetated landfill cover systems, urban green infrastructure, and bioengineered slopes and embankments. The stability of these projects largely depends on the root development and growth of the vegetation cover (Śpitalniak et al. 2019). Low water retention behavior of soil, excess surface runoff, improper management of water resource, and migration of nutrients to deeper layer are responsible for water stress condition. Therefore, unconventional measures, along with conventional water conservation methods, are the need of the hour to reduce the negative influence of drought and increase crop productivity. Addition of soil conditioner is considered as one of the best management practices by researchers, which improves water retention, water infiltration, drainage, aeration, and pore structure of the soil (Hüttermann et al. 1999; Bhardwaj et al. 2007; Inbar et al. 2015; Lentz 2015). The purpose of soil amendment is to increase soil water and nutrient holding capacity over an extended period of time (Andry et al. 2009; Sepaskhah and Shahabizad 2010; Shi et al. 2010; Montesano et al. 2015).

Water absorbing polymers (WAP), also termed superabsorbent hydrogels (SAH), can absorb and retain a large quantity of water and solute molecules in a swollen state, where various hydrophilic groups (e.g., carboxyl groups, amino groups, hydroxyl groups, etc.) attached to the polymeric backbone can readily interact with water molecules through energetically favorable interactions (Li et al. 2004; Bao et al. 2011; Wu et al. 2012; Ahmed 2015). The cross-linking makes the polymer insoluble in water and form a gel, which can trap water within them (Maitra and Shukla 2014; Rivas et al. 2018). The commercially available SAH in the horticulture market has a water absorbing capacity (WAC) of 100-500 g per gram of SAH (Bowman and Evans 1991; Akhter et al. 2004). Due to their high WAC, these polymers

TH-2777_166104034

are receiving much attention in various fields like the hygiene industry, drug delivery, food storage, wastewater treatment, biosensors, and tissue engineering (Zhang et al. 2014; Misiewicz et al. 2019).

The use of SAH for agricultural soil amendment was developed by the United States Department of Agriculture (USDA) in the 1960s. However, most of the commercial SAHs are "fully synthetic copolymer," which are synthesized by copolymerizing acrylic acid and acrylamide in the presence of a cross-linker (Feng et al. 2014). One inherent limitation of the fully synthetic copolymer is that the production cost is very high, may not be eco-friendly, and hence cannot be used for agricultural applications. The other type of SAH is "graft copolymer," where natural materials such as starch (Zhang et al. 2006a), cellulose (Bao et al. 2011), clay (Zhang et al. 2006b), chitosan (Zhang et al. 2007a) are linked with a hydrophilic polymeric chain. These grafted copolymers possess more WAC, salt-resistivity, and higher mechanical stability as compared to the fully synthetic polymer (Bhattacharya and Mishra 2004). For drought management applications, there is a need to develop similar hybrid copolymer, which is semi-synthetic (refers to the integration of synthetic polymer with naturally available substrates/polymers), eco-friendly, utilize waste material for synthesis so that the overall cost of production would be low and serve the purpose of high-water absorption.

Addition of WAP as a soil amendment can improve soil water holding capacity, increase water use efficiency, modify soil hydraulic conductivity/infiltration rates, and reduce surface runoff (Al-Darby 1996; Orts et al. 2007; Abedi-Koupai et al. 2008; Bhardwaj et al. 2009). It also influences the evaporation loss from the soil and soil microbial activity. The application of WAP has also improved crop growth, biomass and successfully reduces the drought stress for different plant species (Lee et al. 2013; El-Tohamy et al. 2014). Recent studies showed the efficacy of WAP for developing polymer-bentonite composites, which can be used as barrier layers in landfill liner (Scalia and Benson 2017; Piqué et al. 2019). The addition of WAP can reduce the hydraulic conductivity of the composite material (Hosney and Rowe 2017). However, there are some anomalies and contrasting observations present in the literature related to the influence of WAP in soils. Another important aspect of WAP as a soil amendment is its variation in water absorbing capacity (WAC) depending on the structure of the polymer and the type of hydrophilic groups attached to its polymer chain. Conflicting results can be seen related to the WAC of WAP in an aqueous salt solution or saline soil (Siriwatwechakul et al. 2012; Almeida and Klemm 2018). These studies indicate that the interaction of soil and WAP depends on the chemical properties of WAP as well as the

TH-2777_166104034

physicochemical properties of the soil. Moreover, the alteration in the soil properties due to WAP amendment can be permanent or temporary, depending on the degradation kinetics of WAP. There are no conclusive studies on the degradability, long-term performance of WAP in soil and specifically WAP-soil interaction.

This research work focuses on the synthesis of novel and ecofriendly water absorbing polymer (WAP) having high water absorbing capacity by grafting partially neutralized polyacrylic acid (PAA) chain on the surface of an industrial waste material, fly ash (FA). The FA is a waste residue from the thermal power plant, which is amorphous ferro-aluminosilicate very similar to soil (Pandey and Singh 2010; Ukwattage et al. 2013). A massive quantity of FA produced annually occupies a large area of land for its disposal. In India, around 40% of FA finds its application in the cement industry and various other infrastructural projects, and the remaining percentage remains unutilized (Basu et al. 2009). The remaining amount of FA was mixed with water and transported as slurry through pipe and disposed in the form of ash ponds. These ash ponds not only utilize a huge area of usable land but also have adverse effects on the environment. Several past studies have shown that FA can be very helpful for plant growth when applied to soil in optimum quantity (Pathan et al. 2003; Mittra et al. 2005). It contains various essential plant nutrients, i.e., macronutrients including P, K, Ca, Mg and S, and micronutrients like Fe, Mn, Cu, B, and Mo, making it suitable for agricultural soil amendment (Basu et al. 2009). Therefore, the transformation of FA to a water sorbing material can alleviate the negative effects of drought along with the nutritional enhancement of soil. It can be noted that FA may contain heavy metals such as Mn, Zn, Cu, Pb, Cr, and Cd, depending on the source of the parent coal (Mittra et al. 2005). However, several past studies have highlighted that the leaching of heavy metals from FA remains well below the recommended value up to an amendment rate of 25% in soil (Pathan et al. 2003; Pandey and Singh 2010). Therefore, FA, being an alumino-silicate compound, can be transformed into water absorbing polymer (WAP) without any pretreatment. Transformation of FA into WAP can alleviate the negative effects of drought along with the nutritional enhancement of soil. However, there are not many studies that explored such a possibility.

1.2 Motivation for the study

The necessity to efficiently utilize water for crops and non-crops species during drought conditions has motivated this study. It is established from the literature that WAP can absorb and retain large quantity of water in a swollen state. However, a thorough investigation is required to evaluate the effectiveness of WAP under water stress conditions considering the

TH-2777_166104034

interaction between soil, water, and WAP particles. The efficacy and suitability of some of the suction and moisture sensors, such as TEROS21, and 5TM, respectively, for the determination of water retention characteristics of WAP amended soils, need to be explored. It will be further advantageous if WAP can be prepared by transforming waste materials, economically. With this motivation, one of the problematic industrial solid wastes, fly ash (FA), has been chosen as a backbone material to synthesize WAP in the present study. The appropriate application rate of WAP and its effect on the irrigation water requirement in different soil textures need to be evaluated. There are no recommendations available in the literature for addressing this problem. Moreover, the moisture transfer mechanism in a soil-WAP system is not well recognized in the previous studies. These research gaps have motivated this study.

1.3 Organization of the thesis

The thesis is organized into eight chapters as follows,

- **Chapter 1** gives a general overview of the thesis, motivation behind this research work, and its importance.
- **Chapter 2** reviews the literature comprehensively on the background research and identifies the gap areas. The objective and scope of the study are listed in this chapter.
- **Chapter 3** deals with the selection and characterization of used materials and the details of the methodologies adopted in this study to meet the research objectives.
- **Chapter 4** describes the transformation process of FA into WAP and the polymerization mechanism related to the synthesis process. The performance of the synthesized WAP in terms of its water absorbing capacity (WAC), swelling kinetics, re-swelling characteristics, sensitivity to various pH and salt solutions were reported and compared with a commercial-grade WAP (Com-WAP).
- **Chapter 5** demonstrates a laboratory procedure to characterize the moisture sorption and moisture transfer mechanism from swollen polymer to soil particle. A diffusion cell was fabricated to measure the soil moisture diffusivity values of three different textured surface soils in contact with the swollen WAP.
- **Chapter 6** presents the performance evaluation of suction and moisture sensors (TEROS21 and ECH$_2$O 5TM, respectively) and summarizes the material-specific calibration parameters, which were used for measurement of water retention characteristics of WAP amended soils.
- **Chapter 7** demonstrates the influence of synthesized and commercial WAP on water retention characteristics curve (WRCC) of WAP amended soils. A WRCC model was proposed to predict the WRCC of WAP amended soils with varying WAP concentrations. The effect of

TH-2777_166104034

both the WAPs on the drying and wetting water retention curves was explored for different textured soils. The degradation kinetics of the used WAPs in three different textured soils were also investigated and reported in this chapter.

➢**Chapter 8** lists the conclusions of this study. The major contribution, limitations and future work of the study are also presented in this chapter.

TH-2777_166104034

Chapter 2

Literature review

2.1 General

A detailed understanding of the physical and chemical aspects of water absorbing polymer (WAP) is essential to evaluate its feasibility as an amendment material in drought management applications. This chapter presents a comprehensive review of the literature on development of different types of WAP and its utilization in drought management. The first section of this chapter discusses the concept of WAP and its synthesis process from different types of waste materials. The second section discusses the application of WAP for soil management and improvement during water stress conditions. As the present study focuses on the development of WAP with maximum utilization of industrial solid waste, the last section includes a review on the potential hazards caused due to fly ash (FA) deposition and its potential use as soil amendment. Towards the drought mitigation practice, an attempt was made to critically understand the effect of incorporation of these hydrophilic polymers into soil for improving its water retention characteristics. A critical appraisal was made on the reviewed literature highlighting the research gaps, followed by the objective and scopes of the present work.

2.2 Drought

Drought is defined as a climatic condition with below average to no rainfall for sufficiently long duration leading to serious environmental and socio-economic issues such as crop failures, water scarcities, and food insecurity in the affected area (Wilhite and Glantz 1985; Mishra and Singh 2010). When a particular region typically receives significant rainfall, undergoes drought, the plants/ crops become highly sensitive to water stress than the species that grow in arid or semi-arid regions. This fact is more worrisome in the last few decades, which has witnessed unprecedented and extreme weather conditions hampering the crop productivity of tropical and subtropical climatic regions. Hence, the drought scenario can be described as a situation where the plants are unable to extract water from the soil and experience water stress conditions. The basic classification of droughts, as shown in Fig. 2.1, includes meteorological drought, hydrological drought, agricultural drought, and socio-economic drought (Wilhite and Glantz 1985). Among these, only meteorological drought is concerned with climate change and lack of precipitation. The other types of droughts are the result of lack of proper water management and unsustainable human activities such as over-cultivation,

TH-2777_166104034

deforestation, and poorly controlled irrigation practice (Nyssen et al. 2009; Bhandari and Panthi 2014; Van Loon 2015; Yu et al. 2018).

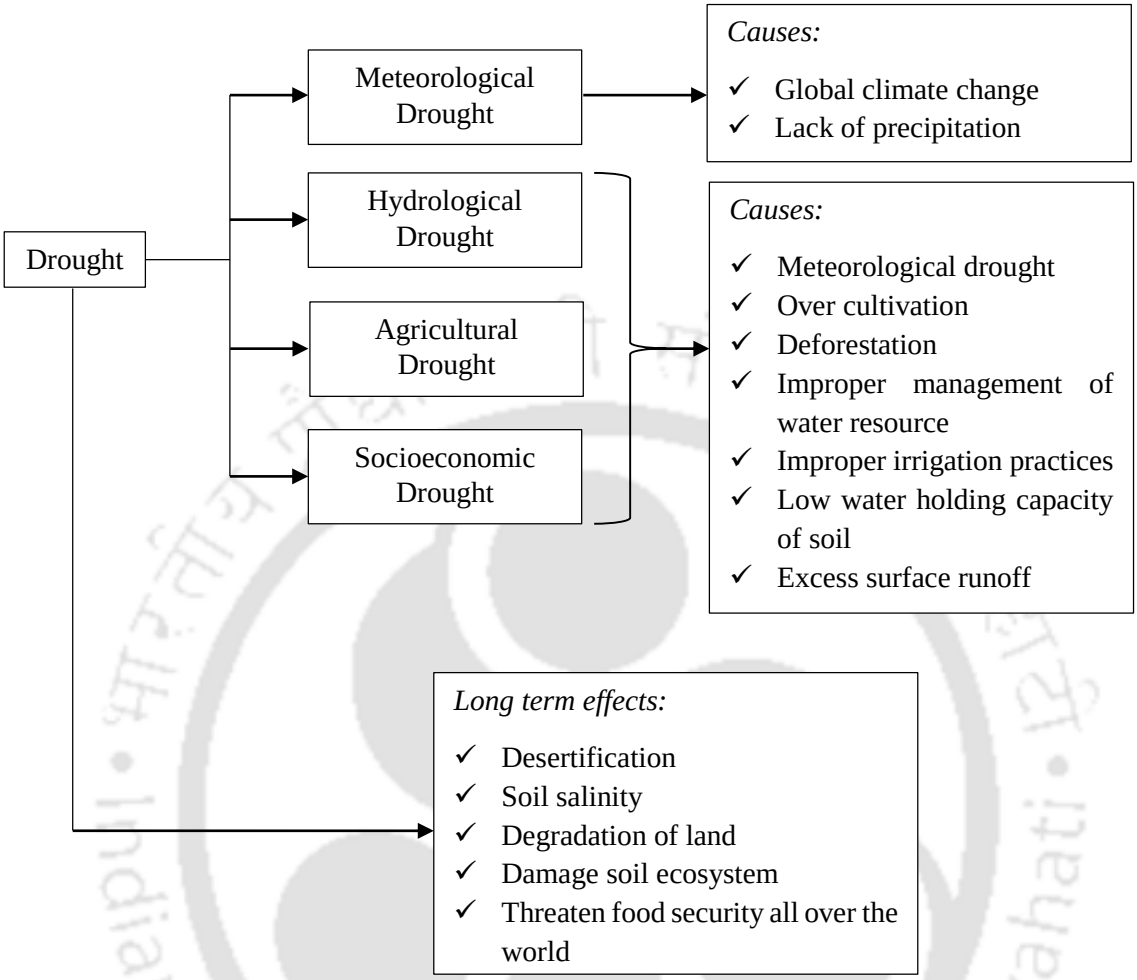

Fig. 2.1 Classification and long-term effects of drought

The low water holding capacity of the soil, migration of water and nutrient into the deeper layer, and excess surface runoff are equally responsible for water stress conditions. The long-term drought can cause desertification, degradation of land, and affect the soil ecosystem. The agricultural ecosystem is very sensitive to drought stress and can threaten food security all over the world (Geng et al. 2015). There are different drought management strategies and policies reported in the literature (Wilhelmi and Wilhite 2002; Van Loon and Van Lanen 2012; Paneque 2015). Most of the strategies are related to early warning systems, identifying vulnerable zones by monitoring the climate data, and water management policies to meet supply and demand of water through rainwater harvesting, reservoir construction, and diversion of streamflow (Merabtene et al. 2002; Garrote et al. 2007; Wilhite et al. 2014; Hasan et al. 2019). Another possible way of circumventing drought conditions (which is not a conventional management strategy) is to engineer and improve the water-holding capacity of the soil, reduce

TH-2777_166104034

the water percolation into the deeper layer, and thereby minimizing the water requirement for irrigation (Fig. 2.2). Addition of soil conditioner is considered as one of the best management practices by researchers, which improve the water and nutrient retention of soil, water infiltration, drainage, aeration, and soil structure resulting in better plant growth (Bai et al. 2010; Shi et al. 2010; Ekebafe et al. 2013; Abdollahi et al. 2014; Xu et al. 2015; Agegnehu et al. 2016; Hansen et al. 2016).

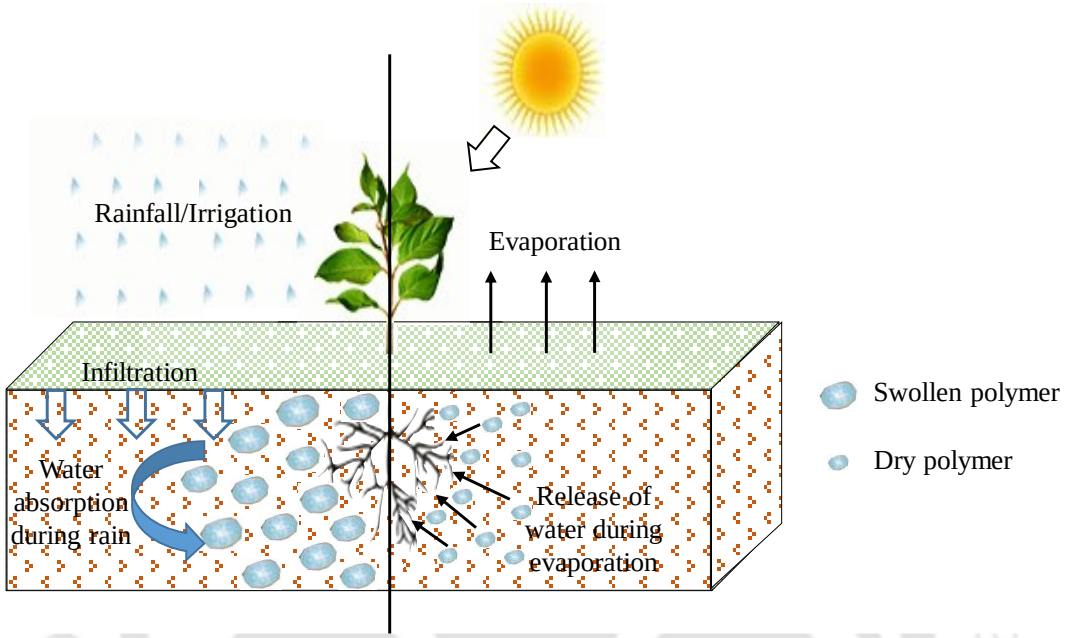

Fig. 2.2 Conceptual diagram to represent the effectiveness of soil amendment for drought

2.3 Water absorbing Polymer (WAP)

There are several synthetic and natural water-absorbing materials such as paper, cotton, pulp that can absorb water by its capillary to an amount of 20g of water per gram of absorbent. However, the absorbed water can be easily squeezed out by applying external pressure. In the 1970s, the United States Department of Agriculture (USDA) have developed new water-absorbing material, which is capable of absorbing water more than 400 times its own weight, which is commonly known as water absorbing polymer (WAP) or superabsorbent polymer (SAP). These WAPs are a special type of polymers, which are highly crosslinked three-dimensional (3D) network, have high molecular weight, and mostly synthesized using acrylamide, potassium acrylate, or acrylic acid (Hüttermann et al. 2009). Crosslink is a bond that connects one polymer chain to another through ionic or covalent bonds (Kabiri et al. 2011), forming a three-dimensional (3D) network. This makes the polymer insoluble in water and forms a gel consistency capable of storing water within them, depending on the crosslinking density (Ahmed 2015).

TH-2777_166104034

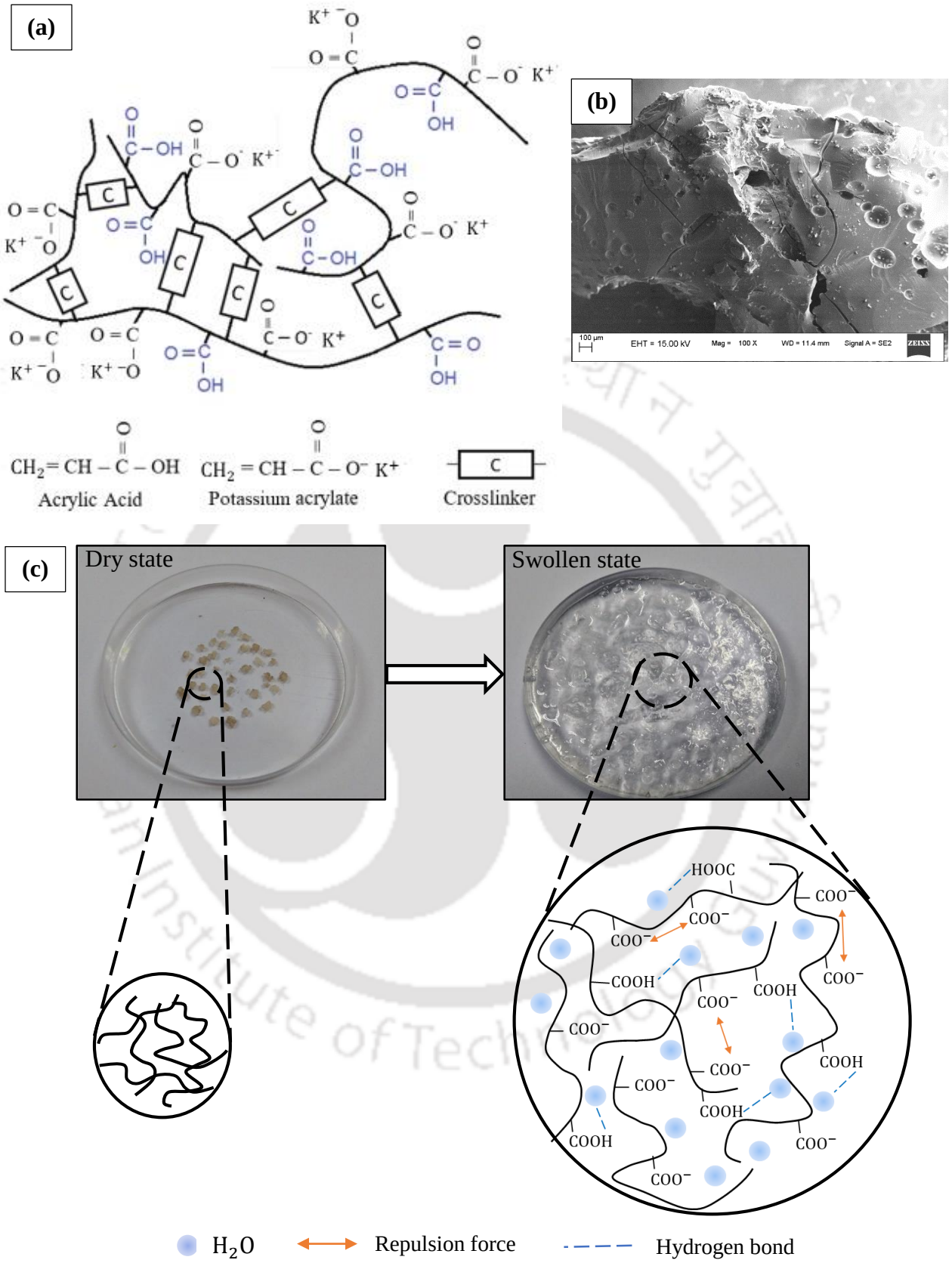

Fig. 2.3 (a) The chemical structure of commercial acrylate WAP (modified after Huttermann et al. 2009), (b) SEM image of acrylate WAP and (c) Swelling mechanism of acrylate WAP

TH-2777_166104034

The chemical structure and surface morphology of a partially neutralized crosslinked acrylic acid-based polymer is presented in Fig. 2.3(a) and (b). The primary hydrophilic group (carboxyl group) present in the polymer structure attach with water molecules through the hydrogen bond. The surface morphology of the WAP suggests the presence of several micro-sized pores that act as active water-absorbing sites resulting in a high water absorbency of the WAP.

During the preparation of WAP, the partially neutralized acrylic salt, such as sodium acrylate or potassium acrylate, is used (Li et al. 2004; Wan et al. 2006). As a result, a large number of strong hydrophilic groups (–COONa/–COOK) are present along with the carboxyl group (–COOH) in the polymer chain. Due to the presence of these strong hydrophilic groups, the negatively charged carboxyl groups ($–COO^-$) create an anion-anion electrostatic repulsion with the polymer chain (Feng et al. 2014) [Fig. 2.3(c)]. When the WAP particles interact with water, a significant osmotic pressure difference develops between the polymer and water. As water molecules penetrate the polymer network, the osmotic pressure difference gradually reduces and approaches equilibrium swelling (Zhang et al. 2014). The equilibrium swelling of WAP is sensitive to different environmental factors such as changes in pH, temperature, ionic strength of the external solution, photo-irradiation, and electric field that can influence the size, shape, solubility, and degree of ionization of the gel (Ahmed 2015).

Depending on the application of WAP, there are various methods reported in the literature to synthesize WAP. The four most commonly used methods of WAP preparation are bulk polymerization, solution polymerization, suspension polymerization, and graft polymerization. The bulk polymerization technique is one of the simplest methods where the bulk WAP can be formed by adding a soluble initiator into the undiluted liquid monomer. One major disadvantage of this technique is the drastic increase in the viscosity of the reaction mass as the polymerization progresses. In the solution polymerization technique, both monomer and initiator are dissolved in a solvent (such as water, ethanol, and benzyl alcohol) to restrict the drastic increase in the viscosity of the solution. After the polymerization reaction, the synthesized product needs to be washed with distilled water to remove the solvent and unreacted monomers. The advantage of the technique is that the presence of solvent restricts the increase in the viscosity and facilitates continuous heat transfer during polymerization. The suspension polymerization technique includes the dispersion of monomer and initiator in an aqueous solution as a homogeneous mixture. This technique needs continuous stirring to restrict the coalesce of monomer droplets. Thus, the shape of the final product remains spherical, and product isolation is relatively easier compared to other techniques. The particle

TH-2777_166104034

shape and size of the final product are governed by the viscosity of the monomer, dispersant type, and agitation speed (Ahmed 2015). Graft polymerization is one of the most promising techniques, where one polymer is linked to the backbone of another polymer or substrate by chemical linkages. Generally, WAP prepared by the previously mentioned techniques have an inherently weak structure and high salt sensitivity.

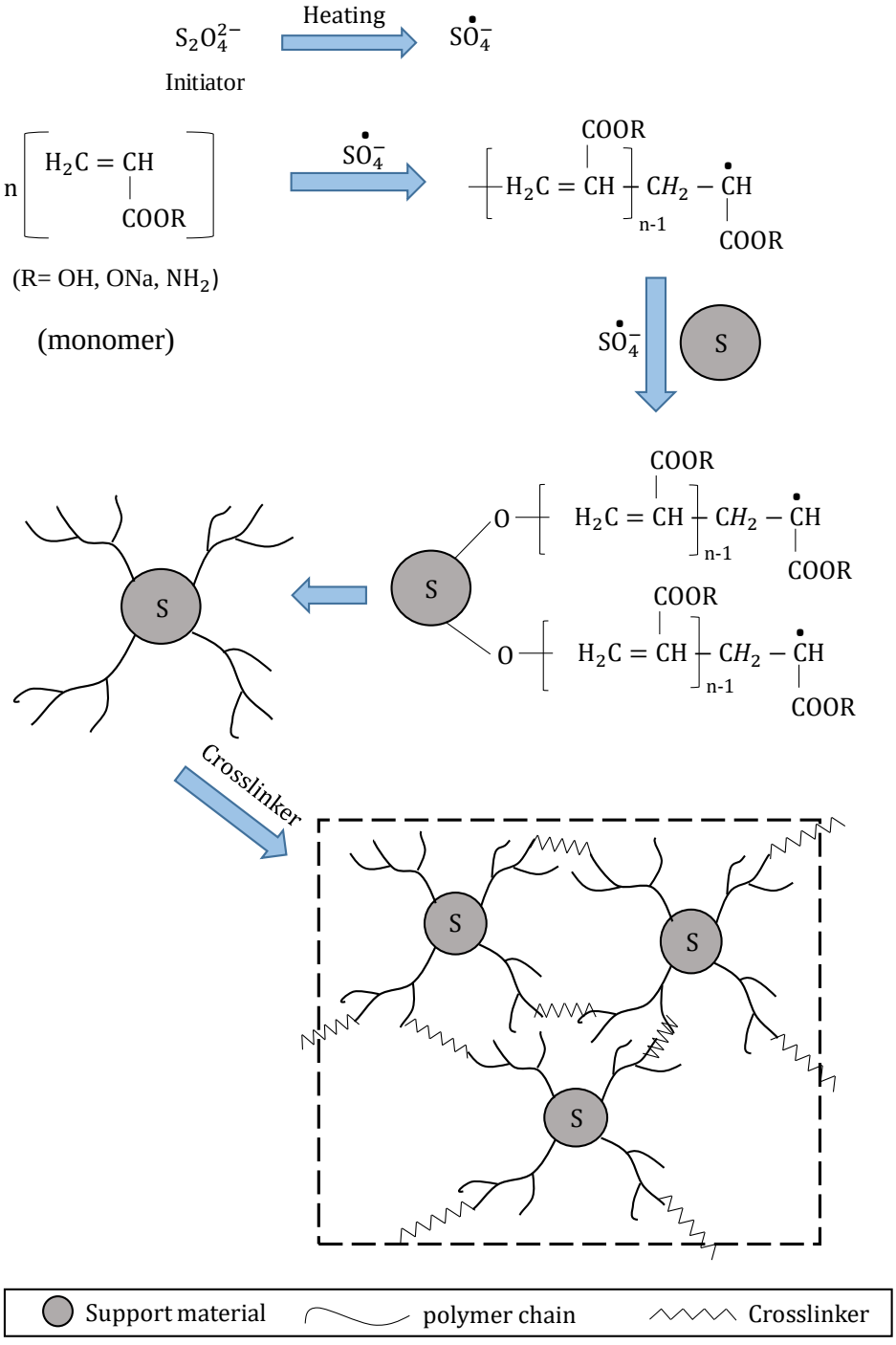

Fig. 2.4 Mechanism involved in the graft polymerization reaction (modified after Feng et al. 2014)

TH-2777_166104034

The thermal, mechanical stability, as well as the water absorbency of the WAP, can be improved when the polymer chains are grafted on the surface of stronger support material (hydrophilic nature). This grafting can be achieved by creating active sites on the support material, initiating polymerization of the monomer to be grafted. The creation of active sites and initiation of the polymerization is achieved by using a free radical initiator, UV irradiation, or enzymes. The detailed mechanism for graft polymerization is explained in Fig. 2.4. Prior to the polymerization process, the initiator is decomposed to free radicals upon heating. The free radical transfers an electron to the monomer to initiate the homo-polymerization. The polymer chain grafted to the surface of the support material causes the growth of the grafted polymer. The cross-linker links two or more polymer chains to produce a three-dimensional (3D) crosslinked polymer network. The various hydrophilic materials that have been used in the previous studies to synthesize a hybrid WAP by graft polymerization technique are listed in Table 2.1. It can be noted that the water-absorbing capacity of the WAP largely depends on the monomer and support material used for the polymerization.

The WAP can be classified based on various criteria depending on the preparation methods and physicochemical properties, as presented in Fig. 2.5. The WAPs can be divided into three categories: natural, synthetic, and hybrid based on their origin (Ullah et al. 2015). Natural WAPs have natural origins such as protein, starch, glycogen, cellulose, chitin, etc., whereas synthetic WAPs are prepared by polymerization of chemicals such as acrylic acid, acrylamide, methacrylic acid, etc. The hybrid WAP consists of both natural polymer and synthetic polymer attached to one another. Thus, the hybrid WAP always possesses better water absorbency and biodegradability as compared to synthetic WAP. Over the past two decades, researches were conducted to synthesize a new type of hybrid WAP known as superabsorbent hydrogel composite (SHC) and superabsorbent hydrogel nanocomposite (SHNC), which showed excellent potential in terms of swelling capacity, salt sensitivity, and mechanical properties due to the incorporation of nano-sized and micro-sized materials in the polymer matrix (Kabiri et al. 2011; Guilherme et al. 2015; Vundavalli et al. 2015). These SHCs and SHNCs are often synthesized using different natural materials such as cellulose, chitin, starch, alginate, clay, and synthetic vinyl monomers such as acrylates, meth-acrylates, acrylamide using different polymerization techniques (Rodrigues et al. 2013). Due to the utilization of natural materials, the SHCs and SHNCs are non-toxic, biocompatible, biodegradable, and cost-effective. However, most of these superabsorbent composites are not commercially available and limited to laboratory stage despite their improved properties and lower price. This is mainly due to the unresolved issues related to scaling up the process for mass commercial production.

TH-2777_166104034

Table 2.1 Details of various hybrid WAP prepared by graft polymerization

Sr. no.	Reference	Monomer used	Backbone material	Weight ratio (monomer:backbone)	Cross-linker used	Water absorbing capacity[#] (g/g)
1	Gao et al. 2001	Acrylic acid	montmorillonite	10:1	MBA*	1834
2	Li et al. 2004	Acrylic acid	Attapulgite	3.5:1	MBA	1325
3	Ye et al. 2004	Acrylic acid	Sodium silicate	10:1	---	1600
4	Wan et al. 2006	Acrylic acid Acrylamide	Kaolinite	10:1	MBA	433
5	Zhang et al. 2006c	Acrylic acid Acrylamide	Sodium humate	3:1	MBA	1184
6	Seki et al. 2007	Acrylic acid	Smectite	10:1	MBA	210
7	Zhang et al. 2007b	Acrylic acid	Bentonite	2:1	Sugar	120
8	Zheng et al. 2007	Acrylic acid	vermiculite	5:1	MBA	1232
9	Zhang et al. 2009	Sodium acrylate	Hydrotalcite	20:1	MBA	1100
10	Wu et al. 2012	Acrylic acid Acrylamide	Cellulose	5:1	MBA	875
11	Feng et al. 2014	Acrylic acid	Yeast	8:1	MBA	358
12	Zhang et al. 2014	Acrylic acid	Maize bran	2.5:1	MBA	2507
13	Leitão et al. 2015	Acrylic acid Acrylamide	Nontronite	10:1	MBA	1104
14	Zhang et al. 2015	Acrylic acid	Starch Zeolite 4A	10:1	MBA	511
15	Xiao et al. 2017	Acrylamide	Starch	1.5:1	MBA	253

*MBA- N, N′-methylene-bisacrylamide,
[#]water absorbing capacity reported in distilled water (g/g of dry WAP)

TH-2777_166104034

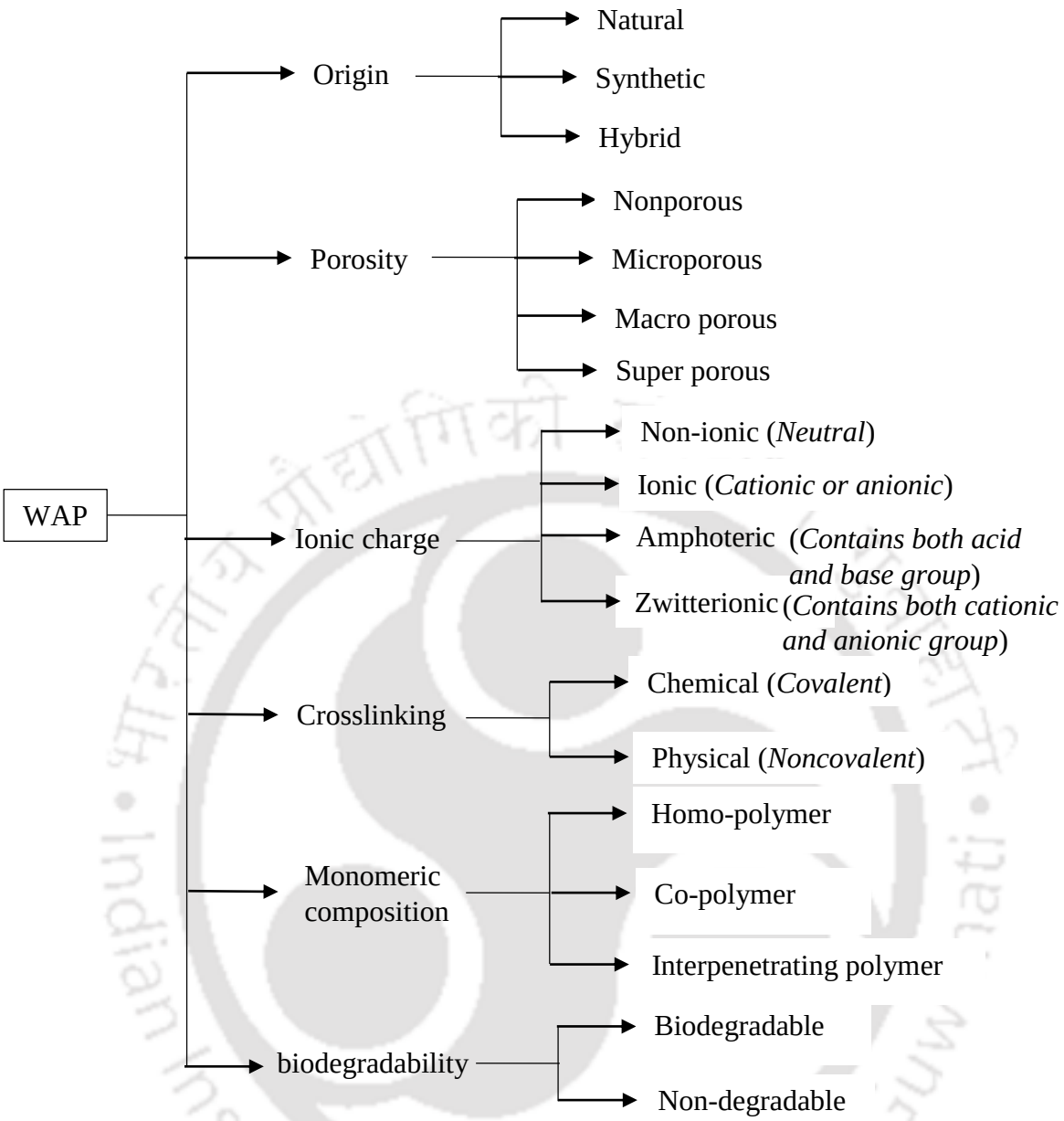

Fig. 2.5 Various criteria for classification of WAP

Based on porosity, the WAPs can be classified into non-porous, micro-porous, macro-porous, and super-porous (Coelho et al. 2010). The porosity of WAP is controlled by the reaction temperature and foaming agent during the polymerization process. The WAPs can be non-ionic, ionic, amphoteric, and zwitterionic based on the presence of electrical charge in the polymer network (Ahmed 2015). Most of the WAP commonly used in the agricultural sector are ionic (either anionic or cationic), whereas non-ionic WAPs are used in the production of contact lenses. The amphoteric WAP contain both acidic and basic group in their polymer network while the zwitterionic WAP contain both cationic and anionic group in their network and used in wound dressing.

TH-2777_166104034

On the basis of crosslinking nature, WAP can be categorized into physically and chemically crosslinked network (Xu et al. 2018). The physically crosslinked networks are not permanent but sufficient to make the WAP insoluble in water. These are reversible crosslinked networks and formed due to hydrogen bonds or ionic interactions. On the other hand, the chemical crosslinked networks are permanent and covalently bonded with the polymer network. Based on the monomeric component, the WAP can be classified into three categories including homo-polymeric WAP (crosslinked network of one type of hydrophilic monomer unit), co-polymeric WAP (consist of two or more different monomers with minimum one hydrophilic component crosslinked together), and interpenetrating WAP (have two independent crosslinked synthetic or natural polymer components). From the degradation perspective, the WAPs can be either biodegradable or non-degradable. Most of the synthetic WAPs are non-biodegradable in nature. Therefore, recent studies are focused on synthesizing different types of biodegradable co-polymeric WAP by attaching a biodegradable waste material (starch, cellulose, chitosan, sodium humate, yeast) into the hydrophilic polymer chain (Wu et al. 2012; Feng et al. 2014; Zhang et al. 2014; Xiao et al. 2017). The practice of using biodegradable WAP in the agriculture field can overcome the environmental jeopardy related to synthetic WAP.

2.4 Influence of WAP amendment on soil and plant properties

This section deals with the influence of WAP on different soil properties (focused on water retention behavior, plant available water content, hydraulic conductivity, and infiltration) [Table 2.2] and plant parameters (such as shoot growth, root growth, leaf area index, and crop yield). A brief literature review on the influence of WAP amendment on the soil salinity and plant survival during water stress conditions was also included in this section, along with the studies related to eco-compatibility and biodegradability assessment of WAP in soil.

2.4.1 Influence on water retention characteristics of soil

Water retention characteristic curve (WRCC), also termed as soil water characteristic curve (SWCC), is a graphical representation of soil suction or negative pore water pressure and the amount of water present in the soil (which can be represented in terms of gravimetric water content, volumetric water content or degree of saturation). Gravimetric water content (w) is the ratio of the weight of water to the weight of dry soil, while volumetric water content (θ) is the ratio of the volume of water to the total volume of soil mass and degree of saturation (S) is defined as the percentage of voids filled with water.

TH-2777_166104034

2.4.1.1 Soil suction

The unsaturated soil is a three-phase system consisting of air, water, and soil particles. The interaction of solid, water, and air phase develop a complex energy state resulting in negative pore water potential known as soil suction. Soil suction is defined as the amount of energy required to expel a unit volume of water from the soil matrix (Lee and Wray 1996). The major component of suction is matric suction (designated as ψ_m), which results from the combined effect of capillary and adsorptive forces that exist in the soil matrix. Osmotic suction (designated as ψ_o) results from the presence of dissolved solutes in soil-water. The sum of these two suction components is termed total suction (ψ). Total suction can be theoretically obtained using Kelvin's equation (Eq. 2.1).

$$\psi = -\frac{R.T}{V_{wo}.\omega_v} \, ln\frac{u_v}{u_{v0}} \qquad 2.1$$

Here, R is the universal gas constant (=8.314 J/mol K), T = absolute temperature in Kelvin, v_{wo} = specific volume of water or the inverse of the density of water (m^3/kg), ω_v = molecular mass of water vapour (=18 Kg/K mol), u_v = partial pressure of pore water vapor and u_{vo} = partial pressure of pore water vapor at sample temperature.

2.4.1.2 WRCC representation

WRCC can be obtained by taking the suction-water content readings during drying of soil sample, which is known as desaturation curve (desorption), or wetting of soil sample, which is known as saturation (adsorption) curve. These curves are distinct from each other for soil due to the hysteresis effect. Drying WRCC always has a greater suction than the wetting WRCC at the same water content value. The saturated water content in drying curve is also greater than the water content in wetting curve at that corresponding suction. This is mainly attributed to the presence of air voids at the end of the wetting process. A typical hysteresis behavior in WRCC is presented in Fig. 2.6. Some of the relevant points for the WRCC are as follows:

a) The volumetric water content at saturation, θ_s, describes the water content at which the soil is completely saturated and typically depicts the initial state for the evaluation of the drying path.

b) The air-entry value (AEV), ψ_a, is the suction at which air enters the largest pore present in the soil sample during the drying process (Brooks and Corey 1964). This is the point where the desaturation process starts.

TH-2777_166104034

c) Residual water content (θ_r) is the minimum water content below which there is no appreciable change in θ. Suction corresponding to θ_r is called residual soil suction, ψ_r (e.g., Yang et al. 2004).

d) The water-entry value, ψ_w, on the wetting WRCC, is defined as the suction at which the water content of the soil starts to increase significantly during the wetting process (Birle et al. 2008).

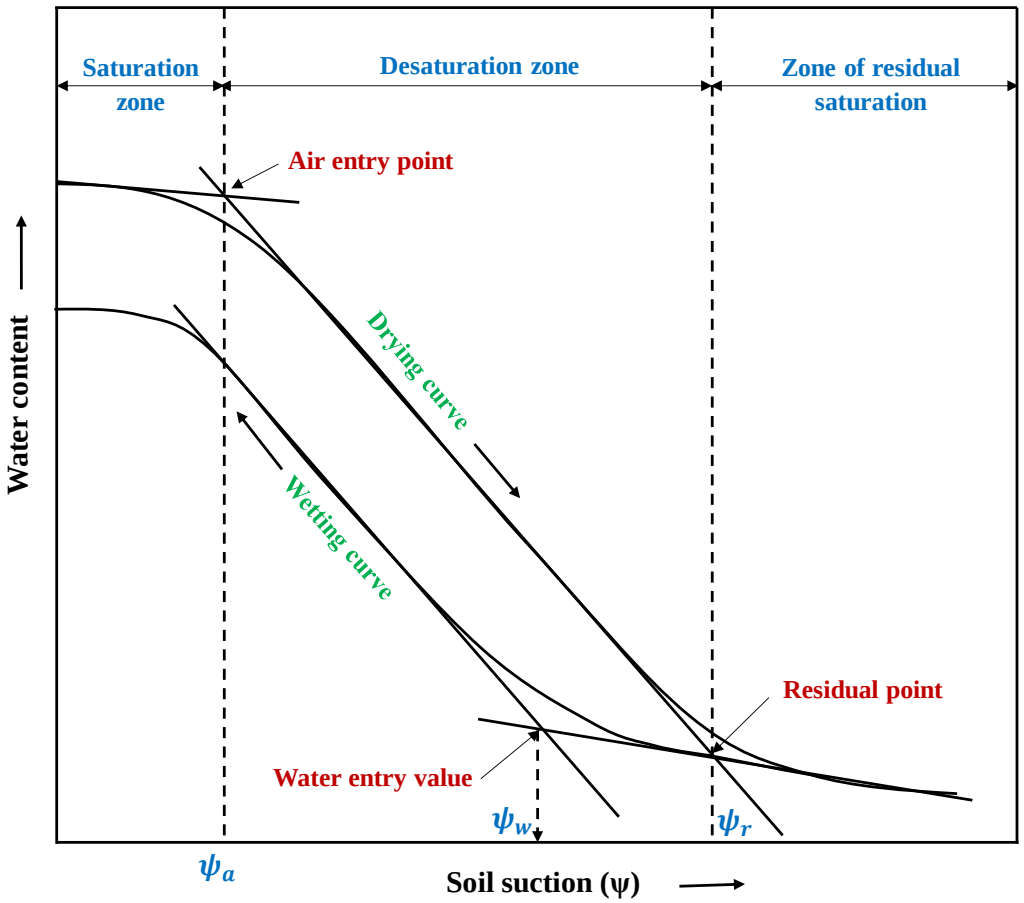

Fig. 2.6 Idealized water retention characteristic curve (WRCC) and important parameters

Sillers et al. (2001) divided the whole drying WRCC into three classified regions, as shown in Fig. 2.6,

i) Capillary saturation zone: In this zone, the soil remains saturated with the pore water held under tension as a result of capillary tension and extends up to air entry value (ψ_a).

ii) Desaturation zone: This region is in between the air entry value and residual water content wherein pore air replaces pore water within the pores of the soil. Water is retained in this zone in the form of thin films on the particle surfaces under the influence of the short-range solid-liquid interaction mechanism.

TH-2777_166104034

iii) Zone of residual saturation: This zone starts from the residual water content and is terminated at oven-dry conditions, i.e., water content equal to zero. Under this zone, pore water is retained by the molecular bonding mechanism, primarily hydrogen bonding with exposed oxygen or hydroxyl on the surface of the soil minerals. An increase in suction in this zone does not result in significant changes in water content.

Past studies have revealed that the water retention behavior of the soil significantly increased with the addition of WAP (Bakass et al. 2002; Dorraji et al. 2010; El-Tohamy et al. 2014; Yang et al. 2014; Mohawesh and Durner 2019). The highly crosslinked WAP has strong adsorption and complexing capacities due to the presence of hydrophilic functional groups. The water enters into the internal polymer network easily and forms a water-blocking layer with the soil particles (Yang et al. 2014). This process prevents moisture evaporation from the soil surface, which resulted in higher retention capacity. Montesano et al. (2015) have observed an increase in the soil moisture up to 400% at field capacity (FC) [ψ= 33 kPa] with 2% WAP (w/w basis) as compared to bare sandy soil. The moisture content at permanent wilting point (PWP) [ψ= 1500 kPa] was also at par with that of FC. The addition of the highest percentage of WAP transformed the WRCC of sandy soil to clay loam. Another important reason behind the increased water retention behavior with the WAP amendment is the alteration of soil pore structure. With the addition of WAP, the median pore diameter and the number of large pores decreased (Narjary et al. 2012). The effect of WAP on water retention was observed to be predominant for coarse-grained soils as compared to fine-grained soils (Koupai et al. 2008; Agaba et al. 2010). The coarse-grained soils have larger pore diameter compared to the fine-grained soils facilitating a higher reduction in pore diameter (Narjary et al. 2012). On the contrary, pore size is smaller for fine-textured soil, causing less effect of WAP on water retention. It was also reported that the improvement in coarse-grained soils could be attributed to the lower cation exchange capacity (CEC) of these soils (Agaba et al. 2010). As the equilibrium swelling capacity of the WAP largely depends on the ionic nature of the polymer, an increase in the CEC of soil can lead to a decrease in WAC. Besides, WAP can alter the specific surface area (SSA) of soil because of the interaction between the soil surface and polymer chain (Dorraji et al. 2010). An increase in SSA with the addition of WAP can lead to an increase in WRCC in the higher suction regime where the water is adsorbed in the form of a thin film on the surface of the soil particle (Lu and Likos 2004).

Koupai et al. (2008) have studied the WRCC of two different textured soils amended with WAP by using pressure plate apparatus. With the addition of WAP, the SWC and the

TH-2777_166104034

RWC of both sand and clay soil were increased. The AEV of the amended soil increased for sandy soil, whereas clay soil exhibited a decrease. Due to larger pore geometry in sandy soils, water is released under lower suction leading to a lower AEV. The reduction in the diameter of the largest pore in the soil due to WAP addition increased the pressure required for water extraction. However, there are not many studies present in the literature, which critically investigated the influence of WAP addition on different WRCC parameters. Moreover, there are not many studies that have measured continuous WRCC of WAP amended soil in the field under ambient drying conditions. The disadvantage of the pressure plate apparatus is that the suction measurements are under applied positive pressure that constricts the pores and drains the water out. The effect of applied pressure on water-swollen WAP is not well understood, and the water release will be different from that within the pores of the soil. There is a possibility that this may induce an error in the suction measurements. Therefore, further investigations are required to quantify the variations in WRCC caused by the WAP amendment for different soil types. This would help to appraise the applicability of WAP in different textured soils.

2.4.2 Influence on plant available water content

It is necessary to understand whether the total amount of water stored in the WAP amended soil will be available for plant root uptake. In general, the plant available water content (PAWC) is defined as the range of water that is readily available to growing crops and determined by the difference between the water content at field capacity (FC) and the permanent wilting point (PWP) [Koupai et al. 2008; Farrell et al. 2013]. The amount of water held in the soil pore after the excess gravitational water has drained and the rate of vertical drainage has substantially decreased is known as FC (Veihmeyer and Hendrickson 1931). To be more precise, FC can be described as the water content below which the specific discharge is sufficiently small that redistribution of soil moisture due to the hydraulic gradient can be neglected. For consistency, the FC is usually denoted as the volumetric water content in the soil after drainage for 2–3 days (with zero evaporation). However, for coarse-textured soils, this reduction in specific discharge may occur within 6–24 h, whereas fine-textured soils may drain for several weeks. Moreover, it was also reported that there is no good alternative for determining FC other than the in-situ field measurement (Cassel and Nielsen 1986). The exact quantification of FC through laboratory experimentation for a given soil type is rarely possible because of the difference in the pore characteristics and drainage conditions in the lab compacted sample. Colman (1947) has proposed the matric suction value of 33 kPa for

TH-2777_166104034

estimating FC for all types of soils, which is widely adopted in the literature. On the other hand, the water content corresponding to 1500 kPa is known as PWP because the plant permanently wilts beyond this suction and fails to recover even after irrigation. The main reason for selecting 1500 kPa for PWP estimation is that the water held at suction 1500 kPa is equivalent to the pores sizes finer than 0.2–0.5 μm. Beyond this range, plant roots cannot extract water from such small pores (Fullen and Catt 2014).

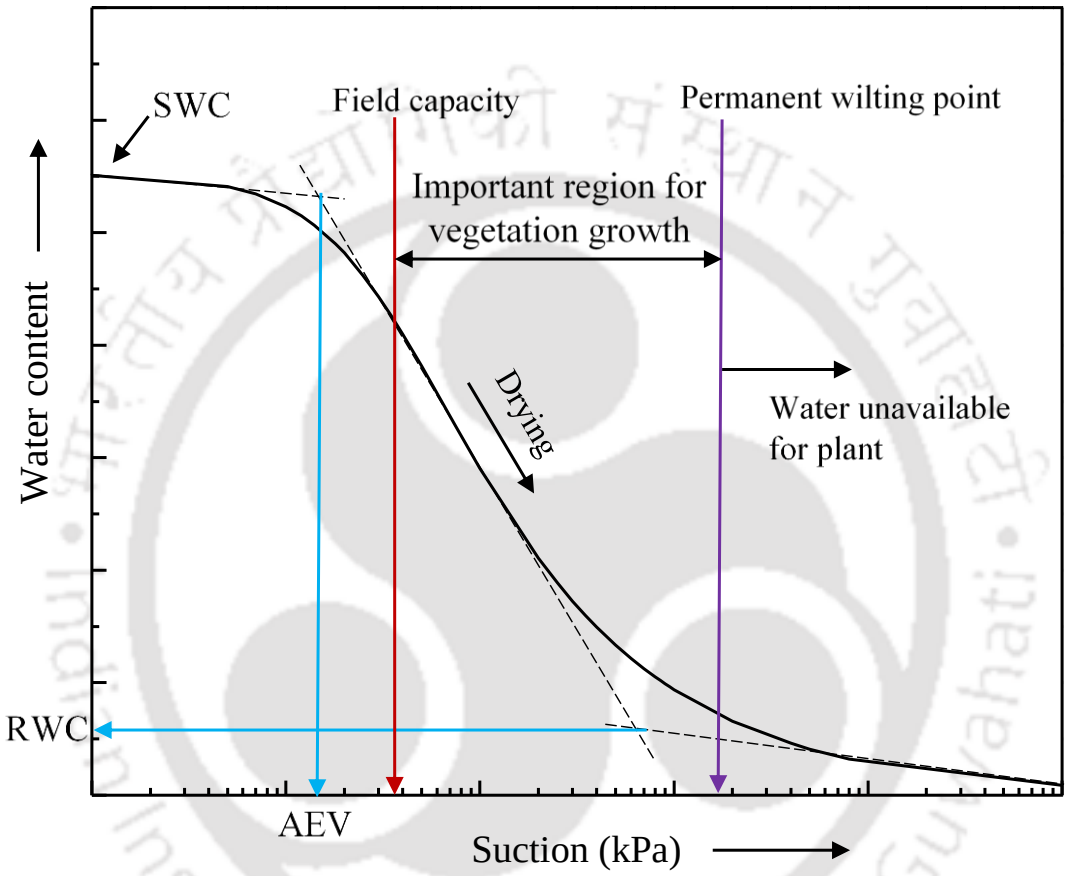

Fig. 2.7 Identifying the important zone of WRCC for vegetation growth

Past studies have reported that the application of WAP in coarse-textured soils substantially increased the water available to the plant. (Huttermann et al. 1999; Andry et al. 2009; Dorraji et al. 2010; Narjary et al. 2012; Yang et al. 2014). Akhter et al. (2004) have observed an increased FC with WAP addition and thereby increasing the PAWC in sandy loam soil. Banedjschafie and Durner (2015) have reported an increase in PAWC by sixty times in sandy soil with 1% WAP amendment as compared to bare sand. It is further noted that PAWC gradually decreased to its initial value (comparable to bare soil) after multiple drying and wetting cycle due to the aging of the polymer. However, the exact quantification of this observation is not mentioned in the literature. Agaba et al. (2010) have observed an increase in PAWC by three times in WAP amended (0.4% addition) sandy soil, whereas the same

TH-2777_166104034

concentration of WAP addition results in a much lesser increase in PAWC for loamy soil and clay. This gives an indication that the WAP amendment is more suitable to the coarse-grained soil as compared to fine-grained soil.

To understand the textural effect of soil on the PAWC of WAP amended soil, the PAWC improvement factor (ratio of PAWC in WAP amended soil to the PAWC in bare soil) was calculated based on the data reported in the literature for different soil texture. Figure 2.8 depicts the variation of the PAWC improvement factor with the soil texture at different concentrations of WAP. It can be noted that the improvement factor gradually decreases as the soil becomes finer. In addition, the PAWC improvement factor increases with the increasing concentration of WAP. For clayey soil, the improvement factor is almost close to 1, which suggests that the addition of WAP has bare minimal effect on the PAWC. However, the small variation in the improvement factor for the same soil texture is attributed to the difference in application rate and composition of the used WAP in the past studies.

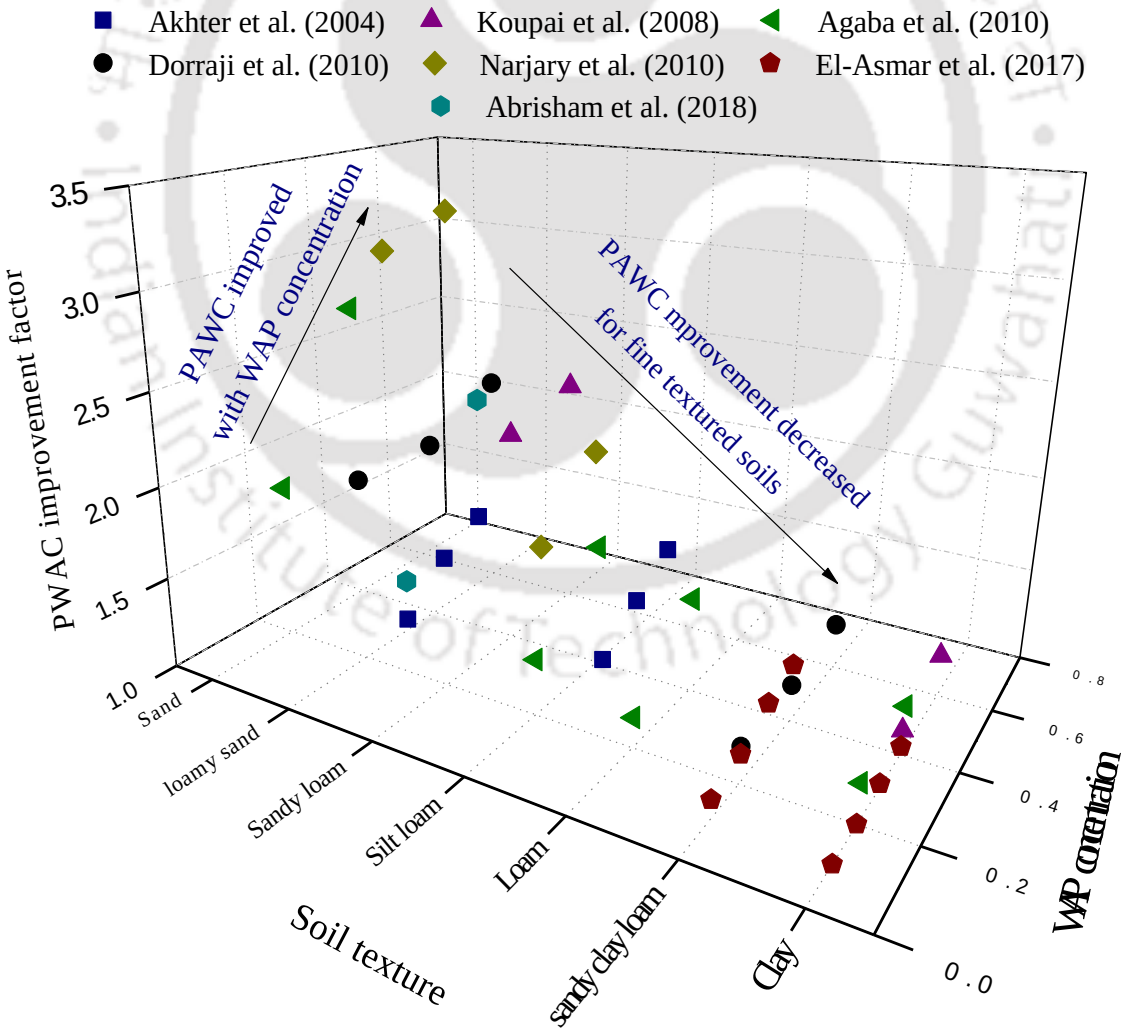

Fig. 2.8 Variation in PAWC improvement factor in different soil texture

TH-2777_166104034

Another important observation from these studies is that the addition of WAP also increases the water content at PWP. Such an observation suggests that a significant amount of water stored in WAP amended soil is not available to the plant. Yang et al. (2015) have demonstrated that the increased water holding capacity of the soil caused by higher addition of WAP does not always lead to a respective improvement in the water use efficiency of plants. The polymer network binds the absorbed water so strong that the plant roots cannot extract a considerable amount of the water. Therefore, further studies should estimate the optimal concentration of WAP in different soil textures, which can be useful to the plant by increasing PAWC rather than improving overall soil-water retention capacity. Efforts should also be made to optimize the synthesis of WAP such that both the water absorption and release are maximum.

2.4.3 Influence on hydraulic conductivity and infiltration characteristics

Influence of the WAP amendment on hydraulic conductivity of soil was studied extensively by the previous researchers, and it is a much-debated subject of research with reported anomalies. Majority of the studies show a decrease in saturated hydraulic conductivity with the application of WAP to coarse-textured soils (Sahid et al. 2012; Narjary et al. 2012; Mohawesh and Durner 2019). It was reported that the total amount of water-accessible pore space at a particular packing density decreases exponentially with the increase in polymer concentration under both restricted and free swelling conditions (Wei and Durian 2013). The pore size distribution is significantly modified by the swollen WAP particles in such a manner that large pores are clogged, and several small pores are formed. This leads to a decrement in the saturated hydraulic conductivity, which is significantly affected by the pore geometry and soil structure (Tuli et al. 2005). However, it is not clear from these studies whether the decrease in the saturated hydraulic conductivity is irrespective of polymer concentration or at an optimum polymer concentration. There are a few studies, which demonstrated that the decrease in saturated hydraulic conductivity is associated with a low concentration of the polymer as the volume of the water-conducting pores gets reduced (Bhardwaj et al. 2007). However, after the concentration of the polymer exceeds an optimum value, the saturated hydraulic conductivity started to increase (Bhardwaj et al. 2009). The higher concentration of swollen WAP can lead to a softer and loose soil matrix through which water can flow easily (Hussien et al. 2012).

In addition to the aforementioned factor, for restricted swelling conditions, the pressure applied by the surrounding soil particles may cause the swollen WAP to drain or lose water leading to an increase in the size of pores available for water flow. The influence of WAP on the saturated hydraulic conductivity of soil is time-dependent. The WAP can create larger pore

TH-2777_166104034

channels in the soil matrix through leaching in the direction of water flow and get accumulated in specific regions (Bharadwaj et al. 2007). Besides, Andry et al. (2009) observed that the saturated hydraulic conductivity of WAP amended soil is dependent on the temperature of the soil. This phenomenon can be associated with changes in the water absorbency of WAP with increasing temperature. The effect of soil texture on the saturated hydraulic conductivity of soil is not extensively studied. There are very few studies, which reported an increase in saturated hydraulic conductivity with the addition of WAP (at a lower concentration of WAP) in fine-textured soil (Hussien et al. 2012; Bagheri and Afrasiab 2013). These studies indicated that soil texture could be an important factor while defining the influence of WAP amendment on the saturated hydraulic conductivity of the soil. This necessitates systematic experimental studies on different textured soil with different percentages of WAP to ascertain these observations beyond doubt.

The infiltration characteristic of soil mainly depends on the soil texture and structure, types of vegetation cover, and water content of the soil. It can be significantly influenced by the addition of WAP as it alters both soil pore structure and water content. The two parameters, including infiltration rate and hydraulic conductivity, are closely related. The rate of infiltration is affected by the hydraulic conductivity of soil, which describes the easiness of fluid flow through the porous media (Schwartz and Zhang 2002). The infiltration rate was found to be decreased with WAP addition, which is obvious as the swollen polymer reduced the pore sizes between the soil particles (Bakass et al. 2002; Lentz 2007; Sepaskhah and Shahabizad 2010; Zhuang et al. 2013). A study conducted by Yang et al. (2015) revealed that WAP addition could alter the advancing wetting front. It was further noted that the horizontal infiltration rate is much higher than the vertical infiltration rate in the WAP amended soil layer. Reddy et al. (2015) reported that the initial vertical infiltration rate was decreased by 38% with the addition of 1% WAP in sandy soil. It was further observed that the time to reach the steady-state infiltration rate was achieved in 60 min for bare soil and 75 min for 1% WAP amended sandy soil. Abrisham et al. (2018) have noted that the steady-state infiltration rate was decreased by 40% in WAP amended sandy loam soil (0.4% WAP). From the aforementioned studies, it was observed that the infiltration rate decreases with WAP addition irrespective of soil texture. The lower rate of infiltration can reduce the migration velocity of water to the deeper layer, which can be a great advantage, as sufficient water would be present in the root zone (Ekebafe et al. 2011).

TH-2777_166104034

Table 2.2 Summary of relevant literatures related to WAP influence on soil properties

Soil Property	Soils used [As per US Department of Agriculture (USDA)]	WAP application rate (w/w)	Used apparatus/ methods	Key conclusions	References
Water retention characteristic curve (WRCC)	✓ Sand ✓ Sandy loam ✓ Sandy clay loam ✓ Loam ✓ Clay loam ✓ Clay	• 0.1% • 0.2% • 0.3% • 0.4% • 0.5% • 0.6% • 0.7% • 1%	• Pressure plate apparatus • Tensiometer • Centrifuge • Dew point potentiameter	➢ An exponential increase in water retention with addition of WAP (0.1 %-0.4 %) for sand. ➢ For sandy loam soil, the saturated volumetric water content is increased by 1.9 times with addition of WAP (0.6%) as compared to bare soil. ➢ The air entry value of sandy loam soil is increased with WAP content. ➢ For clay soil, WAP addition increase aeration by decreasing the air entry value. ➢ The residual water content increases with increasing WAP content and the increment depends on cation exchange capacity of soil. ➢ Water accessible pore spaces at a particular density exponentially decrease with WAP concentration.	Huttermann et al. 1999; Koupai et al. 2008; Andry et al. 2009; Narjary et al. 2012; Wei and Durian 2013; Banedjschafie and Durner 2015; Montesano et al. 2015; Yu et al. 2017; Mohawesh and Durner 2019
Plant available water content (PAWC)	✓ Sand ✓ Sandy loam ✓ Loam ✓ Silt loam ✓ Clay	• 0.1% • 0.2% • 0.3% • 0.4%, • 0.6% • 1%	• Tensiometer • Centrifuge • Field measurement	➢ For sandy soil, the available water content for plants increased up to 5 times with an acrylamide WAP amended soil. ➢ The water content at field capacity of the amended soil improved by 2.4 times with 0.6% WAP amendment in sand. ➢ The PAWC doesn't significantly improved with WAP application in clay soil. ➢ With addition of WAP, the water content at the plant permanent wilting point increases. ➢ Significant part of the stored water in WAP may not available to plant.	Koupai et al. 2008; Andry et al. 2009; Agaba et al. 2010; Dorraji et al. 2010; Yang et al. 2014; Banedjschafie and Durner 2015;

TH-2777_166104034

Soil Property	Soils used [As per US Department of Agriculture (USDA)]	WAP application rate (w/w)	Used apparatus/ methods	Key conclusions	References
Hydraulic conductivity	✓ Sand ✓ Clay loam	• 0.05% • 0.2% • 0.25% • 0.4% • 0.5% • 0.8% • 1% • 2%	• Falling head method	➢ For sandy soil, a reduction of 92% in saturated hydraulic conductivity have been observed with 0.4% WAP application. ➢ Addition of WAP can alter soil structure and pore geometry by clogging the larger pore in coarse textured soil. ➢ After a WAP concentration of 1%, the saturated hydraulic conductivity started to increase in sandy soil. ➢ For clay loam, the saturated hydraulic conductivity increases with the addition of WAP. ➢ With the progression of time, the saturated hydraulic conductivity increases because of the leaching of WAP. ➢ Temperature has a significant effect on saturated hydraulic conductivity as it influences the WAC of WAP.	Bhardwaj et al. 2007; Hussien et al. 2012; Sahid et al. 2012; Bagheri and Afrasiab 2013; Mohawesh and Durner 2019
Infiltration characteristic	✓ Sand ✓ Sandy loam ✓ Loam ✓ Silt	• 0.1% • 0.2%, • 0.4% • 0.5% • 0.75% • 1%	• Mini disk infiltrometer	➢ The initial infiltration rate decreased by 38% in 1% WAP amended sandy soil as compared to bare soil. ➢ The vertical infiltration rate is slower than the horizontal infiltration rate for WAP amended soil. ➢ For sandy loam, the decrease in steady infiltration rate was 40% with 0.4% WAP addition. ➢ The cumulative infiltration of 1% WAP amended soil is almost 1/5th of the infiltration in bare sandy soil.	Bakass et al. 2002; Zhuang et al. 2013; Reddy et al. 2015; Yang et al. 2015; Abrisham et al. 2018

TH-2777_166104034

2.4.4. Influence of WAP on plant parameter

Optimum nutrient retention of soil in the root zone is an important requirement for plant growth and yield. Excessive leaching of water-soluble nutrient during irrigation/rainfall affect both soil properties (soil structure, pH and microbial activity) and plant health. The application of WAP in the agricultural field can bind the nutrient into their polymeric structure along with water and release at a slower rate according to the plant requirement (Islam et al. 2011). Martin et al. (1993) reported that the micropores present in the hydrophilic polymers allow the macronutrients (P, K, Mg, and S) as well as the micronutrient (Fe, Mn, Zn, and Cu) to diffuse through the particles. It was noted that the release of the nutrients depends on the decomposition rate, type of the nutrients, and diffusion properties of the polymer. A nutrient leaching study conducted by Mikkelsen et al. (1993) have revealed that the addition of WAP reduced the nitrogen leaching by 45% compared to bare soil during four weeks of experimentation. It is quite obvious that the reduction in nutrient leaching can improve the root growth as well as the plant biomass.

The influence of WAP amendment on the plant yield, shoot growth, leaf area index (LAI), leaf chlorophyll index reported in the literature are summarized in Table 2.3. As expected, the shoot growth and plant yield increase with the incorporation of WAP (Arbona et al. 2005; Lentz and Sojka 2009; Moslemi et al. 2011). The study reported by El-Tohamy et al. (2014) indicates that the soil amended with 0.7% WAP showed a 60% increase in the LAI (area of a one-sided green leaf per unit area of the ground surface) of a squash plant as compared to bare soil. An increment in LAI results in higher number of leaves per plant and improves yield. Khadem et al. (2010) have observed an increase in leaf chlorophyll index with polymer amendment for corn in water stress conditions. Tongo et al. (2014) have explained that WAP can bind different micronutrients along with the water due to its high absorption capacity, and the chlorophyll synthesis increases with increasing uptake of these micronutrients. Needless to mention that the chlorophyll content of leaves is an important factor that determines the photosynthesis efficiency and plant yield. However, LAI and leaf chlorophyll index are sensitive to the irradiance of solar energy. There is still a lack of knowledge on the correlation between LAI, leaf chlorophyll index, and plant yield with WAP content for different plant species and soil types. This is mandatory for developing efficient guidelines on the use of WAP for engineering water and nutrient retention in soils.

TH-2777_166104034

Table 2.3 Brief overview of the parameter consider for soil-WAP-plant interaction

Reference	Plant species	Soil type	WAP content (w/w)	Plant parameters					Plant survival time
				Root growth	Shoot growth	Leaf area index	Leaf chlorophyll index	Yield	
Johnson and Piper 1997	Tomato	Sand	0.3%	X	✓	X	X	✓	X
Huttermann et al. 1999	Aleppo pine	Sandy soil	0.04%, 0.08%, 0.12%, 0.2%, 0.4%	✓	✓	X	X	X	✓
Arbona et al. 2005	Citrus	Peat	0.2%, 0.4%	✓	✓	X	X	X	X
Koupai et al. 2006	Cupressus arizonica	Clay, Sandy loam	0.4%, 0.6%	X	✓	X	X	✓	✓
Al-Humaid and Moftah 2007	Buttonwood	Sand	0.1%, 0.2%, 0.4%, 0.6%	✓	✓	X	X	X	✓
Yazdani et al. 2007	Soybean	Silt loam	75*, 150*, 225*	X	✓	✓	X	✓	X
Busscher et al. 2009	Maize	Sand	0.1%, 0.6%	X	X	X	X	✓	X
Lentz and Sojka 2009	Bean, Corn	Silt loam	0.1%	X	X	X	X	X	✓
Agaba et al. 2010	Eucalyptus, Pine, Oak, Neem, Afara	Sand, Sandy loam, Loam, Silt loam, Clay	0.2%, 0.4%	X	X	X	X	X	✓
Dorraji et al. 2010	Corn	Loamy sand, Sandy clay loam	0.2%, 0.4%,0.6%	X	X	X	X	✓	X
Khadem et al. 2010	Corn	Loam	200*	X	X	X	✓	✓	X
Chirino et al. 2011	Oak	Clay	0.7%, 1.5%	✓	✓	X	X	X	✓

TH-2777_166104034

Reference	Plant species	Soil type	WAP content (w/w)	Plant parameters					Plant survival time
				Root growth	Shoot growth	Leaf area index	Leaf chlorophyll index	Yield	
Islam et al. 2011	Wheat	Sandy loam	10*, 20*, 30*, 40*	✓	✓	X	X	✓	X
Moslemi et al. 2011	Maize	Clay loam	110*	X	X	X	X	✓	X
Farrell et al. 2013	Wheat, White lupin	Scoria, roof tiles	1%	✓	✓	X	X	X	✓
Orikiriza et al. 2013	Spruce, Pine, Beech	Sand, Loam, Clay	0.4%	✓	✓	X	X	X	✓
Cannazza et al. 2014	Chicory, Tomato	Silty clay, Clay	0.2%, 0.5%, 1%, 1.5%	X	✓	X	X	X	X
El-Tohamy et al. 2014	Squash	Sand	0.1%, 0.2%, 0.3% 0.4%, 0.5%, 0.6%, 0.7%	X	✓	✓	✓	✓	X
Tongo et al. 2014	Bardi bush	Sandy loam	0.2%, 0.4%, 0.6%	✓	✓	✓	✓	X	X
Darini et al. 2015	Grass	Silt loam	0.15%, 0.3%, 0.4%	✓	✓	X	✓	X	X
Dehkordi 2015	Corn	Sand	15†, 30†, 45†	X	X	X	X	✓	X
Mazen et al. 2015	Maize	Loamy sand	0.05%, 0.1%, 0.2%, 0.4%	✓	✓	X	X	X	X
El-Asmar et al. 2017	Maize, Pine	Sandy clay loam, Clay	0.1%, 0.2%, 0.3%, 0.4%	X	✓	X	X	X	✓
Abrisham et al. 2018	Rosemary	Sandy loam	0.2%, 0.4%	X	✓	X	X	X	X
Satriani et al. 2018	Bean	Silty clay loam, silty clay	5†, 10†	X	X	X	X	✓	✓

*WAP content reported in kg/ha; † WAP content reported in g/m^2

TH-2777_166104034

2.4.5. WAP amended soil under drought condition

From the previous section, it is clear that the addition of WAP as a soil amendment can increase the water retention capacity, plant available water content and reduce infiltration rate, especially in coarse-textured soils. As a result, the WAP application can reduce the irrigation frequency and improve plant growth under drought conditions. Apart from these aspects, the most important relevance of utilizing WAP is the survival of plants under water stress conditions. Geng et al. (2015) have reported that the water stress condition affects the soil ecosystem directly and results in soil degradation. The long-term effect of drought on the soil ecosystem is so severe that it could not be easily recovered even after heavy rainstorms or rehabilitation. Therefore, there is a need to restrict excess moisture loss during water stress conditions to prevent soil degradation. It was reported that WAP amendment could alleviate the negative effect of drought stress on plants by prolonging their survival time (Johnson and Piper 1997; Nazarli et al. 2010; Ekebafe et al. 2011; Islam et al. 2011; Moslemi et al. 2011; Orikiriza et al. 2013; Darini et al. 2015). According to Huttermann et al. (1999), there is a significant increase in the plant survival time (by 32 days) with 0.4% WAP amendment under drought conditions. The increase in survival time may be a result of decreased hydraulic conductivity and loss of water from the top layer (Chirino et al. 2011).

The efficiency of WAP for improving the plant survival time for different soil textures was obtained by calculating the plant survival time improvement factor (ratio of plant survival time in WAP amended soil to that of bare soil) from the available data reported in the literature, as shown in Fig. 2.9. It was observed that irrespective of the soil texture, the WAP addition had prolonged the survival of plants under water stress conditions. The maximum improvement in the survival time in sandy soil and clayey soil was found to be 3.8 times and 1.9 times, respectively, as compared to bare soil. These studies give an indication that the addition of WAP in semi-arid, arid, and drought-prone areas can be effective in circumventing the shortage of irrigation water. Shi et al. (2010) have found that the application of WAP can delay the drought stress-induced leaf injury by a significant amount of days. Keshavars et al. (2012) have observed that the application of WAP at a rate of 0.4% has compensated the adverse effects of drought stress in a plant species and increased total plant biomass (both root and shoot). These studies indicate the possibility of water uptake from WAP during water distress. de Vasconcelos et al. (2020) reported an increase in root and shoot growth of melon seedling with the application of a laboratory synthesized WAP (based on starch and rice husk ash) under drought conditions.

TH-2777_166104034

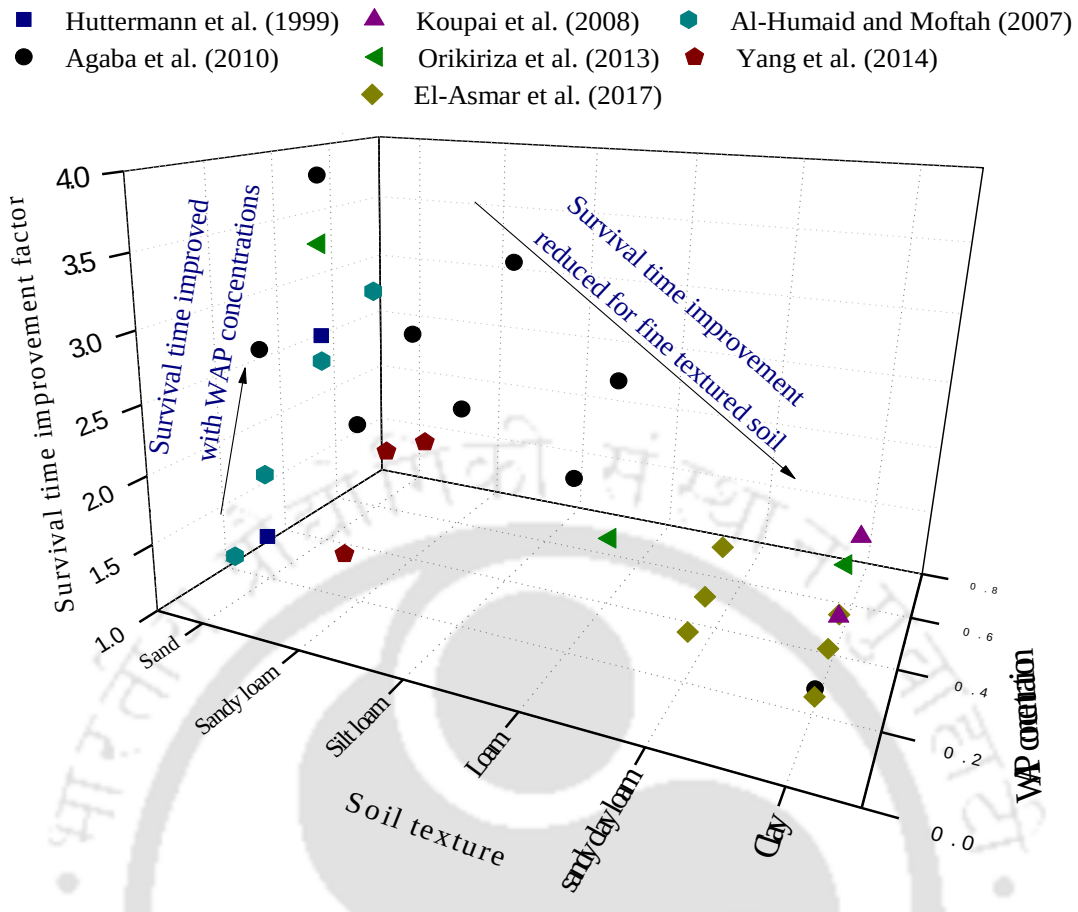

Fig. 2.9 Variation in survival time improvement factor for different soil texture

Another important aspect of WAP amendment is that it reduces the rate of evaporation of water from the soil (Abedi-Koupai and Asadkazemi 2006; Marandi et al. 2009; Agaba et al. 2010; Yang et al. 2014; Fallahi et al. 2015), which is a crucial factor during water stress condition. This phenomenon can be explained from the concept of hydraulic lift, which is defined as the movement of water from the deeper soil layer to the surface soil (Agaba et al. 2010). As the hydraulic conductivity of the WAP amended soil is less compared to bare soil, the upward movement of water is also less in the amended soil. Rabat et al. (2016) reported that the evaporation loss from the polymer amended soil is significantly lower as compared to bare soil due to the macromolecular network of polymer and its interaction with water. The water in WAP can be classified into bound water, half-bound water, and free water (Marandi et al. 2009). The percentage of half-bound and bound water in the swollen gel is proportional to the number of hydrophilic groups present in unit volume. The free water present in WAP has high mobility compared to bound water and half-bound water and can easily be lost during evaporation. After the full evaporation of water outside the WAP, the water inside the WAP is slowly released to the soil (Demitri et al. 2013). However, there is a gap in the literature on the

TH-2777_166104034

quantification of moisture release mechanism from WAP to the soil and how much percentage of water stored in the WAP will be available for water uptake. Such quantifications are necessary to evaluate the efficiency of WAP for drought applications.

2.4.6. Effect of soil salinity on WAP amended soil

Soil salinity is prominent in the agricultural field due to improper irrigation practice, lowering of water levels during drought, and soil erosion (Al Jabri et al. 2015). All source of water, including natural rainfall, contains some amount of dissolved solids resulting in soil salinity. However, proper irrigation management can minimize salt accumulation by providing sufficient drainage water to leach out the added salts from the soil. Lowering of groundwater table during drought can cause the salts in groundwater to rise to the root zone by capillary action. It is a well-known fact that soil salinity has an adverse effect on plant water uptake due to osmotic pressure in soil retaining more water. A high concentration of salt in soil can create a nutrition imbalance, which restricts plant growth and causes deformed leaves (Dorajji et al. 2010; Sudhir and Murthy 2012). Excessive salt accumulation near the root zone can reduce the plant water uptake capacity and affect plant health (Shi et al. 2010; Zhao et al. 2016). Hamdy and Sfeir (2002) have investigated the use of WAP as a soil conditioner to mitigate the effect of saline irrigation with four different salt concentrations in irrigated water. It was noted that the application of hydrophilic polymer increased the salt tolerance of the plant and thereby increased the crop yield by three times compared to bare soil for a maximum soil salinity of 9 dS/m.

Shi et al. (2010) have reported the effect of two different WAP on the tolerance of salt-sensitive plant species. The addition of WAP in saline soil can lower the salt concentration of the pore water by binding the salt ions in the large chain structure of the polymer. Also, salt ion concentrations in the hydrophilic polymers get diluted due to a large amount of water retained in the polymers and restrict the accumulation of salt ions near the root area (Al Jabri et al. 2015). However, there are some observations presented in the literature, which states that the presence of salt has an adverse effect on the water absorption capacity of WAP. Bowman and Evans (1991) have studied the absorption capacity of three different types of polyacrylamide gels in eight saline solutions. It was observed that the water absorbency was highly affected by the presence of the salt ions. Subsequently, the covalence of the salt ions also influences the hydration or water absorbency of the WAP. The effect of trivalent and divalent cations was more than the monovalent cations due to the increased ionic strength of the higher covalent ions. Zhang et al. (2014) have reported that the presence of salt cation has

TH-2777_166104034

an adverse effect on the absorption capacity of WAP due to the formation of additional ionic crosslinks in the gel network. It can be noted that the most common fertilizer used in the agricultural field (urea) does not influence the water storage capacity of WAP due to the non-ionic nature of the compound (El-Rehim et al. 2006). Despite these shortcomings associated with the WAP under saline conditions, application of the WAP can improve the water holding capacity of soil as well as the plant growth and yield compared to the bare soil (Huttermann et al. 2009; Dorraji et al. 2010; Dehkordi 2017).

2.4.7. Eco-compatibility and biodegradability of WAP

The compatibility of WAP with the environment is an important aspect to be ensured before using it as a soil amendment under water stress conditions. Previous studies have highlighted the fact that commercially available WAP is a non-toxic material and can be considered environmentally-friendly (Haselbach et al. 2000; Zohourian and Kabiri 2008; Pandey et al. 2014; Guezennec et al. 2015). However, it is obvious that WAP can be prepared from the polymerization of different monomers and support materials using the crosslinking agent. Thus, the chemical properties and the biodegradability of any WAP completely depend on the type of monomer and support material used. Most of the commercially available WAPs are acrylate and acrylamide-based products, which is a non-biodegradable product. Though polyacrylamide based WAP is non-toxic in nature, the degradation of the polymer can produce acrylamide residue (Caulfield et al. 2002; Young et al. 2007; Weston et al. 2009; Labahn et al. 2010), which is considered hazardous for the aquatic environment as well as for human and reported as a carcinogenic (level 2) compound (World Health Organization 1985). On the contrary, Sojka et al. (2007) have reported that acrylamide undergoes quick degradation in the presence of soil moisture and produces acrylic acid and ammonia. These resultant products could be a source of carbon and nitrogen for the growing media. Besides, the degradation of acrylamide can also be influenced by the microbial activity of the soil. Arrowood (2008) have investigated the microbial degradation pattern of acrylamide in a soil column with three different types of soils. The results indicated that acrylamide was quickly degraded, and the half-life of acrylamide was less than 3 hours. Further research is needed for quantifying the degradation kinetics and the resulting bioactivity in the root zone before using the polyacrylamide-based WAP for agricultural purposes. None of the above-mentioned concerns are applicable for acrylate-based WAP and can be used in the agricultural field during drought conditions.

TH-2777_166104034

The biodegradability of acrylate-based WAP in different types of soils at different temperatures was studied in previous literature using carbon isotopes (Wilske et al. 2014; Bai et al. 2015). It was noted that the polyacrylate chain degraded at a very slow rate of 0.12–0.24 % per 6 months in soil and the degradation rate did not vary significantly with an increase in temperature. It can be expected that the degradation rate in the experimental laboratory setup may be less compared to the field soil as microbial activities will be more intense and controlled by the type of crops. There are several studies present in the literature that highlighted biodegradation of synthetic WAP is very poor and generally takes long time to degrade in the soil (Entry et al. 2008; Guezennec et al. 2015). One of the possible methods to enhance the degradability is the incorporation of white root fungi into the soil that results in causing solubilizing and mineralizing WAP (Cameron et al. 2000; Stahl et al. 2000; Mai et al. 2004). Moreover, recent studies are focusing on the development of biodegradable polymer, having similar physio-chemical properties as the commercial WAP. These laboratory-synthesized WAPs are prepared from natural waste materials like starch (Ismail et al. 2013; Hua and Wang 2008; Zhang et al., 2014; Zhang et al., 2015), cellulose (Bao et al. 2011; Wu et al. 2012; Demitri et al. 2013), chitosan (Zhang et al. 2007a; Spagnol et al. 2012b; Cheng et al. 2017; Pereira et al. 2017), yeast (Feng et al. 2014) and clay powder (Li et al. 2004; Wan et al. 2006). There are several literatures that reported the performance of the lab-made WAP in terms of water absorbing capacity (as observed from Table 2.1), salt sensitivity, and reswelling ability, which is better than the commercial WAP (Zhang et al. 2006c; Zheng et al. 2007; Wang et al. 2008; Zhang et al. 2009; Zhang et al. 2014; Xu et al. 2015; Xue et al. 2016). Apart from that, the added advantage of lab-made WAP is its low cost and excellent degradation kinetics in soils. The utilization of natural/waste material for the synthesis makes the lab-made WAP cost-effective as compared to commercial WAP. The lab-made WAP showed a higher degradation rate in soil. Wang et al. (2008) reported the degradation rate of 43% after three months in soil for carboxymethyl cellulose-based WAP. Xie et al. (2012) observed a degradation rate of 34% after one month for a synthesized WAP composite (prepared from wheat straw, acrylic acid, acrylamide). Jin et al. (2013) synthesized a nitrogen-phosphorus (NP) coated starch-based WAP with a degradation rate of 40% after two months. Sharmah and Karak (2020) have also reported a similar degradation rate (40%) after three months of a starch modified poly (acrylic acid) WAP, using soil burial method. From these studies, it is conclusive that the development of such biodegradable WAP can reduce the environmental jeopardy associated with the synthetic polymer as well as reduce the cost of production.

TH-2777_166104034

A cost comparison of commercial WAP with the common fertilizers used in the agricultural field is presented in Table 2.4 to explore the cost-effectiveness. It is quite evident from Table 2.4 that the total expenditure (per year) for WAP is much lesser than fertilizers. From the eco-compatibility perspective, there is no conclusive observation about the toxicity of the acrylate-based WAP. Moreover, the laboratory-synthesized WAP showed a higher biodegradability rate as compared to the commercial-grade WAP.

Table 2.4 Cost comparison of commercial WAP with fertilizer

		WAP	Fertilizer (Urea+ Phosphate)
Cost per kg weight	Maximum cost, dollars	6	0.6[*2]
	Minimum cost, dollars	4	0.4[*2]
Cost per ha of land	Maximum cost, dollars	180[*1]	98[*3]
	Minimum cost, dollars	120[*1]	66[*3]
Service life	years	3	1
Total expenditure per year	Maximum cost, dollars	60	98
	Minimum cost, dollars	40	66

[*1]Application rate 30 kg/ha (Islam et al. 2011), [*2]Schnitkey, 2017, [*3]Fertilizer rate 165 kg/ha (Food and Agriculture Organization, 2006)

2.5 Current scenario of FA production and utilization

Fly ash (FA), a coal combustion solid waste residue from the thermal power plant, is one of the most complex and anthropogenic materials (Yao et al. 2015; Gollakota et al. 2019). In India, the coal-based thermal power plants contribute about 80% of the total power demand (Fig. 2.10). Though there are a lot of discussions are going on to utilize natural gas, oil, nuclear, and renewable energy sources to meet the growing electricity demand, the thermal power plant will still remain the major source of electricity in the next few decades (Nawaz 2013). According to the Central Electricity Authority (CEA), India produces around 196 million tons of FA annually (CEA 2018b). With the rapid rate of industrialization and urbanization, the production of FA is expected to cross 250 million tons by the year 2020. However, FA utilization rate has not improved much in the last ten years (utilization rate 53% in 2007-2008 and 67% 2017-2018) in comparison with the growth in FA production [Fig. 2.11]. The unutilized portion of FA is mixed with water and transported as slurry, and disposed in the form of ash ponds. These ash ponds can cause soil contamination and disruption of ecological

TH-2777_166104034

balance by altering the soil pH and clogging natural drainage (Malik and Thapliyal 2009). Moreover, the toxic substances present in these uncovered ash ponds can reduce the quality of air and pose severe risks to the environment. This necessitates more innovative, economical, and green technologies to maximize the utilization of FA in order to reduce the burden of storage and disposal of FA.

As per the report published by CEA, India in 2018, the utilization rate of FA for agriculture, concrete, and road construction is only about 0.3%, 0.7%, and 3.4%, respectively (Fig. 2.12). The reason for such a low utilization rate in these applications is the unavailability of advanced and cost-effective technologies. Moreover, there are some conflicting observations and anomalies exist in the literature related to the adverse effects of FA on the environment due to the presence of heavy metals. Therefore, there is a need to develop a clear understanding of the potential benefits and threats of FA in those applications to increase its utilization. Most of the recent studies are more focused on the transformation of FA into various innovative materials to achieve a valuable addition of FA. Transformation of FA into geopolymer or biodegradable polymer opens up a huge area of research to achieve 100% utilization of FA and maintain the ecological balance.

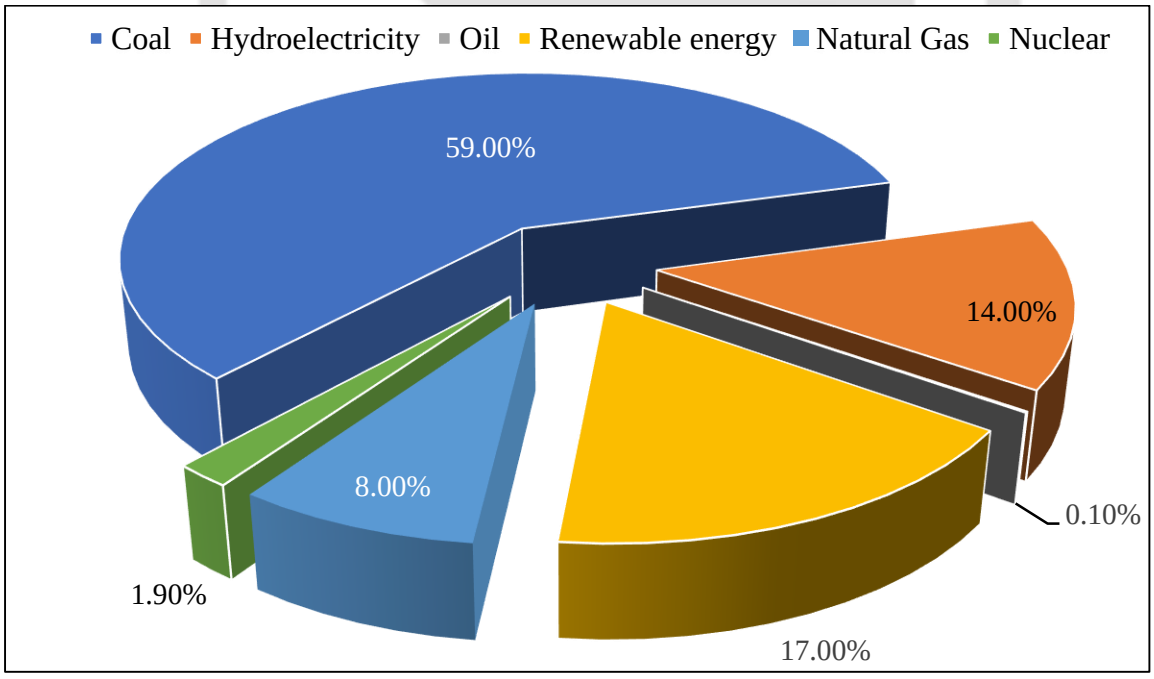

Fig. 2.10 Different sources of electricity generation in India (adapted from CEA, 2019a)

2.5.1 Physicochemical properties of FA

A thorough knowledge of the physicochemical properties of FA, such as chemical composition, mineralogy, and surface morphology, is required to explore the possibility of

TH-2777_166104034

alternate and value-added applications of FA. The physical properties of FA can vary significantly depending on the type of coal (Anthracite, Bituminous or Lignite), ash content in coal, combustion method, boiler type, and collector setup (Basu et al. 2009). FA obtained from the combustion of bituminous coal is generally finer as compared to FA obtained from lignite coal (Gallakota et al. 2019). FA particles are mostly silt loam texture with particle sizes ranging from 0.5µm to 300µm (Chang et al. 1977). Yao et al. (2015) have reported that the surface morphology of FA suggested that the particles are spherical in shape and consist of hollow spheres (cenospheres), solid spheres, irregular-shaped debris (minerals that do not undergo melting), and unburnt carbon (porous). The physical appearance of FA can vary from light grey to dark brown, depending on the percentage of unburnt carbon content after combustion. The darker color of FA represents the higher percentage of unburnt carbon content. The particle size distribution and surface area of FA are essential parameters as they influence the texture and sorption behavior of FA. A summary of the physical properties of FA is presented in Table 2.5.

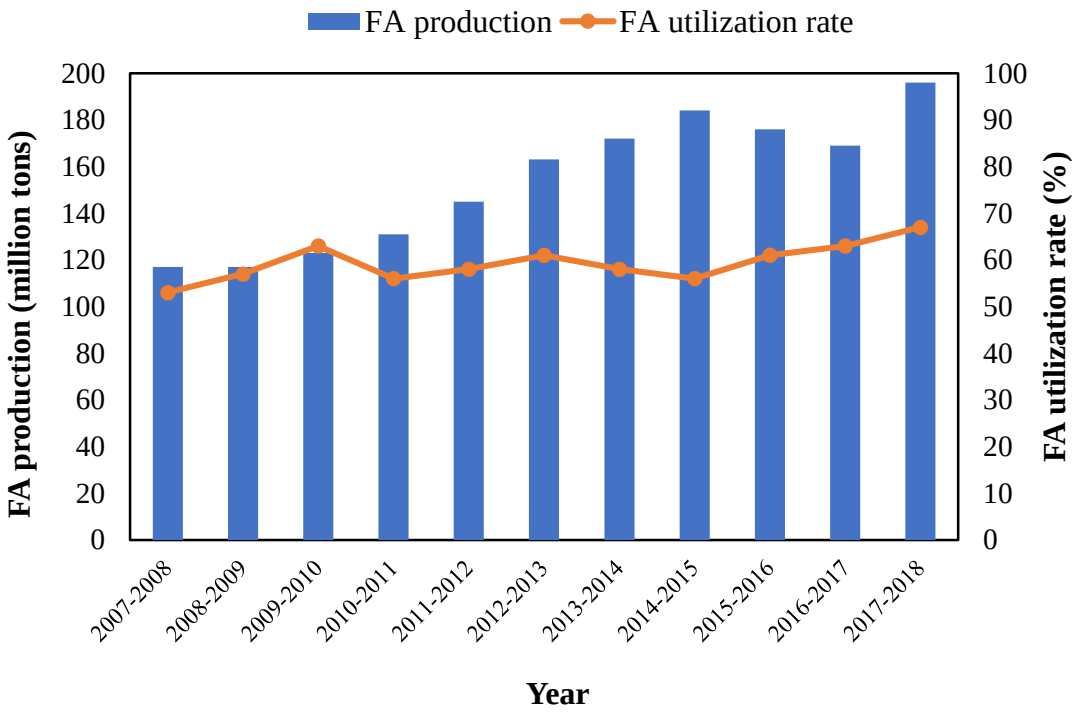

Fig. 2.11 FA production and utilization rate in India for the past 10 years (adapted from CEA, 2018b)

The chemical characterization of FA is one of the most complicated methods as a wide range of minerals can be present depending on the source of FA. Vassilev and Vassileva (2005) reported the presence of approximately 316 minerals and 188 mineral groups in various coal

TH-2777_166104034

FA. However, the major constituents of FA are mainly oxides of silicon, aluminum, and iron, with a smaller fraction of magnesium (Mg), calcium (Ca), sodium (Na), potassium (K), and Phosphorus (P) (Abhijit and Sreedeep 2015). FA also contents various trace elements, some of which are beneficial for plant growth, whereas some minerals may have toxic effects. According to Gatima et al. (2005), about 95-99% of FA consists of oxides of silicon, aluminum, and iron, and about 0.5-3.5% consists of sodium, phosphorus, potassium, and sulfur, and the remaining portion is consisting of trace elements. Page et al. (1979) reported the presence of many trace elements such as arsenic (As), boron (B), molybdenum (Mo), Selenium (Se), mercury (Hg), cobalt (Co), and Strontium (Sr) in FA.

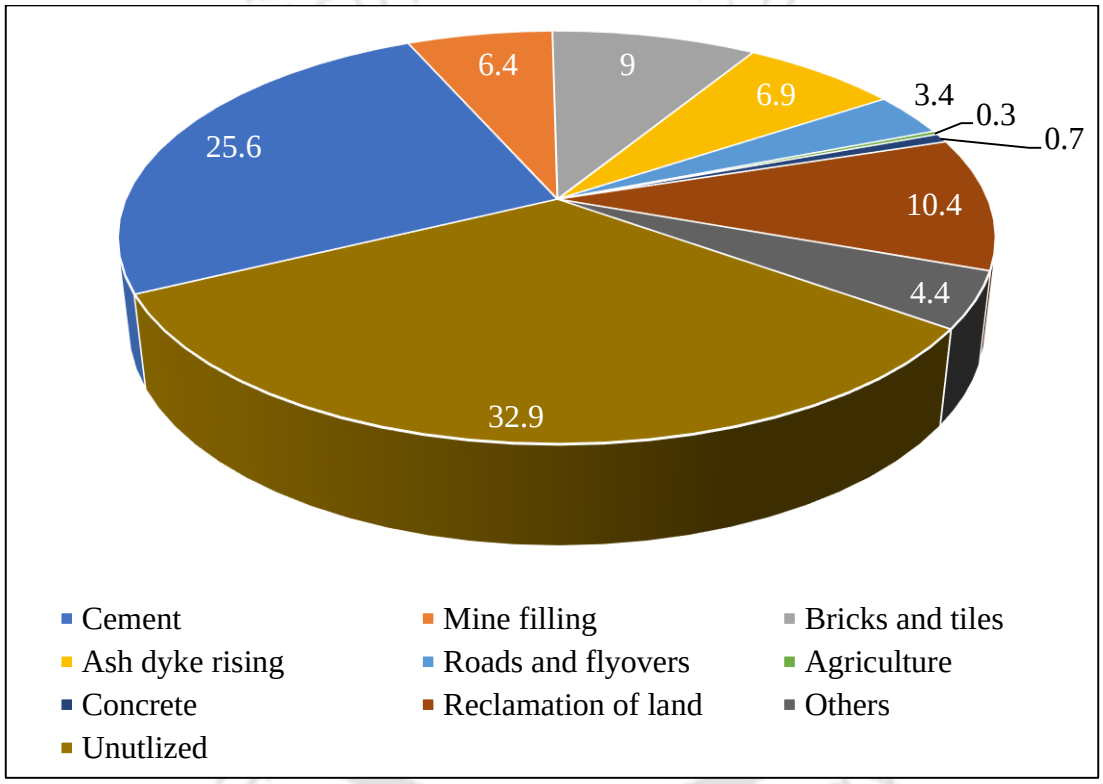

Fig. 2.12 Modes of utilization of FA in India (adapted from CEA, 2018b)

As per the American Society of Testing and Materials (ASTM) standard, the FA has been classified into class C and class F based on the chemical composition and the origin of coal (ASTM C618, 2019). The class C FA, which originated from the combustion of sub-bituminous and lignite coals, has self-cementing properties because of the presence of high calcium (Ca) content (more than 20%). On the other hand, class F FA, derived from anthracite and bituminous coals, has lower Ca content (less than 20%).

From the mineralogy point of view, FA can contain quartz, mullite, magnetite, hematite, char, feldspars, clay, calcite, and mica minerals (Vassilev and Vassileva 2005). These minerals

TH-2777_166104034

and phases can be classified into three categories such as primary, secondary, and tertiary constituents. The primary constituents are those materials, which are initially present in the coal and have not undergone any phase transformation during coal combustion such as quartz, mica, feldspar. The secondary constituents include new minerals formed due to the combustion of coal, namely mullite, magnetite, hematite, lime. The tertiary constituents include the new minerals and phases that originated during the transport and storage of FA, such as calcite and amorphous materials.

Table 2.5 Summary of basic physical properties of FA

Physical properties	FA	Reference
Bulk density (kg/m^3)	900-1300	Gallakota et al. 2019
Water holding capacity (%)	35-40	Basu et al. 2009
Specific gravity	1.6-2.5	Prakash and Sridharan 2009
Free swell index	Negligible	Gallakota et al. 2019
Coefficient of Uniformity (%)	3.1-10.7	Gallakota et al. 2019
Porosity (%)	50-60	Basu et al. 2009
Plasticity	Non-plastic	Deka and Sreedeep 2017
Specific surface area (m^2/s)	1.6-5	Gallakota et al. 2019
pH	4.5-12	Gorai 2018
Maximum dry density (kg/m^3)	8-15.5	Prakash and Sridharan 2009
Optimum moisture content (%)	15.5-59.9	Prakash and Sridharan 2009
Hydraulic conductivity (m/s)	10^{-8} to 10^{-6}	Prakash and Sridharan 2009

2.5.2 Potential hazards of FA to environment

Past studies have highlighted several environmental impacts of FA resulting from the dumping of FA in open land. The inappropriate disposal of FA in the form of ash pond not only requires a vast area of land but also leads to soil degradation. The FA particles are small enough to reach the subsoil and can clog natural drainage and contaminate the groundwater due to the leaching of heavy metals. In addition, the smaller particles of FA can remain in the atmosphere in a suspended state and can become a major source of air pollution. It can be noted that long-time exposure to FA can cause irritation of the eyes, nose, throat, and infection in the

TH-2777_166104034

respiratory tract (Yao et al. 2015). It is quite known that coal contains various types of trace elements (Such as Cu, Co, Cd, Mn, Ni, Pb Zn). Akar et al. (2012) have reported that the concentration of trace elements increased by 4-10 times in FA than their concentration in the parent coal. A substantial amount of these trace elements can leach out from the FA during its interaction with water in the ash ponds (Bhattacharyya et al. 2009). Thus, the water-soluble elements can easily contaminate the groundwater as well as surface water (Sushil and Batra 2006). Saikia et al. (2006) observed that the movement of these trace elements in the aqueous environment is generally governed by the size of the particle, pH of the external solution, initial concentration of elements, and leaching time. Patra et al. (2012) reported that the presence of trace elements such as Cd, V, Cr, Ni, and Pb are hazardous to the environment even at very low concentrations. Wang et al. (2008) used a column leaching experiment to evaluate the leachability of various trace elements, including As, Cd, Co, Cr, Hg, Mo, Ni, and Pb in FA. The results showed that the leached concentration of the trace elements exceeds the recommended concentration during acid rain. Gong et al. (2010) conducted an in-situ leaching test to investigate the leaching behavior of Cd, Zn, Cu, Pb, Cr, and Co in the FA dump and observed that the surrounding soil hugely affected by the FA dump. The radioactivity assessment of FA indicated that their radiation characteristic is typically dependent on the presence of radioactive elements in the parent coal (Jala and Goyal 2006). Mahur et al. (2008) have reported the presence of ^{238}U, ^{232}Th, and ^{40}K radionuclides in FA samples collected from Durgapur thermal power plant, India. Bhangare et al. (2014) collected FA samples from six different sources across India and found that all samples are enriched with radionuclides such as ^{238}U, ^{226}Ra, ^{232}Th, and ^{40}K.

2.5.3 Utilization of FA as soil amendment

The influence of FA on the physical and geotechnical properties has been extensively studied. Several studies are available in the literature that reported an improvement in soil texture, bulk density, water-holding capacity, and an increase in the essential plant nutrients in coarse-textured soil (Basu et al. 2009; Pandey and Singh 2010; Yunusa et al. 2012; Yao et al. 2015). An addition of FA up to 15% by weight significantly reduced bulk density and improved the soil structure, porosity, aeration, and root penetrability in fine-grained soils (Garg et al. 2005). Malaya and Sreedeep (2016) reported an increase in water retention capacity in the sandy soil with an increase in FA concentration (up to 70% by weight). Kalra et al. (2000) investigate the influence of FA addition on field capacity (FC) and wilting point on four different textured soils. The results showed an increase in FC by 16.2%, 38.5%, and 295.7%

TH-2777_166104034

for sandy loam, sandy clay loam, and sandy soils, respectively, with 40% FA amendment, while in clayey soil, FC was decreased by 10% as compared to bare soil. These results indicate that the FA amendment in the agricultural field can increase water availability to the plants, especially in coarse-textured soil. Moreover, the hydraulic conductivity and infiltration rate significantly reduce with the addition of FA and thereby reducing the excess leaching of water and water into the deeper layer (Yunusa et al. 2012). Another important advantage of FA addition is that it can ameliorate soil acidity as most of the FA produced in India is alkaline (pH >8) in nature. It can be noted that the efficacy of class C FA in ameliorating soil acidity is relatively higher than class F FA due to higher CaO content (more than 20%) in the former one (Manoharan et al. 2010). Moreover, Matsi and Keramidas (1999) showed that the use of FA in two acidic soils had improved soil fertility and crop production.

FA also contains various essential plant nutrients, including P, K, Ca, Mg, Cu, and Zn, which are beneficial for plant growth. Pandey and Singh (2010) showed that the application of FA could enhance crop yield by increasing the microbial activity of soil. It was also reported that utilization of FA, along with the chemical and organic fertilizer in an integrated way, could increase the fertilizer use efficiency (FUE) [Mittra et al. 2005; Basu et al. 2009]. However, there exist few conflicting studies regarding the presence of trace elements in FA and its influence on the soil-plant-human system. Mishra et al. (2007) reported the accumulation of trace elements such as Cu, Pb, Cr, and Cd in plants grown in FA amended soils. Dwivedi et al. (2007) found arsenic (As) accumulation in the leaves of rice. On the other hand, Pathan et al. (2003) reported that the release of trace elements in FA remains well below the regulatory levels. Pandey et al. (2009) evaluated that a low-level utilization of FA ensures the translocation of heavy metals in the plant within the critical limit. Therefore, there has to be an optimum quantity of FA amendment rate so that the uptake of trace elements remains within the permissible limit.

2.6 Critical appraisal of the reviewed literature

Drought is one of the devastating disasters that have hit India from a very long time, and it has a wide range of effects in a developing country. Apart from the climate change and shortening of monsoon, the other important causes of the drought involve low water holding capacity of soil, improper management of water resources, and undue use of chemical fertilizer. Hence, there is a need for an appropriate methodology for handling water stress conditions. This could be done using water absorbing material as soil amendment so that the soil can draw water from the material under water stress conditions. A review of the existing literature have

TH-2777_166104034

demonstrated that WAP could be very useful under drought stress to prolong the survival of plants and minimize the irrigation water requirement. The critical review highlights the anomalies associated with the influence of some key parameters, such as the effect of soil texture, presence of salt ions, and application rate on the performance of WAP. It was observed that plant available water content (PAWC) increased by several times as the field capacity of the soil has been increased with the WAP amendment. However, it is not clear from these studies whether the application rate has a significant effect on the PAWC as most of the stored water in the soil is not available to the plant in case of a higher application rate of WAP.

Moreover, the interaction of the WAP with the soil-water system is not systematically studied in the previous literature. The development of negative pore pressure (known as soil suction) in the WAP amended soil and its variation with stored water in the soil under drought conditions is not addressed. The water uptake process and the release mechanism of the WAP in soil under water stress conditions need to be studied in detail. Since the primary concern of soil-WAP-water interaction is the movement of water from swollen WAP to dry soil, a systematic investigation is required to explore the water release mechanism of WAP to soil and the percentage of water available for root uptake. Such a type of study will help to understand the efficacy of WAP as a soil amendment.

The review also highlights the physicochemical properties of FA and its potential hazards to the environment. It is quite evident from the past studies that the open disposal of FA in the form of ash ponds or landfills has several adverse impacts on plant and human life. Therefore, various innovative and cost-effective methods are required for 100% utilization of the generated FA and to enhance the value of FA. It was observed that the bulk utilization of FA in various field is limited due to the complex composition of FA. Based on the composition (physicochemical properties), the suitability of FA needs to be assessed for various applications. It was well established in the literature that FA can be utilized as a fertilizer or growth promoter for crop and non-crop species, as it contains multiple macro and micronutrients, suitable for plant growth. The radioactivity and the heavy metal content remain well below the safe limit if the optimum quantity of FA is being utilized.

In general, most of the commercially available WAP is prepared from the polymerization of partially neutralized acrylic acid. Some previous studies showed that WAP could be prepared by grafting various natural materials, such as starch, cellulose, chitosan, clay, into the polymeric chain of acrylic acid. Fly ash, being an alumino-silicate material, has the

TH-2777_166104034

potential to be used for the development of eco-friendly, low-cost WAP. However, there are not many studies that have explored such a possibility.

2.7 Objective and scopes of the proposed work

The primary objective of the proposed research work is to study the performance of laboratory synthesized WAP as well as commercial-grade WAP for drought stress management considering WAP-soil interaction. The study aims to transform an industrial solid waste, i.e., FA into WAP, and evaluate its utilization, application rate, impact on the soil properties under water stress conditions. Accordingly, the scopes of the study are outlined as follows,

(i) Development of an ecofriendly, low-cost WAP by transforming FA to maximize the water absorption and release capacity of WAP.

(ii) Characterize the moisture sorption mechanism of WAP and its transfer mechanism from swollen WAP to dry soil.

(iii) Establish a reliable suction and moisture content measurement technique that can measure the water retention characteristics of WAP amended soil.

(iv) Study the water retention characteristics of WAP amended soil.

(v) Evaluate the effect of aging, alternate drying/ wetting cycle on the degradation kinetics of WAP.

TH-2777_166104034

Chapter 3

Materials and Methodology

3.1 General

The materials used and salient experimental methodologies related to the current work are presented in this chapter. It includes characterization of the basic physical, and chemical properties of the used soils, fly ash, and commercial WAP along with its morphological characteristics. Apart from this, details of the different generic instruments/ sensor used and their working principles are presented in this chapter.

3.2 Materials selection

Three natural soils of different texture suitable for vegetation growth were selected for this study from different parts of the north-eastern region of India (Table 3.1). All three selected soils were surface soils and collected within a depth of 15 cm from the ground surface. The fine sand (FS) and Brahmaputra silt (BS) were collected from two different locations of Brahmaputra river bank, while the red soil (RS) is a hill soil collected within the Indian Institute of Technology (IIT), Guwahati campus. As most of the previous studies have mainly focused on cohesionless sandy soil, the present work includes soils varying widely in terms of their grain size distributions, plasticity, and texture. A commercially available WAP, Stockosorb (neutralized potassium polyacrylate, granular type), supplied by SargaGreen, India, was used in this study. Stockosorb has been widely used in the horticulture and agriculture sector as it is non-toxic to plant and environment, with a service life of 3 to 5 years (Islam et al. 2011). The raw fly ash (FA) sample was collected from the electrostatic precipitator of National Thermal Power Corporation (NTPC) Limited, Farakka, India.

Table 3.1 Details of various materials used in the study

Material	Designation	Source
Fine sand	FS	Brahmaputra river sand, Assam
Brahmaputra silt	BS	Brahmaputra river bank, Amingaon, Assam
Red soil	RS	Hill slopes, IIT Guwahati, Assam
Fly ash	FA	NTPC, Farakka, West Bengal, India
Commercial WAP	Com-WAP	SargaGreen, Kerala, India

TH-2777_166104034

3.3 Characterization of the used soils

The basic geotechnical characterization of soils used in this study was performed following the guidelines reported in ASTM international code in Table 3.2. The specific gravity was determined using the small density bottle or pycnometer. The hygroscopic water content of soils was determined by the standard oven drying method. The consistency limits (i.e., liquid, plastic limit, and plasticity index) of the soil samples were evaluated in the laboratory by the Casagrande method. The grain size distribution was obtained based on dry, wet sieve, and hydrometer analyses. Based on these above characterizations, the soil samples were classified according to the unified soil classification system (USCS) and the United States Department of Agriculture (USDA). The pH value and cation exchange capacity (CEC) of the used soils were also determined for the chemical characterization of each soil. Each of the tests was repeated at least thrice and the average results obtained from these tests are shown in Table 3.3. The mineralogical composition of the selected soils was obtained using the X-Ray diffraction (XRD) technique. The XRD spectrums of the soil samples were determined by the X-Ray Diffractometer (Company: Rigaku, Model No: TTRAX III). The selected range of 2θ was 5° to 70° with a scanning speed of 2°/min. For the identification of minerals, X'pert HighScore Plus software was used and reported in Table 3.3.

Table 3.2 Details of the references used for basic characterization of the soils

Geotechnical properties	References
Specific gravity	ASTM D854 (2014a)
Hygroscopic water content	ASTM D4959 (2016a)
Free swell index	ASTM D4546 (2014b)
Grain size distribution	ASTM D422-63 (2007)
Liquid limit and plastic limit	ASTM D4318 (2017b)
Shrinkage limit	ASTM D427 (2004)
USCS classification	ASTM D2487 (2017a)
USDA classification	USDA (2010)
pH value	ASTM D4972 (2019a)
Cation exchange capacity	ASTM D7503 (2018)

TH-2777_166104034

Table 3.3 Basic geotechnical properties of the used soils

Physical Properties			Soils		
			FS	BS	RS
Specific Gravity (G_s)			2.65	2.73	2.69
Grain Size Distribution (%)		Gravel (> 4.75 mm)	0	0	0
		Coarse sand (2 mm – 4.75 mm)	14	0	0
		Medium sand (0.425 mm – 2 mm)	40	0	6
		Fine sand (0.075 mm – 0.425 mm)	46	32	19
		Silt (0.002 mm – 0.075 mm)	0	58	47
		Clay (< 0.002 mm)	0	10	28
Atterberg Limits (%)		Liquid limit (LL)	NA	31	40
		Plastic limit (PL)	NA	21	19
		Shrinkage limit (SL)	NA	22	21
Plasticity Index (PI) [%]			NA	10	21
USCS Classification			SP	CL	CL
USDA Classification			Sand	Silt Loam	Clay Loam
Free swell index (%)			NA	NA	12
pH value (L/S=10)			NA	7.9	6.4
Cation exchange capacity (meq/100g)			NA	3	10
Minerals present			Quartz	Quartz, Calcite	Quartz, Hematite

*NA = Not Applicable/Negligible

The elemental compositions of the selected soils were obtained from the energy dispersive X-ray (EDX) analysis. Prior to EDX analysis, soil samples were mounted on aluminum stubs over double-sided carbon tape followed by double gold coating using a sputter coater (Quorum, SC7620, Quorum Technologies, Lewes, UK and Edwards, RV3, Czech Republic). The elemental compositions of the soil samples, as obtained from the EDX analysis, are presented in Fig. 3.1. From the EDX spectrum, it can be observed that Si/Al ratio is higher for coarse-grained soil (FS) and progressively reduces with the increasing finer content. The BS contains some amount of calcium (Ca), which is also reflected in the XRD analysis in the form of calcite. A high percentage of iron (Fe) and aluminum (Al) can be seen in RS, which typical characteristics of laterite soils.

TH-2777_166104034

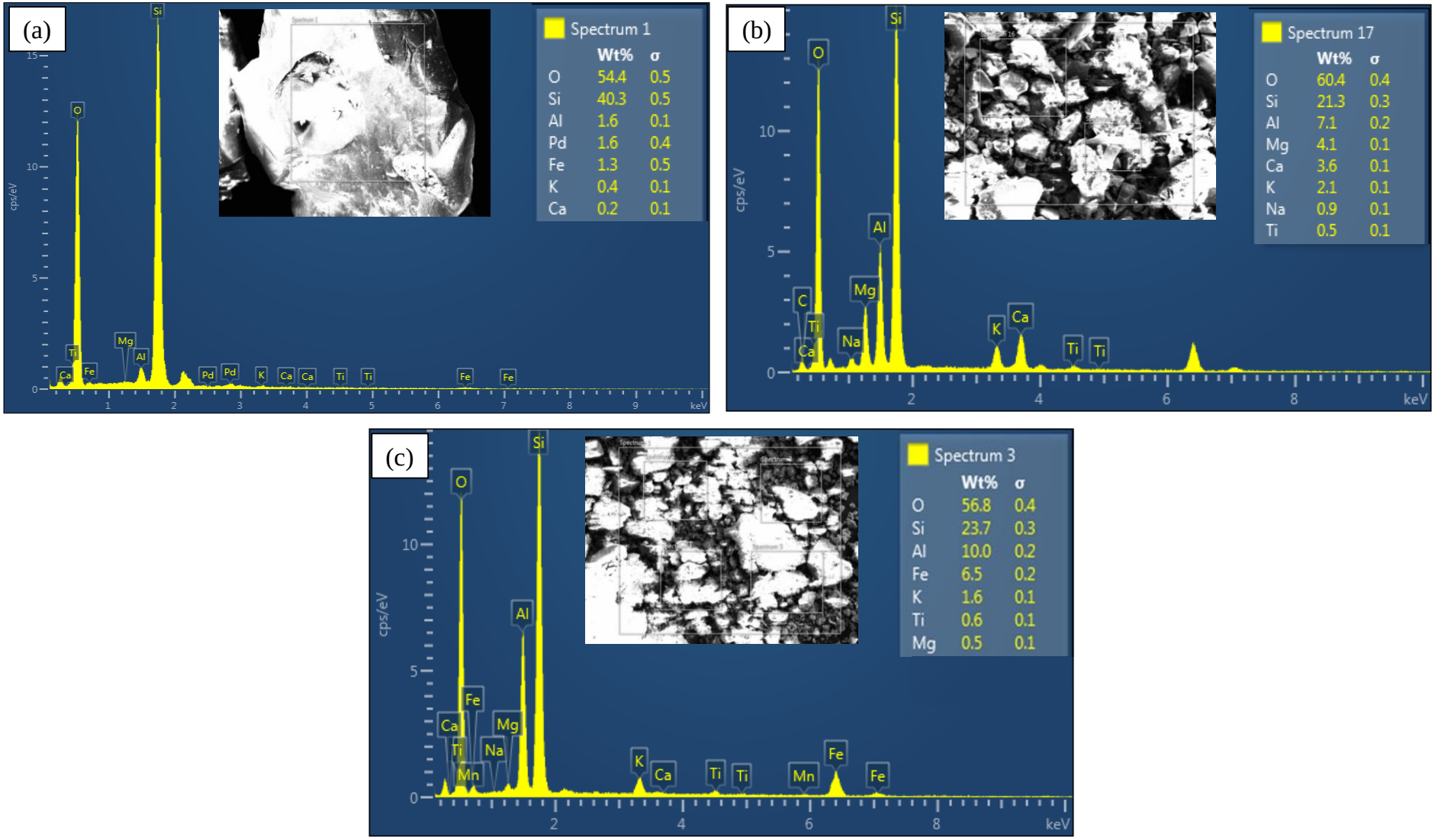

Fig. 3.1 Elemental compositions (EDX analysis) of (a) fine sand (FS), (b) Brahmaputra silt (BS), and (c) Red soil (RS)

TH-2777_166104034

3.4 Characterization of the used FA

The used FA was characterized for its basic physical properties, including specific gravity (G_s), grain size distribution, mineralogical composition, cation exchange capacity (CEC), and reported in Table 3.4. The chemical oxide composition of the FA was determined using X-ray Fluorescence (XRF) test (AXIOS, PANalytical, Netherlands), and the results are shown in Table 3.5. The classification of FA was made based on the oxide composition (SiO_2+ Al_2O_3+ Fe_2O_3), as recommended by ASTM C618 (2019b), which indicated that the used FA belongs to class F type.

Table 3.4 Basic physical properties of the used FA

Physical properties		FA
Specific Gravity (G_s)		2.02
Grain Size Distribution (%)	Gravel (> 4.75 mm)	0
	Coarse sand (2 mm – 4.75 mm)	0
	Medium sand (0.425 mm – 2 mm)	0
	Fine sand (0.075 mm – 0.425 mm)	24
	Silt (0.002 mm – 0.075 mm)	74
	Clay (< 0.002 mm)	2
pH (L/S=10)		10.9
Cation exchange capacity (meq/100g)		2
Minerals present		Mullite, Quartz, Hematite

3.5 Characterization of Commercial WAP

The selected commercial WAP (com-WAP) [Fig. 3.2(a) and (b)] was characterized for its basic functional groups, surface morphology, elemental compositions. The functional groups of the WAP surface were characterized by Fourier transform infrared (FTIR) spectroscopy, operated in a range from 4000 cm^{-1} to 450 cm^{-1}. The dry WAP particles were mixed with potassium bromide powder (KBr, optical grade) and pressed into a small slice for the measurement of the FTIR spectrum. It can be observed from Fig. 3.2(c), the broad peak observed at 3427 cm^{-1} is due to intermolecular and intramolecular hydroxyl stretching vibration. The characteristic peaks at 1410 cm^{-1}, 1170 cm^{-1} were due to the existence of carboxylate (COO^-) groups. The absorption band at 2935 cm^{-1} was assigned to the alkyl C–H stretching, whereas the absorption peak at 1580 cm^{-1} was assigned to the bending vibration of

TH-2777_166104034

hydroxyl groups. Presence of these hydrophilic groups (hydroxyl, carboxyl) is suggestive of high water absorbency of the used com-WAP.

Table 3.5 Chemical composition of the used FA

Oxide	**FA**
SiO_2	46.5
Al_2O_3	27.5
Fe_2O_3	1.0
MnO	2.9
MgO	0.1
CaO	2.8
Na_2O	0.6
K_2O	0.8
TiO_2	6.6
P_2O_5	5.2
$SiO_2+Al_2O_3+Fe_2O_3$	75
LOI	6
Classification (ASTM C618, 2019b)	Class F

The surface morphology of the dry WAP was analyzed using a field emission scanning electron microscope (FESEM) at two different magnifications and presented in Fig. 3.2(d) and (e). It can be observed from the figure that the surface morphology of WAP displayed loose and porous surfaces with a considerable number of cavities. Such a surface morphology is indicative of water-absorbing site, which permits water molecules to penetrate into the polymeric network.

The elemental composition (as obtained from the EDX analysis) of the used WAP was presented in Fig. 3.3, which showed major elements are C, O, and K. The presence of potassium (K) confirms that the used WAP is a partially neutralized potassium acrylate compound. The dry com-WAP particles consist of several (–COOH) groups and (-COOK) groups (ref. Fig. 3.4), creating an anion-anion electronic repulsion within their polymeric network. On contact with water, a significant osmotic pressure difference between the polymer network and water

TH-2777_166104034

is developed due to which water molecules penetrate into the polymer network (Zhang et al. 2014).

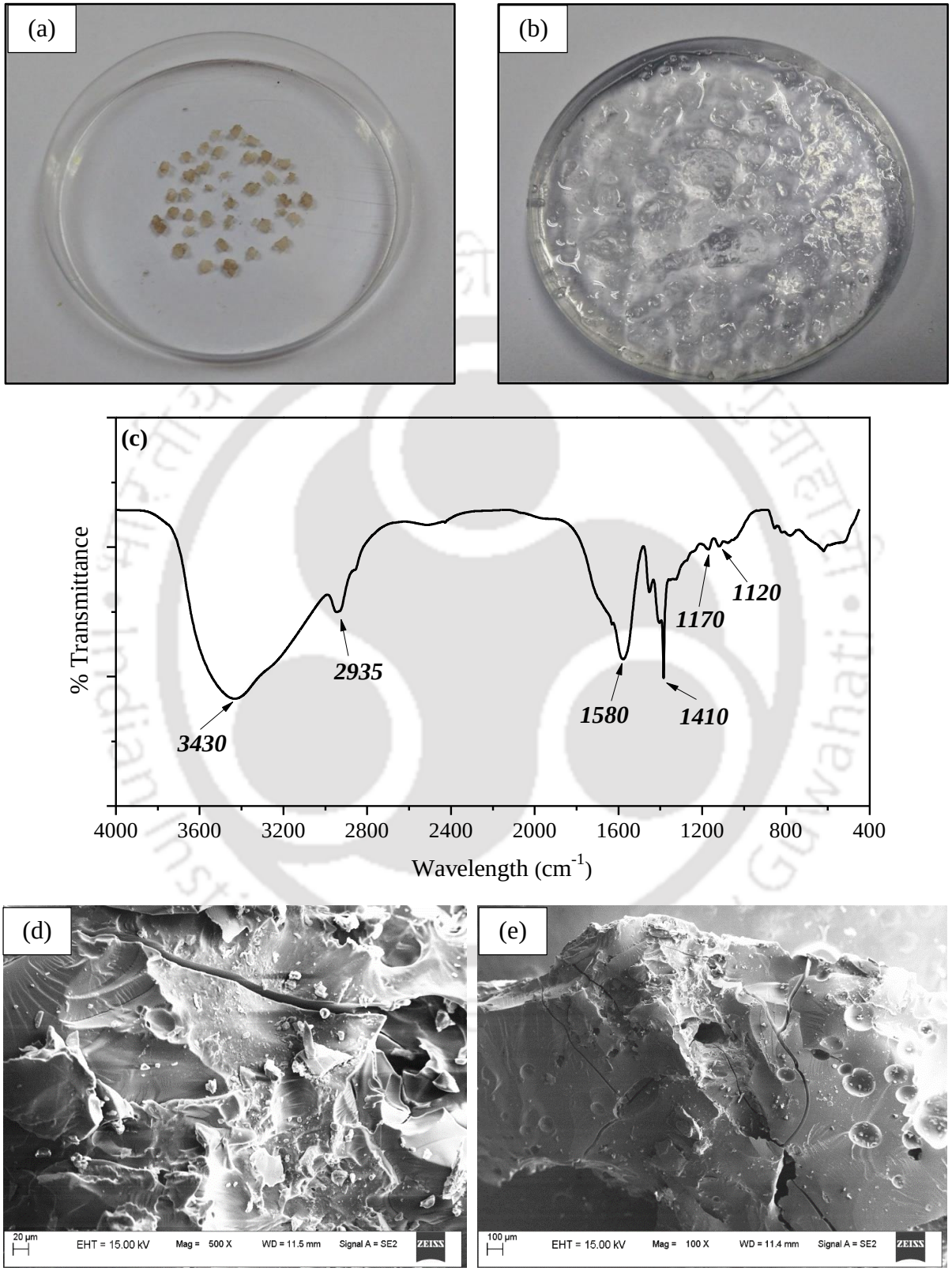

Fig. 3.2 Commercial WAP at (a) dry state, (b) swollen state, (c) FTIR spectrum, and surface morphology at (d) 500X and (e) 100X magnification.

TH-2777_166104034

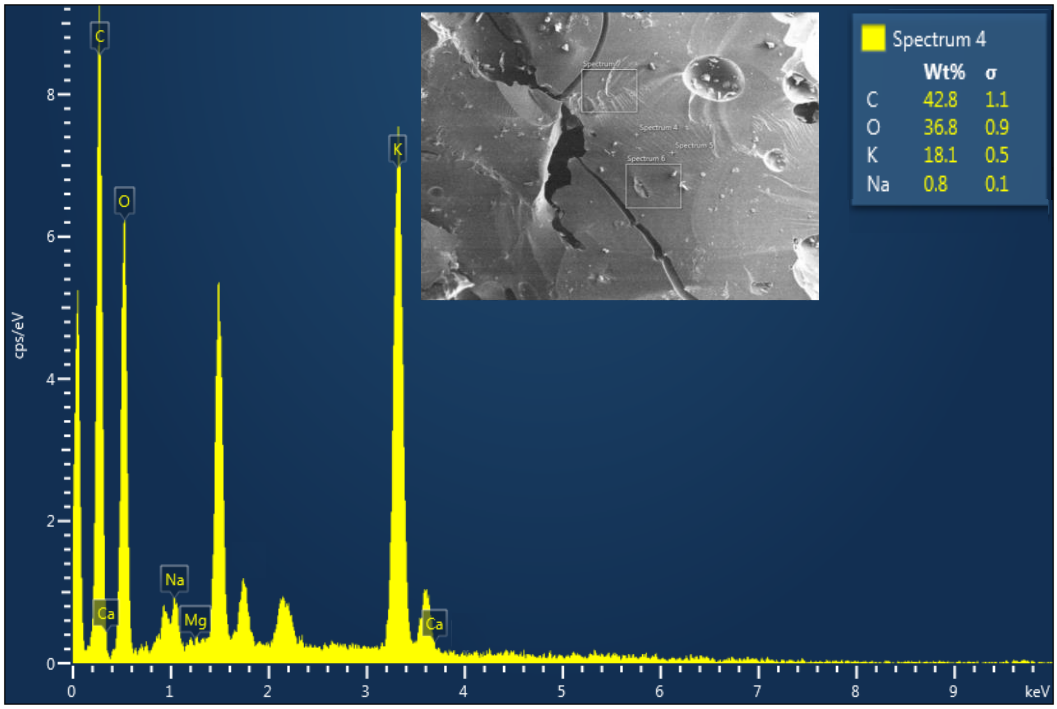

Fig. 3.3 Elemental composition (EDX spectrum) of the used WAP

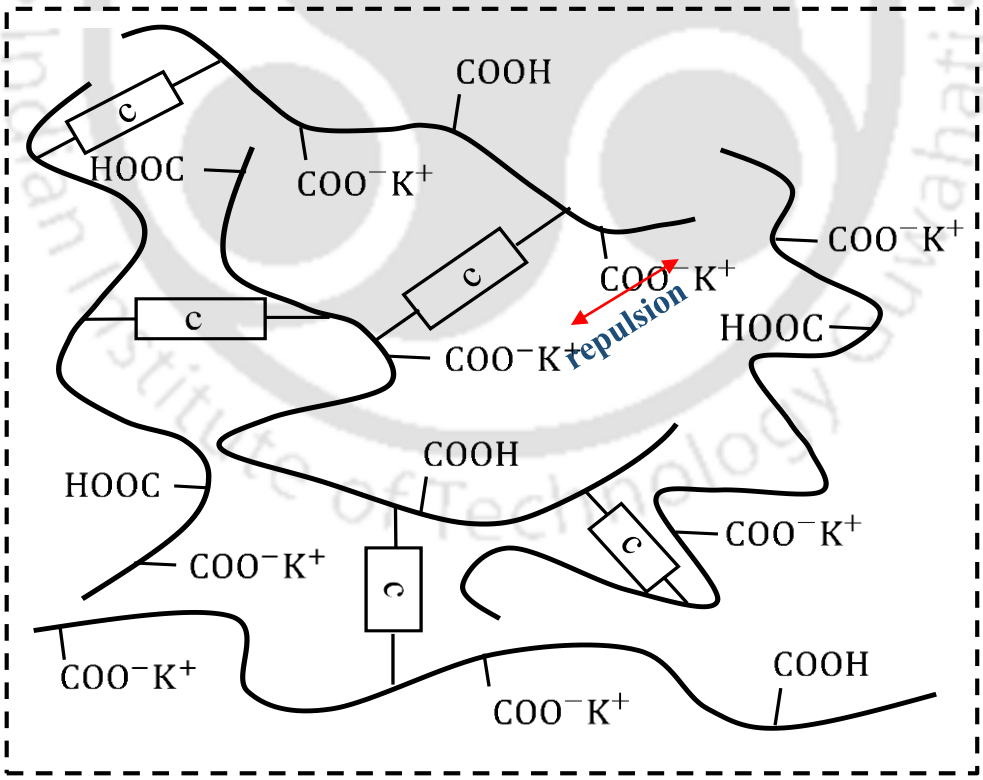

Fig. 3.4 Chemical Structure of the used WAP

TH-2777_166104034

3.6 Measurement of soil suction

The unsaturated soil is a three-phase system consisting of air, water, and soil particles. The interaction of solid, water, and air phase develops a complex energy state resulting in negative pore water potential known as soil suction. Soil suction is defined as the amount of energy required to expel a unit volume of water from the soil matrix (Lee and Wray 1996). It represents how tightly the soil holds the pore water or how easily the water can be expelled out from the soil. The higher the value of suction, the higher will be the energy required to extract water from the soil matrix. The suction is expressed in kPa, atm, pF, cm, or m in terms of the head. The unit pF is defined as the logarithm of negative pore water potential (head) in centimeters of water (Fredlund and Rahardjo 1993).

The major component of suction is matric suction (designated as ψ_m), which results from the combined effect of capillary and adsorptive forces that exist in the soil matrix. Osmotic suction (designated as ψ_o) results from the presence of dissolved solutes in soil-water. The sum of these two suction components is termed total suction (ψ). It has been proven that when there is no salt or impurity present in the soil, the total suction is equal to the matric suction (Sreedeep and Singh 2006). Total suction can be theoretically obtained using Kelvin's equation (Eq. 2.1).

There are a large number of instruments available for measurement of suction, but none of them alone can measure the soil suction for the entire measurable range for a geomaterial (i.e., saturated state to air dry state). Measurement of suction is mainly divided into direct and indirect methods for matric and total suction measurements. The ψ_m is obtained by measuring the pore water pressure (u_w). The pore air pressure (u_a) is equal to the atmospheric pressure at the site, and matric suction is the difference between the pore air pressure and pore water pressure ($\psi_m = u_a - u_w$). The direct measurement of ψ_m requires a separation between the water and air phase by means of a ceramic disk or a ceramic cup. The maximum value of matric suction that can be measured is limited by the air entry value (AEV) of the ceramic disk or the ceramic cup used. The commonly used instruments for direct suction measurement are the pressure plate apparatus, tensiometer, and hanging column method [ASTM D6836 (2016b)]. Indirect methods do not measure the pore water pressure directly. Rather they measure the soil properties such as the vapor pressure, moisture content, resistivity of the soil, thermal conductivity, or electrical conductivity of the porous medium and correlate it with soil suction with the help of calibration equation (Bulut and Leong 2008; Pan et al. 2010). Some of the instruments used for indirect measurement of suction are time domain reflectometry (TDR),

TH-2777_166104034

electrical conductivity sensor, thermal conductivity sensor, contact filter paper technique for matric suction, pore fluid squeezer for osmotic suction, psychrometer, relative humidity sensor, chilled mirror hygrometer, non-contact filter paper method for measurement of total suction. The indirect method can measure up to a very high range of suction, but its accuracy largely depends on the reliability of the calibration procedure and equation.

3.6.1 T5 tensiometer

A miniature tensiometer (T5), as depicted in Fig. 3.5(a), has been used to measure matric suction up to 85 kPa. The technical specifications of the used sensor, as reported in the operator's manual, are listed in Table 3.6. As shown in Fig. 3.5(a), the tensiometer can be divided into three important parts, tensiometer body, shaft, and ceramic cup. The tensiometer body consists of a pressure transducer that is capable of continuously measuring the vacuum pressure or negative pressure created in the shaft during ψ_m measurement. This pressure transducer consists of a plastic body with a thin silicon chip semiconductor that is capable of capturing the vacuum or negative pressure created in the shaft. The tensiometer body is threaded to a transparent acrylic shaft, which is filled with distilled water free from air bubbles. The other end of the shaft is connected to a tensiometer ceramic cup. This ceramic cup acts as an interface between soil and the shaft and maintains continuity of water through its pores.

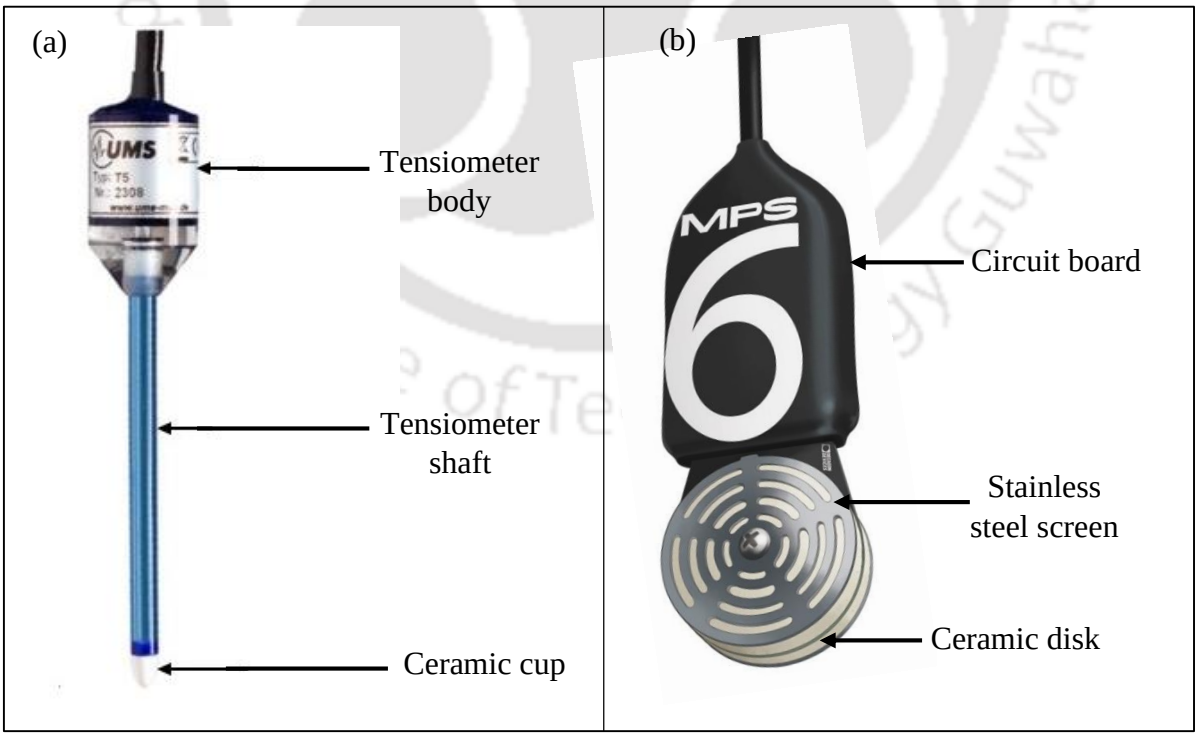

Fig. 3.5 Details of (a) T5 tensiometer and (b) capacitance sensor (TEROS21)

TH-2777_166104034

Table 3.6 Technical specifications of T5 tensiometer

Measurement	Matric potential (ψ_m)
Measurement range	(ψ_m): +100 kPa to -85 kPa
Accuracy	(ψ_m): ±0.5 kPa
Resolution	(ψ_m): 0.1 kPa
Operative temperature	4° C to 70° C
Equilibrium time	10 seconds
pH range	pH 3 to pH 10
Compatible data logger	DL6 Data logger

When the tensiometer is inserted into soil for ψ_m measurement, the water present in the shaft tries to equilibrate with the suction present in the soil-water via the ceramic interface. For an efficient equilibrium, the continuity of water between the shaft and soil-water becomes extremely important. The continuity ensures that the negative pressure of soil-water will be identical with the water tension developed in the shaft. The changes in water tension in the shaft water result in the deformation of the silicon chip. The silicon chip is thin and therefore extremely sensitive to such pressure (water tension) variations. The strain or deformation of the silicon chip induces a change in its specific electric resistance, which is converted to a defined voltage signal via a Wheatstone bridge (T5 User Manual, UMS 2001). The changes in water tension in the shaft are captured electronically and converted to pressure units in hectopascal (hPa) by a calibration procedure. A proper contact must be ensured between the soil mass and the tensiometer ceramic cup for the proper functioning of tensiometer.

3.6.2 Capacitance sensor (TEROS21)

A dielectric matric potential sensor, TEROS21 (METER Group, USA), as depicted in Fig 3.5(b) was used in the present study to measure the suction of the WAP amended soils. The technical specifications of the sensor are listed in Table 3.7. The sensor consists of two ceramic disks sandwiched between two stainless steel screens and a circuit board. When the TEROS21 is inserted into the sample, the water present in the sample tries to equilibrate with the two-ceramic disk. Therefore, at equilibrium, the water potential of the ceramic disk will be equal to the potential of the soil sample. The sensor circuit board comprises an oscillator that generates an electromagnetic (EM) field during ψ_m measurement. The EM field charges the ceramic disks around the sensor circuit board. This stored charge is proportional to dielectric permittivity, ε of the ceramic disks, and measure the water content of the ceramic disk. The matric suction

TH-2777_166104034

was found out from the previously establish the suction-water content relationship of the ceramic disk.

Table 3.7 Technical specifications of TEROS21

Measurement	Matric potential (ψ_m), Soil temperature
Measurement range	(ψ_m): -9 to -100,000 kPa, Soil temperature: -40° C to 60° C
Accuracy	(ψ_m): ± (10% of reading) from -9 to -100 kPa
	Soil temperature: ± 1° C
Resolution	Matric Potential: 0.1 kPa, Soil temperature: 0.1° C
Operative environment	-40° C to 60° C
Measurement speed	150 ms (millisecond)
Equilibrium time	10 min to 1 hour depending on matric potential
Sensor type	Frequency domain with calibrated ceramic discs, thermistor
Compatible data logger	Em50 Data logger

3.6.3 Dew point potentiameter (WP4)

A dew point potentiameter (model WP4C, METER Group, Inc., USA), as shown in Fig 3.6, has been used to measure the total suction (ψ) of the soil samples. This instrument works on the principle of chilled mirror dew point technique and estimates the relative humidity of the sample. The device consists of a sealed chamber with a cooling fan, a mirror, a photoelectric cell, and an infrared thermometer. The soil sample is placed in a plastic or stainless-steel container with a diameter of 40 cm. The container is then placed in the tray and moved into the temperature-controlled chamber. There the sample specimen gets equilibrated with the chamber environment. A peltier cooling system is used to reduce the temperature on the surface of the mirror to the dew point temperature. The photoelectric cell detects the first sign of condensation on the mirror, and the temperature at which the moisture appears at the mirror corresponds to the dew point. The temperature of the mirror at that point is measured by a thermocouple. The infrared thermometer measures the temperature of the chamber, which is equal to the temperature of the sample at equilibrium condition. The vapour pressure above the soil specimen in the chamber and the saturated vapour pressure at the same temperature are computed using the dew point temperature and the sample temperature. The total suction of the sample is then calculated by Kelvin's equation, as shown in Eq. 3.1 (Fredlund and Rahardjo 1993). This whole calculation part is performed by the device, and the suction value is displayed on the LED panel along with the temperature of the sample. A

TH-2777_166104034

cooling fan is used to circulate the air and reduce the equilibration time, which is approximately 5 to 10 minutes. The main limitation of this instrument is its inaccuracy in suction measurement in the lower suction range (below 1 MPa), and a small change in temperature can affect the suction value in that range (Fredlund and Rahardjo 1993). The detailed technical specifications of the instrument are listed in Table 3.8.

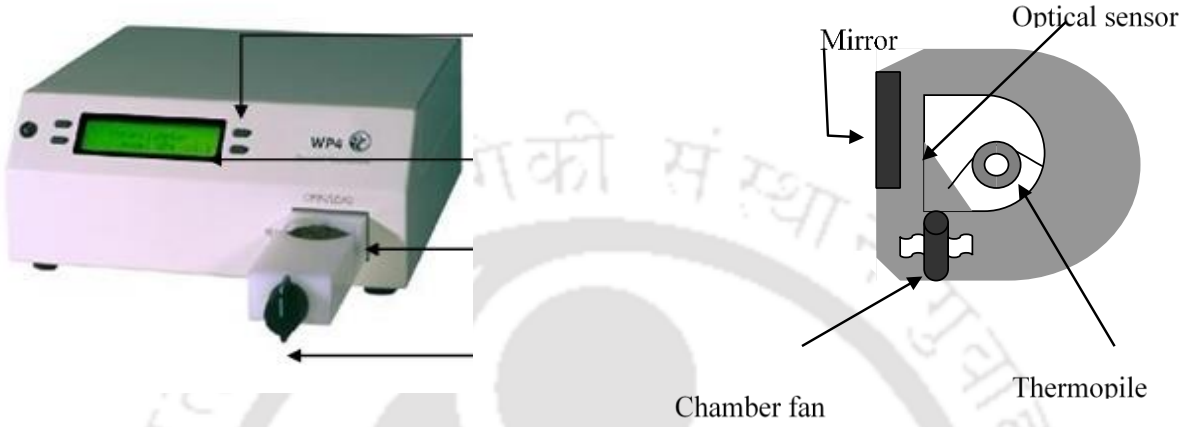

Fig. 3.6 Details of (a) WP4C and (b) block chamber

Table 3.8 Technical specifications of WP4C

Measurement	Total suction (ψ), Soil temperature (T)
Measurement range	(ψ): -0.1 to -300 MPa, Soil temperature: 15° C to 60° C
Accuracy	(ψ): ± 0.05 MPa from -0.1 MPa to -5 kPa, ± 1% from -5 MPa to -300 kPa Soil temperature: ± 0.2°C
Resolution	Matric Potential: 0.01 MPa, Soil temperature: 0.1°C
Measurement speed	10-15 minutes (Precise mode) < 5 minutes (fast mode)
Operative environment	5° C to 40° C
Sensor type	Chilled-mirror dew point sensor, Infrared temperature sensor
Sample cup capacity	15 mL (full); 7 mL (recommended)

3.7 Measurement of soil moisture content

Measurement of soil moisture content is vital for establishing the relationship with the soil suction. In this study, a volumetric water content (θ) measurement sensor, namely ECH$_2$O 5TM (developed and supplied by METER Group, Inc., USA), as shown in Fig 3.7, was used.

TH-2777_166104034

The technical specifications of the sensor are listed in Table 3.9. The 5TM determines θ by measuring the dielectric constant of the soil (or other porous media) using capacitance/frequency domain technology. This robust sensor can be pushed directly into undisturbed soil to ensure good accuracy. The 5TM is installed and plugged into the Em50 data logger.

The basic principle behind the working of the sensors is that the dielectric constant of the soil medium changes with its water content. Dielectric permittivity (ε_a) is dependent on the capacitance property of the soil mass. For highly saturated and dry soil mass, the value of ε_a would vary between 80 and 4. This broad range of permittivity helps in measuring θ of the soil from saturated to dry state condition. The sensor is equipped with an oscillator working at a frequency of 70 MHz, which generates an electromagnetic field. The electromagnetic field charges the soil around the probe. This stored charge is proportional to permittivity and θ, and is measured by the copper traces of the prongs. The 5TM microprocessor outputs a value of dielectric permittivity from the sensor. The dielectric permittivity was converted to the VWC by Topp's equation. A zone of influence of 50 mm from the edge of the probe surface is reported in the manual for this stored charge.

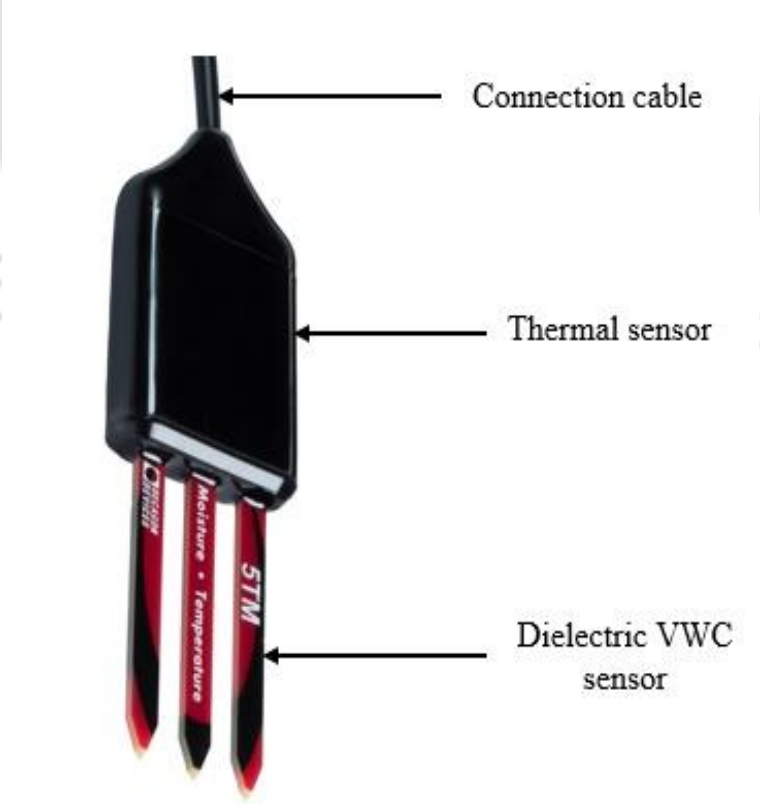

Fig. 3.7 Details of 5TM sensor

TH-2777_166104034

Table 3.9 Technical specifications of ECH$_2$O 5TM

Measurement	Volumetric water content (θ), dielectric constant (ε_a), and temperature (T)
Measurement range	θ: 0 to 1 m^3/m^3; ε_a: 1 (air) to 80 (water); T: –40 °C to 60 °C
Accuracy	θ: ± 3% (mineral soils that have solution electrical conductivity < 10 dS/m). ε_a: ± 1 (1 – 40) and ± 15% (40 – 80); Soil temperature: ± 1°C
Resolution	ε_a: 0.1 (1 – 20), < 0.75 (20 – 80); θ: 0.08% (from 0 to 50% VWC); T: 0.1°C
Operative environment	-40°C to 60°C
Measurement speed	150 ms (millisecond)
Compatible data logger	Em50 Data logger

TH-2777_166104034

Chapter 4

Transformation of fly ash to water absorbing polymer

4.1 General

This chapter presents the detailed methodology and the reagents used for the transformation of fly ash (FA) to water absorbing polymer (WAP). Basic characterization of the synthesized polymer. Previous researchers have used different waste materials, such as yeast, starch, cellulose, chitosan, paper-industry waste, for the preparation of WAP. This study demonstrated a method to synthesize an eco-friendly fly ash-based water absorbing polymer (FA-WAP) by grafting the polyacrylic acid (PAA) onto the surface of FA in the presence of a crosslinker, N, N′-methylene-bisacrylamide (MBA). The proposed mechanism for chemically grafting and crosslinking the PAA on the FA surface was also presented in detail. Further, the performance of the synthesized WAP was compared with the commercial WAP to check its effectiveness for drought management.

4.2 Methodology

4.2.1 Used reagents

Acrylic acid (AA) [purity 99 %], and N, N′- methylene-bisacrylamide (MBA) [purity 99.5 %] was purchased from Sigma Aldrich, Bangalore, India. Ammonium persulfate (APS) [purity 98 %] and sodium hydroxide (NaOH) [Purity 98 %] were procured from Merck Specialties Private Limited, India. All the procured reagents were of analytical grade and used without further refinement. Distilled water was used to prepare all the stock solutions throughout this work.

4.2.2 Preparation of FA-WAP

A series of FA-WAP samples were prepared by considering different combinations of various amounts of FA (backbone material), N, N′- methylene-bisacrylamide (MBA) (crosslinker), ammonium persulfate (APS) (initiator), and AA (monomer) with different neutralization degree (neutralized with NaOH). Every combination was repeated thrice to ensure repeatability of test results. A total of 360 numbers of combinations (including repetitions) were performed for the synthesis of FA-WAP. Out of these, the most important combinations (i.e., 24 numbers) are listed in Table 4.1, which was further used to optimize the reagent quantities for achieving maximum WAC. For optimizing the reagent content, only one reagent amount was varied at a time while others were kept constant. It may be noted that the

TH-2777_166104034

monomer content was kept constant at 8 g, and the polymerization reaction temperature was chosen as 70 ℃ throughout this study based on the literature (Bao et al. 2011).

Table 4.1 Important combinations of reagent quantity for the preparation of FA-WAP

Trial No.	Monomer (AA)	Cross-linker (MBA)		FA		Initiator (APS)		Neutralization degree	Water
	(g)	(mg)	(%)	(g)	(%)	(mg)	(%)	(%)	(g)
Optimization of FA content									
1	8	40	0.5	0	0	120	1.5	60	50
2	8	40	0.5	0.5	6.3	120	1.5	60	50
3	8	40	0.5	1	12.5	120	1.5	60	50
4	8	40	0.5	1.5	18.8	120	1.5	60	50
5	8	40	0.5	2	25	120	1.5	60	50
Optimization of Cross-linker									
6	8	40	0.5	1	12.5	120	1.5	60	50
7	8	80	1	1	12.5	120	1.5	60	50
8	8	120	1.5	1	12.5	120	1.5	60	50
9	8	160	2	1	12.5	120	1.5	60	50
Optimization of Initiator									
10	8	40	0.5	1	12.5	72	0.9	60	50
11	8	40	0.5	1	12.5	96	1.2	60	50
12	8	40	0.5	1	12.5	120	1.5	60	50
13	8	40	0.5	1	12.5	144	1.8	60	50
14	8	40	0.5	1	12.5	168	2.1	60	50
Optimization of neutralization degree									
15	8	40	0.5	1	12.5	120	1.5	40	50
16	8	40	0.5	1	12.5	120	1.5	50	50
17	8	40	0.5	1	12.5	120	1.5	60	50
18	8	40	0.5	1	12.5	120	1.5	70	50
19	8	40	0.5	1	12.5	120	1.5	80	50
Optimization of water added									
20	8	40	0.5	1	12.5	120	1.5	40	20
21	8	40	0.5	1	12.5	120	1.5	50	30
22	8	40	0.5	1	12.5	120	1.5	60	40
23	8	40	0.5	1	12.5	120	1.5	70	50
24	8	40	0.5	1	12.5	120	1.5	80	60

TH-2777_166104034

To begin with the synthesis, a certain amount of partially neutralized AA monomer was dissolved in 30 mL of distilled water in a 250 mL three-neck flask equipped with a reflux condenser, thermometer, mechanical stirrer, and nitrogen line, as shown in Fig. 4.1. FA powder was then added to the aforementioned partially neutralized monomer solution, and the flask was connected to a nitrogen cylinder for 30 min to remove the dissolved oxygen from the solvent. Thereafter, under the nitrogen environment, a certain amount of MBA, initiator APS, and 20 mL of distilled water was added to the mixture with effective stirring. The mixture was slowly heated in an oil bath at 70° C for 2 h to complete the polymerization reaction. Subsequently, the resultant product was dried at 80° C to a constant weight in an oven. The dried product was washed several times with distilled water and ethanol to remove the unreacted reagent. Finally, the obtained FA-WAP was dried at 80° C and milled to particle size in the range of 10-50 mesh (0.3-2 mm). A flow chart was presented in Fig. 4.2 to describe the synthesis process for the FA-WAP production. A control sample without the FA was also prepared following the same process as described above, designated as polyacrylic acid (PAA).

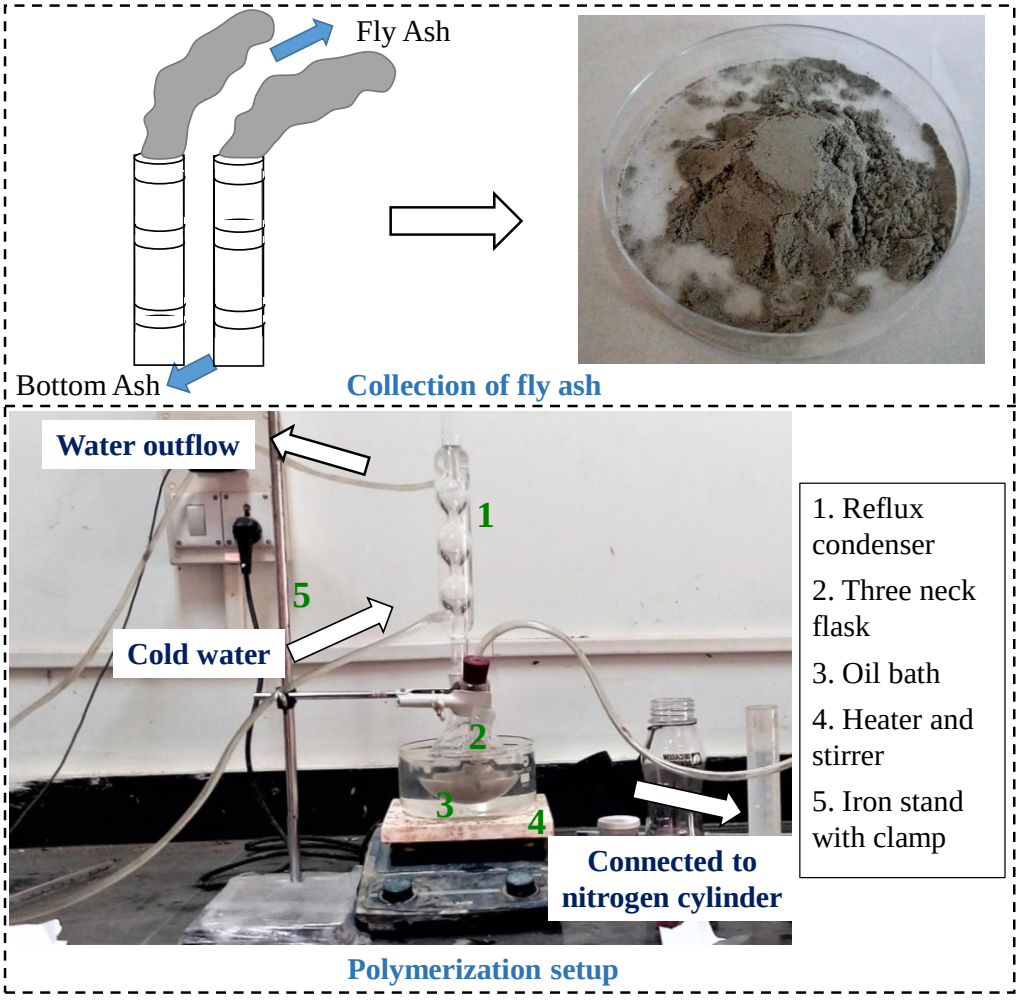

Fig. 4.1 Collection of FA and polymerization setup for the preparation of FA-WAP

TH-2777_166104034

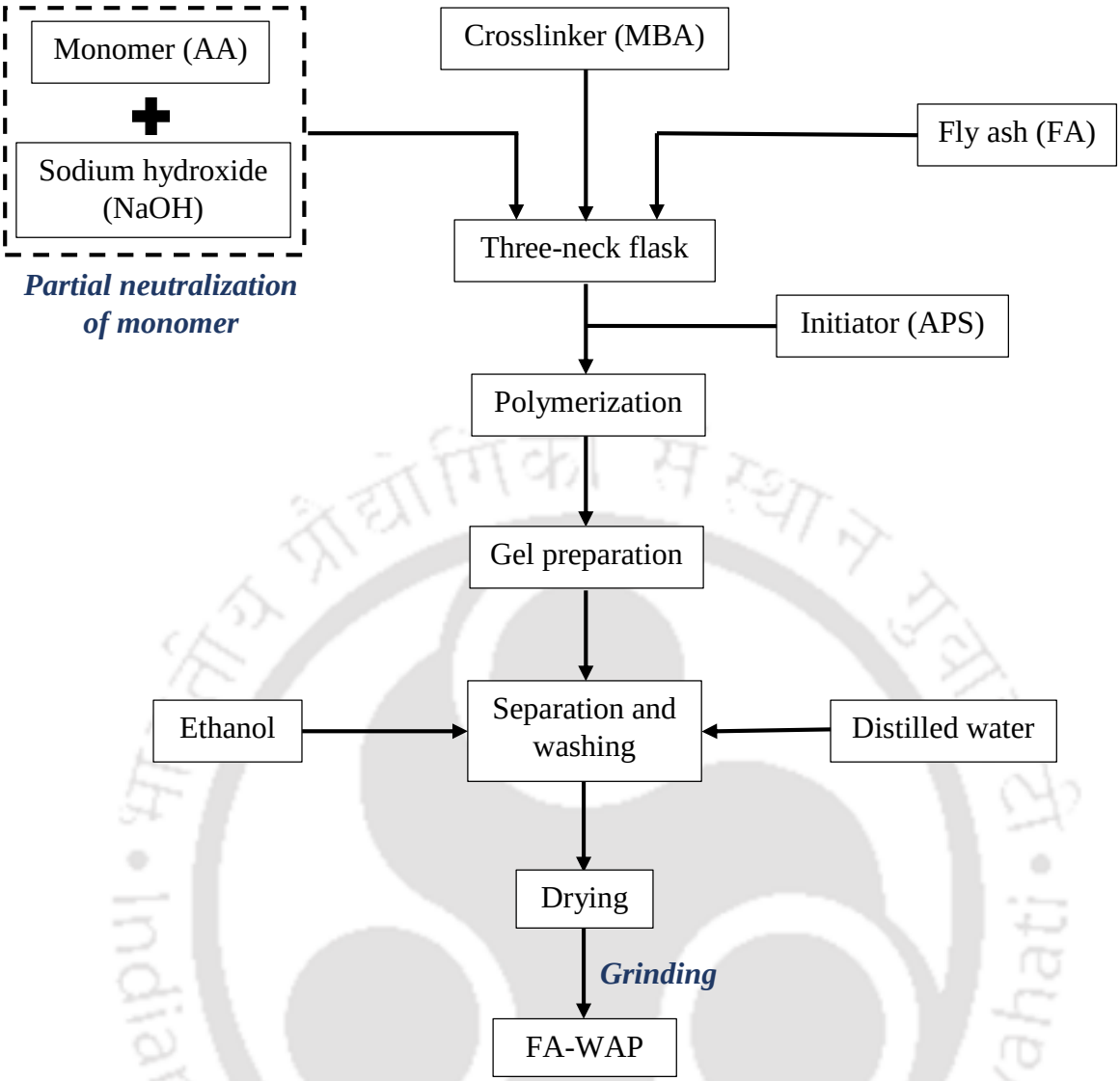

Fig. 4.2 Synthesis scheme of FA-WAP production process

4.2.3 Characterization of FA-WAP

The functional groups of FA, PAA, and FA-WAP were characterized using a Perkin-Elmer FTIR operated in a range from 4000 cm^{-1} to 450 cm^{-1}. For this purpose, the dried sample was mixed with dried potassium bromide (KBr, optical grade) powder and pressed into small slices for further measurement of the spectrum.

The mineralogy of the parent and final products were determined by the X-Ray Diffractometer (Company: Rigaku, Model No: TTRAX III). The selected range of 2θ was 5° to 70° with a scanning speed of 2°/min.

The surface morphology of FA, PAA, and FA-WAP was obtained using a field emission scanning electron microscope (FESEM) (Zeiss Sigma, Oberkochen, Germany). For

TH-2777_166104034

FESEM analysis, the samples were mounted on aluminum stubs coated with double-sided carbon tape.

The Brunauer–Emmett–Teller (BET) surface area of FA and FA-WAP was determined by N_2 adsorption-desorption isotherm. Prior to the analysis, 0.5 g of sample was degassed at 130 ℃ for 4 h, followed by N_2 adsorption at 77K.

The zeta potential and dynamic light scattering (DLS) analysis of FA, FA-WAP was carried out using Zetasizer Nano ZS90 (model no. ZEN3690). The samples were added to distilled water at a temperature of 25 ℃ prior to the measurement. Three identical samples were prepared, and the mean value, along with the standard deviation, was considered and reported.

4.2.4 Measurement of swelling characteristics

The swelling characteristics of FA-WAP include swelling kinetics, water absorbing capacity (WAC), and re-swelling capability under alternate wetting-drying. These characteristics are mandatory for establishing the efficacy of FA-WAP for drought management.

4.2.4.1 Swelling kinetics

Evaluation of swelling kinetics is important to understand the mechanism of the swelling process as well as the absorption rate and time to reach swelling equilibrium. To evaluate the swelling kinetics of the FA-WAP, 0.2 g of dry material was taken in a nylon teabag and immersed into 250 mL beaker with a sufficient amount of distilled and tap water (pH= 6.5; Electrical conductivity= 0.11 mS/cm). The teabag was lifted from the water at predetermined time intervals and drained for 2 minutes. Thereafter, the sample was weighed, and the water absorbency with time was calculated by Equation (4.1) after deducting the weight of the teabag. A highly sensitive high precision microbalance (readability = 0.1 mg) was used for weighing the samples. The procedure was repeated until the water absorbency reached the equilibrium swelling.

$$Q_t = \frac{W_{wet(t)} - W_{dry}}{W_{dry}} \qquad 4.1$$

Here, Q_t (g/g) is the water absorbency at time t; $W_{wet(t)}$, and W_{dry} represent the water-swollen weight at time t, and dry weight of FA-WAP. The WAC was obtained from the

TH-2777_166104034

equilibrium swelling and reported as grams of water per gram of dry FA-WAP. For all the cases, three samples were used to ensure repeatability of the measured data.

4.2.4.2 Water absorbing capacity (WAC)

For cross-verification of water absorbing capacity (WAC) [or equilibrium water absorbency] of the WAP, a sufficient amount of solvent (distilled and tap water) was taken in a beaker, and weighed amount of dry WAP was added into it as shown in Fig. 4.3. The dry WAP particles were allowed to absorb water at ambient temperature until it reaches its maximum equilibrium swelling. Swollen samples were separated from the excess solution by filtering through a filter paper for 30 minutes and drained under gravity until no excess water remained in the swollen WAP. After draining out the free water, the swollen sample was weighed to calculate the amount of absorbed water, and the WAC (maximum swelling) was calculated by Eq. 4.1.

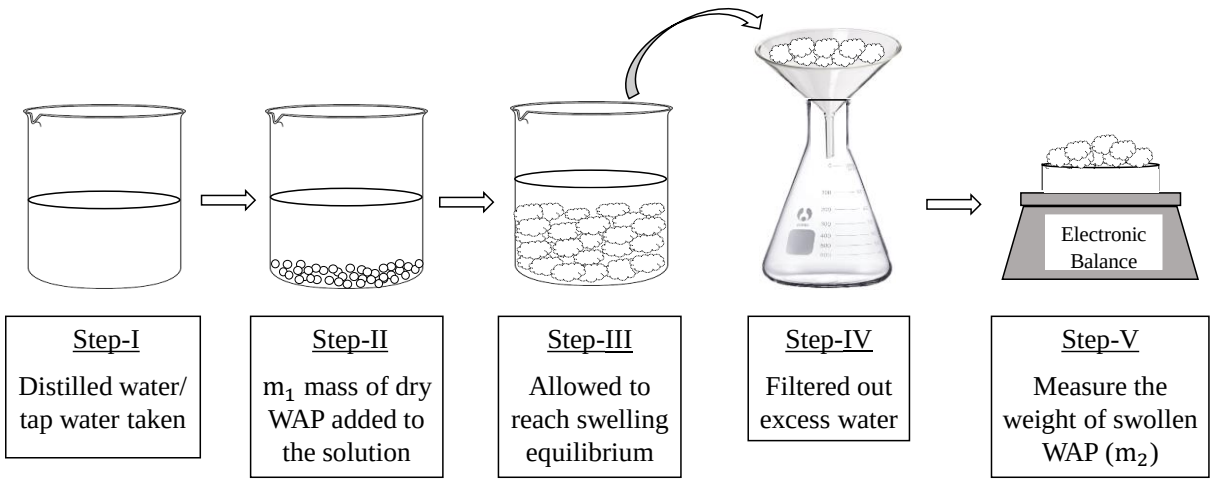

Fig. 4.3 Methodology adopted for the measurement of WAC

4.2.4.3 Drying characteristics at different temperature

Drying characteristics of the swollen WAPs (in terms of amount of retained as a function of time) were obtained by taking the swollen sample in a glass beaker and continuously dried in two conditions, including air drying at ambient temperature (average temperature= 25° C) and oven drying at a constant temperature of 50° C. The oven-drying method has been used in this study to simulate the actual drought conditions, where temperature can reach up to 45° C-50°C. The drying characteristic was obtained by measuring the weight of the sample after certain time intervals until the WAP was completely dried.

4.2.4.4 Re-swelling characteristics

TH-2777_166104034

Re-swelling characteristic is one of the most crucial factors determining the performance of FA-WAP for field applications. The re-swelling ability of the FA-WAP was investigated through multiple alternate wetting-drying cycles and measuring their WAC. For this purpose, a weighed amount of FA-WAP was added in 250 ml of the swelling medium at ambient temperature for 4 hrs to achieve complete saturation (based on swelling results). The swollen FA-WAP was filtered, and WAC was measured following a similar procedure, as discussed above. The swollen material was then dried in an oven at 80 °C until a constant weight was reached. Thereafter, the dried sample was again added in 250 ml of swelling medium for the next cycle of WAC measurement. The procedure was repeated for eight cycles of wetting-drying to obtain the re-swelling ability of the FA-WAP. These results are needed to assess the deterioration of FA-WAP in the field with time due to seasonal effects.

4.2.4.5 Salt sensitivity

To investigate the effect of salt concentration, a known quantity of dry FA-WAP was added to different concentrations of salt solution and allowed to swell until the equilibrium is reached. The WAC at the particular salt concentrations was calculated from Equation (1). The WAC of FA-WAP was evaluated in seven different inorganic salts including sodium chloride, potassium chloride, ammonium chloride, calcium chloride, sodium nitrate, sodium carbonate, and sodium sulfate at six different molar concentrations (0.01 M, 0.05 M, 0.1 M, 0.15 M, 0.2 M, and 0.3 M). The choice of the salts facilitated to compare the sensitivity of FA-WAP to various cations (Na^+, K^+, Ca^{2+}, NH_4^+) and anions (Cl^-, NO_3^-, CO_3^{2-}, SO_4^{2-}) specifically.

4.2.4.6 pH sensitivity

To verify the influence of pH, four different stock solutions, including HCl, H_2SO_4, NaOH, and CaO, having pH ranging between 2.0 to 12.0, were used. No additional ions were added through the buffer solution for setting the pH as the WAC is strongly affected by the ionic strength of the solution. The stock solutions were diluted with distilled water to reach the desired acidic and basic pH values. The main reason for using different valence stock solutions was to critically evaluate any effect of the composition of the stock solutions on WAC of FA-WAP. In each of the cases, WAC for a particular pH was calculated following the method discussed earlier.

4.2.5 Toxicity assessment of FA and FA-WAP

Past studies have reported that FA may contain different heavy metals and trace elements, including Zn, Cu, Pb, Mn, Fe, Ni, Cr, and Cd, depending on the source of the parent

TH-2777_166104034

coal (Yao et al. 2015; Pandey et al. 2009). Therefore, it is important to evaluate the toxicity characteristics of the parent FA as well as the synthesized FA-WAP before using it as soil amendment. The Toxicity Characteristic Leaching Procedure (TCLP), as proposed by United States Environmental Protection Agency (USEPA) in 1990 (method 1331), was adopted in the present study to determine the toxicity characteristics of FA and FA-WAP. The method is designed to determine the mobility of both organic and inorganic contaminants present in liquid, solid, and multiphasic wastes. There are two types of extraction fluids (Extraction fluid #1 and Extraction fluid #2), as described in TCLP, depending on the alkalinity of the waste material. Very high alkaline materials require a fixed quantity of glacial acetic acid (CH_3CH_2OOH) diluted with distilled water [Extraction fluid #2], whereas other waste materials require a fixed quantity of glacial acetic acid, distilled water, and sodium hydroxide (NaOH) [Extraction fluid #1]. According to USEPA TCLP method 1311, the solid phase is extracted with an amount of extraction fluid equal to 20 times the weight of the solid phase. Therefore, the liquid to solid ratio (L: S) was fixed at 1:20 during TCLP of FA. However, it was found that the FA-WAP forms a gel like consistency at L: S of 1:20 due to its higher water absorbency, and the TCLP of FA-WAP was conducted at a L: S of 1:200.

Measured quantities of FA and FA-WAP were added to the extraction fluid in a conical flask, as described in USEPA protocol. The mixture was then subjected to horizontal shaking at 30 rpm in an oscillating shaker for 18±2 h and 22±3 °C. After agitation on the shaker, the solution was centrifuged at 3000 rpm for 10 min to separate solids and liquid. The leachate was collected using a pipette and filtered through Whatman grade 42 filter paper by the vacuum filtration system. Element concentrations in the leachates were determined by using Perkin Elmer atomic absorption spectrometer (AAS). Further, toxicity assessment was performed for 0.4% FA-WAP amended soils (at L: S ratio of 1: 20) also to understand the leaching characteristics of different trace elements from the FA-WAP amended soils. Three identical samples were prepared for the measurement of different metal concentrations, and the average value was reported.

4.3 Observations and discussion

The FA-WAP is formed by graft polymerization of acrylic acid (AA) monomer on the surface of FA in the presence of crosslinker MBA and radical initiator APS. In the presence of FA, a large amount of AA monomer could be captured on the surface of FA due to hydrogen-bond interaction between the functional group present in FA and AA molecule. During heating at 70 °C, the initiator (i.e., APS) in the solution was decomposed to generate sulfate anion

TH-2777_166104034

radicals (SAR). Subsequently, SAR initiates the polymerization process by activating the monomer (AA). These active monomer radicals act as a free radical donor to the adjacent monomers, and thus, the propagation of the homo-polymer started. The SAR also creates a chemically active group in the FA, which acts as an active center for chain propagation. The polymer chain was captured on these active FA centers, leading to the growth of the grafted polymeric chain. During the polymerization reaction, these grafted polymer chains react with the end vinyl group present in the crosslinker, MBA, to produce an interpenetrating, three-dimensional (3D) polymeric network with a lot of free carboxyl groups. In this way, the FA particle plays two significant roles in the formation of FA-WAP. Firstly, the functional group present in FA captures AA monomer and crosslinker MBA, resulting in the graft polymerization reaction. Secondly, the FA particle in the polymer network acts as an additional network point, which enhances the mechanical stability and salt resistivity of the water-absorbing polymer.

4.3.1 Characterization of FA-WAP

The FTIR spectroscopy was used to characterize the functional groups of parent material and the final product. The FTIR spectrum of the FA, PAA, and FA-WAP are presented in Fig. 4.4. As observed from the figure, the broad peak in FA observed at 3427 cm^{-1} is due to the existence of H-bonded (i.e., intermolecular and intramolecular) hydroxyl stretching vibration. The peaks observed at 1088 cm^{-1} and 795 cm^{-1} were assigned to asymmetrical stretching of Si-O-Si and symmetrical stretching of Si-O-Si, which can also be seen in the FA-WAP. In addition to this, the new absorption peaks in the region of 2920 cm^{-1} and 2853 cm^{-1} in FA-WAP were ascribed to the stretching of the alkyl C-H bond. The characteristic IR signature at 1410 cm^{-1} and 1630 cm^{-1} for symmetric and asymmetric stretching of carboxylate groups (COO^{-}) validating the successful grafting of AA on the surface of FA. Overall, the FTIR spectrum of synthesized FA-WAP indicated the existence of both PAA and FA.

The XRD spectrum of FA, PAA, and FA-WAP are presented in Fig. 4.5. The XRD pattern of FA clearly indicates that it consists of quartz (Q) and mullite (M). The XRD pattern of PAA exhibit a broad peak at $2\theta = 22°$, which indicates an amorphous structure with low crystallinity. A Similar peak for PAA was reported in the previous literature (Zhang et al. 2016; Swain and Prusty 2018). The presence of quartz and mullite in FA-WAP, along with the same crystalline peak of PAA, confirmed the incorporation of FA in the PAA chain network.

TH-2777_166104034

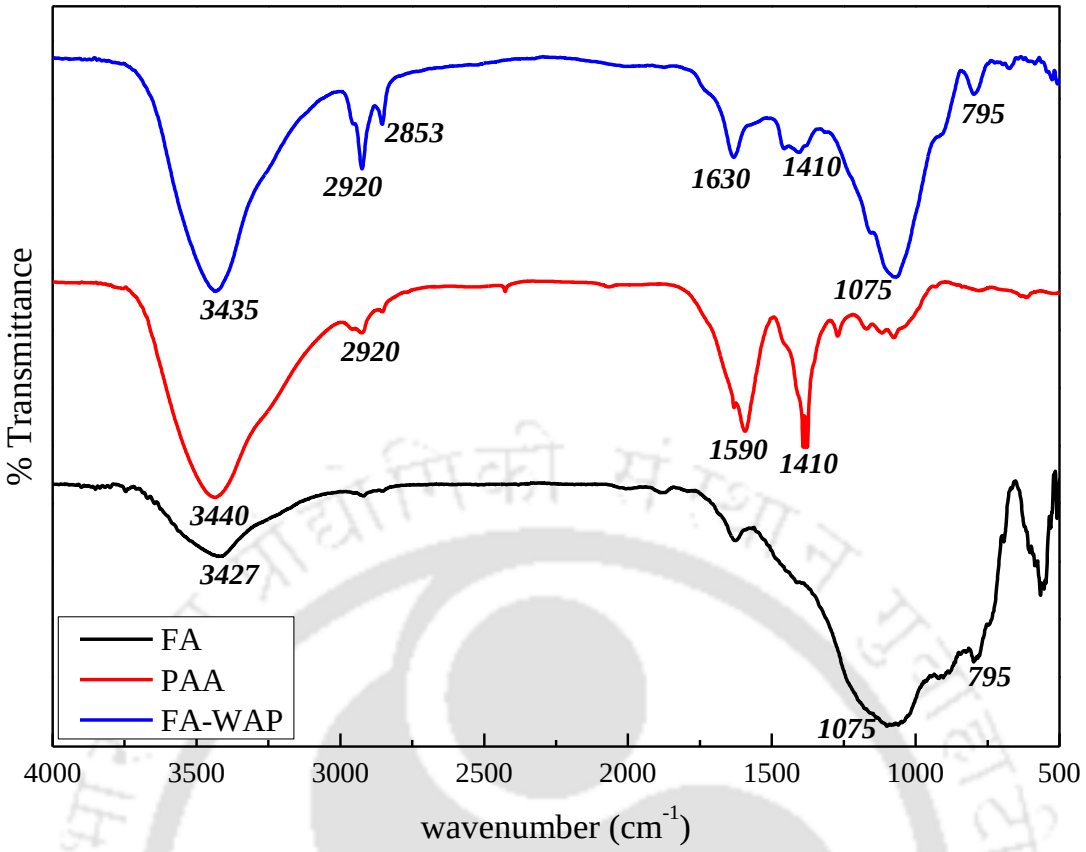

Fig. 4.4 FTIR Spectrum of FA, PAA and FA-WAP

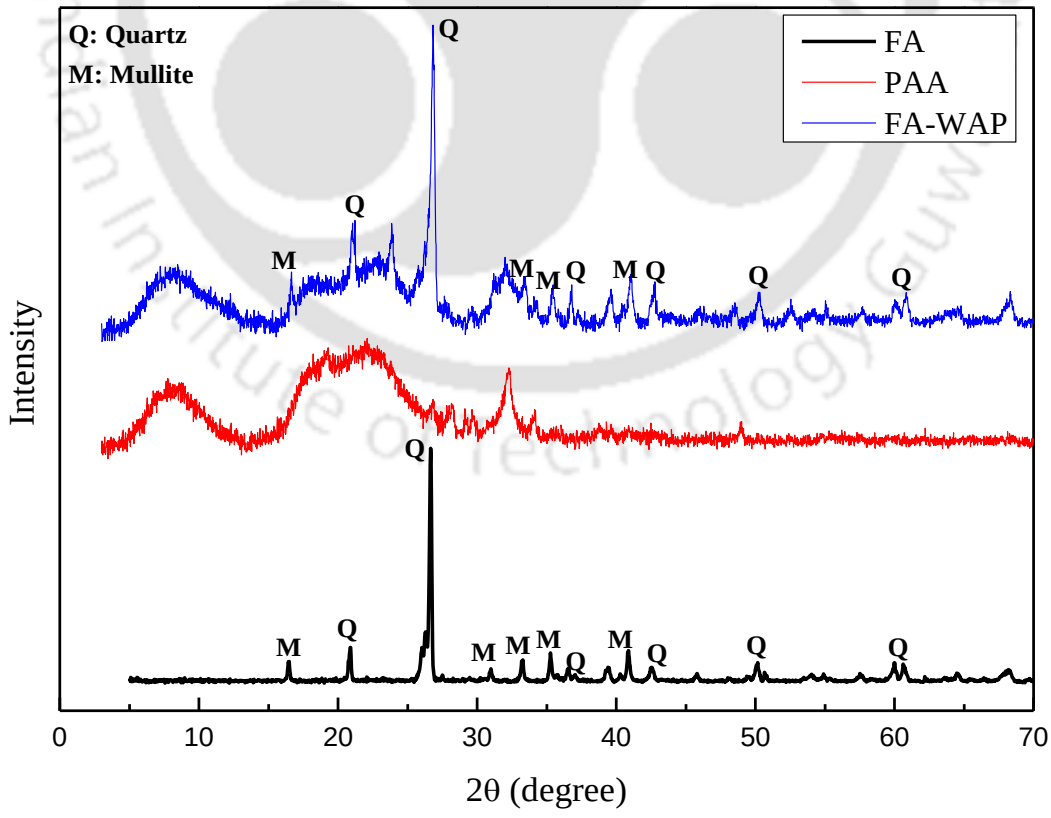

Fig. 4.5 XRD analysis of FA, PAA and FA-WAP

TH-2777_166104034

The graft polymerization of PAA on the surface of FA can be further verified through their surface morphology. For this purpose, the surface morphology of the FA, PAA, and FA-WAP, as visualized from FESEM, is presented in Fig. 4.6. Figure 4.6(a) depicts the FA particles, which are relatively smooth and spherically shaped. On the other hand, the morphology of the PAA displayed a compact, flat, and porous surface [Fig. 4.6(b)]. The surface profile of FA-WAP, as shown in Figs. 4.6(c) and (d) are distinctly different from PAA. The FA-WAP portrayed a comparatively coarse, loose, and porous surface with a considerable number of cavities, indicating more water-absorbing sites as compared to PAA. The change in the surface morphology was due to the grafting of FA, which destroyed the tight, smooth surface of the PAA, leading to a heterogeneous and loose structure with a lot of cavities.

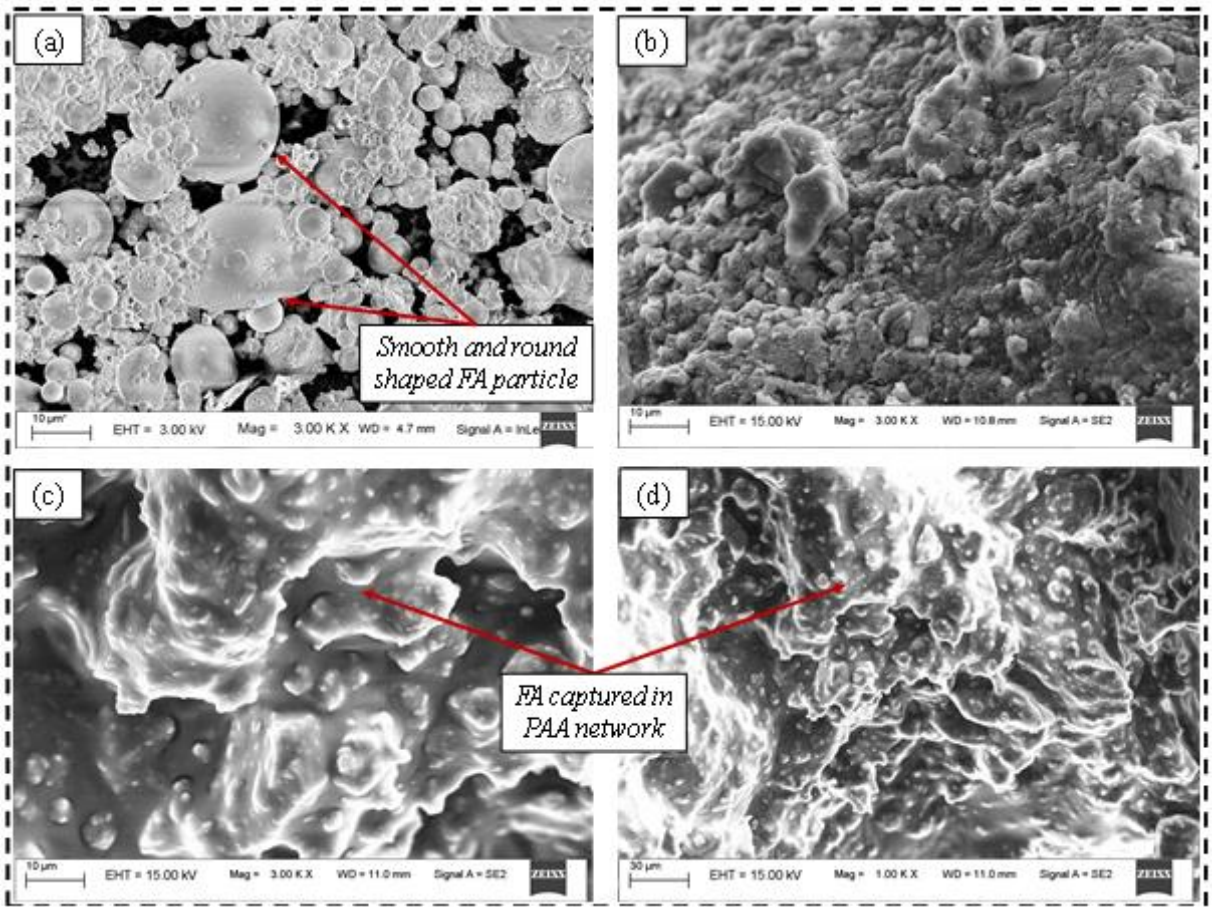

Fig. 4.6 FESEM image of (a) raw FA, (b) PAA, (c) FA-WAP at 3000X and (d) FA-WAP at 1000X magnification

The adsorption-desorption isotherm and pore size distribution of FA and FA-WAP were presented in Fig. 4.7, along with the BET surface area and average pore diameter in Table 4.2. It can be observed that the surface area decreased from 2.07 m^2/g (for FA) to 0.08 m^2/g in FA-WAP. This is attributed to the pore-blocking effect as a significant part of pores in FA-

TH-2777_166104034

WAP is occupied by sodium polyacrylate. A similar pore-blocking effect was also reported in He et al. (2016). Moreover, such a low surface area of FA-WAP suggests that the water absorption mechanism is not related to the surface adsorption phenomenon.

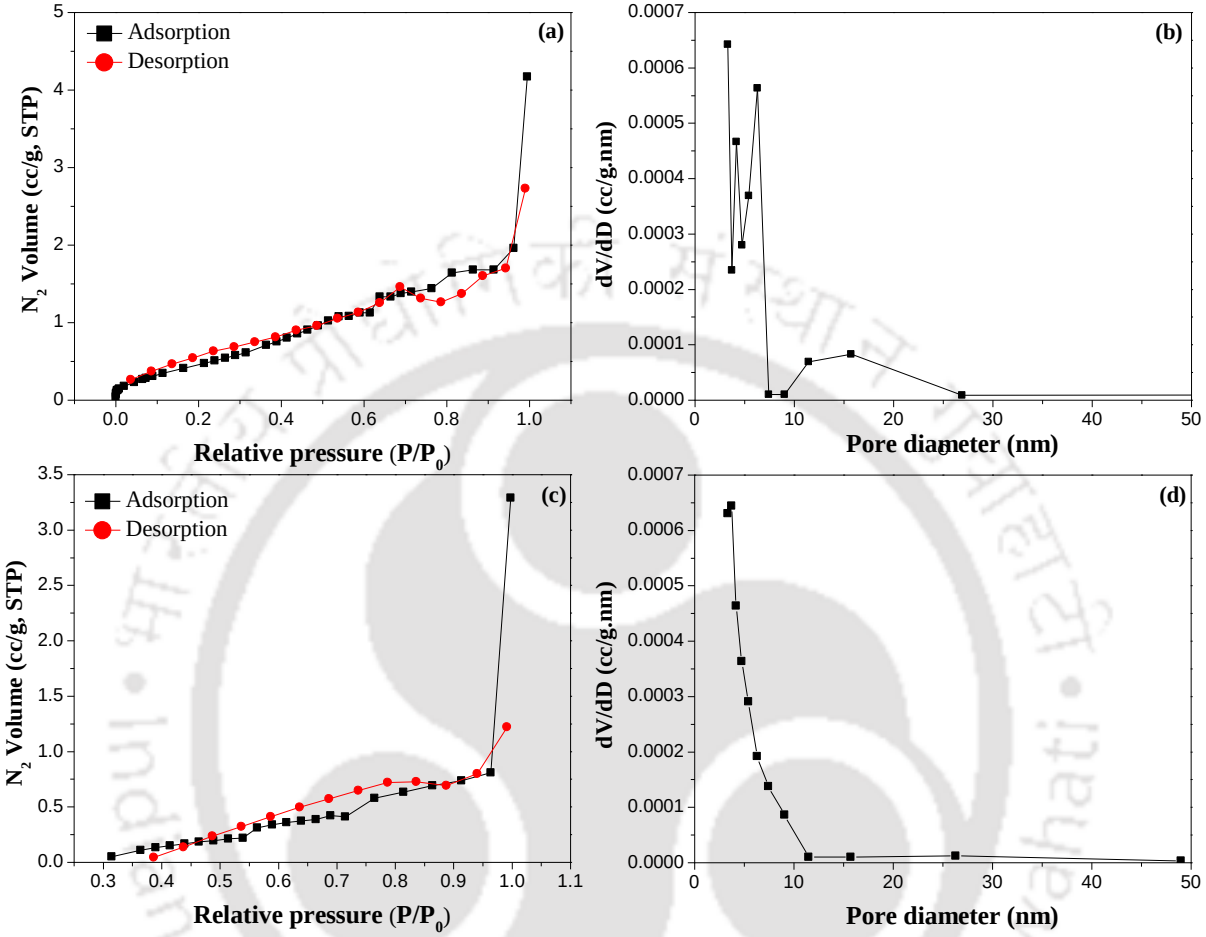

Fig. 4.7 BET N_2 adsorption-desorption isotherm of (a) FA, and (c) FA-WAP, and pore size distribution of (b) FA and (d) FA-WAP

Table 4.2 BET surface area and average pore diameter of FA and FA-WAP

Material	Surface area (m^2/g)	Average pore diameter (nm)	Pore volume (cc/g)
FA	2.07	12.5	0.0065
FA-WAP	0.08	273.4	0.005

The zeta potential (reflects the surface charge of the material) of FA and FA-WAP were found to be -3.44±0.18 mV, and -4.82±0.76 mV. The increase in zeta potential in FA-WAP can be attributed to the existence of carboxylate groups (COO^-) on the surface after modification.

TH-2777_166104034

4.3.2 Optimizing the synthesis of FA-WAP for maximum WAC

The maximum WAC of FA-WAP is governed by the optimal content of parent materials used in graft polymerization, which include FA content, crosslinker content (MBA), initiator content (APS), neutralization degree of AA, and water dilution. The influence of these parameters on the WAC was evaluated and presented in Fig. 4.8. The variation in FA content, crosslinker content, and initiator content was expressed as a weight percentage with respect to the dry weight of monomer AA. The effect of different amounts of FA content on the WAC in distilled water and tap water can be observed from Fig. 4.8(a). With an increase in FA content from 0 to 25%, the WAC of FA-WAP increased to 310 g/g and then decreased to 255 g/g in distilled water. A small quantity of FA act as an additional network point and react with the monomer, which enhances the three-dimensional polymeric network due to which the water absorbency increases. A further increase in FA content increases the density of crosslinking in the polymer network. It is, therefore, invariably necessary to identify an optimal FA content (=12.5% according to this study) for WAC of FA-WAP. The quantity of FA proposed for the synthesis of FA-WAP is well below the recommended maximum value of FA application rate in agriculture (=25%) [Pandey et al. 2009].

Figure 4.8(b) shows the effect of crosslinker content on the WAC. The figure depicts that the WAC is inversely proportional to the crosslinker content. With the increase in crosslinker content, the crosslinking density of the polymer increases, leading to a much tighter network with fewer free nodes in the polymer chain. It can be noted that crosslinker content less than 0.5% resulted in a water-soluble polymer composite, and its WAC cannot be evaluated. Therefore, the crosslinker content was fixed at 0.5%.

The effect of initiator content on the WAC is presented in Fig. 4.8(c). The WAC increases with an increase in initiator content from 0.8% to 1.5% and then decreases with a further increase in the initiator. The purpose of the initiator in the polymerization reaction is to produce free radical sites on FA particle and AA monomer so that the monomer could be grafted well on the surface of FA. Hence, the WAC increases with the initial increase in initiator content. However, exceeding the initiator content beyond 1.5% lead to an increased number of radical active sites in the monomer, and chain propagation gets terminated (Cowie and Arrighi 2007; Li et al. 2007; Feng et al. 2014). This results in a decrease in the molecular weight of the polymer chain, and subsequently, the WAC is reduced.

TH-2777_166104034

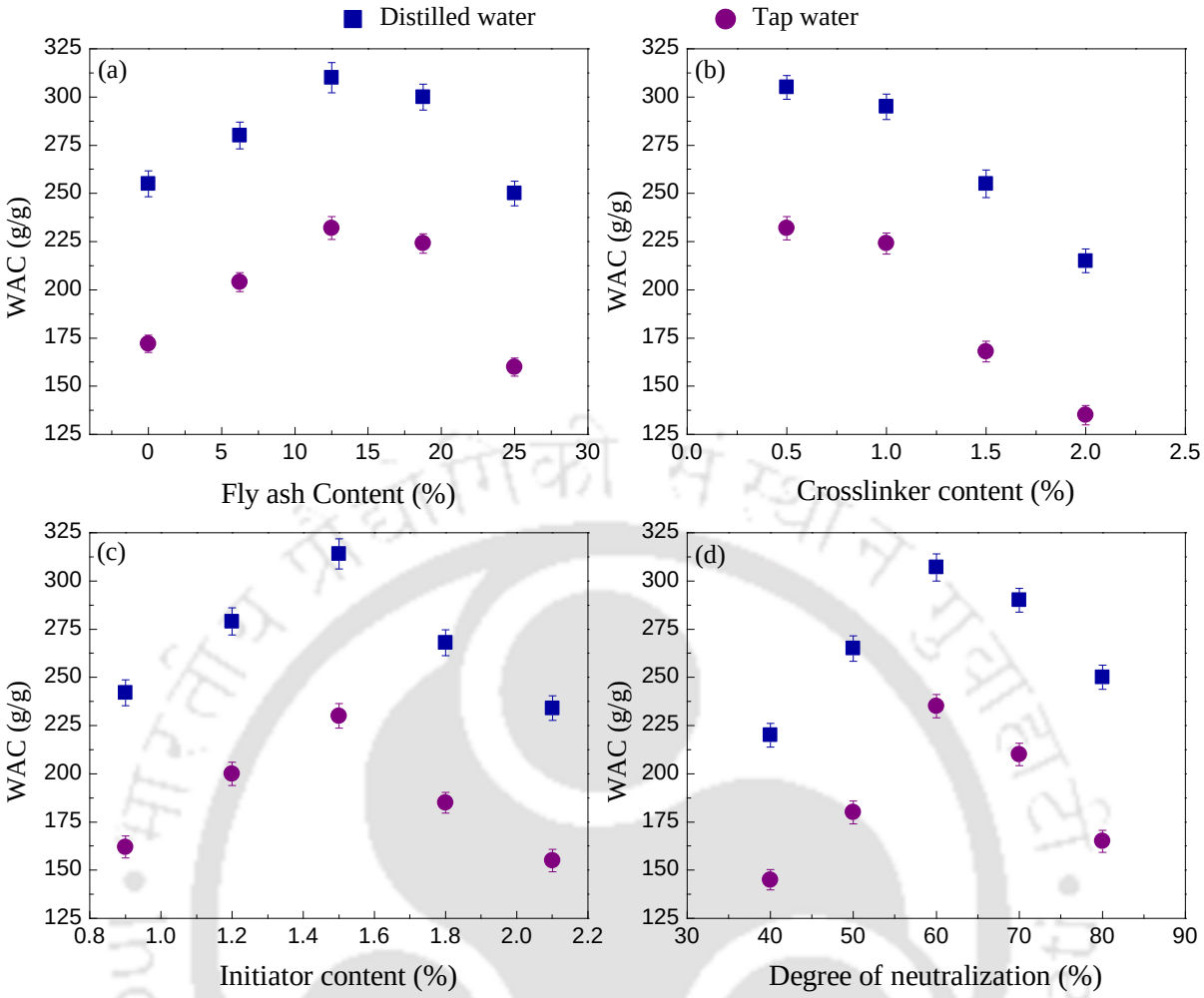

Fig. 4.8 Effect of (a) FA content, (b) Crosslinker content (c) initiator content and (d) neutralization degree of AA on WAC of the synthesized FA-WAP

Figure 4.8(d) shows that the neutralization degree of AA has a significant effect on the WAC of the FA-WAP. The optimum WAC of 310 g/g in distilled water and 230 g/g in tap water was obtained at 60% neutralization degree of AA. Neutralization of AA with sodium hydroxide (NaOH) leads to an increase in the strong hydrophilic group (-COONa) in the polymer network [ref Fig. 4.9]. The negatively charged carboxyl groups ($-COO^-$) creates an anion-anion electronic repulsion within their polymeric network. On contact with water, a significant pressure difference is developed between the polymer network and water, which supports the penetration of water molecules into the polymer network. After exceeding the optimum value of the neutralization degree, the WAC decreases because of the increase in Na^+ counter ions, which shields the negatively charged carboxyl group (Wang and Wang 2010; Zhou et al. 2011).

TH-2777_166104034

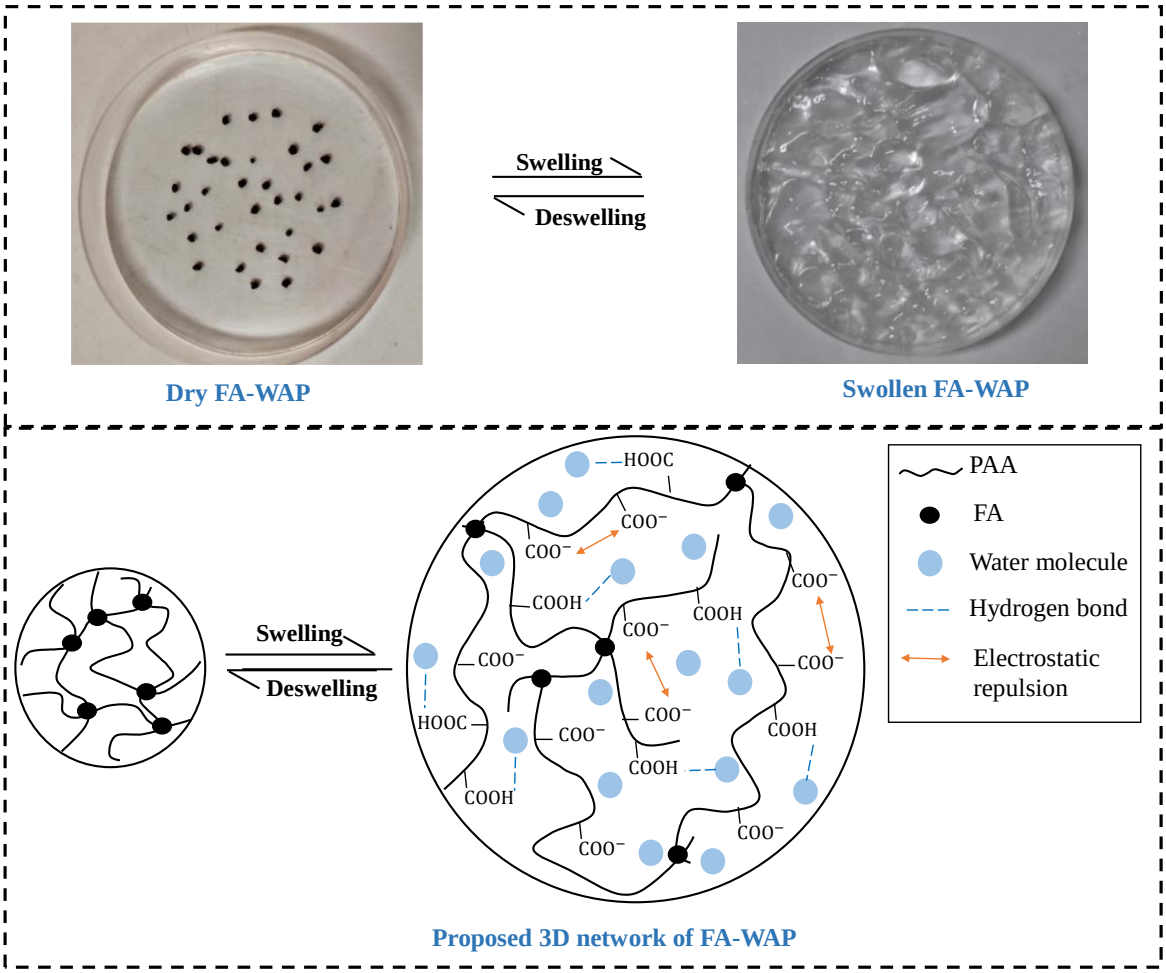

Fig. 4.9 Swelling and deswelling mechanism of FA-WAP

To evaluate the effect of water, the polymerization reaction was performed by adding 20 ml, 30 ml, 40 ml, 50 ml, and 60 ml of distilled water into the reaction mixture. It was observed that the polymerization did not take place when the amount of water was lower than 30 ml and higher than 60 ml. The WAC of synthesized FA-WAP remained constant (= 310 g/g) for the amount of water ranging between 30 ml and 60ml. It can be noted that the WAC of the synthesized FA-WAP is comparable with the WAC of other laboratory-grade WAP and commercial grade WAP (Table 4.3).

4.3.3 Swelling characteristics

4.3.3.1 Swelling kinetics

The swelling kinetics of FA-WAP, as well as the Com-WAP in distilled and tap water, are presented in Fig. 4.10. The swelling trend of both WAPs is found to be similar. The swelling capacity increased rapidly in the initial stage and then attained a constant equilibrium swelling capacity, which is similar to the trends reported in the previous literature (Li et al. 2007; Zhou

TH-2777_166104034

et al. 2011; Wan et al. 2013). It can be noted that FA-WAP and Com-WAP reach their swelling equilibrium within 4 hrs., and 2 hrs., respectively, from the beginning of the test.

A pseudo-first-order kinetic model (Equation 4.2) was fitted to the experimental data to describe the swelling mechanism.

$$Q_t = Q_e[1 - \exp(-k_1 t)] \quad 4.2$$

Here, Q_e (g/g) is the equilibrium water absorbency, t is the time (min), and k_1 denotes the first-order rate constant (min^{-1}). The value of k_1 was calculated from the measured swelling kinetics data using the non-linear curve fitting technique and presented in Table 4.4.

Table 4.3 Comparison of WAC of FA-WAP with other available WAP

Reference	WAC in distilled water (g/g)	Composition
Wan et al. (2006)	430	Polyacrylic acid, acrylamide, kaolinite
Rodrigues et al. (2012)	225	Polyacrylic acid, chitosan, rice husk
Wan et al. (2013)	360	Polyacrylic acid, acrylamide, corn stalk
Xu et al. (2015)	252	Polyacrylic acid, sea buckthorn
Xiao et al. (2017)	253	Polyacrylic acid, acrylamide, corn starch
Abdallah (2019)	244	Polyacrylamide (commercial grade)
Present study	310	Polyacrylic acid, fly ash
Present study	279	Crosslinked potassium polyacrylate (commercial WAP)

Table 4.4 Rate constant of FA-WAP and Com-WAP in distilled and tap water

WAP	Rater parameter (min^{-1})			
	Distilled water	R^2	Tap water	R^2
FA-WAP	0.015	0.96	0.013	0.97
Com-WAP	0.051	0.98	0.065	0.99

TH-2777_166104034

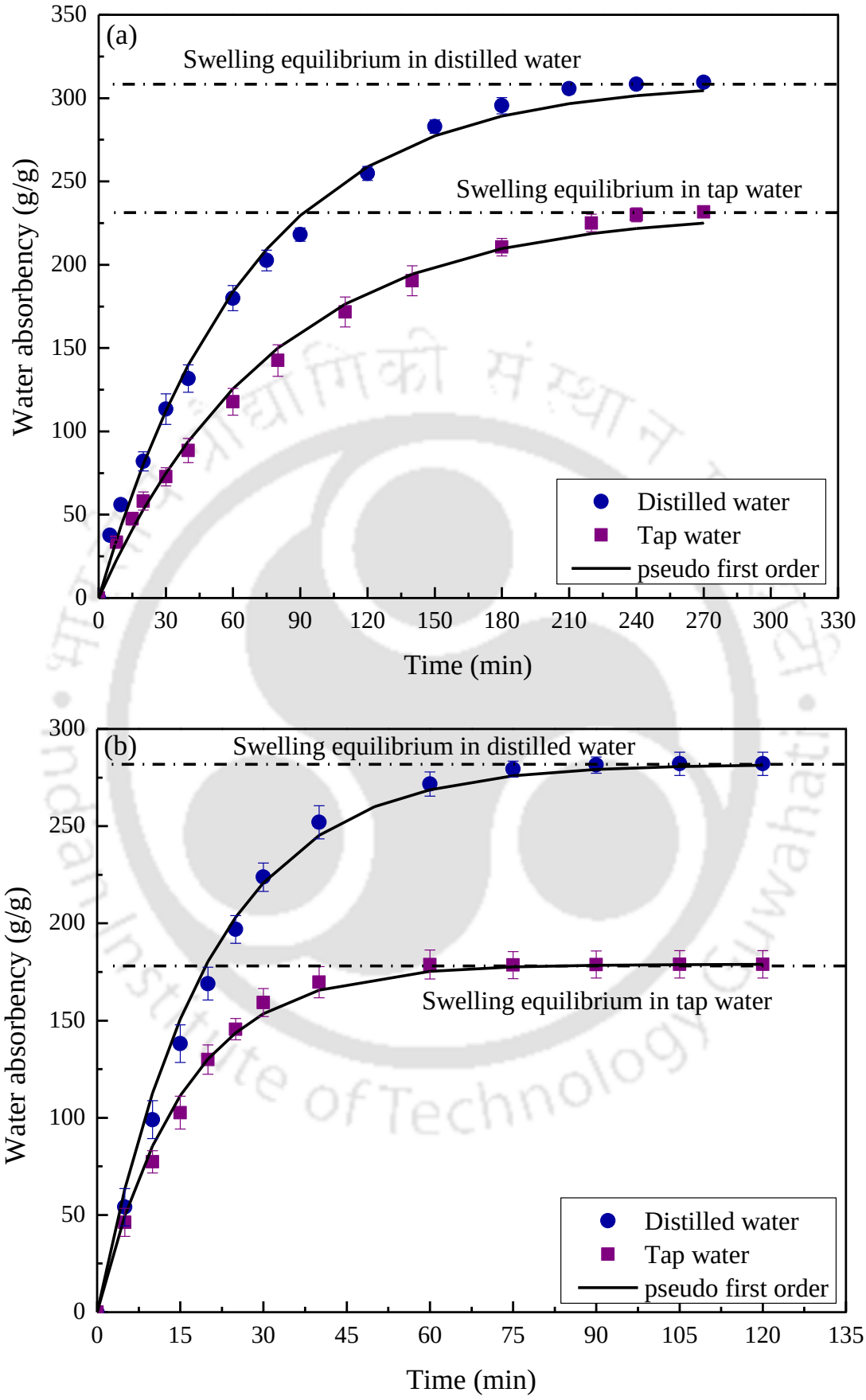

Fig. 4.10 Swelling kinetics of (a) FA-WAP and (b) Com-WAP in distilled and tap water

TH-2777_166104034

4.3.3.2 Drying characteristics at different temperature

The drying characteristics of the com-WAP and FA-WAP are presented in Fig. 4.11 at two different temperatures (ambient temperature and 50° C). The drying rate of WAP at higher temperature remains almost constant from the equilibrium absorbency to complete dry condition. On the other hand, the initial drying rate is relatively high for the samples dried in ambient conditions, followed by some decrement in the drying rate as the sample approaches towards the residual state. It can be observed that the Com-WAP took 400 hrs for complete drying in ambient temperature, whereas the FA-WAP took 520 hrs for the complete desaturation. The higher drying time in FA-WAP as compared to the Com-WAP is attributed to the higher WAC of the former one. For a better understanding of the drying rate, the moisture evaporation rate from the swollen WAPs at two different temperatures were calculated using Eq. (4.3) and presented in Fig. 4.12.

$$ER\ (mm/hr) = \frac{Amount\ of\ water\ evaporated\ per\ hr\ (mm^3)}{Cross\ sectional\ area\ of\ container\ (mm^2)} \qquad 4.3$$

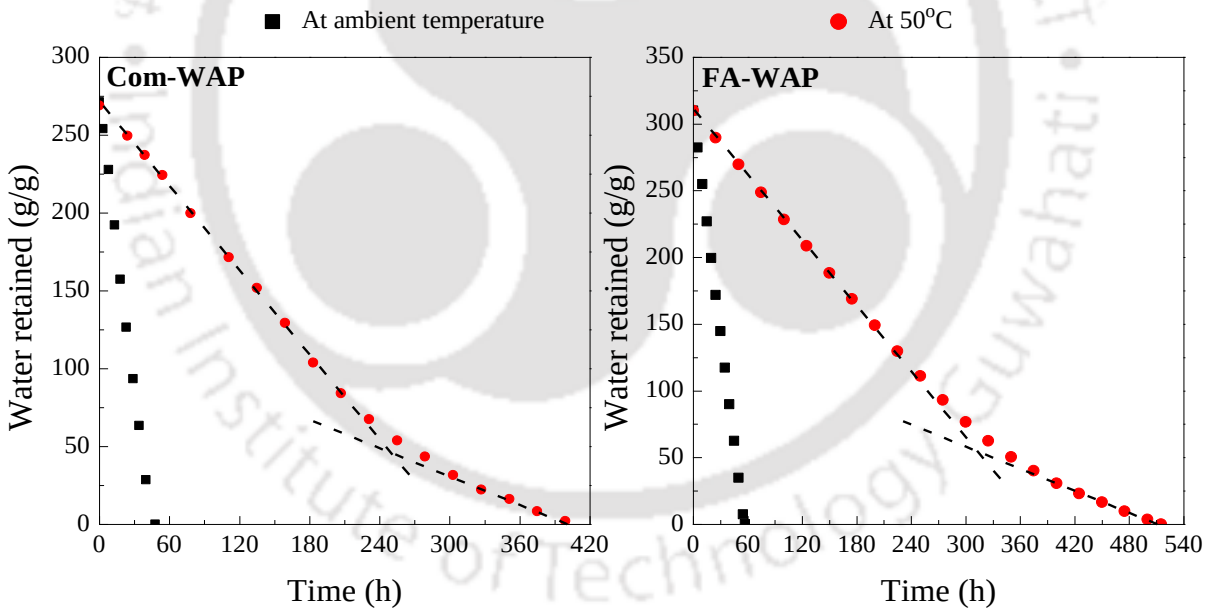

Fig. 4.11 Deswelling kinetics of com-WAP and FA-WAP at two different temperatures

As it can be observed in Fig. 4.12, the evaporation rate remains almost constant in FA-WAP during oven drying conditions with some decrement in evaporation rate for Com-WAP. Moreover, the rate of evaporation was found to be higher in Com-WAP as compared to FA-WAP. At ambient temperature, the variation of evaporation rate with time shows three distinct phases. At the initial stage (Phase I), the evaporate rate is maximum and remains constant. Phase II drying begins when the surface of the polymer cannot allow sufficient moisture flow

TH-2777_166104034

due to the conductive properties of the polymer. The evaporation rate further declines with progressive drying, reaching to a low residual value defined as phase III drying (Wilson et al. 1994). It can be observed that the evaporation rate is higher in Com-WAP as compared to FA-WAP in phase I drying, whereas the evaporation rate followed the opposite trend in phase II drying. Both the WAP attained the same evaporation rate in the phase III drying.

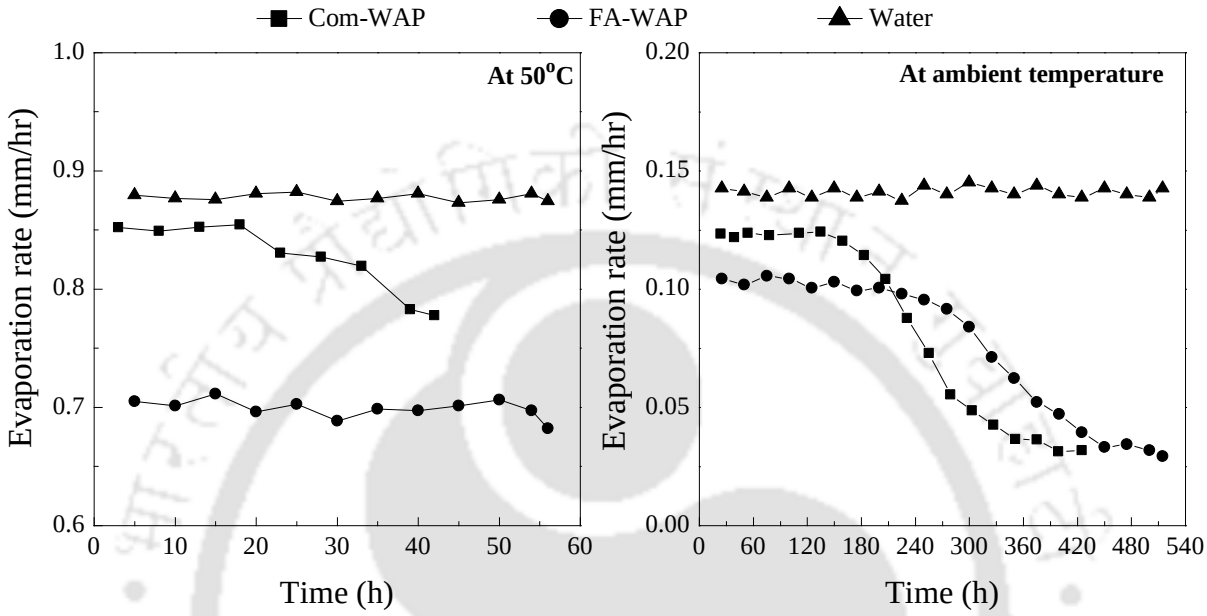

Fig. 4.12 Variation in the moisture evaporation rate from WAP at different temperature

4.3.3.4 Re-swelling characteristics of FA-WAP

Figure 4.13 represents the re-swelling characteristics of FA-WAP in distilled and tap water as a function of alternate wetting-drying cycles (8 cycles). A negligible decrease in the WAC was noticed after eight wetting-drying cycles for FA-WAP in distilled water, whereas a sharp decrease in the WAC can be observed in tap water. The minimal decrease in WAC associated with distilled water may be due to change in the polymeric network as the FA-WAP was dried in the oven. However, the sharp decrease in the WAC in tap water could be a result of the presence of salt and other impurities in tap water, which affected the polymer chain and weakened the chemical bond between different hydrophilic groups, leading to degradation of the polymeric structure. The decrement in WAC for FA-WAP in tap water was found to be 73% after eight wetting-drying cycles. In contrast, the WAC decrement was only about 6% in the case of distilled water. These results indicate that the FA-WAP has an excellent re-swelling ability and can efficiently contribute towards water retention during drought stress even after the eighth alternate drying-wetting cycle. A similar observation was also observed in Com-WAP. However, the water absorbency of Com-WAP after eight alternate cycles was found to

TH-2777_166104034

be lower than FA-WAP. This indicates that the quality of pore water has a significant influence on the re-swelling capability of WAP. This opens up the need for further research for deciding the time interval for replenishing FA-WAP in the field based on soil quality.

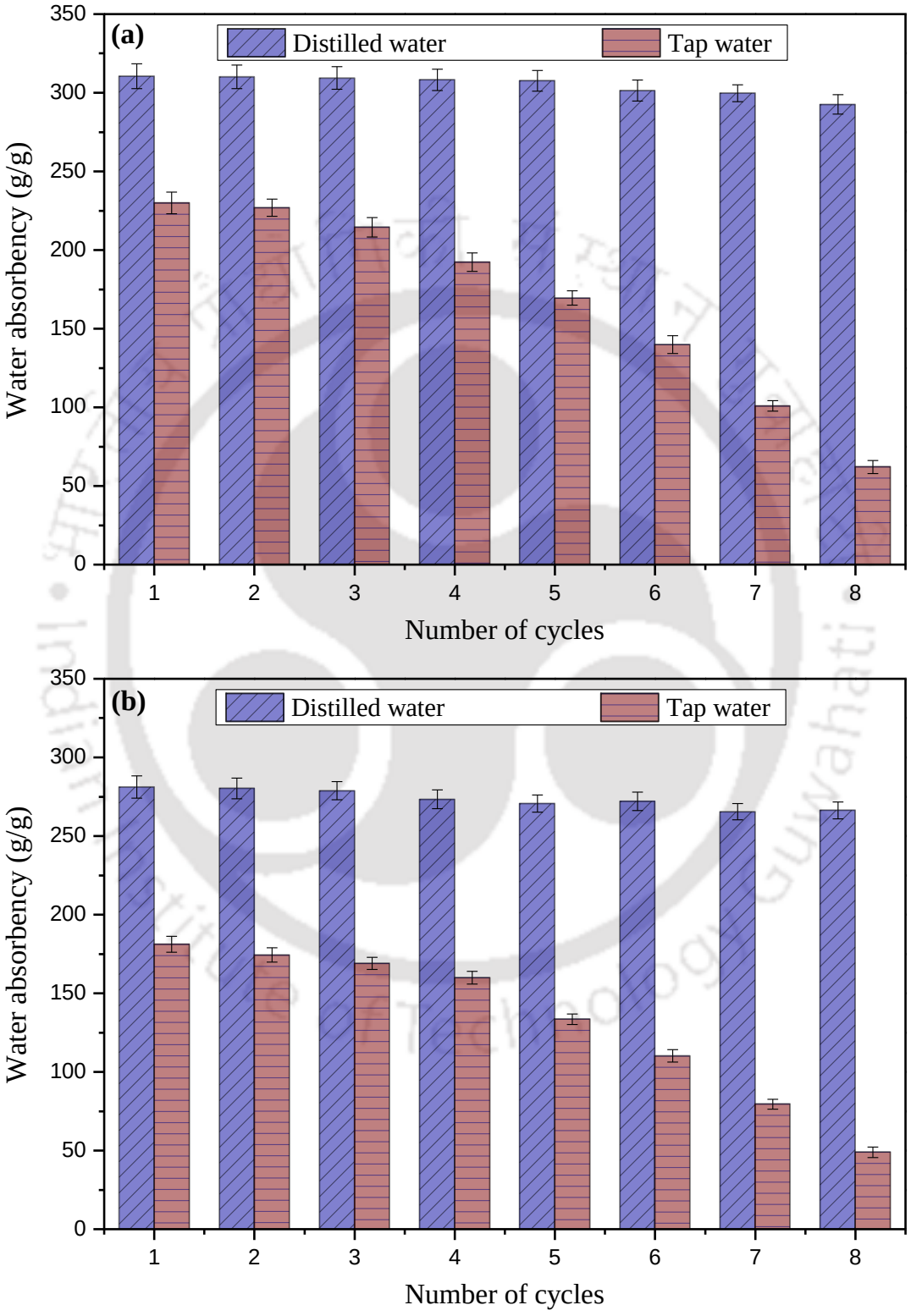

Fig. 4.13 Re-swelling characteristics of (a) FA-WAP and (b) Com-WAP

4.3.3.5 Salt sensitivity of FA-WAP

TH-2777_166104034

The effect of various inorganic salt ions on the WAC of the FA-WAP and Com-WAP was investigated and presented in Fig. 4.14 and Fig. 4.15, respectively. It can be observed that the WAC was significantly decreased with the increase in the salinity level. A rapid decrease in the absorbency can be noticed up to a salt concentration of 0.05 M, followed by a minimal decrement beyond 0.05 M. This was attributed to the increase in ionic strength of the salt solution and subsequent reduction in the osmotic pressure difference between the solvent and polymer network. It was also observed that the presence of divalent ions affected the WAC more than monovalent ions. This was due to the higher ionic strength of divalent ionic salt compared to the monovalent ionic salt. According to Equation (4.4), as suggested by Hermans (1953), the swelling characteristics of any WAP are significantly influenced by the ionic strength of the solution.

$$Q^{\frac{5}{3}} = A + B\frac{i^2}{I} \tag{4.4}$$

Here, *Q* denotes the WAC, *i* denotes the concentration of the charges bound to the gel, *I* denote the ionic strength of the solvent, and *A*, *B* are empirical parameters.

Figures 4.14(a) and 4.15(a) show the effect of different monovalent (Na^+,K^+,NH_4^+) and divalent (Ca^{2+}) cations on WAC of FA-WAP and Com-WAP in the presence of a common anion (Cl^-). The order of WAC of FA-WAP in the chloride salt solution was found to be NH_4Cl >NaCl >KCl >$CaCl_2$. Out of the three monovalent cations, the effect of NH_4^+ ions on WAC of FA-WAP was found less effective as the other two cations are more electro-positive since they belong to S-block elements in the periodic table. Both the WAPs showed higher WAC in NaCl solution compared to KCl as the size of the Na^+ ion is small compared to the K^+ ion. On the other hand, the effect of divalent Ca^{2+} ion on WAC was found to be much higher in comparison to the monovalent ions because of the higher ionic strength. In addition, Ca^{2+} ion can increase the crosslinking density of the polymer leading to a reduction in free available water-absorbing sites within the polymer network (Zhang et al. 2014).

The effect of monovalent (Cl^-, NO_3^-) and divalent (CO_3^{2-}, SO_4^{2-}) anions on WAC in the presence of a common cation (Na^+) are presented in Fig. 4.14(b) and Fig. 4.15(b). The decreasing order of WAC of both the polymer in different sodium salts were found to be $NaNO_3$ >NaCl >Na_2CO_3 >Na_2SO_4. It is obvious that the WAC was found to be more in nitrate (NO_3^-) and chloride (Cl^-) compared to carbonate (CO_3^{2-}) and sulfate (SO_4^{2-}) ions as the former ions are monovalent. Among the monovalent anions, the effect of Cl^- on WAC was more than NO_3^-

TH-2777_166104034

ions. This was attributed to the fact that NaCl is formed from a more acidic group [HCl (pK_a= -7)], whereas $NaNO_3$ is formed from a less acidic group [HNO_3 (pK_a= -1.3)]. Due to the same reason, among the divalent anions, the effect of Na_2CO_3 salt is lesser than Na_2SO_4 salt on the WAC of WAP.

Soil salinity is a condition characterized by a high concentration of soluble salts, of which NaCl is the most soluble and widespread salt (Munns and Tester 2008). Although soil salinity is a complex phenomenon that resulted from different salt sources, irrigation combined with poor drainage is the principal source of adding calcium (Ca^{2+}), magnesium (Mg^{2+}), and sodium (Na^+) to soil (Zhu 2007). As a result of water evaporation, Ca^{2+} and Mg^{2+} often precipitate into carbonates, leaving Na^+ dominant in the soil (Serrano et al. 1999), and therefore, Na^+ concentrations often exceed those of most macronutrients by one or two orders of magnitude, and by even more in the case of micronutrients. Increases in cations and their salts, NaCl in particular, in the soil generates external osmotic potential, which prevents or reduces the water influx into the root, resulting in water deficit similar to drought conditions. The use of water-absorbent like FA-WAP can improve the water availability to the plant roots as compared to the bare soil.

Though the effect of salt ions on the WAC of FA-WAP was investigated up to 0.3 M, the crop species can only sustain up to a soil salinity level of 0.1 M (Munns and Termaat 1986; Tavakkoli et al. 2010). Beyond this salinity level, the plants start to wilt due to ion toxicity, and the plant growth is completely prevented by the salt ions (Acosta-Motos et al. 2017). It can be observed that the synthesized FA-WAP has WAC of 80 g/g even up to 0.1 M salinity level for monovalent ions, which showed its excellent potential for agricultural application under water stress conditions.

For a comparative measure of the sensitivity of FA-WAP and Com-WAP to a particular type of aqueous fluid, a dimensionless salt sensitivity factor (*f*) was calculated from Equation (4.5). The calculated *f* value for the used salts at different molar concentrations was presented in Fig. 4.16 and compared with the f value of different laboratory-grade WAP, as reported in the previous studies (Li and Wang 2005; Zhang et al. 2005; Bao et al. 2011; Zhang et al. 2014; Fan et al. 2018).

$$f = 1 - \frac{WAC\ in\ salt\ solution}{WAC\ in\ distilled\ water} \tag{4.5}$$

TH-2777_166104034

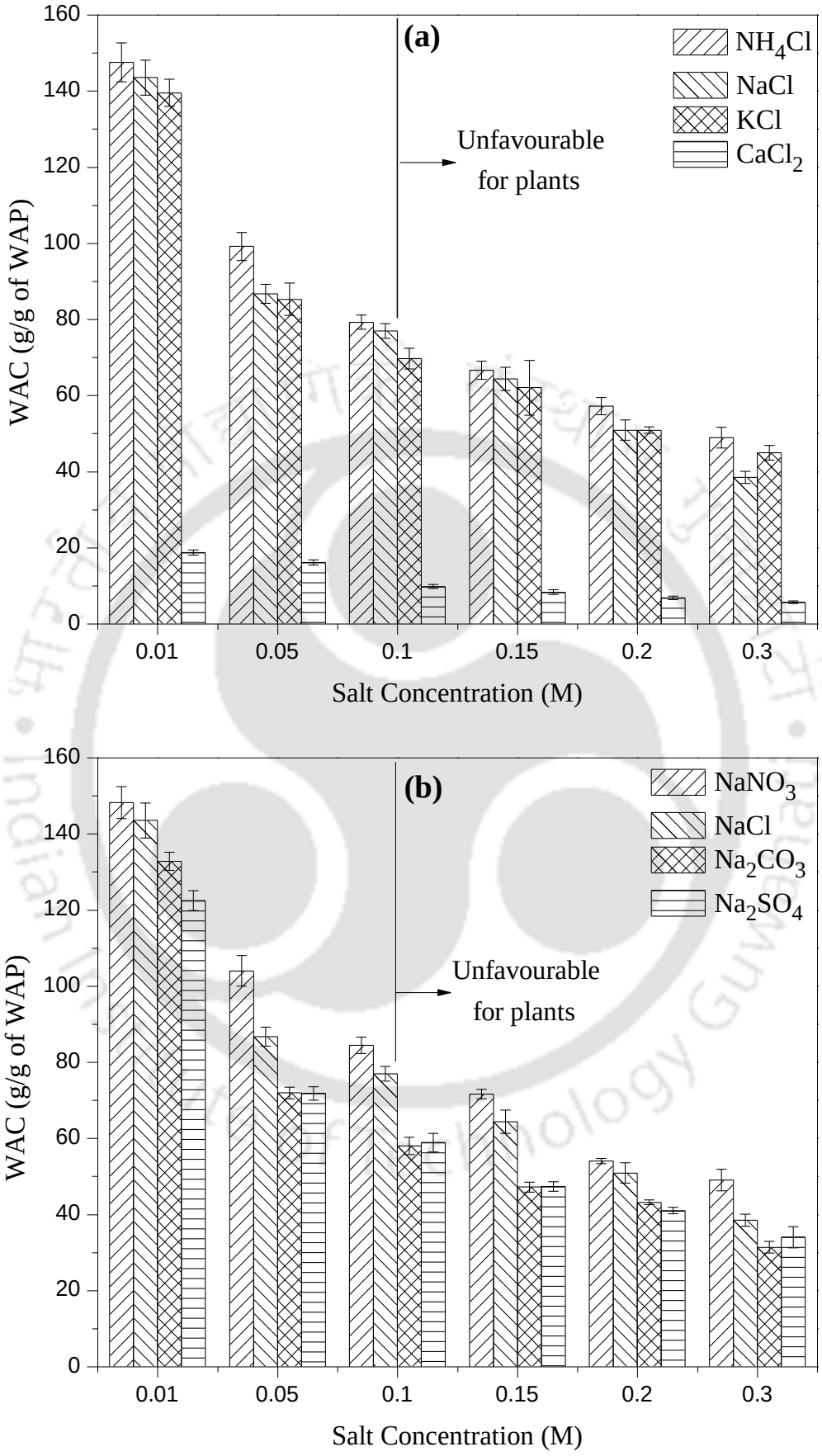

Fig. 4.14 Effect of various (a) cations and (b) anions on WAC of FA-WAP

TH-2777_166104034

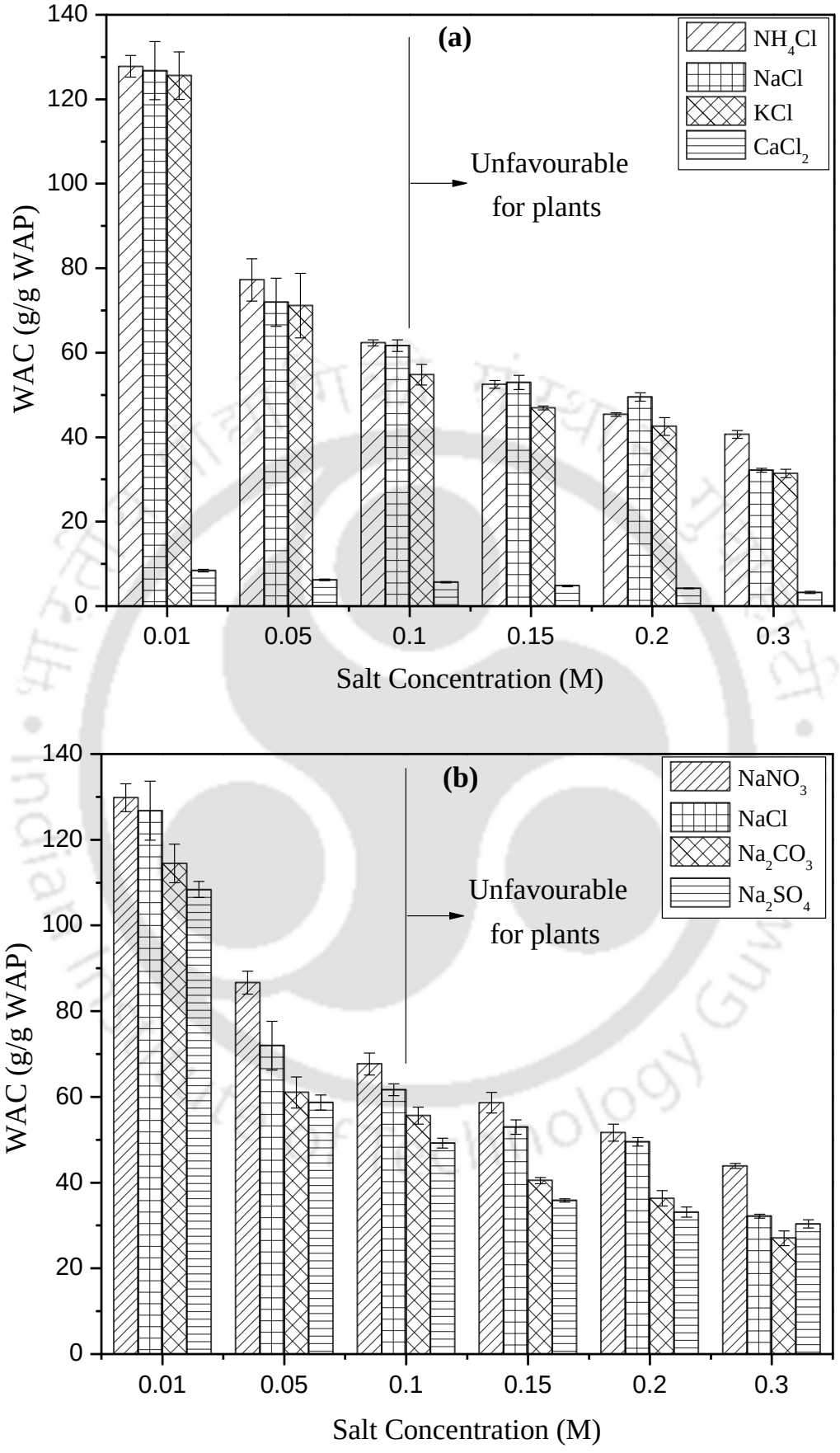

Fig. 4.15 Effect of various (a) cations and (b) anions on WAC of Com-WAP

TH-2777_166104034

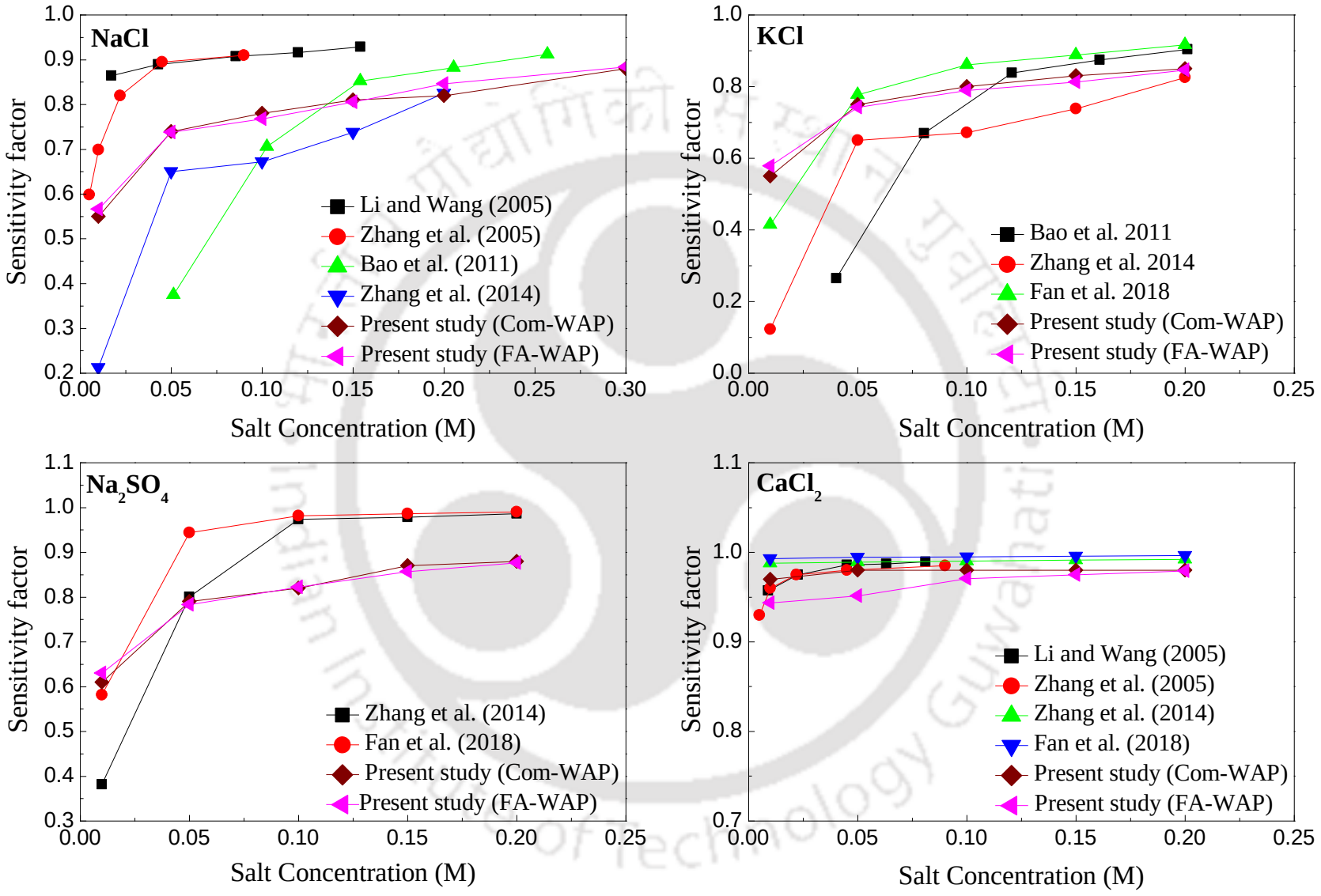

Fig. 4.16 Sensitivity factor of different WAPs in different salt solutions

TH-2777_166104034

As it can be observed in Fig. 4.16, the obtained sensitivity value is different for different laboratory-grade WAP. The sensitivity factor of a particular WAP to salt solution depends on the physicochemical properties of WAP and its composition (monomer and backbone material). The *f* value of FA-WAP and Com-WAP was more or less similar in monovalent salts, whereas for divalent ions, the *f* value was much higher in FA-WAP than Com-WAP.

4.3.3.6 pH sensitivity of FA-WAP

The sensitivity of FA-WAP and Com-WAP in terms of WAC to various pH solutions was presented in Fig. 4.17. A significant variation in the WAC can be observed in FA-WAP at a wide range of pH due to the presence of different interacting species in the swelling medium. The influence of different stock solutions on the WAC was found very minimal at the same pH value. Various phenomenon and mechanisms are involved during the swelling of FA-WAP at different pH range. At very low pH (pH <3.0), the main interacting species present in the solution are protonated ($-COOH_2$), and excess acid anions (Cl^-, SO_4^{2-}). Presence of these excess anions shield the charge of protonated carboxyl cation, which prevent the electrostatic repulsion between protonated ($-COOH_2$), resulting in a remarkable decrease in WAC. At pH range 5.0-6.0, an intense repulsion between protonated ($-COOH_2$) cause a significant increase in osmotic pressure inside the FA-WAP. This high osmotic pressure difference between the polymer network and the external solution is balanced by the swelling of the FA-WAP particles. At neutral pH, the majority of base and acid groups are in non-ionized form. As a result, the intermolecular hydrogen bond form between some of the carboxyl groups (-COOH) of the monomer leading to some minor decrease in the WAC. Similarly, for the pH range 8.0-10.0, electrostatic repulsion between multiple deprotonated ($-COO^-$) increase the charge density inside the particle resulting in high swelling in the solution. With the increase in pH (pH> 10.0), the presence of different basic cation like Na^+, Ca^{2+} increases, which shield the charge of deprotonated ($-COO^-$) that causes a significant decrease in the WAC. A similar type of observation was reported in Mahdavinia et al. (2004). According to USDA (United States Department of Agriculture) Natural Resources Conservation Service (USDA 1993), soil pH can vary from 5.5-8.5 with extreme scenarios of 3.5-9.0. It was reported that the optimum soil pH range for most of the plants is 5.5-7.5, beyond which the plants are susceptible to aluminum toxicity (for pH less than 5.5) and nutrient deficiency (for pH higher than 7.5) [Queensland Department of Environment and Heritage Protection 2013]. From Fig. 4.17, it is evident that the WAC of the synthesized FA-WAP is negligibly affected by soil pH.

TH-2777_166104034

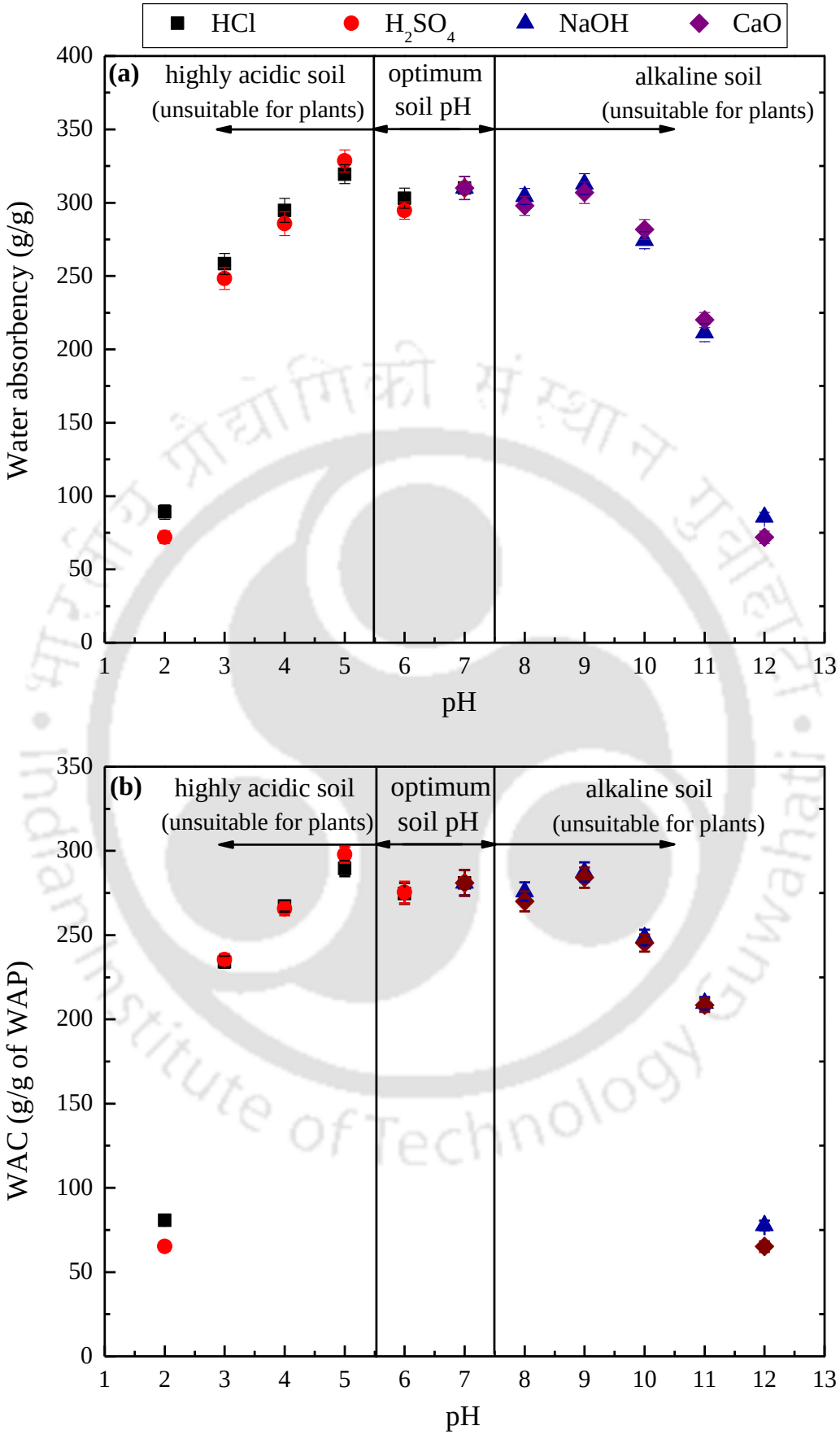

Fig. 4.17 Effect of pH on WAC of (a) FA-WAP and (b) Com-WAP

TH-2777_166104034

4.3.3.7 Combined effect of various salt and pH

A combined influence of pH and salinity on the performance of both the WAP was also evaluated in the present study. The WAC of both the WAPs were measured at three different pH (5, 7, and 9) along with the previously mentioned salt solutions. Two stock solutions, HCl and NaOH, were used for preparing pH solutions of 5 and 9, respectively. After adding the desired concentration of the salt, the stock solutions were diluted with distilled water to obtain the required acidic and basic pH. The electrical conductivities (EC) of different concentrations of salt solutions at three different pH (pH 5, 7, and 9) were measured using an EC meter (Company: Systronics, India) to incorporate in influence of both salinity and pH on WAC.

Fig 4.18 represents the measured experimental data points for the WAC of the FA-WAP and Com-WAP in different salt and pH solutions (in terms of EC). A logarithmic curve was fitted to the data points, which relates the WAC and EC of swelling medium as presented below (Eq. 4.4 and Eq. 4.5),

$$WAC_{FA-WAP} = -31.8 \times \ln EC + 141.4 \quad 4.4$$

$$WAC_{Com-WAP} = -28.1 \times ln\, EC + 121.2 \quad 4.5$$

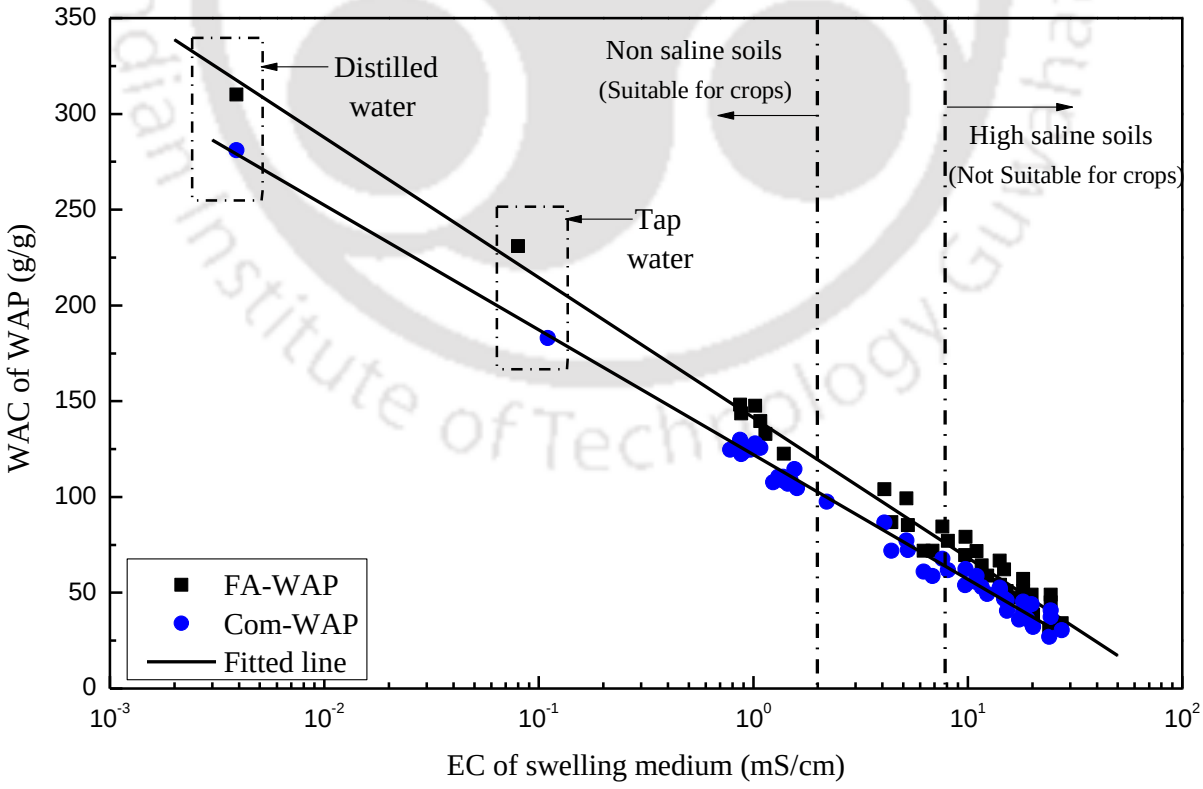

Fig. 4.18 Relationship between WAC of WAP and EC of swelling medium

TH-2777_166104034

The range of electrical conductivity exist in the agricultural land, which is suitable for the crop growth were also included in Fig. 4.18. Most of the crop species can sustain up to an EC value of 2 mS/cm and the corresponding soils are termed as non-saline soils (Abrol and Yadav 1988). For extreme drought case, the soil salinity level can reach up to an EC of 4 mS/cm where some special types of crops can survive. After the salinity exceeds an EC value of 8 mS/cm, plants start to wilt because of the higher salt concentrations. The synthesized FA-WAP has WAC of 97g/g at the maximum level for soil salinity suitable for agricultural lands (EC=8 mS/cm), which is higher than the WAC of Com-WAP at the same EC value.

4.3.4 Toxicity assessment of FA and FA-WAP

The leachability of various trace elements from FA and FA-WAP, as obtained with the TCLP test, were reported in Table 4.5 along with the permissible limits of these metals in soil, as proposed by the United States Environmental Protection Agency (USEPA 2002) and World Health Organization (WHO 1996). It can be observed that the leachability of different heavy metals (Pb, Cd, Cr, Ni, Cu, Zn) remains well below the regulatory values. Moreover, the leachability of these heavy metals was not detectable in 0.4% FA-WAP amended soil (except Copper). It may be noted that some of these trace elements, such as Cu, Mn, Fe, are essential plant micronutrients and useful for promoting plant growth. Therefore, the synthesized FA-WAP can alleviate the negative effects of water stress conditions, along with the nutritional enhancement of soil.

Table 4.5 Leachability of various metals from FA, FA-WAP and FA-WAP amended FS

Metals	Metal concentrations in mg/kg			Permissible concentrations of metals in soil (mg/kg) [USEPA]	Permissible concentrations of metals in soil (mg/kg) [WHO]
	FA (L/S=20)	FA-WAP (L/S=200)	0.4% FA-WAP amended FS (L/S=20)		
Pb	2.4	22	ND	200	100
Cd	ND	ND	ND	0.48	3
Cr	2.2	18	ND	11	100
Ni	0.8	2	ND	72	50
Cu	6	54	0.4	270	100
Zn	36	16	ND	1100	300
Mn	5.8	42	0.2	NG	NG
Fe	1.6	112	0.8	NG	NG

ND: Not detectable; NG: Not given

TH-2777_166104034

4.4 Summary

A novel and eco-friendly fly ash-based water absorbing polymer (FA-WAP) was synthesized by grafting polyacrylic acid (PAA) chain on the surface of FA, using a crosslinker (N, N'-methylene bisacrylamide) and an initiator (Ammonium persulfate). The FTIR, FESEM, and XRD results confirm the successful grafting of PAA on the FA surface. A total of 360 number of combinations (including three repetitions) were performed to optimize the reagent quantities. The FA-WAP showed an excellent water-absorbing capacity (WAC) of 310 g/g and 230 g/g in distilled and tap water, respectively, at optimized synthesis conditions, which is higher than commercially available water absorbing polymer (Com-WAP).

The salt sensitivity of both WAP was evaluated in seven different inorganic salts (NaCl, KCl, NH_4Cl, $CaCl_2$, $NaNO_3$, Na_2CO_3, Na_2SO_4) at six molar concentrations (0.01 M, 0.05 M, 0.1 M, 0.15 M, 0.2 M, 0.3 M). Similarly, the sensitivity to pH solution was evaluated in HCl, H_2SO_4, NaOH, CaO, having pH between 4.0 to 12.0. The water absorbing capacity (WAC) of the FA-WAP was significantly affected by the salinity and pH of the external solution. The FA-WAP is more sensitive to multivalent ions as compared to monovalent ions due to the higher ionic strength of the former. The order of sensitivity of the FA-WAP for various cations was found to be in the order of $NH_4^+ < Na^+ < K^+ < Ca^{2+}$, while for anions, it was found to be $NO_3^- < Cl^- < CO_3^{2-} < SO_4^{2-}$. However, the FA-WAP showed WAC of 80 g/g at a salt concentration of 0.1 M, which is the limiting value for plant survival under ion toxicity. Hence, the application of FA-WAP will be beneficial under the saline condition as well. The effect of solution pH on the WAC was negligible for the pH range of 5.5 to 7.5, which is the recommended pH range of soil for plant and vegetation growth. The synthesized FA-WAP was performed better in terms of its reswelling characteristic, water absorbency in different salt and pH solutions as compared to Com-WAP. Moreover, the toxicity characteristics of the parent FA, synthesized FA-WAP, and 0.4% WAP amended soils were evaluated by measuring the leachability of different trace elements (such as Pb, Cd, Cr, Ni, Cu, Zn, Mn, Fe) using toxicity characteristic leaching procedure (TCLP). The TCLP results showed that the leaching potential of the trace elements remains well below the regulatory values, and the FA-WAP can be used as soil amendment.

TH-2777_166104034

Chapter 5

Moisture movement in WAP-soil system

5.1 General

As discussed in the earlier chapters, water absorbing polymer (WAP) particles act like an additional water reservoir, which absorbs the water during rain or irrigation and releases the water back to the soil when it is dry. Therefore, it is very important to understand the basic phenomenon involved in the movement of moisture from swollen polymer to dry soil to evaluate its effectiveness under drought conditions. There are few studies present in the literature that evaluated the moisture sorption mechanism of WAP (Witono et al. 2013; Zhang et al. 2014; Fan et al. 2018). However, the moisture movement mechanism in a soil-WAP system is not well recognized in any of the previous studies. Such type of study will be helpful in understanding the performance of WAP as a soil amendment under water stress conditions. The moisture diffusivity is one of the fundamental parameters for the characterization of water transport in unsaturated soil. Therefore, estimation of moisture diffusion mechanism and moisture diffusivity values become an important aspect for the characterization of moisture movement from swollen WAP particles to the soil.

5.2 Horizontal absorption test for moisture diffusion

A method for measuring soil moisture diffusivity, $D(\theta)$, where θ is the volumetric water content (VWC), was first presented by Gardner (1956) using pressure plate apparatus data. Later, Bruce and Klute (1956) used the horizontal absorption test to relate $D(\theta)$ to the volumetric water content when the gradient of the gravitational component of soil water potential is negligible. For this case, wetting front distance and time can be combined with the Boltzmann transformation factor (1894), which converts Richards' equation for horizontal water flow into an ordinary differential equation. Whisler et al. (1968) have introduced a method with the same theoretical analysis as presented in Bruce and Klute (1956), but the moisture diffusivity value was estimated based on moisture distribution with time at a fixed position. The advantage of the method is that it is non-destructive and relatively simpler and faster than the Bruce and Klute (1956) method. However, it utilizes the gamma-ray attenuation method for moisture content measurement, which is expensive and implies radioactive hazards (Selim et al. 1970). Clothier et al. (1983) adopted a fitting function in order to correlate the experimentally observed volumetric water content with the Boltzmann constant, which gives an analytical moisture diffusivity function that may not be valid for all types of soil. Shao and

TH-2777_166104034

Horton (1998) have developed a new method for estimating soil water diffusivity by general similarity theory. They have reported a power function to represent *D(θ)* and soil water content, which might not be applicable for all soil types. Evangelides et al. (2005, 2010) have presented a tangential fitting function to relate Boltzmann constant and water content, which can be useful for all types of soil. Espejo et al. (2014) have developed a field method for estimate *D(θ)* from successive water content sensors readings at a specific depth during the desiccation period. Villarreal et al. (2019) modified the Whisler et al. (1968) method of measuring the soil moisture profiles with the use of capacitance-based moisture sensors (EC5, METER Group, USA). It should be noted that all the aforementioned studies have conducted a horizontal water flow test with different soil samples to measure *D(θ)*. There is a need to extend the present concept of horizontal absorption to characterize the moisture transfer from swollen WAP particles to the soil layer.

In the present study, the sorption kinetics was first used to characterize the moisture sorption mechanism of WAP. For moisture movement characterization, a horizontal absorption test was performed in a diffusion cell (Shackelford 1991; Sreedeep and Singh 2008), where two portions of the cell, containing swollen polymer and dry soil were placed together to allow movement of moisture in the liquid phase from swollen polymer to dry soil. Thereafter, the classic method of Bruce and Klute (1956) was followed for the measurement of soil moisture profiles (by destructive gravimetric sampling) and inspection of wetting front versus time along the horizontal soil column in contact with swollen WAP. The obtained moisture profiles were further used to validate Fick's second law of diffusion for the description of moisture movement through the horizontal soil column. A tangential fitting function was proposed to obtain the relationship between the Boltzmann constant and VWC for the determination of moisture diffusivity function in terms of VWC.

5.3 Theory

5.3.1 Sorption kinetics of WAP

The governing mechanism of mass transport phenomena through diffusion is based on Fick's second law, as presented below.

$$\frac{\partial C(x,t)}{\partial t} = D\frac{\partial^2 C(x,t)}{\partial x^2} \qquad 5.1$$

where C is the concentration, x is the distance parameter, t and D is the time and moisture diffusivity into the polymer matrix, respectively.

TH-2777_166104034

For diffusion into a sphere and cylinder, the parameter *x* can be replaced by the radial distance,

$$\frac{\partial C}{\partial t} = \frac{1}{r}\frac{\partial}{\partial r}\left(rD\frac{\partial C}{\partial r}\right) \qquad 5.2$$

where *r* represents the radius of the sphere or cylinder.

Crank (1975) derived an analytical solution for Eq. (5.2) for many materials and shapes based on Fick's law. However, it was reported that the model could not describe the system, where the diffusing molecules cause extensive swelling of the material. The mass transport in macromolecular material such as WAP involves a complex process, which can be influenced by various factors, including the internal structure of the polymer (De Kee et al. 2005), chemical nature of the diffusing molecules (Rogers 1985), swelling, and relaxation time of the polymer matrix (Puri et al. 2008), and mechanical deformation (De Kee et al. 2005). To overcome the situation, a general model has been proposed (Frisch 1980; Bajpai and Johnson 2005), simplifying Eq. (5.2) in the form of an empirical equation given as,

$$\frac{M_t}{M_e} = kt^n \qquad 5.3$$

Where, M_t and M_e represent the mass of water absorbed at time t and at equilibrium, respectively. *k* is the characteristic constant, and *n* is diffusional exponent, dependent on the transport mechanism (Fickian or non-Fickian). For a value of $n < 0.5$, the movement of solute molecules into the polymer structure is described by the Fickian diffusion mechanism. Ritger and Peppas (1987) have demonstrated the transition from Fickian to non-Fickian diffusion at the value of 0.5 could differ depending on the geometry of the absorbing materials. For example, the limiting values of diffusion exponent (*n*) are 0.43, 0.45, and 0.5 for Fickian diffusion in spherical, cylindrical, and thin-film shaped materials, respectively.

5.3.2 Moisture movement through soil

The movement of water in unsaturated soil can be described by Richard's Equation (one-dimensional horizontal flow),

$$\frac{\partial \theta}{\partial t} = \frac{\partial}{\partial x}\left[k(\theta)\frac{\partial h}{\partial x}\right]$$

$$\frac{\partial \theta}{\partial t} = \frac{\partial}{\partial x}\left[k(\theta)\frac{\partial h}{\partial \theta}\frac{\partial \theta}{\partial x}\right]$$

TH-2777_166104034

$$\frac{\partial \theta}{\partial t} = \frac{\partial}{\partial x}\left[D(\theta)\frac{\partial \theta}{\partial x}\right] \qquad 5.4$$

Where θ is the volumetric soil water content ($m^3.m^{-3}$), $k(\theta)$ is the soil hydraulic conductivity ($cm.hr^{-1}$), h is the pressure head (cm), $D(\theta)$ is the moisture diffusivity ($cm^2.hr^{-1}$), x is the horizontal distance from the interface (cm), and t is time (hr).

The initial and boundary conditions for the moisture diffusion test are,

$$\theta(x,t) = \theta_i \qquad for\ x \geq 0\ and\ t = 0$$

$$\theta(x,t) = \theta_f \qquad for\ x = 0\ and\ t > 0$$

$$\theta(x,t) = \theta_i \qquad for\ x = \infty\ and\ t > 0$$

Here, θ_i is the initial water content ($m^3.m^{-3}$), and θ_f is the final water content ($m^3.m^{-3}$).

To convert Eq. (5.4) to an ordinary differential equation, a constant λ (Boltzmann transformation variable) has been introduced, where $\lambda = \frac{x}{\sqrt{t}}$. With this transformation variable, Eq. (5.4) was transformed to

$$-\frac{\lambda}{2}\frac{d\theta}{d\lambda} = \frac{d}{d\lambda}\left[D(\theta_x)\frac{d\theta}{d\lambda}\right] \qquad 5.5$$

Subjected to the boundary conditions,

$$\theta_x = \theta_i \qquad for\ \lambda = \infty$$

$$\theta_x = \theta_f \qquad for\ \lambda = 0$$

Integrating the Eq. (5.5) with respects to λ yields,

$$D(\theta_x) = -\frac{1}{2}\left(\frac{d\lambda}{d\theta}\right)_{\theta_x}\int_{\theta_i}^{\theta_x}\lambda d\theta \qquad 5.6$$

The above expression of moisture diffusivity is valid for all soil conditions except where solute and soil surface interaction exists, for soils with high clay content that swells upon wetting, and for organic soils where the presence of organic solutes affect wetting angles, vapor transfers, and viscosity (Selim et al. 1970). Further, the movement of moisture from the WAP particle to the soil can be described by the above equation only if the transformed water content and time-distance data give a unique $\lambda(\theta)$ function irrespective of the positions of x in the column.

TH-2777_166104034

From the experimental setup, volumetric water content distribution can be obtained with time *t*, and the value of λ can be calculated at different *x* values, which provide a unique relationship between θ and λ. A simple tangential equation (modified from Evangelides et al. 2010) with three constants (*a*, *b*, and *c*) was used to describe the transformed moisture profile,

$$\lambda = a\left[\tan\left(\frac{\theta}{b}\right) + c\right] \qquad 5.7$$

Now, $$\left(\frac{d\lambda}{d\theta}\right)_{\theta_x} = \frac{a}{b} sec^2\left(\frac{\theta_x}{b}\right)$$

and $$\int_{\theta_i}^{\theta_x} \lambda d\theta = -abln\left[\frac{\cos\left(\frac{\theta_x}{b}\right)}{\cos\left(\frac{\theta_i}{b}\right)}\right] + ac(\theta_x - \theta_i)$$

Therefore, moisture diffusivity as a function of θ becomes,

$$D(\theta_x) = -\frac{1}{2}\frac{a^2}{b} sec^2\left(\frac{\theta_x}{b}\right)\left[c(\theta_x - \theta_i) - bln\left\{\frac{\cos\left(\frac{\theta_x}{b}\right)}{\cos\left(\frac{\theta_i}{b}\right)}\right\}\right] \qquad 5.8$$

5.4 Test Setup and Procedures

A diffusion cell, as depicted in Fig. 5.1, was fabricated to monitor the moisture movement from swollen WAP particles to dry soil. The diffusion cell consists of a 5 mm thick acrylic cylinder of internal diameter 20 mm and length 110 mm. One side of the cell was fixed with a base plate, and the other side of the cell was closed with a lid after placing the soil and polymer particles. The collected soils were first air-dried and sieved as per ASTM D2487 (2011) to consider the particle size finer than 2 mm. The air-dry soil samples were hand compacted to the diffusion cell up to a length of 80 mm, and then a 30 mm thick layer of swollen polymer particles was placed. The amount of swollen WAP was selected in such a manner that the used soil can able to achieve full saturation. Multiple duplicate samples were prepared for each of the used soil for the measurement of water content at different time intervals. The diffusion cells were dismantled after the predetermined time intervals, and soil samples at the soil-polymer interface and a distance of every 10 mm from the soil-polymer interface were scooped out to measure the gravimetric water content (*w*). The volumetric water content, θ (VWC), was then determined by multiplying the obtain *w* with the dry density (γ_d) of the packed soil. As per the boundary conditions, Fick's diffusion equation, as presented in Eq. 6, is valid for an infinite soil column. Therefore, the test procedure was carried out until

TH-2777_166104034

the moisture profile (i.e., wetting front) reaches the other end of the container. The advancement of the wetting front in BS is presented in Fig. 5.2 at different time intervals. It is evident from Fig. 5.2 that the moisture movement is governed by one-dimensional (1D) horizontal flow as the sample thickness is very less (20 mm). For each soil texture, three identical samples were prepared for a particular time interval for the assessment of the repeatability of the data points.

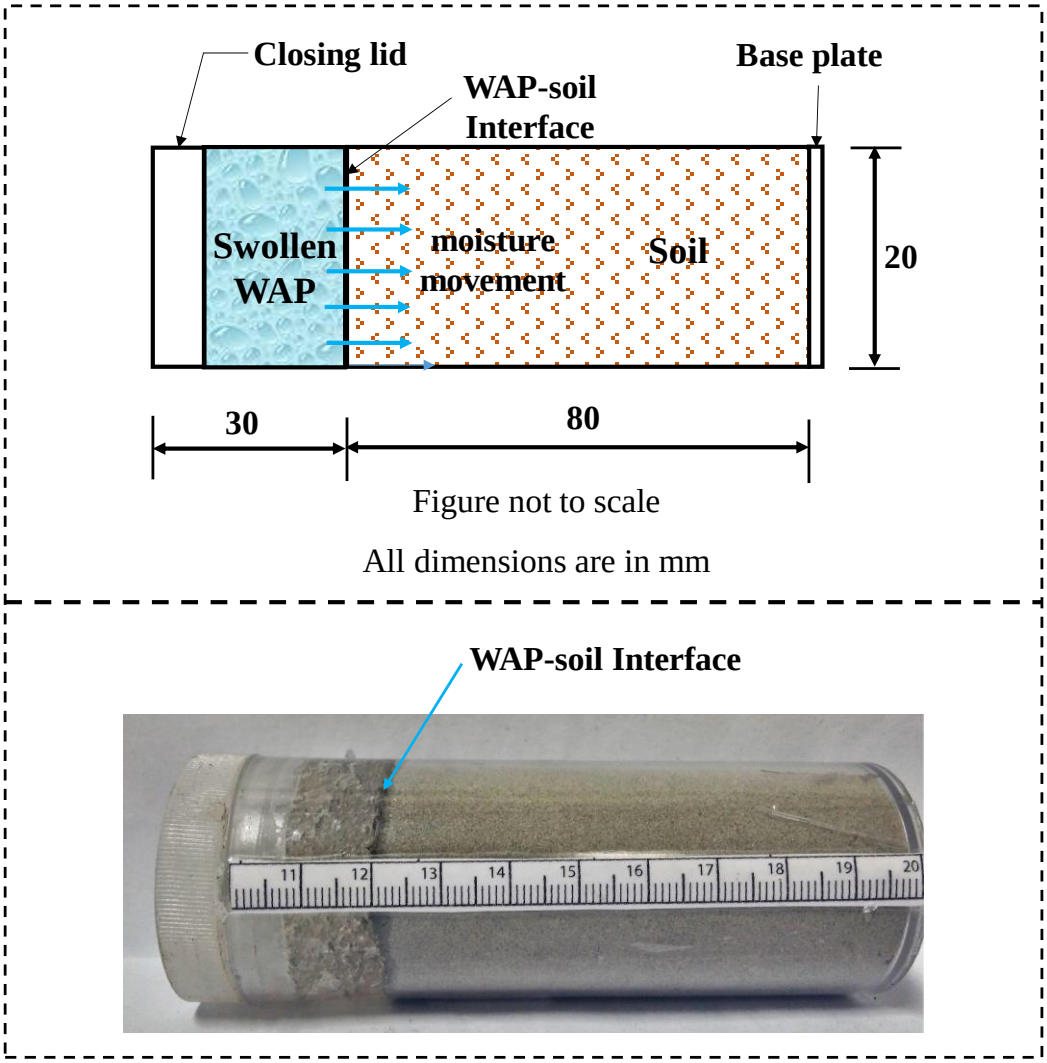

Fig. 5.1 Experimental setup for the measurement of moisture movement from swollen WAP to soil

5.5 Sorption mechanism of WAP

The moisture sorption kinetics of the used WAPs were used (as presented in Chapter 4) to characterize the moisture sorption mechanism of WAP. The moisture movement into the polymer network was described by modifying Eq. (5.3) to the following equation,

TH-2777_166104034

$$\ln\left(\frac{w_t}{w_e}\right) = \ln(k) + n \times ln\,(t) \qquad 5.9$$

Here w_e and w_t represent water absorbency at equilibrium condition and at time, t, respectively. To obtain the value of n and k parameter, the sorption kinetics data of Com-WAP and FA-WAP were plotted as $\ln\left(\frac{w_t}{w_e}\right)$ versus ln(t) [Fig. 5.3]. The diffusion parameters, n, and k were calculated from the slope and intercept of the plot and summarized in Table 5.1. It can be observed that the diffusion exponent (n) value remains the same in different swelling mediums (distilled and tap water) for a particular type of WAP. On the other hand, the characteristics constant (k) varies depending on the type of swelling medium, indicating that this value depends on the rate of water absorption in different swelling mediums. In the present study, n value of 0.5 was taken as the reference value to describe the transition from Fickian to non-Fickian diffusion as the particle size of the WAP was close to spherical and thin-film shaped. As it can be observed from Table 5.1, the n value exceeds 0.5 for all the cases (distilled and tap water as well as Com-WAP and FA-WAP). These results confirmed that the moisture moving into the polymer is dominated by non-Fickian diffusion, in which the polymer chain relaxation rate is higher than the moisture diffusion rate.

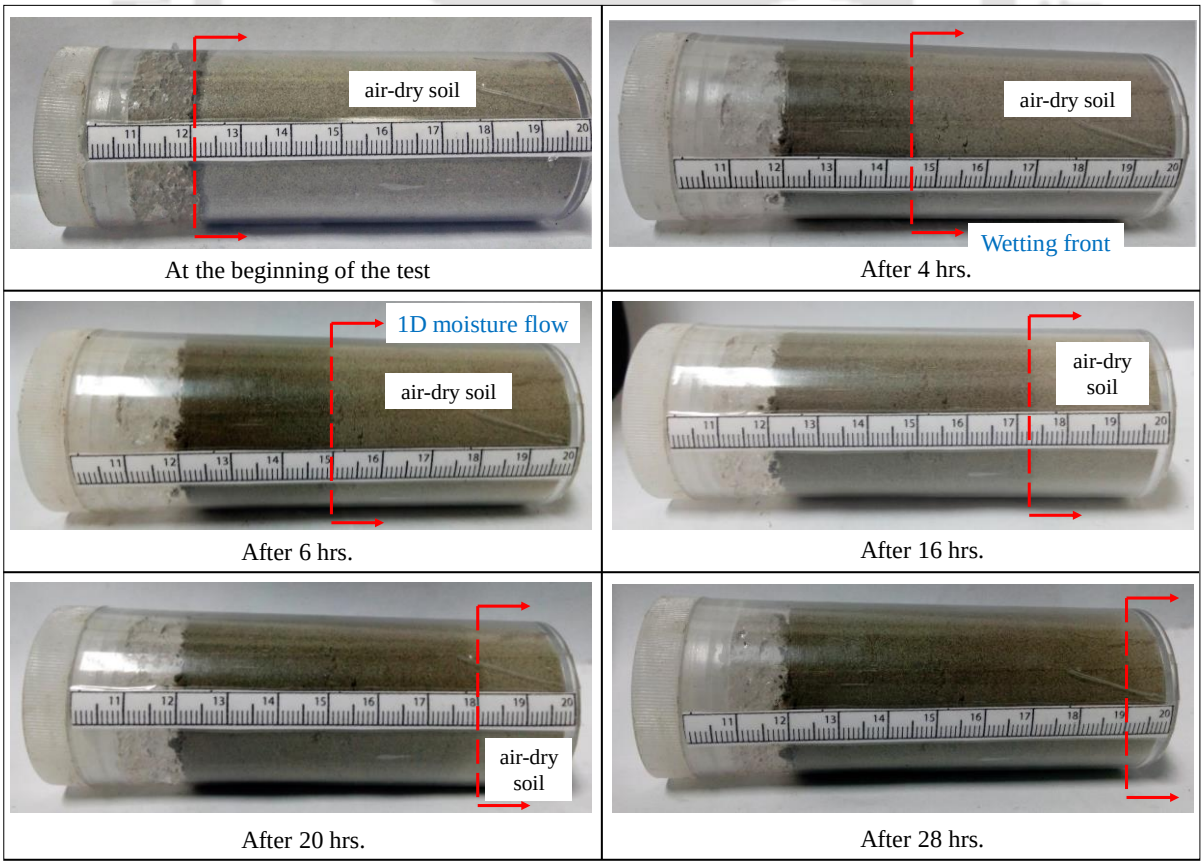

Fig. 5.2 Advancement of wetting front at different time intervals in BS for commercial WAP

TH-2777_166104034

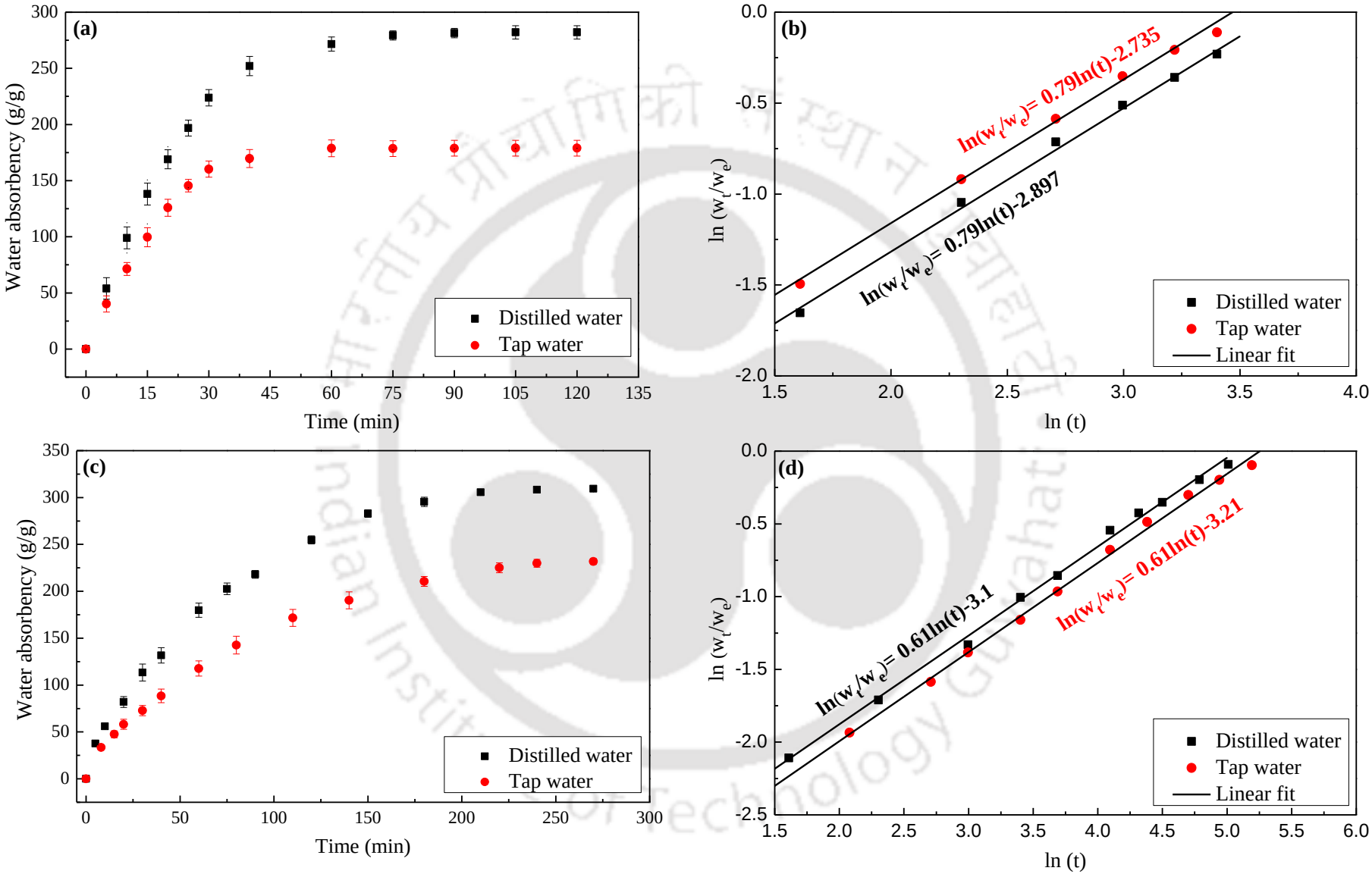

Fig. 5.3 Sorption kinetic of (a) Com-WAP, (c) FA-WAP, and moisture diffusion behavior (b) Com-WAP, (d) FA-WAP

TH-2777_166104034

Table 5.1 Details of the parameters for moisture diffusion into WAP particles

Diffusion parameters	Com-WAP		FA-WAP	
	Distilled water	Tap water	Distilled water	Tap water
Characteristic constant (k)	0.055	0.065	0.044	0.04
Diffusional exponent (n)	0.79	0.79	0.61	0.61
Correlation coefficient (R^2)	0.99	0.99	0.99	0.99

5.6 Moisture movement from swollen WAP to soil

The moisture movement from swollen WAP to soil was characterized by placing the swollen WAP and compacted soil sample side by side in a diffusion cell. The bulk density and the porosity of the hand compacted soils were determined with nine duplicate samples, which were further used to measure the moisture profiles at different time duration. The variability in the measured data was found very little for a particular type of soil, and the average of the nine values was reported in Table 5.2. The bulk densities decreased from 1.84 g/cc in FS to 1.65 g/cc in the RS, whereas the porosity values followed the opposite trend. This increase in porosity is attributed to the increase in clay percentage in the RS compared to the FS. As the inter-granular space between the individual grains is much more in the case of clay than sand, the porosity of clay is much higher than sand for the compacted sample. The theoretical saturated VWC (θ_s) [Table 5.2] of the used soils for the particular compaction state was calculated from the porosity value of the compacted sample as the porosity of soil at a fully saturated state represents θ_s.

Table 5.2 Details of the compaction properties of the used soils

Parameters		FS	BS	RS
Compaction properties	Bulk density (g/cc)	1.8	1.75	1.6
	Dry density (g/cc)	1.78	1.7	1.5
	Void ratio (e)	0.49	0.61	0.79
	Porosity (n)	0.33	0.38	0.44
Saturated VWC (θ_s)		0.33	0.38	0.44

The variation wetting front distance (x_f), as obtained by visual inspection of the sample, at different time intervals for the used three soils, were presented in Fig 5.4-5.6. As it can be observed, the wetting front advancement in FS was 7.6 cm after 32 hrs with Com-WAP, whereas the wetting front advancement was 7.7 after 12 hrs with FA-WAP. A similar trend of

TH-2777_166104034

higher wetting front advancement with FA-WAP as compared to Com-WAP was observed for the other two soils. These results indicate that FA-WAP can quickly release the stored water into the dry soil. The measured wetting front distances at different time intervals were fitted to the power curve (Eq. 5.10) to quantify the time duration after which the wetting front touches the other end of the cell.

$$x_f = pt^q \qquad 5.10$$

Here, p and q are two empirical constants, which were obtained from the measured data. It can be noted that the value of q parameter remains the same (q=0.5) for all the cases, whereas the p parameter varies depending on the WAP type and soil texture. The higher value of p parameter denotes a higher water front advancement rate. The wetting front reached the other end of the cell after 13.1 hrs, 13.3 hrs, and 36.8 hrs from the beginning of the test in FS, BS, and RS, respectively with FA-WAP, which is much less as compared to Com-WAP. It was observed that the advancement rate of the wetting front decreases as the soil becomes finer, which is in good agreement with the previous studies (Liu et al. 2009; Villarreal et al. 2019). Based on these values, the measurement of soil moisture profiles was continued until the wetting front touches the other part of the cell.

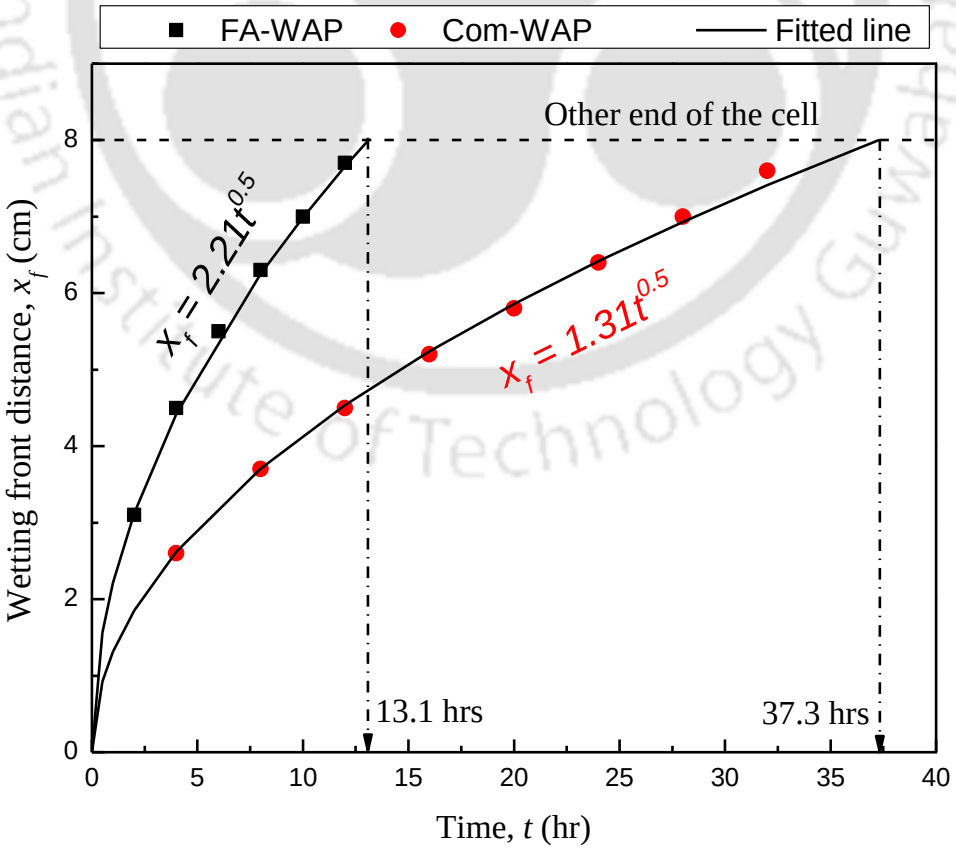

Fig. 5.4 Variation of wetting front distance with time for FS

TH-2777_166104034

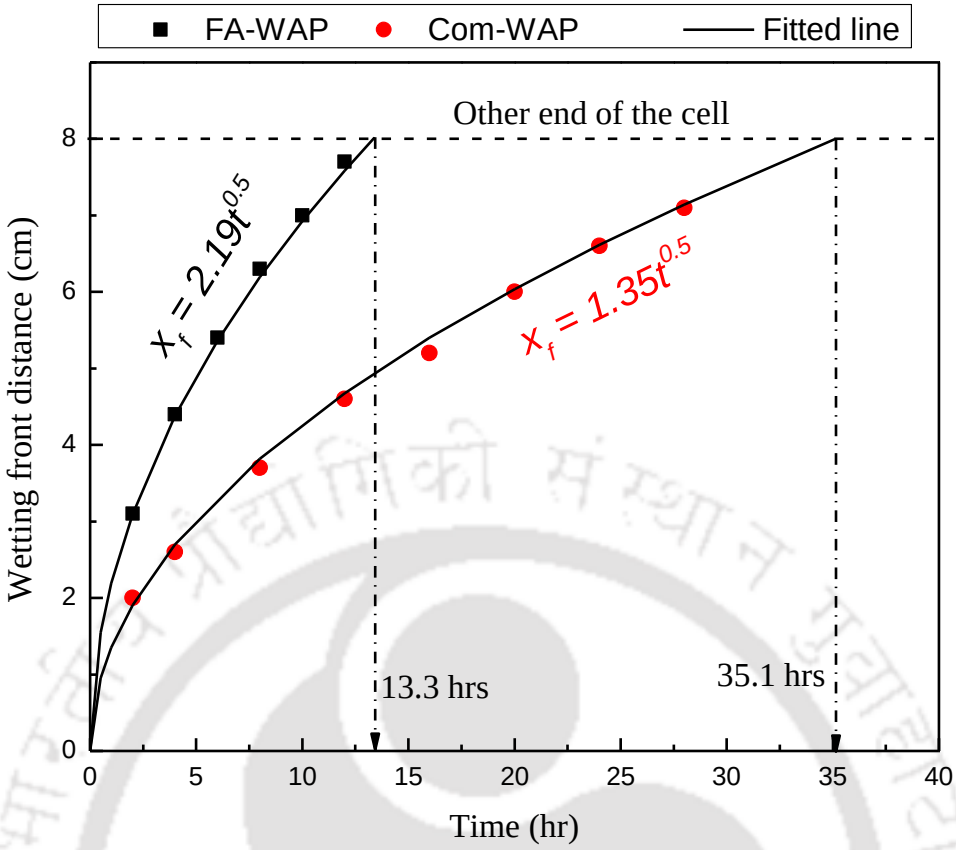

Fig. 5.5 Variation of wetting front distance with time for BS

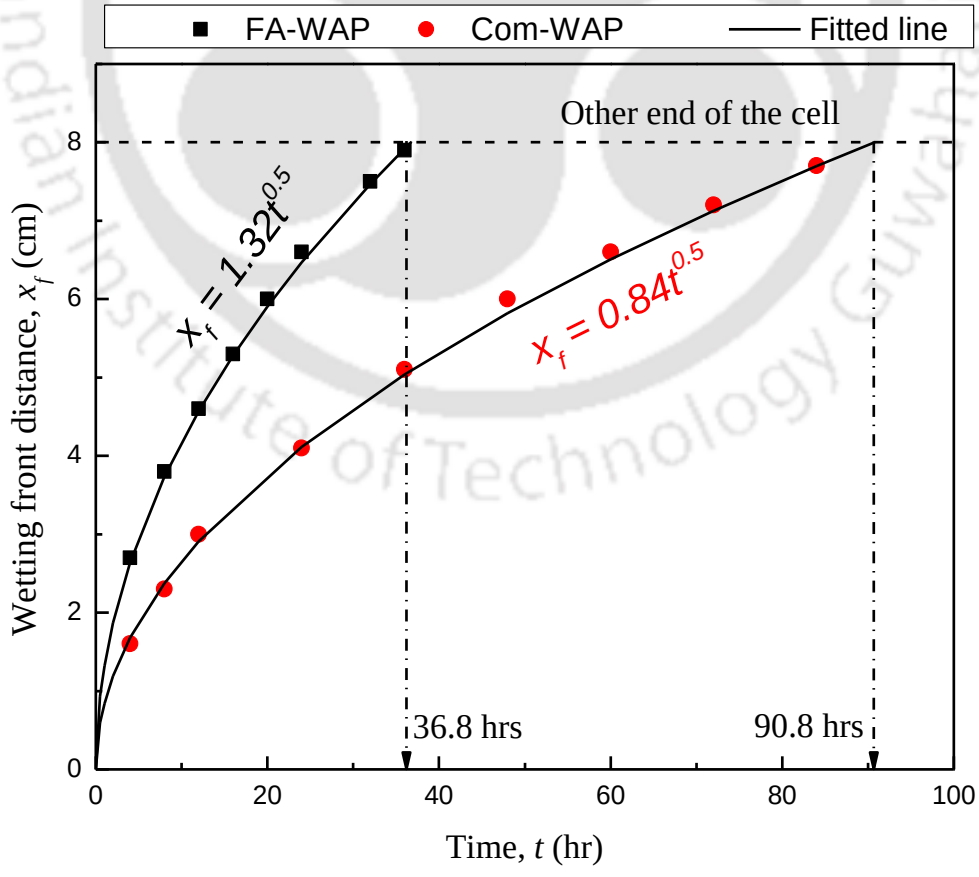

Fig. 5.6 Variation of wetting front distance with time for RS

TH-2777_166104034

The observed horizontal moisture profiles at different time intervals for the used three soils with both the WAPs were presented in Fig. 5.7 and 5.8. These figures also indicated the movement of moisture from the swollen polymer particle to the dry soil. As time progresses, soil present at the interface and different locations from the interface slowly absorbs water from the swollen WAP and reaches the near-saturated state. It can be noted that the moisture profiles were measured up to 32 hrs in both FS and BS, and 84 hrs for RS with Com-WAP. Similarly, the moisture profiles were measured up to 12 hrs in both FS and BS, and 36 hrs for RS with FA-WAP.

Figure 5.9 represents the degree of saturation achieved by soil particles present at different locations from the interface for the used three soils with both the WAPs. With the increase in VWC of the WAP-soil interface, the soils present at the different locations absorb moisture from the interface. It can be observed that a maximum saturation degree of 97% was achieved in FS with FA-WAP till the wetting front reached the other end of the cell, whereas the maximum saturation degree achieved in RS was 99%. However, the maximum degree of saturation in FS, BS, and RS were only 75%, 77%, and 92% with Com-WAP. Similarly, the saturation degree was higher with FA-WAP as compared to Com-WAP at any time duration for a certain soil texture. The moisture movement from swollen WAP to soil is governed by both soil and WAP properties. It was clear from the previous section that FA-WAP can release more quickly as compared to Com-WAP. The moisture movement through horizontal soil column is governed by two parameters, including the easiness of water transmittance through the soil, which is represented by hydraulic conductivity and the potential energy gradient. The hydraulic conductivity of the soil with higher clay content is low due to a highly tortuous flow path. On the other hand, coarse-grained soils have relatively larger pore-space and lower tortuosity factors that facilitate rapid moisture movement (ref. Fig. 5.10). Due to this reason, the wetting front advancement through the soil matrix is generally lower in the case of soil with high clay content. On the other hand, the amount of moisture absorbed (or degree of saturation) is a function of the potential energy gradient between dry soil and swollen WAP. Because of the higher clay content and smaller pore structure in RS, the negative pore pressure (known as soil suction) is much higher in dry RS as compared to dry FS and BS. This could result in a higher energy gradient between RS and swollen WAP, leading to an increased VWC in RS as compared to the other two soils. Due to this higher energy gradient, RS can absorb and retain more water as compared to the other soils, and this phenomenon was reflected by the degree of saturation value of the soil samples at the end of the test.

TH-2777_166104034

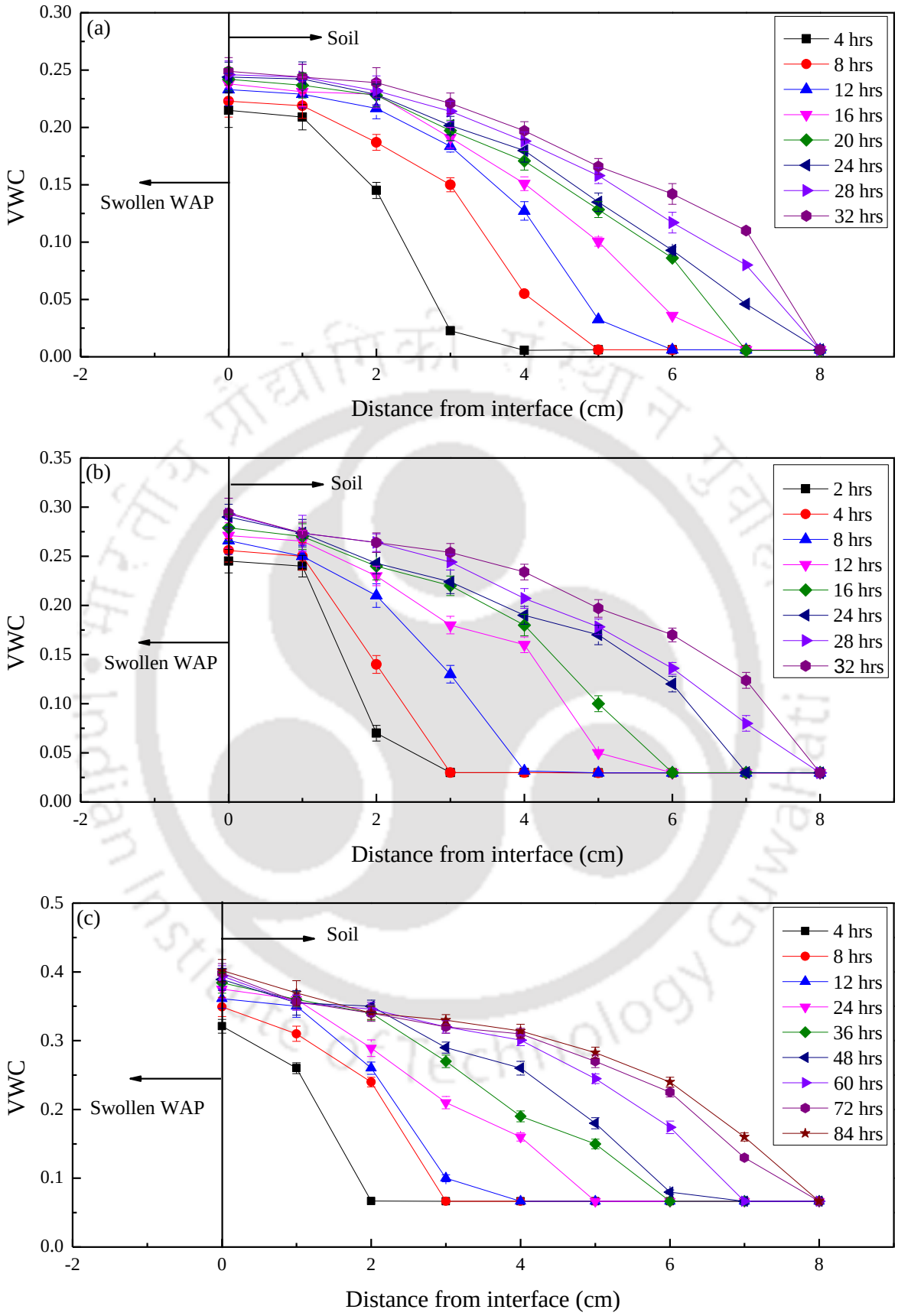

Fig. 5.7 Measured moisture profiles through (a) FS, (b) BS, and (c) RS at different time intervals with Com-WAP

TH-2777_166104034

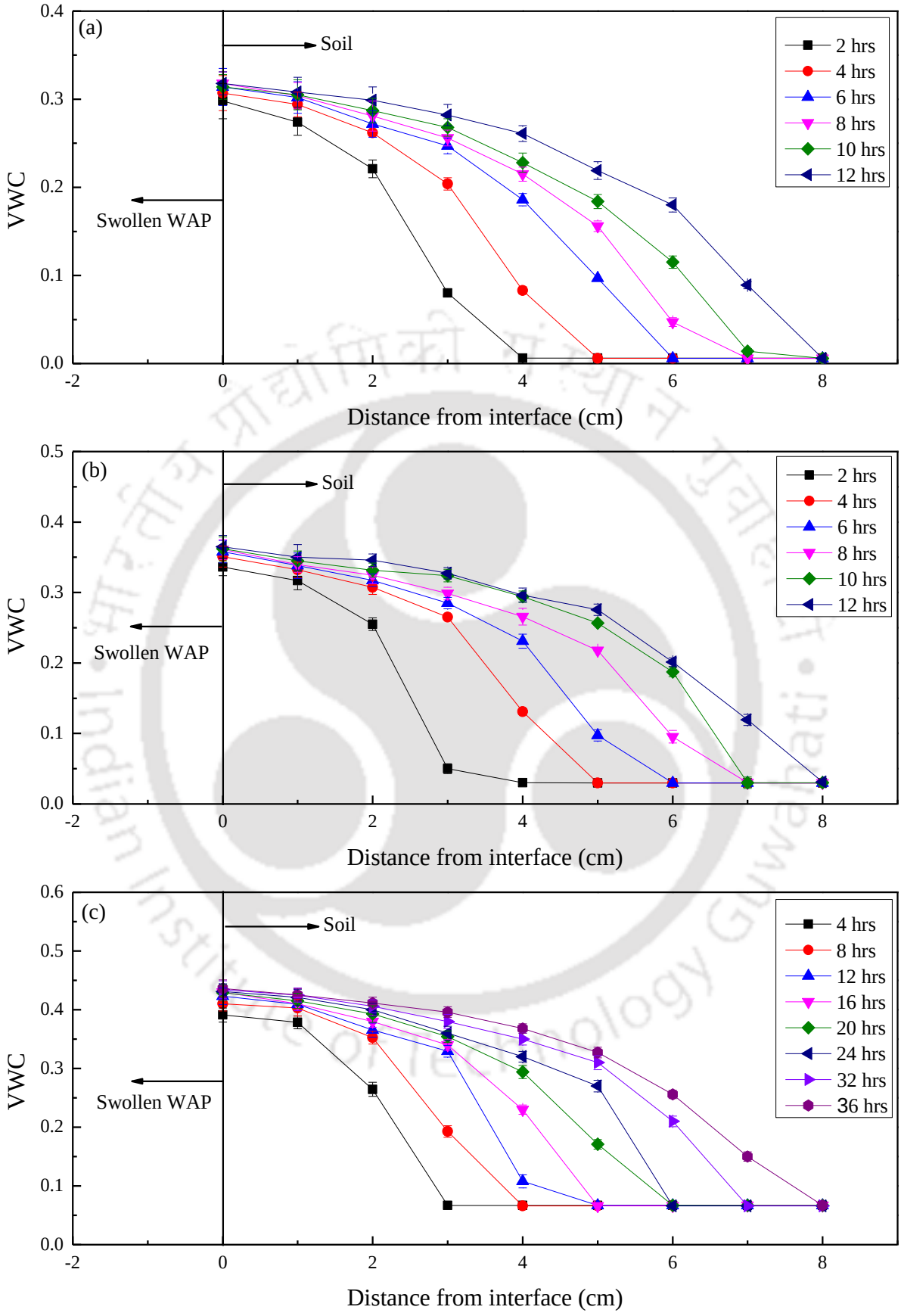

Fig. 5.8 Measured moisture profiles through (a) FS, (b) BS, and (c) RS at different time intervals with FA-WAP

TH-2777_166104034

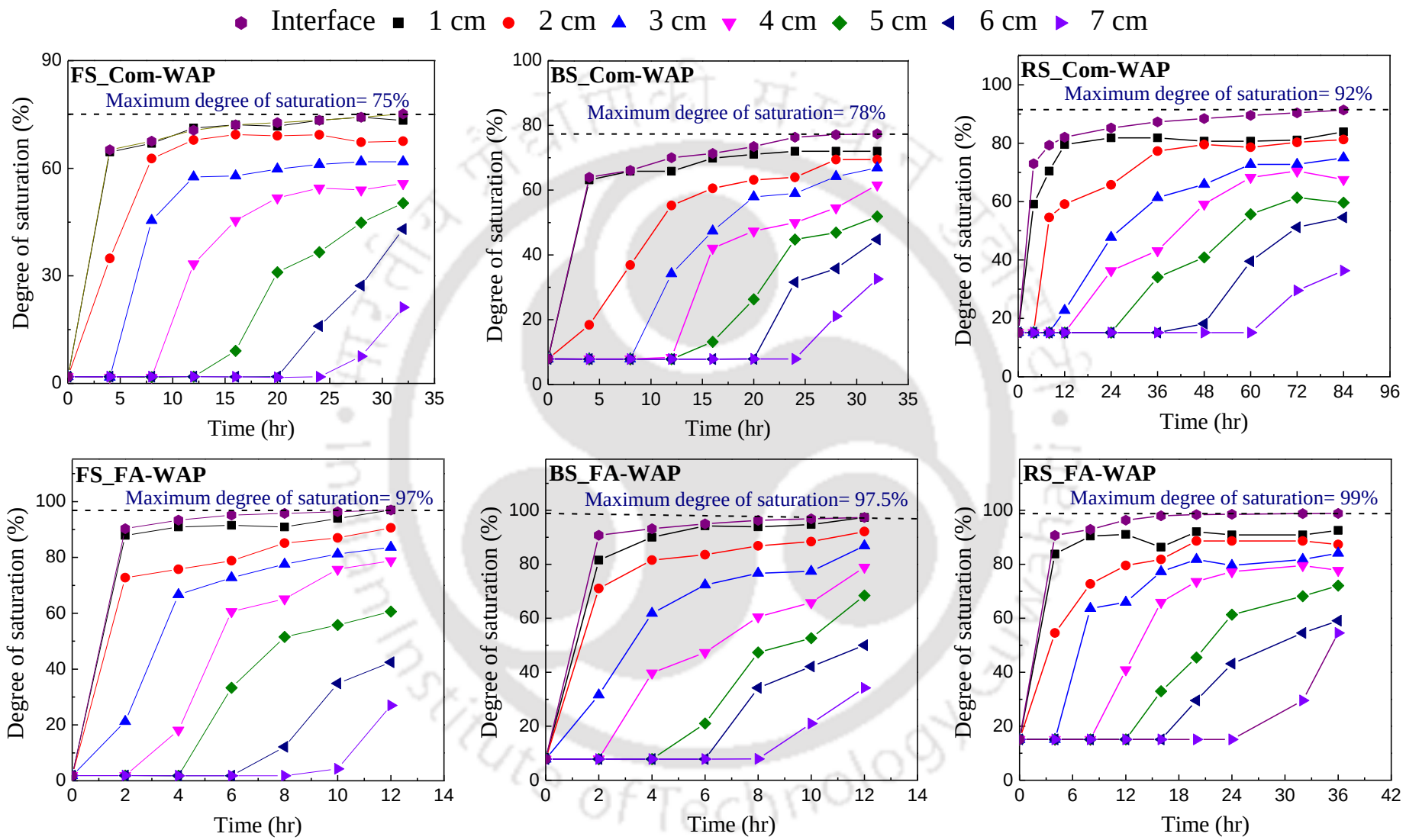

Fig. 5.9 Comparison of degree of saturation achieved by soil at different locations from the WAP-soil interface

TH-2777_166104034

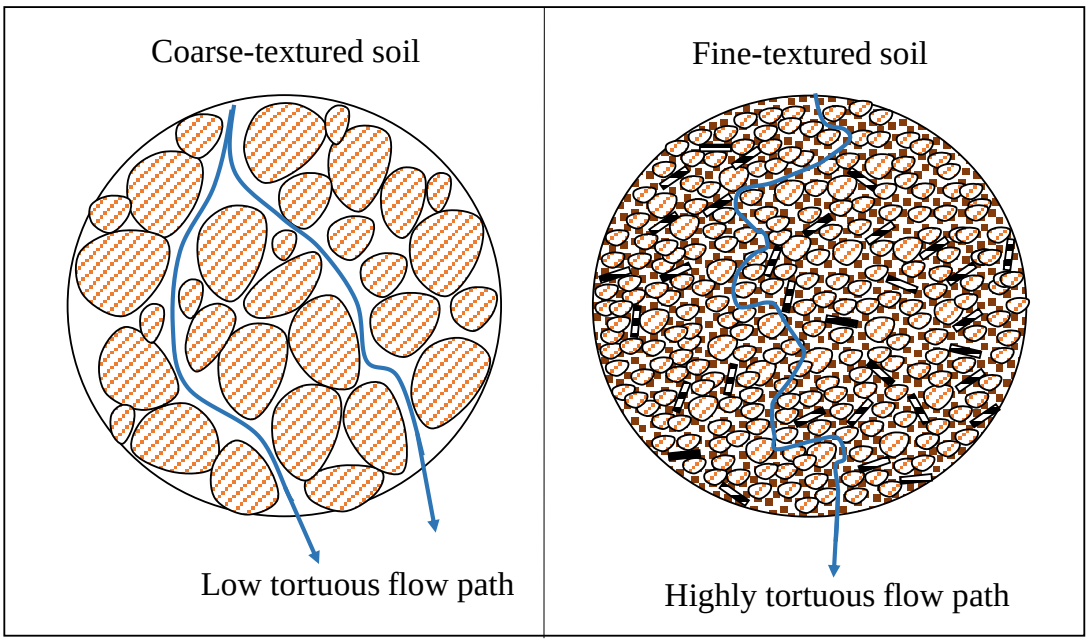

Fig. 5.10 Difference in the moisture flow path in different textured soils

To test the validity and applicability of the diffusivity theory for the description of the moisture movement, the measured θ was plotted versus the Boltzmann function λ for the used soils (Fig. 5.8 and Fig. 5.9). It can be seen from these figures that for each of the soils, θ vs. λ relationship obtained at different distances from the interface were coinciding with each other, which means that θ is a unique function of λ. Therefore, the diffusivity equation is valid for moisture movement from WAP to the dry soil.

The proposed tangential equation (Eq. 5.7) was fitted to the measured experiment data (Fig. 5.11 and Fig. 5.12), and the *a*, *b*, and *c* parameter was obtained (Table 5.3) using nonlinear regression analysis to represent λ as a function of θ. It can be noted that the value of three parameters (*a*, *b*, and *c*) are valid for a particular range of water content, as presented in Table 5.3. It may be noted that the value of fitting parameters (*a*, *b*, and *c*) for Com-WAP are valid for the range $0.007 < \theta < 0.25$, $0.03 < \theta < 0.28$ and $0.07 < \theta < 0.36$ for FS, BS, and RS, respectively as the boundary condition of the diffusion equation exceed after the mentioned range. On the other hand, the value of fitting parameters for FA-WAP are valid for the range $0.007 < \theta < 0.32$, $0.03 < \theta < 0.36$ and $0.07 < \theta < 0.42$ for FS, BS, and RS, respectively. It was reported in the previous studies that the high error in the moisture diffusivity value could be observed in the near-saturated zone as moisture diffusivity becomes very sensitive to the change in soil moisture with λ in this zone (Clothier et al. 1983; Villarreal et al. 2019). Therefore, the proposed horizontal absorption method is inadequate to obtain soil moisture diffusivity values in the near-saturated zone.

TH-2777_166104034

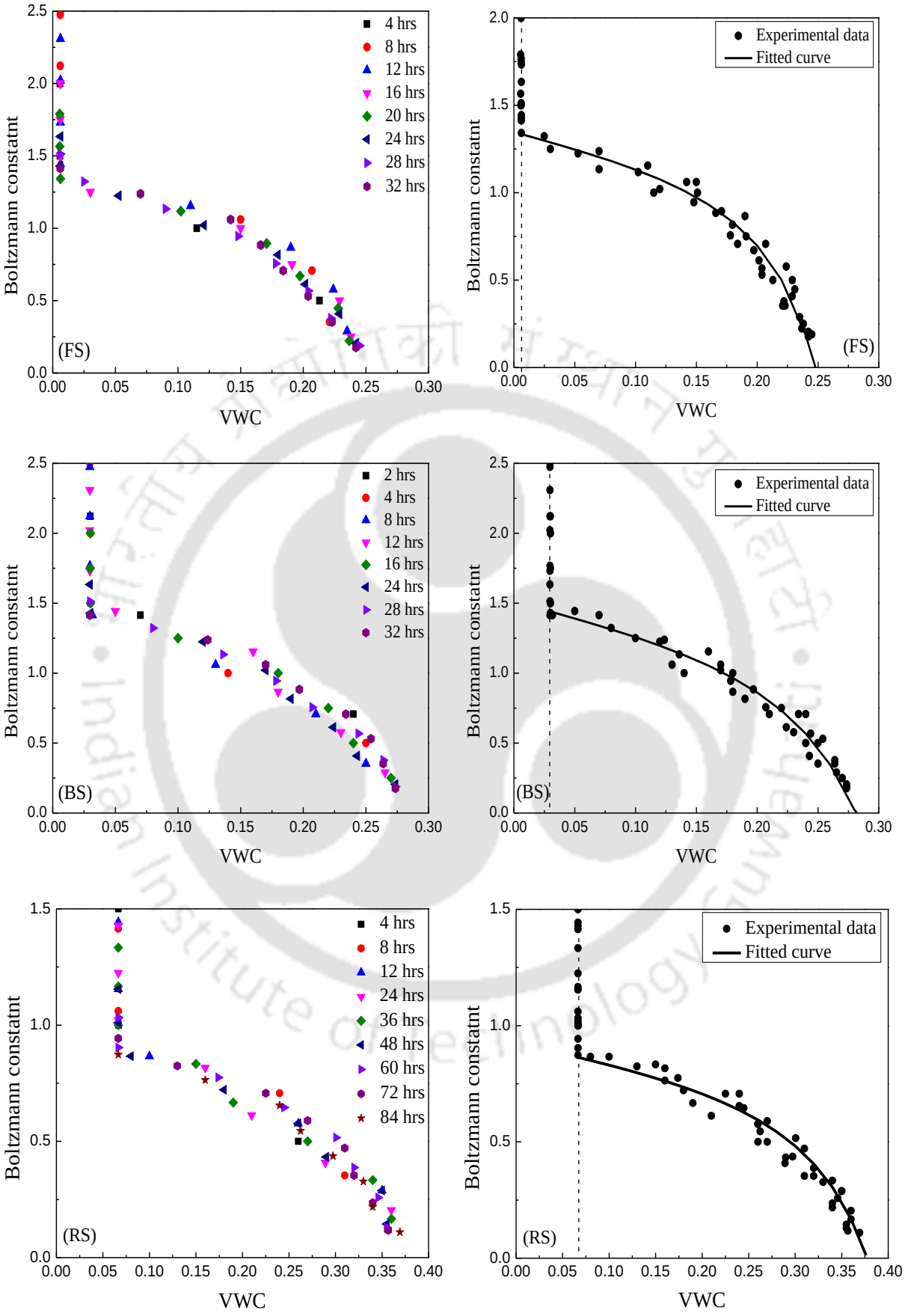

Fig. 5.11 Boltzmann constant variation with VWC for the used soils with Com-WAP

TH-2777_166104034

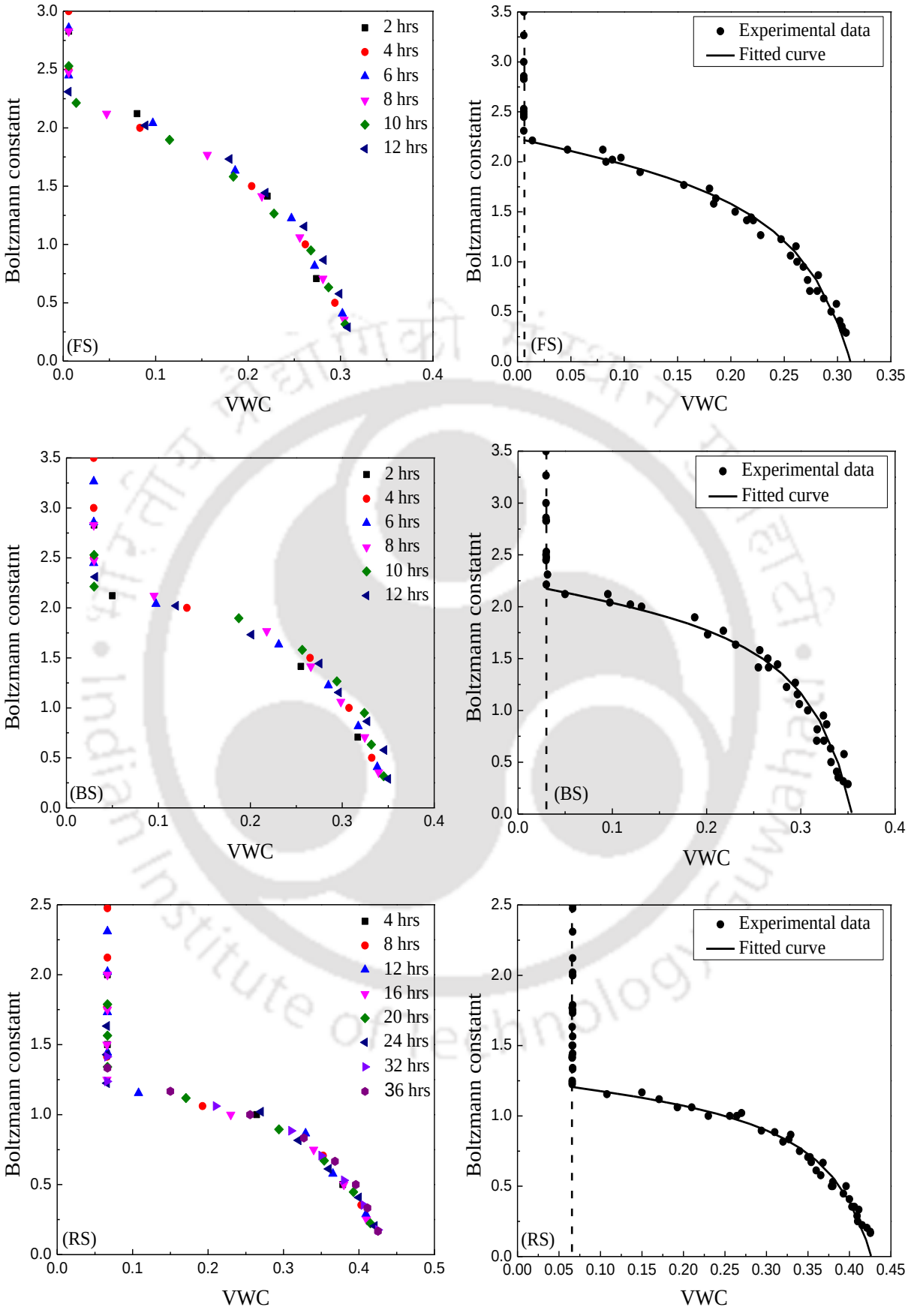

Fig. 5.12 Boltzmann constant variation with VWC for the used soils with FA-WAP

TH-2777_166104034

Table 5.3 Summary of the parameters related to moisture diffusion through soil

Diffusion parameter	FS		BS		RS	
	Com-WAP	FA-WAP	Com-WAP	FA-WAP	Com-WAP	FA-WAP
a	-0.4	-0.48	-0.45	-0.53	-0.42	-0.54
b	0.19	0.23	0.22	0.27	0.31	0.36
c	-3.45	-4.45	-3.31	-4.29	-2.54	-2.69
R^2	0.97	0.99	0.96	0.99	0.97	0.99
RMSE	0.05	0.04	0.06	0.04	0.04	0.03

The moisture diffusivity value as a function of VWC [$D(\theta)$] for the used soils, as obtained with two different WAP, were calculated from the obtained fitting parameters using Eq. 8 and presented in Fig. 5.13. The trend of the obtained moisture diffusivity curve is in good agreement with the several authors (Clothier et al. 1983; Evangelides et al. 2010; Han et al. 2013; Ma et al. 2016; Villarreal et al. 2019) that reported an exponential relationship between moisture diffusivity and VWC. It was also observed that the particle size distribution of soil and pore characteristics significantly influence the moisture diffusivity function. The diffusivity value corresponding to a particular VWC is higher for FS as compared to BS and RS. This is attributed to the higher pore-space and lesser tortuous flow path for FS than BS and RS, as discussed above. Another important observation is that the moisture diffusion curves obtained with different WAPs are almost similar for the same soil texture, indicating that the moisture diffusivity value of soil is governed by the soil properties.

The moisture diffusivity values obtained from the present study (with FA-WAP) were further compared with the moisture diffusivity value reported in the past literature (obtained with the traditional horizontal water infiltration test of soil column) in Fig. 5.14. As it can be observed, the moisture diffusivity values are in a good match (i.e., same order of magnitude) with the literature reported data (Selim et al. 1970; Evangelides et al. 2010; Espejo et al. 2014; Li et al. 2017). It may be noted that there is considerable difference in packing density between the literature-reported diffusivity value and the present study. Therefore, some difference in the moisture diffusivity values can be observed. These results clearly suggest that the addition of WAP in the soil is as good as a mini-water reservoir in the soil matrix from which moisture can slowly diffuse into the dry soil.

TH-2777_166104034

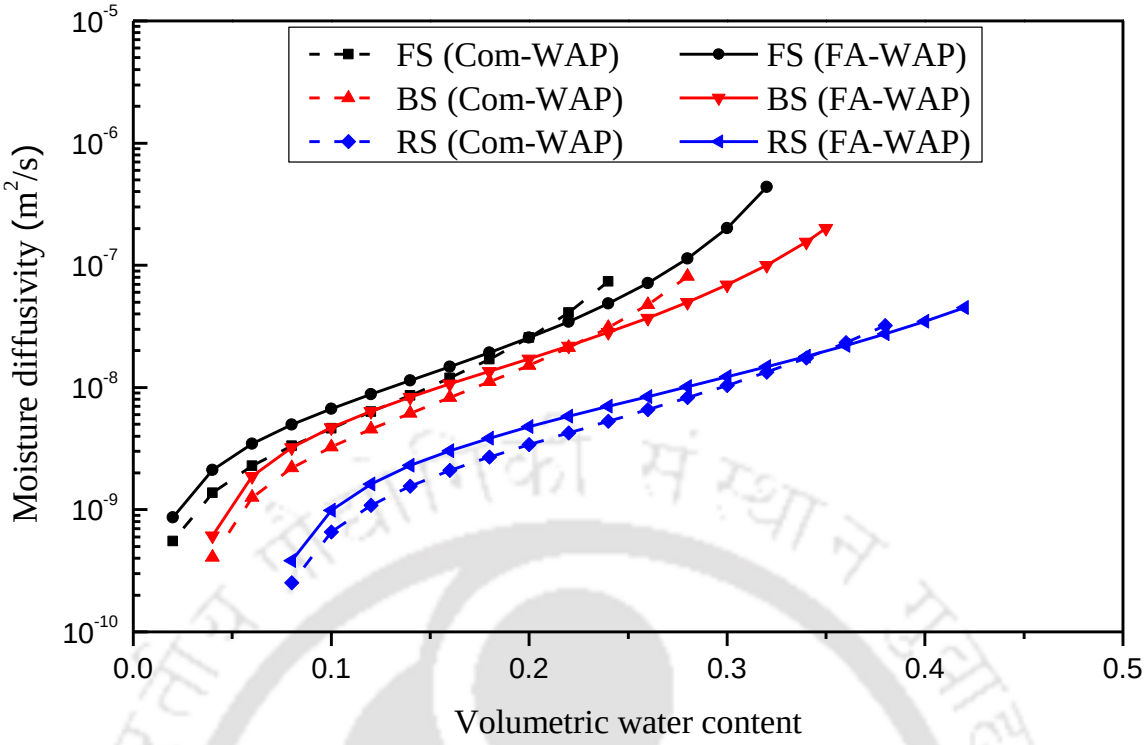

Fig. 5.13 Soil moisture diffusivity as a function of VWC obtained in the present study

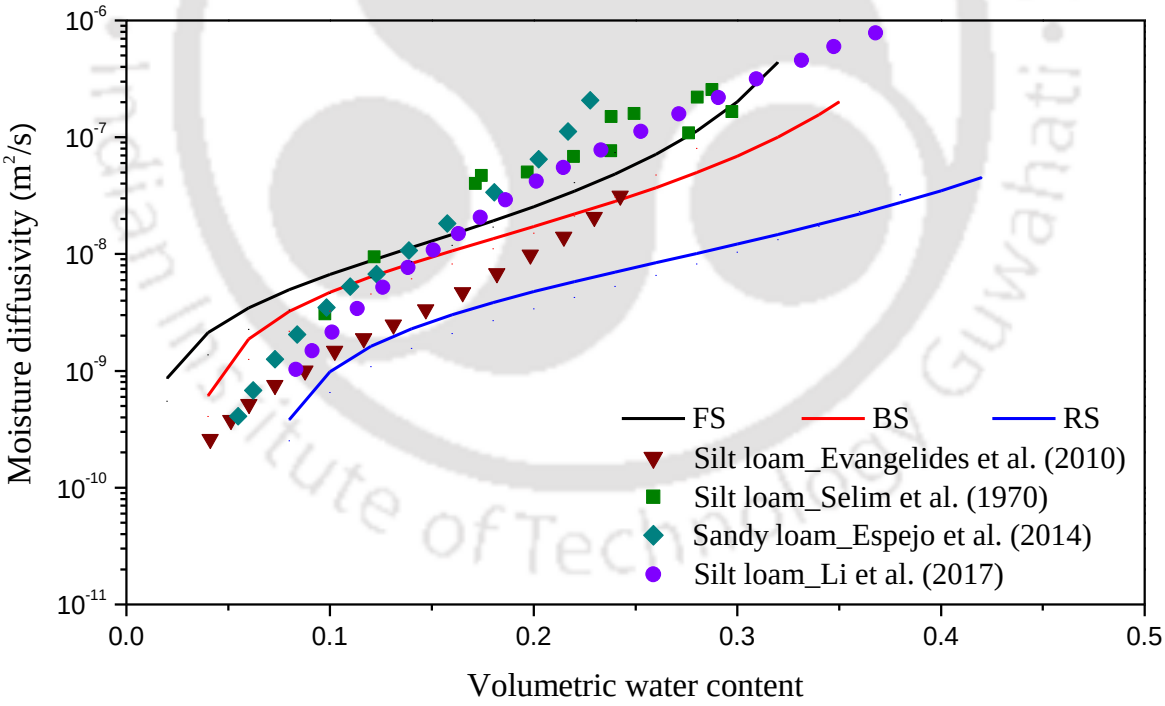

Fig. 5.14 Comparison of the obtained soil moisture diffusion value with the literature data

5.7 Moisture desorption from swollen WAP

For a better understanding of the higher rate of water front advancement (which is dependent on the WAP characteristics), the moisture desorption kinetics of the WAPs were

TH-2777_166104034

measured at different time intervals for the used soils. To establish the moisture desorption kinetic of WAP in soil, the weight of the remaining swollen WAP was taken (by dismantling the diffusion cell) after certain intervals of time and presented in Fig. 5.15 for the used soils. It is quite evident from the figure that the moisture desorption rate was higher in FA-WAP as compared to the commercial WAP. The dry soil particles can easily draw water from the FA-WAP, which could be an additional advantage under water stress conditions. The moisture desorption rate was very high at the beginning due to a higher energy gradient in the dry soil and swollen WAP. As the soil samples absorbed the moisture, the difference in the energy gradient reduced, leading to a decrease in the release rate. It may be noted that the moisture desorption curve matches with one another for both the WAPs as the water content of the soil column reaches to near-saturated state.

A moisture desorption isotherm, as proposed by Peleg (1988), was used to describe the moisture desorption kinetics of swollen WAP. The two-parameter mathematical model (Eq. 5.11) was fitted to the measured desorption data for further analysis.

$$w_t = w_0 - \frac{t}{k_1 + k_2 t} \qquad 5.11$$

Here, w_0 is the initial weight of the swollen WAP; w_t is the weight of swollen WAP after time t; k_1 and k_2 are the kinetic constant and characteristic constant, respectively.

The obtained model parameters k_1 and k_2, along with the R^2 value and RMSE value for the fitting, were presented in Table 5.4. It can be observed that the characteristic constant (k_2) depends on the soil type, whereas the kinetic constant (k_1) depends on the WAP type. Based on these above observations, it is quite evident that the FA-WAP is more effective than Com-WAP for moisture transfer to dry soil under water stress conditions.

Table 5.4 Details of the desorption kinetic model parameters

Parameters		k_1	k_2	R^2	RMSE
FS	Commercial WAP	0.6	0.055	0.99	0.61
	FA-WAP	0.25	0.056	0.99	0.65
BS	Commercial WAP	0.55	0.039	0.99	0.76
	FA-WAP	0.26	0.04	0.99	0.42
RS	Commercial WAP	0.57	0.034	0.99	0.68
	FA-WAP	0.32	0.034	0.99	0.82

TH-2777_166104034

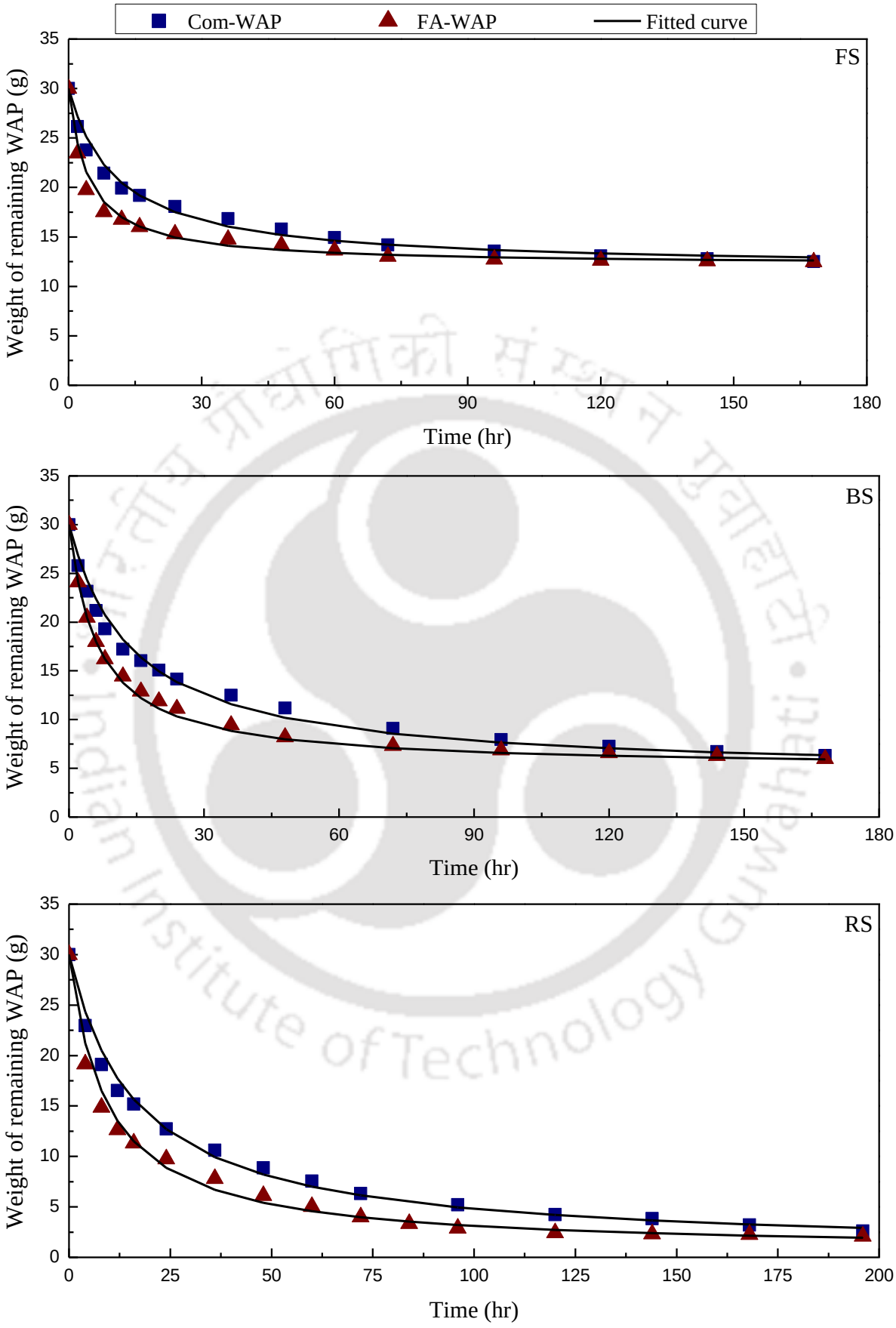

Fig. 5.15 Moisture desorption kinetics of the used WAPs in different soils

TH-2777_166104034

5.8 Summary

This chapter presents a simple and efficient laboratory method to characterize the moisture sorption of water absorbing polymer (WAP) and its movement mechanism from the swollen WAP particle to soil particle in the WAP-soil system is proposed. The moisture sorption mechanism of WAP was characterized from the measured swelling kinetics of both the WAP in distilled and tap water. The mathematical analysis of the moisture sorption kinetics indicated that the moisture transport into the polymer network is governed by non-Fickian diffusion mechanism, in which the polymer chain relaxation rate is higher than the water diffusion rate.

The water transfer mechanism from swollen WAP to dry soil was characterized by conducting a horizontal absorption experiment in a diffusion cell with WAP and soil placed in contact with each other. The wetting front advancement in the soil column was obtained by visual inspection of the sample using both the WAPs. The time required for wetting front to reach the other end of the cell is much less in FA-WAP as compared to Com-WAP for the used soils. The classic method of Bruce and Klute (1956) was followed to obtain the moisture profiles (VWC variation with time) of the horizontal soil column in contact with the swollen WAP. The experimental results presented in terms of VWC and Boltzmann constant (λ) for three different textured soils verified the moisture movement through the soil column is governed by the Fickian diffusion mechanism. Hence, the moisture diffusivity equation was employed to obtain the diffusivity function for the used soils with different WAPs. A tangential equation was proposed to describe the variation of VWC with λ, which was further used to calculate the moisture diffusivity function in terms of VWC. It was observed that the moisture diffusivity value largely depends on the soil texture and soil pore structure. Sand (FS) has the highest moisture diffusivity values as compared to the silt loam (BS) and clay loam (RS) due to the higher available pore space between sand particles. However, the moisture diffusivity function was found more or less similar for both the WAP (synthesized and commercial), indicating the fact that the diffusivity function is independent of WAP type.

The moisture desorption kinetic from swollen WAP to soil was evaluated to understand the moisture release rate from swollen WAP. The measurement was carried out in the same diffusion cell, in which the weight of the remaining quantity of WAP at different time intervals. The results indicated a higher rate of moisture released from the synthesized FA-WAP as compared to commercial WAP. This quick release of moisture from FA-WAP could be an added advantage during water stress conditions.

TH-2777_166104034

Chapter 6

Performance evaluation of suction and moisture sensors

6.1 General

Accurate measurement of soil suction and volumetric water content (VWC) is key for the reliable measurement of water retention characteristic curve (WRCC) of WAP amended soil. WRCC is an essential input parameter for the estimation of soil-water storage, flow characteristics of WAP amended soils. Moreover, some of the important physical properties of soil, including field capacity (FC), permanent wilting point (PWP), and plant available water content (PAWC), can be obtained from the measured WRCC of soils. A knowledge of soil-water content at FC and PWP is extremely important to assess the irrigation water requirement, irrigation scheduling, and modeling the solute transport through the soil.

6.2 Performance evaluation of TEROS21

The capacitance sensor, TEROS21 (METER Group, USA), with manufacturer specified measurement limit of 10^5 kPa, holds promise in field monitoring of suction. However, not many studies exist in the literature that evaluates the applicability of this capacitance sensor (TEROS21) for a wide range of suction measurement. Therefore, it is essential to evaluate the performance of TEROS21 for suction measurement in the used soils under controlled laboratory conditions to ensure its applicability for field instrumentation in the WAP amended soil. According to the available literature (Operator's manual, TEROS21), the capacitance sensor adopts a six-point calibration technique where five points are within 100 kPa in comparison with a tensiometer. The sixth point corresponds to the sensor placed in the air, assuming the suction to be 10^5 kPa. This gross assumption may or may not be valid for the measurement of high suction in soils accurately. There are no studies in the literature that verifies the preciseness of TEROS21 for suction greater than 100 kPa by comparing it with established measurement methods (Operator's manual, TEROS21).

6.2.1 Test plan and procedure

In the present study, the accuracy of TEROS21 up to 80 kPa was established by comparing the measurements with a well-established T5 miniature tensiometer. For suction greater than 80 kPa, the TEROS21 measurements were compared with the relative humidity (RH) based dew point potentiameter (WP4C). It is a known fact that WP4C measures total soil suction (ψ), which is a combination of matric suction (ψ_m) and osmotic suction (ψ_o). For a

TH-2777_166104034

meaningful comparison of TEROS21 and WP4C, it is important to prove that there is no osmotic suction measured by the latter. It is established in the literature that osmotic suction of soil is attributed to the dissolved salt present in the pore solution (Krahn and Fredlund 1972; Abedi-Koupai et al. 2008; Tripathy et al. 2016). Therefore, repeated washing of the soils (BS, RS) was done with deionized water to nullify the measurable osmotic suction, as reported in the literature (Sreedeep and Singh 2006; Sreedeep and Singh 2011; Abhijit and Sreedeep 2015).

Soil washing was performed by mixing the soil with deionized water to achieve a dilution ratio (DR, which is liquid to solid ratio) of 2. The slurry was continuously stirred for 24 hours and filtered through Whatman's No. 42 filter paper. The filtrate was analyzed for electrical conductivity (EC) to verify the presence of dissolved salts. The process of washing was repeated until the filtrate exhibited a negligible value of EC (< 1 mS/cm) and osmotic suction. The results of soil washing are presented in Table 6.1. It can be noted that the EC of the pore solutions becomes negligible by 4th washing, which is indicative that both the soils are free from the influence of dissolved salts.

Table 6.1 Details of soil washing with deionized water

Washing	Cumulative DR		EC (mS/cm)	
	BS	RS	BS	RS
1	2	2	5.4	7.6
2	4	4	2.1	3.2
3	6	6	0.9	1.2
4	8	8	0.5	0.8
5	10	10	0.4	0.6
6	12	12	0.4	0.6

For further verification, the osmotic suction of the filtrate after every washing (obtained from RS) was measured by WP4C and presented in Fig. 6.1. By third washing, the osmotic suction dropped down to the lower measurement limit of WP4C. This indicates that beyond third washing, the total suction measured by WP4C does not include osmotic suction. To prove this point emphatically, the osmotic suction of a known concentration of NaCl salt solution was measured using WP4C and plotted as a function of EC, as shown in Fig. 6.1. It is worth noting that a low concentration of the salt solution (< 0.02 M) gave osmotic suction equal to the lower limit of WP4C measurement. The results are in good agreement with the USDA

TH-2777_166104034

handbook (Richards 1954) for measuring osmotic suction in saline soil. It was reported that the osmotic suction is 22 kPa for a pore solution with EC equal to 0.6 mS/cm, which is comparable with the results from this study. It is explicit that osmotic suction measured using WP4C is not sensitive to the salt concentration below 0.02 M (corresponding EC value 2.5 mS/cm). Comparing both the figures depicted in Fig. 6.1, it can be concluded that beyond EC <2.5 mS/cm, the osmotic suction measured by WP4C for both the soils are negligible. In all our subsequent WP4C measurements, the soil samples after 6th washing were used for reliable comparison with TEROS21 measurements.

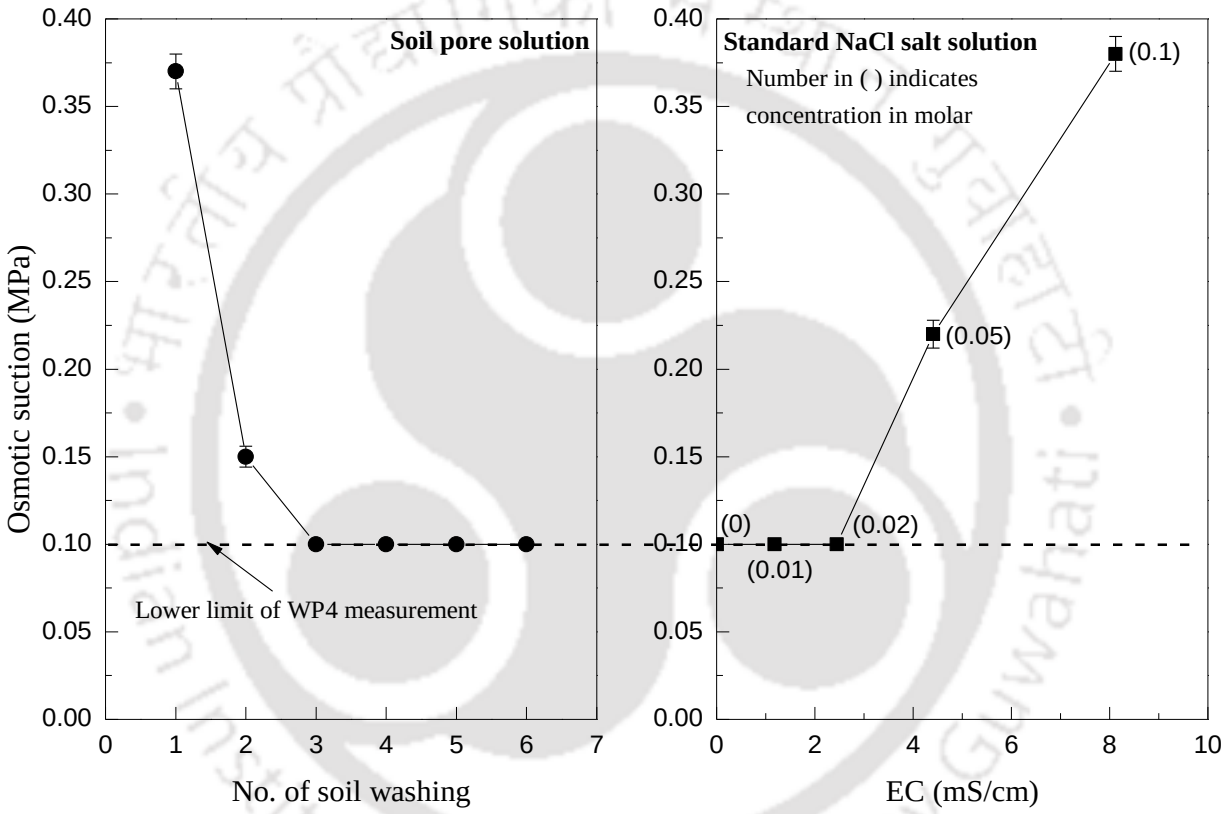

Fig. 6.1 Osmotic suction of soil-pore solution (RS) after soil washing and standard NaCl solution

The washed soil samples (BS, RS) were mixed with sufficient amounts of deionized water to obtain a high-water content close to the liquid limit for ensuring suction close to zero as the initial point. The mixed sample was placed in an airtight chamber for three days for the uniform distribution of water content. The wet samples were placed in a PVC container of 20 cm diameter and TEROS21, 5TM sensors inserted into the soil, as shown in Fig. 6.2. Special care was taken to place the ceramic tip of T5, TEROS21, and 5TM at the same level to avoid any influence of locational variability. The whole setup was subjected to ambient drying for 40

TH-2777_166104034

days until the sample became air dry. Similarly, continuous drying suction measurement was performed in WP4C for soil samples with the same initial state used in the TEROS21 measurement. The WP4C measurements were carried out by following the standard procedure reported in the literature (Shah et al. 2006; Thakur et al. 2006; Sreedeep and Singh 2011).

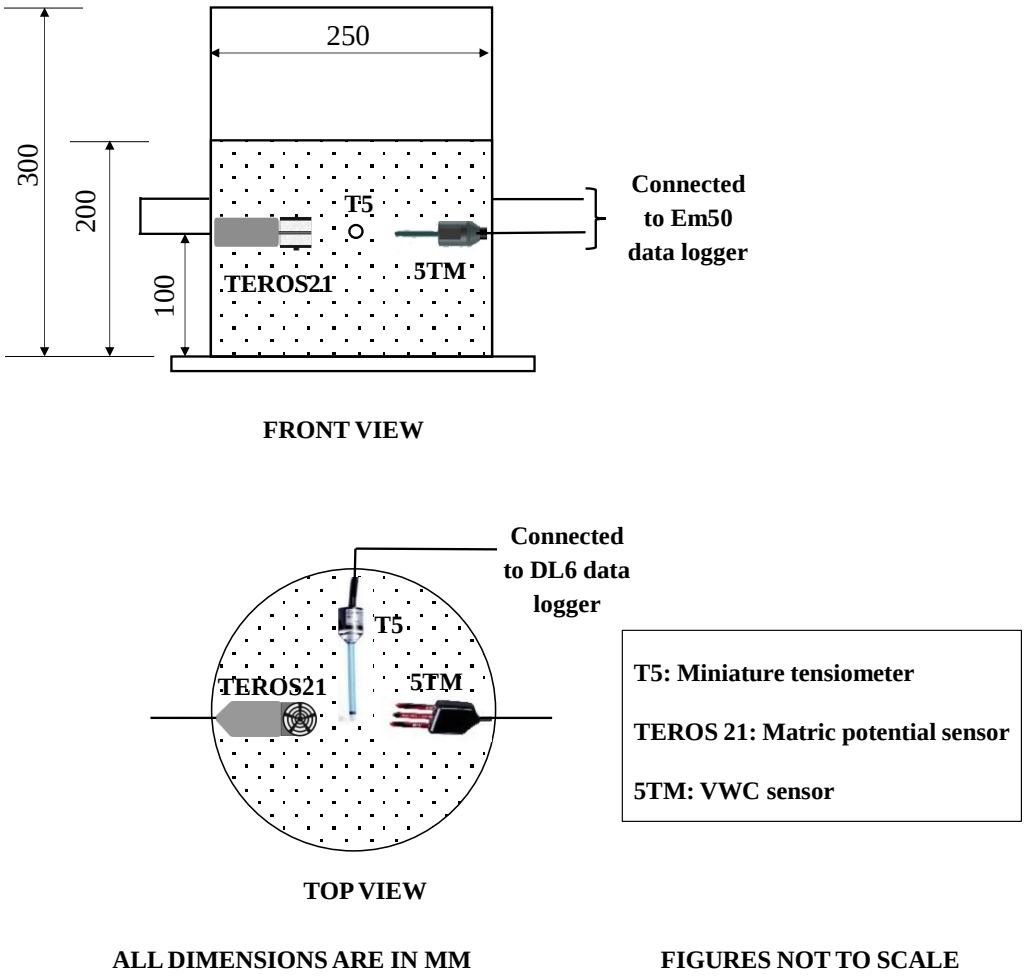

Fig. 6.2 Methodology adopted for the measurement of WRCC of the soil

6.2.2 Observations and Discussion

The continuous suction-water content variations, as measured by TEROS21, T5, and WP4C, for both BS and RS during air drying are presented in Fig. 6.3. The results indicate an excellent match between T5 and TEROS21, reiterating the accuracy of the latter in the range 9 kPa to 100 kPa. Further, the TEROS21 measurements matched well with WP4C results up to 1850 kPa for BS and 1700 kPa for RS considered in this study. It may be noted that a good matching of TEROS21 and WP4C for ψ_m< 1700 kPa is a confirmation on the accuracy of both the instruments, which works on an entirely different measurement principle. Moreover, it also suggests that there is no influence of osmotic suction for the washed soil sample (as discussed

TH-2777_166104034

earlier). For ψ_m> 2000 kPa, the TEROS21 measurements are significantly less than WP4C. As discussed earlier, the difference in TEROS21 and WP4C cannot be attributed to the osmotic suction (as shown in Fig. 6.1). The difference is due to the inadequacy of TEROS21 calibration for measuring ψ_m> 2000 kPa.

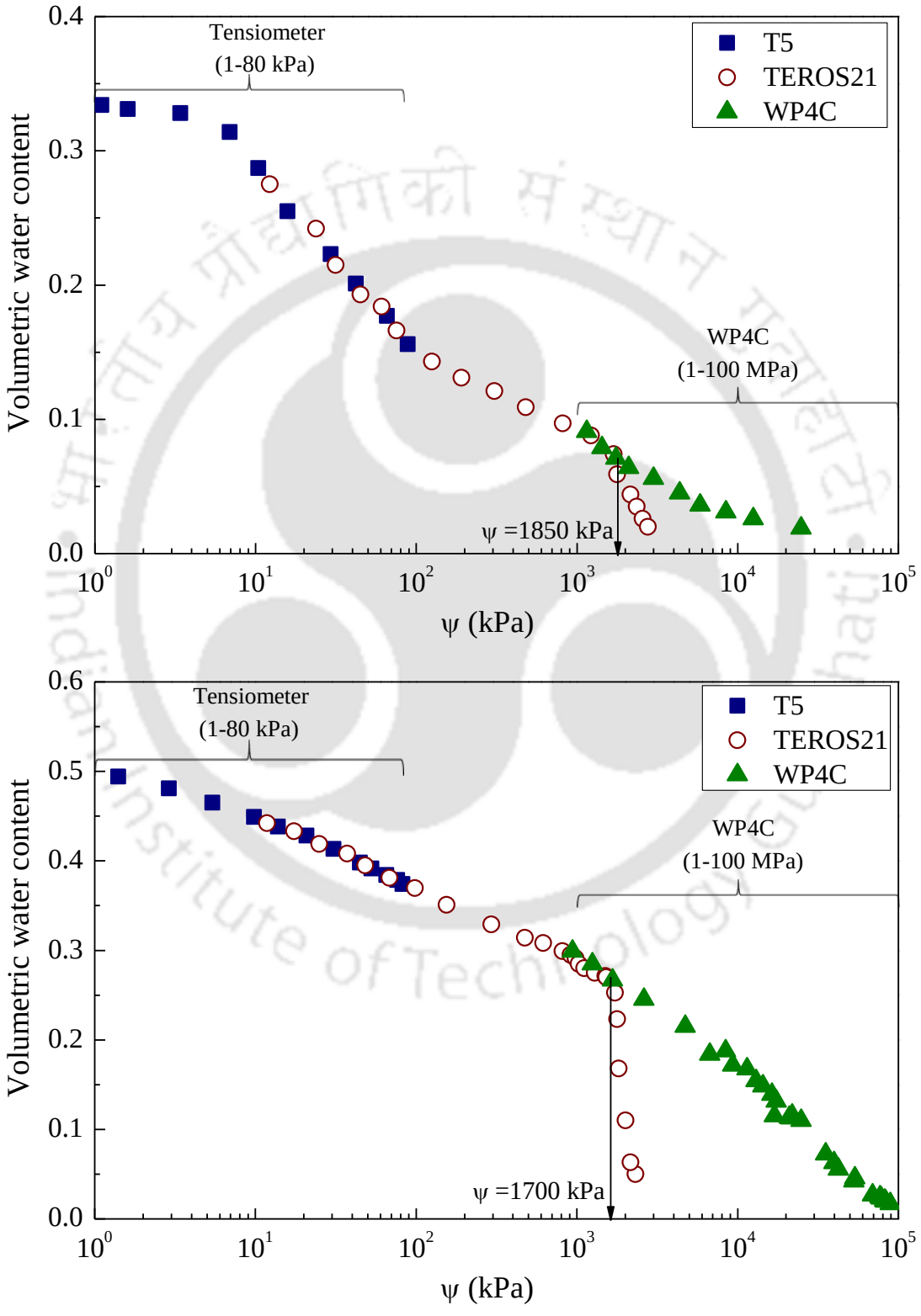

Fig. 6.3 Measured SWRC of (a) BS and (b) RS using T5, TEROS21, and WP4C

TH-2777_166104034

It is further observed from Fig. 6.3 that the difference between WP4C and TEROS21 significantly increases as the sample dries. The ceramic portion of the TEROS21 interfacing with the soil may not be sensitive to low water content as the soil dries. The loss of moisture from the ceramic beyond 2000 kPa may not be directly proportional to the water content changes in the soil, thereby inducing a significant deviation between the TEROS21 and WP4C measured suction values. The low suction measured by TEROS21 as compared to WP4C also indicates the inadequacy of the last point calibration (factory calibration) in the air, as discussed earlier. It was confirmed as part of this study that the ceramic of TEROS21 is not sensitive to the relative humidity (RH) changes in the closed atmosphere (in air). To demonstrate this, a series of salt solutions representing different RH (from 97% to 53%) (Greenspan 1977; ASTM D5298, 2016) was prepared and kept in an airtight relative humidity chamber (Malaya and Sreedeep 2011). The TEROS21 sensor was placed inside the relative humidity chamber to check its sensitivity to the ambient RH, as shown in Fig. 6.4. It can be observed that the sensor reading remains within 9 kPa to 13 kPa, with the RH value decreasing from 97.3% to 53%, which is indicative of the insensitivity of the TEROS21 sensor to the changes in ambient relative humidity. This confirms that last point calibration in ambient air cannot ensure the accuracy of TEROS21 for a higher suction range.

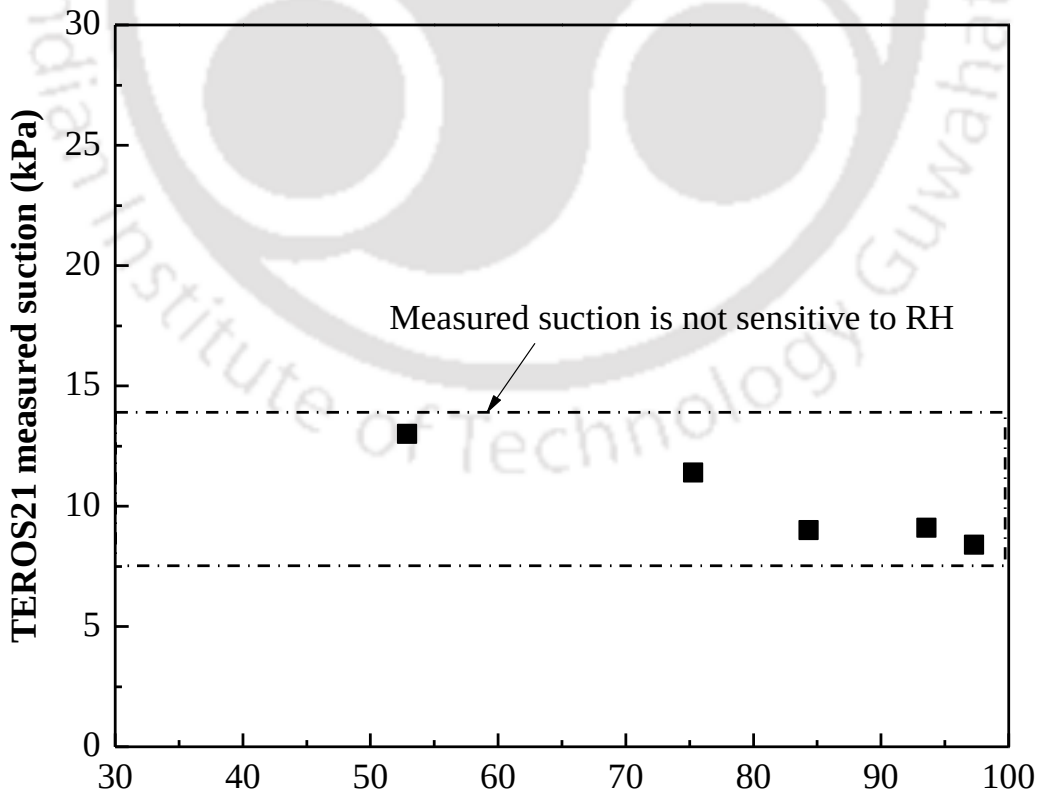

Fig. 6.4 Sensitivity of TEROS21 to ambient relative humidity (RH)

TH-2777_166104034

For better understanding of the factory calibration of TEROS21, the relationship between measured suction value and raw data (electronic output) of TEROS21 was plotted, as shown in Fig. 6.5. For the variation of suction in the range 10 kPa to 5873 kPa, the raw data varies from 20131 to 47776, respectively. An exponential equation, as presented in Eq. (6.1), was fitted to correlate the measured raw data and the suction value.

$$\psi_m(in\ kPa) = 0.098 \times \exp(0.00023 \times raw\ data) \qquad 6.1$$

It is well understood from Fig. 6.5 that the trend of variation is nonlinear, and the raw data approaches a value of 42040 correspondings to the suction of 1550 kPa. Beyond this, the sensitivity of TEROS21 is negligible as the curve becomes asymptotic. This means that for suction variation from 10 kPa to 1550 kPa, the raw data changes from 20131 to 42040. A further change of suction from 1550 kPa to 5879 kPa, the raw data variation is minimal from 42040 to 47776. Therefore, it is reasonable to state that the factory calibration has a significant effect on the inaccuracy of TEROS21 for ψ_m higher than 2000 kPa. Due to the inaccuracy of the factory calibration, all the suction measurement using TEROS21 was carried out up to a suction value of 2000 kPa for the selected soils amended with different concentrations of WAP.

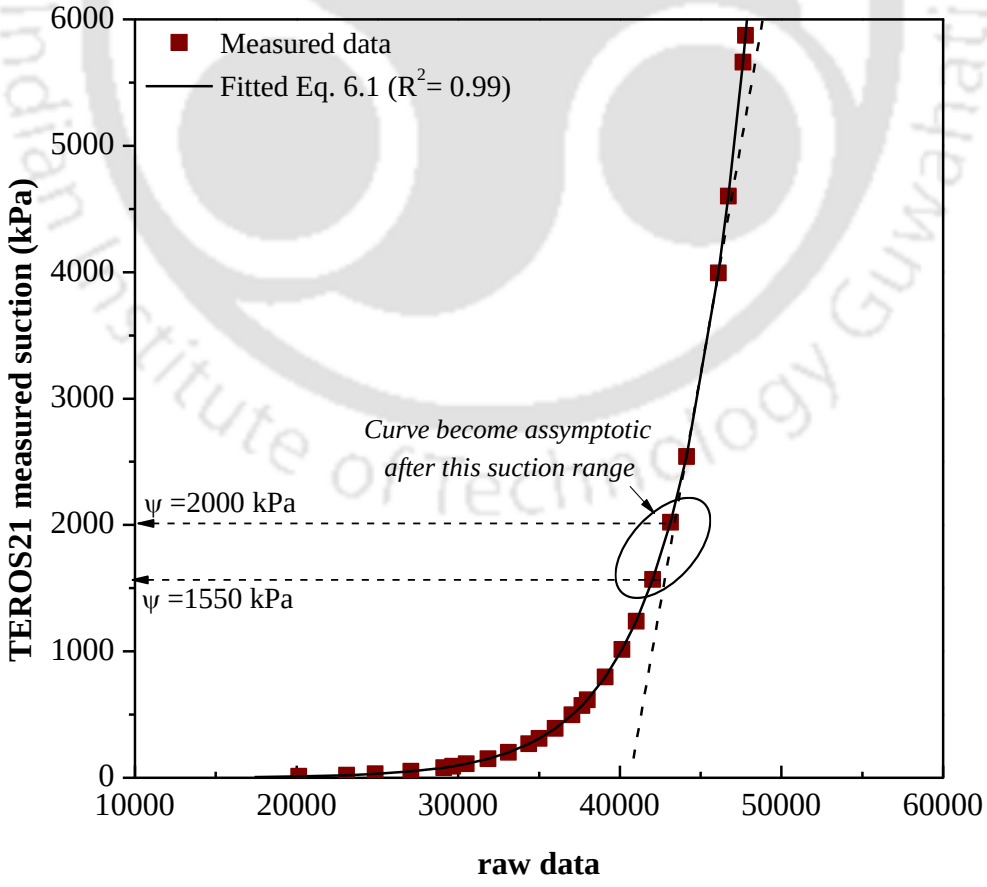

Fig. 6.5 Relationship between TEROS21 measured suction (kPa) and raw data

TH-2777_166104034

6.3 Performance evaluation of moisture sensor

Measurement of WRCC under field conditions also requires continuous and accurate monitoring of volumetric water content (VWC) in WAP amended soils. The conventional gravimetric method of water content determination is time-intensive and destructive process, and hence not preferable for real-time field monitoring of VWC. There are several non-destructive VWC measurement sensors available in the market, which works on the principles of time-domain reflectometry (TDR), frequency domain reflectometry (FDR), electromagnetic wave propagation, X-Ray, and neutron scattering (Evett and Steiner 1995; Huang et al. 2004; Polyakov et al. 2005; Visconti et al. 2014; Shaikh et al. 2019). Due to high accuracy, these sensors are extensively used for field monitoring of VWC in various applications, such as agriculture/irrigation, waste management, landfill covers, water resource and hydrology, and slope stability (Fares and Alva 2000; Gong et al. 2003; Chen et al. 2012; Ataka et al. 2014). Most of the available sensors are dielectric sensors (FDR, TDR, and capacitance) and measures the apparent dielectric permittivity (ε_a) of soil, which predominantly depends on soil-water content. Subsequently, the VWC of the soil is indirectly estimated from the measured ε_a value using specific calibration equation, which is considered valid for a wide range of soils. It has been reported in the previous literature that the measured ε_a value of the soil does not only depend on the soil water content but also influenced by the soil texture, soil salinity, mineralogical composition, bulk density (Gong et al. 2003; Visconti et al. 2014; Parvin and Degre 2016). Dielectric losses associated with the soil salinity (caused by soil electrical conductivity) and the presence of clay content (caused by the bound water at particle surface) can also result in an inaccurate measurement of VWC using capacitance sensor. To overcome this issue, past researchers have highlighted the importance of soil-specific calibration equations, which can improve the measurement accuracy from ±4% to ±1% (Chandler et al. 2005; Vaz et al. 2013; Shaikh et al. 2019).

6.3.1 Background

The ECH$_2$O 5TM (METER Group., Inc., USA) sensor uses a capacitance technique to measure the apparent dielectric permittivity (ε_a) of the soil with its prongs. The circuit board of the sensor consists of an electronic oscillator, which generates a repetitive square waveform with a characteristic frequency (≈70 MHz) [Bogena et al. 2012]. The capacitance (C) of the sensor is obtained from the average charge time (t) of the capacitor, from a starting voltage (V_i) to a voltage V, with an applied voltage (V_f) of the capacitor. If the resistance of the sensor circuit

TH-2777_166104034

(R), V_i, and V_f are kept constant, then the capacitance of the sensor can be determined from the following equation (Bogena et al. 2012),

$$C = -\frac{t}{\left[Rln\left(\frac{V - V_f + V_i}{V_i - V_f}\right)\right]} \quad 6.2$$

The capacitance is related to the soil apparent dielectric permittivity (ε_a) through the Eq. (6.3),

$$C = C' + g\varepsilon_0\varepsilon_a \quad 6.3$$

Here, ε_0 is the vacuum dielectric permittivity; g is the geometrical factor associated with the length, shape, and separation of sensor prongs; C' is the parasitic capacitance occurring due to the stray electric field. The parameters g and C' are jointly calibrated by the manufacturer taking the measurement of capacitance in several liquids with a wide range of ε_a value.

The ε_a of soil is a combination of soil solids (ε_{solid} ≈3-5), soil-pore water (ε_{water} ≈80), and soil air (ε_{air} ≈1). The contribution of soil-pore water permittivity can be divided into the permittivity of free water in the soil pores and permittivity of bound water in the diffuse double layer (DDL) for clay particles. Topp et al. (1980) proposed an empirical relationship (third-order polynomial equation) for the estimation of VWC (θ) from the measured ε_a of soil, including all the above-mentioned interaction and factors, as reported below,

$$\theta = a\varepsilon_a^3 + b\varepsilon_a^2 + c\varepsilon_a + d \quad 6.4$$

where a, b, c, and d represent the empirical coefficients. The ECH_2O 5TM uses Eq. (6.4) for the measurement of θ with the empirical parameters $a = 4.3 \times 10^{-6}$, $b = -5.5 \times 10^{-4}$, $c = 2.92 \times 10^{-2}$, and $d = -5.3 \times 10^{-2}$. These empirical parameters may not be valid for the WAP amended soils, where the permittivity of solid polymer particles and permittivity of absorbed water (within the polymer network) also contributes to the permittivity of WAP amended soils. There are not many studies present in the literature that evaluates the performance of 5TM for VWC measurement in WAP amended soils. The water absorption mechanism of the WAP particle is significantly different from the soil particle, as the absorbed water is stored within the polymer network due to an osmotic pressure difference between water and polymer network (Feng et al. 2014).

TH-2777_166104034

The present study aims to evaluate the performance of a capacitance sensor (ECH_2O 5TM) for real-time monitoring of VWC in WAP amended soils (Fig. 6.6). The WAP amended soils are often exposed to the real climatic conditions and undergo cyclic changes in VWC, influencing its hydraulic characteristics. Hence, it is necessary to verify and improve the accuracy of the 5TM sensor for VWC measurement before employing it in the soil.

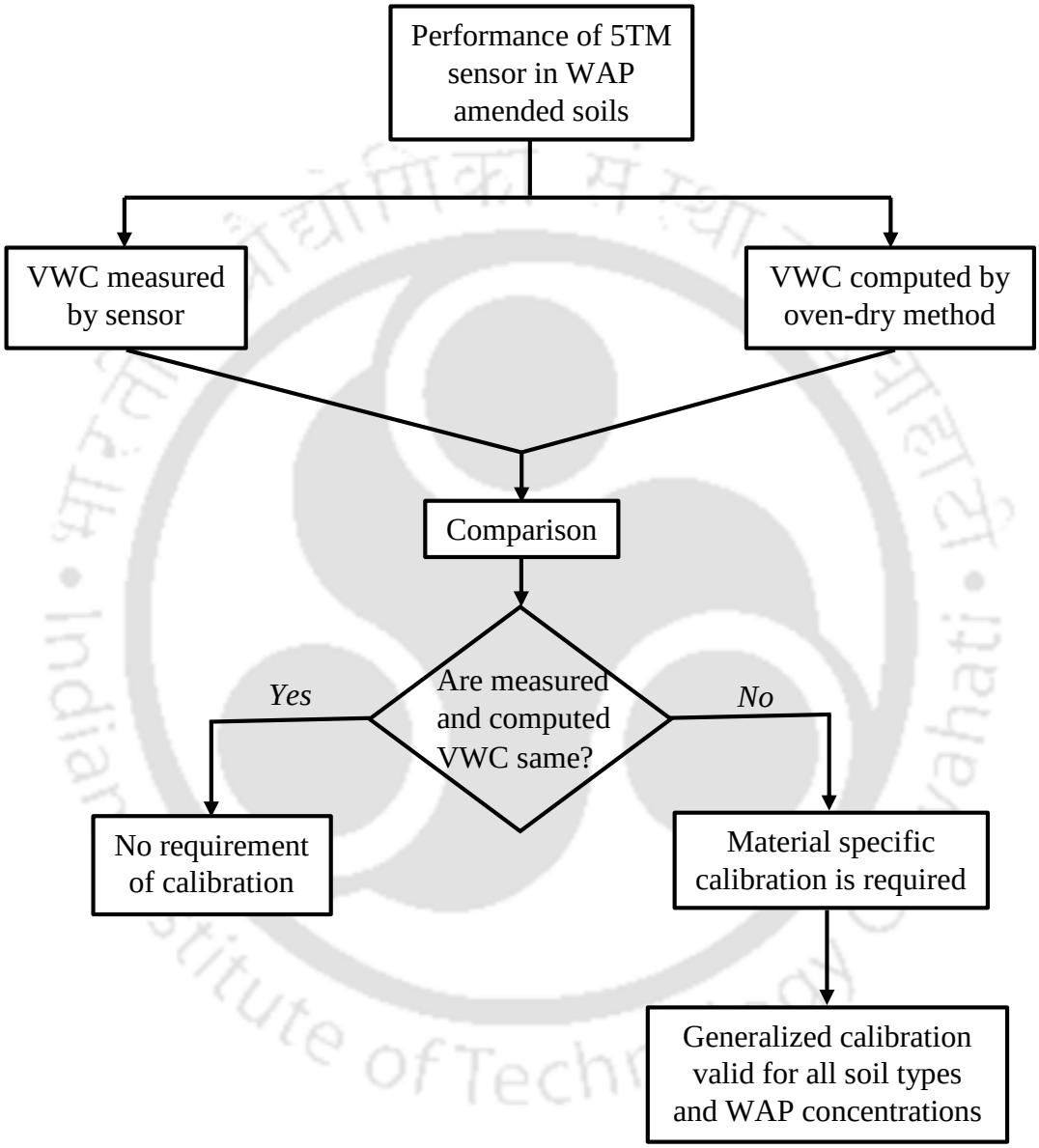

Fig. 6.6 Schematic diagram to represent the motivation of the study

6.3.2 Test procedure

The air-dried soil samples, passing through 2 mm sieve, were thoroughly mixed with dry WAP at four different concentrations (0, 0.1%, 0.2%, and 0.4% on w/w basis). The WAP concentrations were selected based on the previously reported literature (Dorraji et al. 2010; El-Asmar et al. 2017). The WAP amended soils were mixed with different quantities of

TH-2777_166104034

deionized water to obtain five different soil-water contents, from relatively dry side to wet side. The mixed samples were kept in polythene bags for 72 h to allow uniform distribution of moisture. The WAP amended soil samples were then compacted to specific bulk density (ρ_b) [close to the field density] in a cylindrical PVC column (diameter 25 cm and height 20cm), as shown in Fig. 6.7. To ensure uniform ρ_b during compaction, the total volume of soil sample was divided into three uniform parts, and each layer was compacted using a 2.6 kg rammer. The 5TM sensor was inserted horizontally in the middle of the soil layer in such a way that the tip of the sensor remains at the center of the soil column. A dummy sensor was placed during the compaction in the middle of the soil layer to facilitate easy installation of 5TM sensor in the compacted soil layer. The dimensions of the dummy sensor were chosen slightly smaller than the 5TM sensor to ensure proper contact between the sensor and soil. The sensor was then connected to the Em50 data logger, and the VWC of the samples (designated as θ_m) along with the unprocessed raw data (R_w) were measured. This R_w was further used to obtain ε_a of soil sample at that particular water content. A total of 36 numbers of samples were prepared (three repetitions for each WAP concentration), and 12 numbers of 5TM sensors were tested to verify the repeatability and reproducibility of the measured data.

After the measurement of θ_m, an accurate VWC (θ_a) of the soil samples was computed theoretically by measuring the gravimetric water content (w) and dry density (ρ_d) of the samples. For this purpose, the top layer of the soil along with the sensor was removed, and steel rings (with known volume) were inserted into the soil sample at three different locations within the influence zone of the sensor to collect samples for w measurement. The θ_a values of the samples were calculated using the following equation,

$$\theta_a = \frac{w \times \rho_d}{\rho_w} \tag{6.5}$$

Here, ρ_w is the density of water.

The sensor measured θ_m and accurate θ_a for all the soil samples were compared to evaluate the accuracy of the sensor in WAP amended soils. If the deviation between these two VWC exceeds ±10%, then a corrective procedure (as stated in the following section) must be incorporated to evolve a new material-specific calibration equation for 5TM sensor, which can be useful for WAP amended soils. In the present study, two calibration procedures, including polynomial calibration and linear calibration, were proposed to correlate the accurate θ_a with the measured ε_a and θ_m, respectively.

TH-2777_166104034

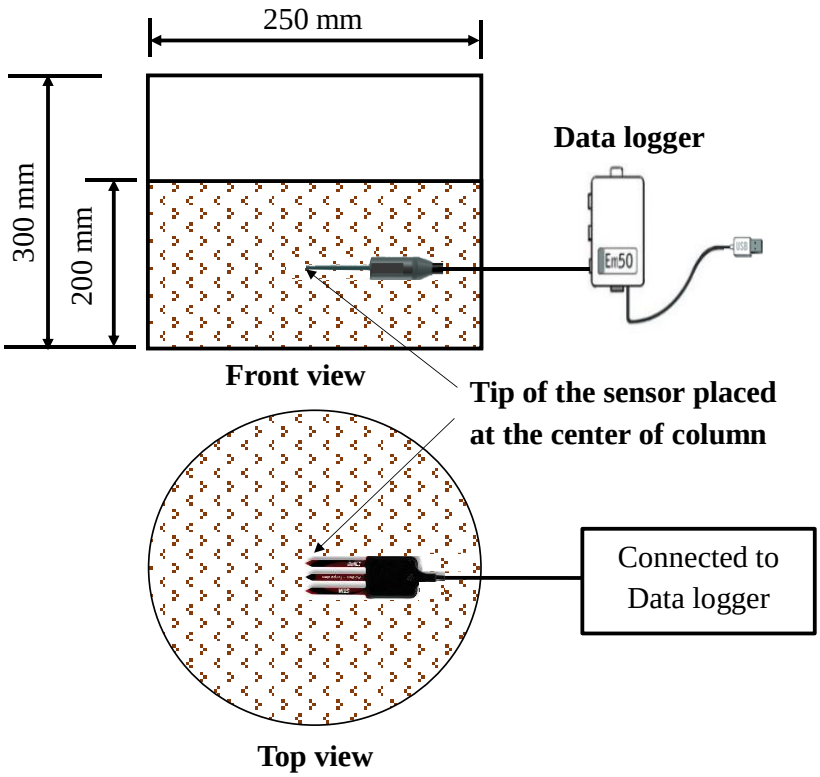

Fig. 6.7 Experimental methodology adopted to evaluate the performance of 5TM sensor

6.3.3 Observations and Discussion

Figure 6.8 illustrates the variation in the average values of θ_m, measured using 5TM sensor, and the theoretical accurate θ_a value (measured by oven-dry method) for the soils at four different WAP concentrations. It can be observed that the factory calibration is satisfactory for the measurement of θ in bare soils, except for RS. A significant difference in the measured θ_m and accurate θ_a value was observed for bare RS, and the difference increases with an increase in the water content. This observation is in line with the past studies (Visconti et al. 2014; Parvin and Degré 2016; Shaikh et al. 2019), which reported the inaccuracy of capacitance-based sensors for θ measurement in soils with higher clay content. It can be further observed from Fig. 6.8 that the sensor measured θ_m significantly different from the accurate θ_a value of WAP amended soils at all three WAP concentrations. All the measured data falls above the 1:1 line, and the accurate θ_a of the WAP amended soils (at highest WAP concentration) was 1.5 times to 2 times higher than the measured value. This clearly shows the extent of error that can occur if the sensors are used directly for WAP amended soils. The observations in Fig. 6.8 suggest the necessity of a corrective procedure to minimize the error in θ measurement of WAP amended soil using 5TM sensor. Therefore, WAP-specific

TH-2777_166104034

calibration was performed using the methodology presented in Fig. 6.8 in two ways, including (i) polynomial calibration (correlating the sensor measured ε_a to accurate θ_a), and (ii) linear calibration (correlating the sensor measured θ_m to accurate θ_a).

The measured ε_a of bare soils and WAP amended soils are obtained from the raw output, as recorded in the Em50 data logger, and presented as a function of accurate θ_a in Fig. 6.9. It can be noticed that higher ε_a values are recorded (at near-saturated state) in WAP amended soils as compared to bare soil (except for RS), indicating an increase in saturated water content with the addition of WAP. As the permittivity of soil solid (ε_{solid} ≈3-5) and entrapped air (ε_{air} ≈1) is very less as compared to the permittivity of free water (ε_{water} ≈80), the permittivity of soil (ε_a) largely depends on the amount of soil-pore water and physical states of the water (free or bound). Free water can be defined as the water retained in the soil macro-pores against the gravitational force, whereas bound water is defined as the thin layer of water surrounding the soil particles held by the molecular and electro-molecular force (Boyarskii et al. 2002). Bound water is subjected to different forces, which may hinder its response to an external electromagnetic field leading to a lower permittivity (dielectric loss) than free water (Mohamed and Paleologos 2017). Due to this reason, the factory calibration often underestimates the θ for soils with higher clay content, where the water retained by the soil matrix is governed by both capillary mechanism and surface adsorption phenomenon (bound water). On the other hand, the water absorption mechanism and other allied parameters contributing to the relative permittivity of WAP amended soils are different than the bare soil (Fig. 6.10). At the air-dry state, the WAP particles occupy the free pore space or macro-pores in the soil matrix (depending on the soil texture). With the addition of water, the WAP particles absorb water within their polymer network due to the osmotic pressure difference (as explained in the earlier section) and swell depending on the availability of pore space and the amount of water added. At the same time, some percentage of the added water is also retained by the soil particles against the gravitational force (i.e., free water). The stored water inside the polymer network (bound water held by negatively charged carboxyl group) significantly contributes to the dielectric loss, leading to a lower permittivity value than the actual one. The influence of dielectric loss is clearly visible in Fig. 6.9, where the WAP amended soils possess higher moisture content at the same permittivity (ε_a) value. This phenomenon of dielectric loss is also prominent for WAP amended RS (due to higher percentage of clay particles), where the maximum measured ε_a value remains almost the same with the increasing WAP concentrations, resulting in a higher degree of error in θ measurement.

TH-2777_166104034

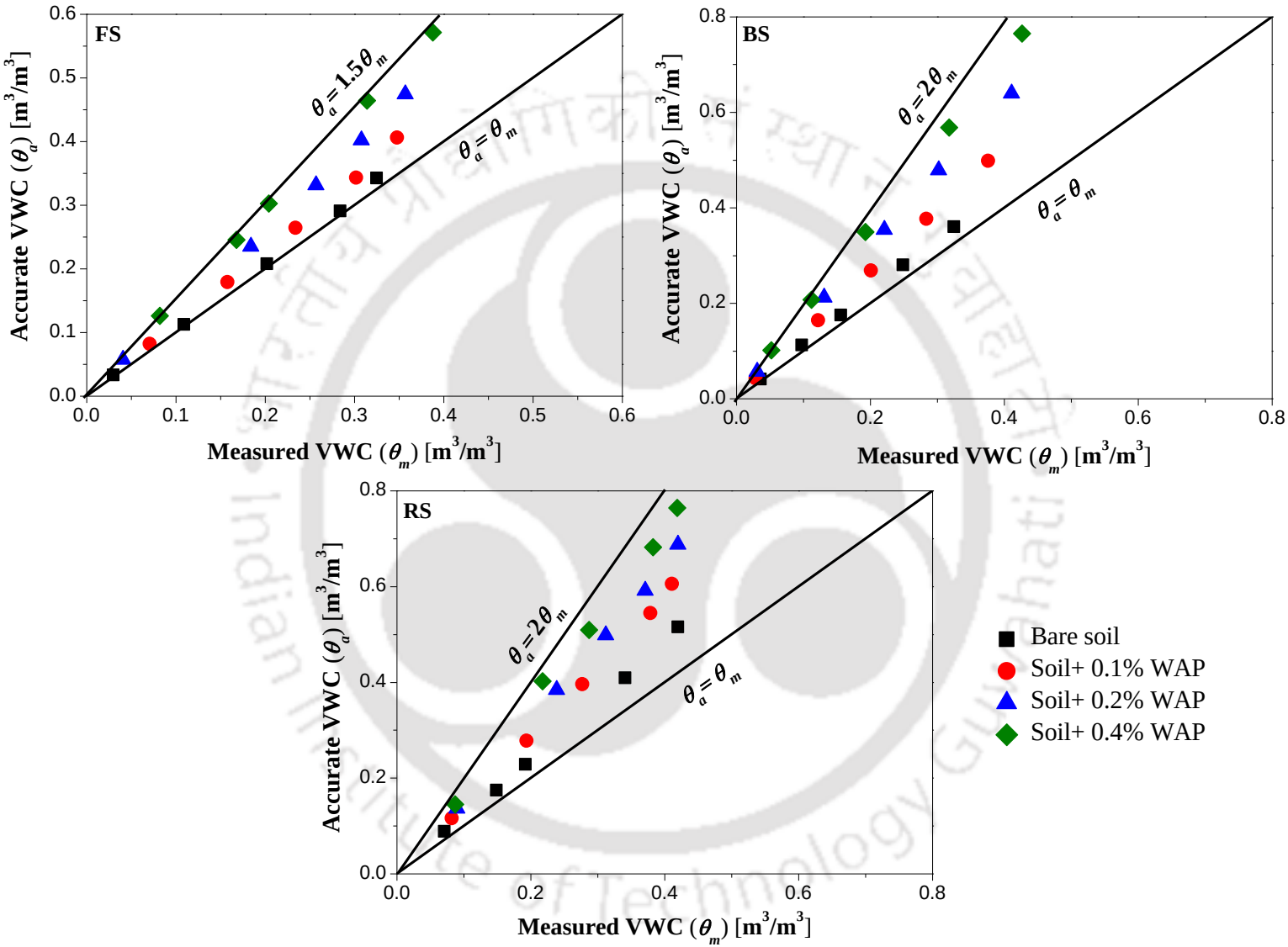

Fig. 6.8 Comparison between 5TM sensor measured VWC and accurate VWC at different concentrations of WAP

TH-2777_166104034

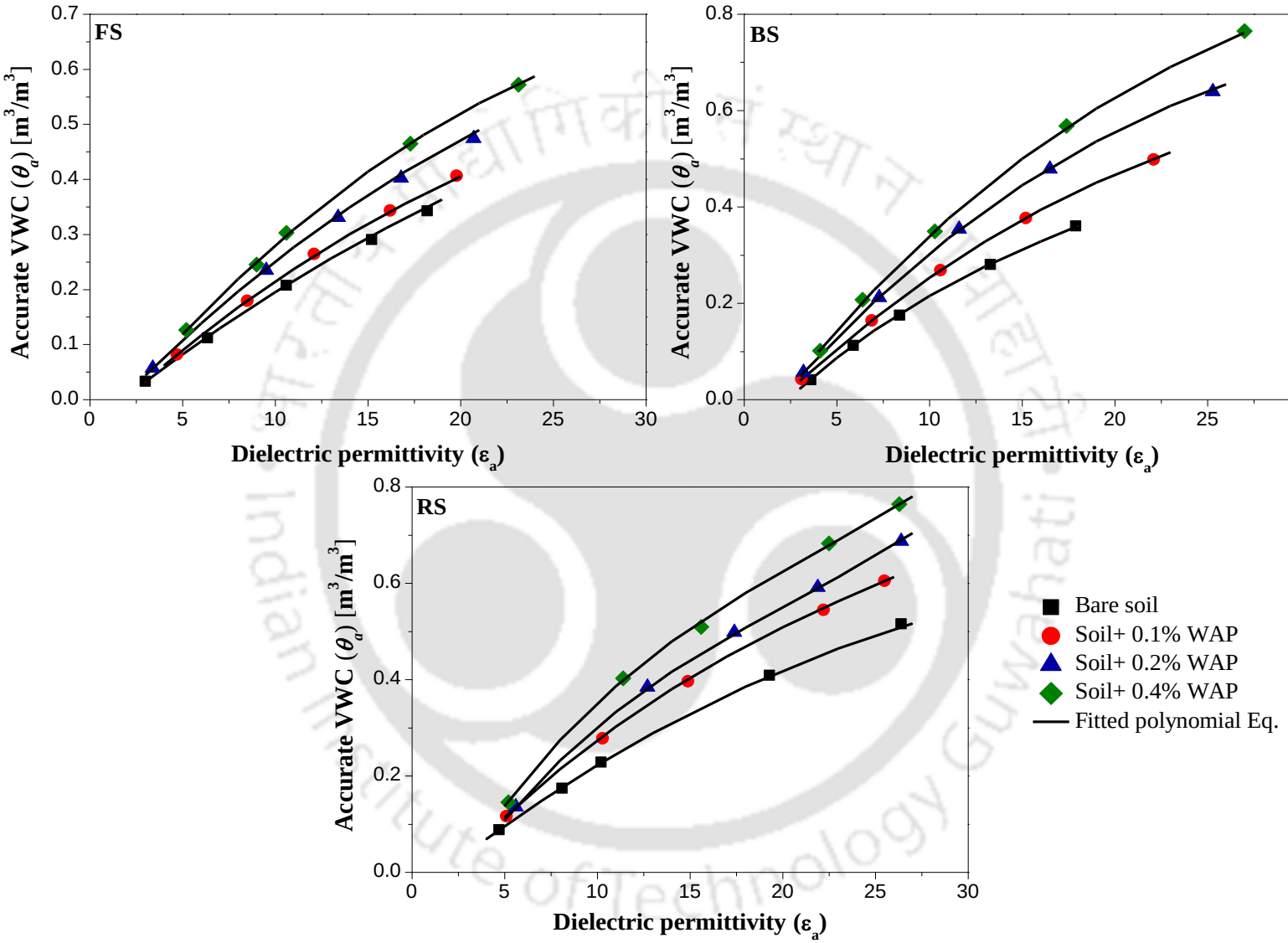

Fig. 6.9 Polynomial calibration procedure for accurate measurement of VWC of WAP amended soils

TH-2777_166104034

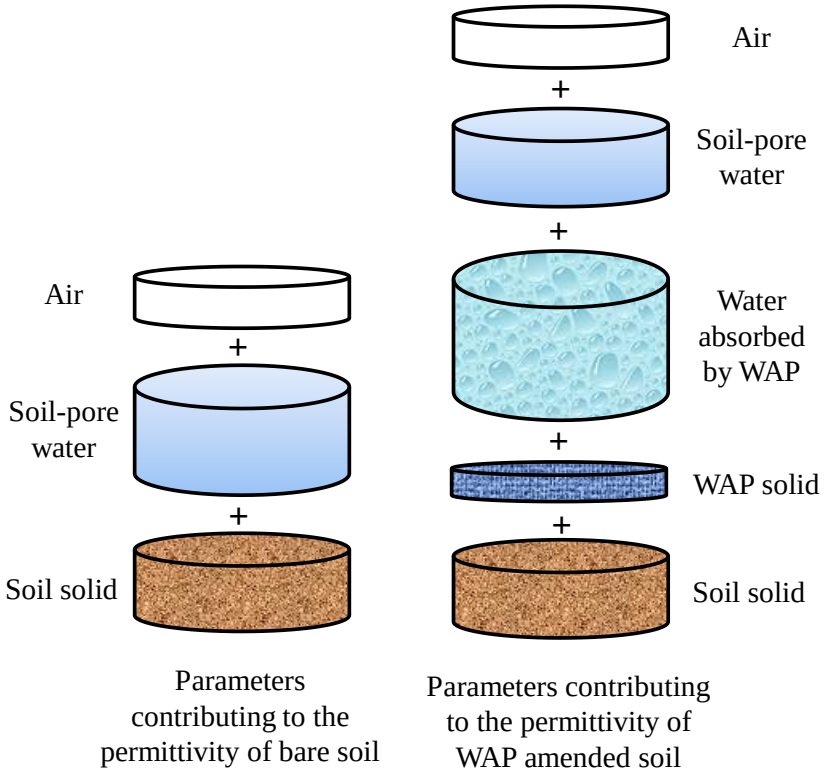

Fig. 6.10 Illustrations of different parameters contributing to the permittivity (ε_a) of bare soil and WAP amended soil

For polynomial calibration (PC), a third-order polynomial function, similar to Topp Equation (Eq. 6.4), was fitted to the measured ε_a and accurate θ_a to obtain the empirical parameters valid for WAP amended soils. The variation of θ_a with the measured ε_a and the fitted polynomial equations are compared in Fig. 6.9, whereas the obtained calibration parameters are summarized in Table 6.2 along with the regression coefficient (R^2) value. It can be observed that the fitted equations yield R^2 values close to unity, indicating an excellent fit to the measured data. The data reported in Table 6.2 indicates that the obtained calibration parameters for WAP amended soils are quite different from the empirical parameters suggested by Topp et al. (1980). Moreover, the calibration parameters are different for different soil types and WAP concentrations, and hence adopting a single set of calibration parameters can result in an erroneous value of θ for WAP amended soils. It is also very difficult to propose a generalized relationship to obtain these calibration parameters (based on soil properties and WAP concentrations) that are valid for all WAP concentrations and soil texture.

In the next approach, the variation of sensor measured θ_m and accurate θ_a for all the WAP concentrations are plotted in Fig. 6.11, which showed a linear response between θ_m and

TH-2777_166104034

θ_a. Therefore, a linear equation (Eq. 6.6) was fitted to the observed variation to correlate the θ_m value with the θ_a value. It can be observed that all the fitted lines are passing through the origin, and therefore the vertical intercept value (k_2) is equal to zero. The slope (k_1) of the fitted line can be termed as the correction factor (k) [Table 6.3] that needs to be multiplied with the sensor measured θ_m for accurate measurement of θ in WAP amended soils.

$$\theta_a = k_1\theta_m + k_2 \quad 6.6$$

Table 6.2 Details of the calibration parameters (PC) for WAP amended soils

Soil	WAP concentrations	*a*	*b*	*c*	*d*	R^2
FS	Bare soil	2 x10^{-6}	-4.5 x10^{-4}	2.8 x10^{-2}	-4.9 x10^{-2}	1
	Soil+0.1% WAP	2 x10^{-6}	-5 x10^{-4}	3.2 x10^{-2}	-5.8 x10^{-2}	1
	Soil+0.2% WAP	2 x10^{-6}	-5 x10^{-4}	3.6 x10^{-2}	-5.9 x10^{-2}	0.99
	Soil+0.4% WAP	2 x10^{-6}	-5.5 x10^{-4}	4.2 x10^{-2}	-7.4 x10^{-2}	0.99
BS	Bare soil	2 x10^{-6}	-7 x10^{-4}	3.7 x10^{-2}	-8.2 x10^{-2}	0.99
	Soil+0.1% WAP	2 x10^{-6}	-6 x10^{-4}	3.8 x10^{-2}	-7.1 x10^{-2}	1
	Soil+0.2% WAP	5 x10^{-6}	-8 x10^{-4}	4.6 x10^{-2}	-8.4 x10^{-2}	1
	Soil+0.4% WAP	7 x10^{-6}	-1 x10^{-3}	5.3 x10^{-2}	-9.8 x10^{-2}	0.99
RS	Bare soil	1 x10^{-6}	-4 x10^{-4}	3.1 x10^{-2}	-4.9 x10^{-2}	0.99
	Soil+0.1% WAP	1 x10^{-5}	-1 x10^{-3}	4.4 x10^{-2}	-8.6 x10^{-2}	1
	Soil+0.2% WAP	3 x10^{-5}	-2.1 x10^{-3}	6.4 x10^{-2}	0.165	0.99
	Soil+0.4% WAP	4 x10^{-5}	-2.2 x10^{-3}	7 x10^{-2}	0.162	1

Table 6.3 Obtained *k* parameter for linear calibration (LC) of WAP amended soils

Soil type	Bare soil	Soil+0.1% WAP	Soil+0.1% WAP	Soil+0.1% WAP
FS	1.04	1.15	1.31	1.49
BS	1.12	1.33	1.57	1.78
RS	1.2	1.44	1.6	1.79

TH-2777_166104034

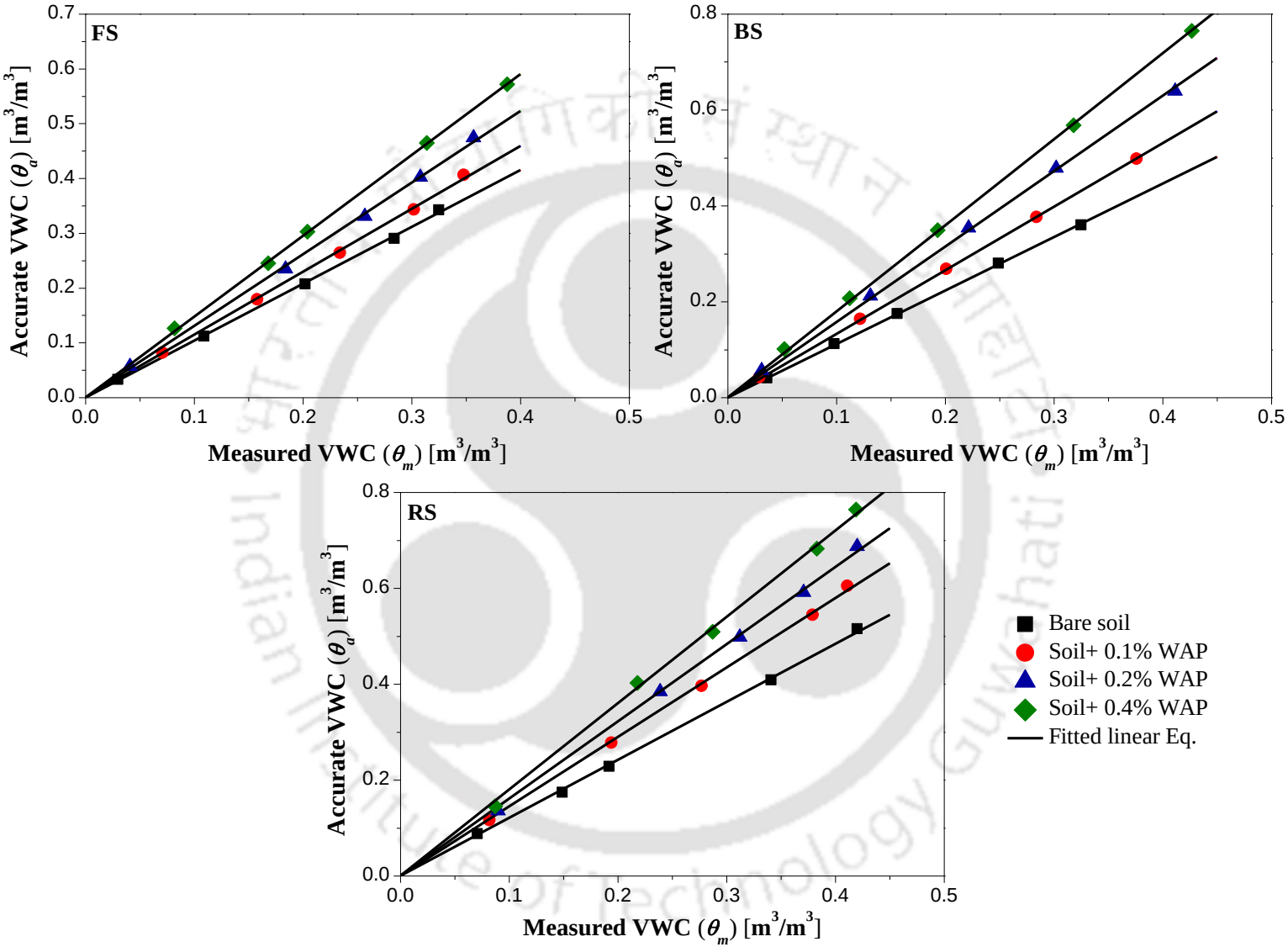

Fig. 6.11 Linear calibration procedure for accurate measurement of VWC

TH-2777_166104034

The obtained correction factor (k) for the soils at different WAP concentrations are presented as a function of soil clay content in Fig. 6.12(a). As the dielectric loss in WAP amended soils is mainly associated with the soil clay content and WAP concentrations, the figure showed an increase in the k value with increasing clay content and WAP concentrations. The k values of other bare soils (with different clay content) were calculated from the data reported in Shaikh et al. (2019) and presented in Fig. 6.12(a). It can be observed that the k values for the other bare soils (as obtained from the literature) are in line with the k values obtained in the present study. Therefore, this result can be effectively used to calculate the k value (by simple linear interpolation method) of different textured soils with clay content varying from 0% to 28%. The k value for a wide range of soils at three different WAP concentrations (0.1%, 0.2%, 0.4%) can also be obtained using Fig. 6.12(a), and the accurate VWC can be estimated from the sensor measured θ_m value. To calculate k value for WAP concentration other than the above three concentrations, the obtained k values (from Fig. 6.12a) were presented as a function of WAP concentrations for the three soils in Fig. 6.12(b), which showed a nonlinear variation. A second-order polynomial equation, as reported in Fig. 6.12(b), was fitted (with $R^2 > 0.99$) to the measured dataset to calculate the k value corresponding to any other WAP concentrations. A similar approach can be applied to calculate the k value for any soil texture with different WAP concentrations. Therefore, the combination of Fig. 6.12(a) and (b) can serve as a useful method to measure VWC accurately under laboratory and field conditions using 5TM sensor for a wide range of WAP amended soils.

The correction factor (k) values, as obtained from LC using Com-WAP, were used to calibrate the 5TM sensor for FA-WAP amended soils. Different concentrations of dry FA-WAP were mixed with the dry soil, and the moisture content was measured at different water content using 5TM following the same procedure as discussed earlier. The sensor measured VWC was then multiplied with the obtained k values (from Fig. 6.12), and the calibrated VWC was compared with the actual VWC (obtained with the oven-dry method) in Fig. 6.13. It can be observed that all the measured points lie on the 1:1 line, indicating that the k values obtained with Com-WAP for different textured soils can be used for FA-WAP amended soils as the difference of water absorbency between Com-WAP and FA-WAP is not very high. It can be noted that adopting the material-specific calibration parameters can increase the measurement accuracy to less than ±5% for WAP amended soil.

TH-2777_166104034

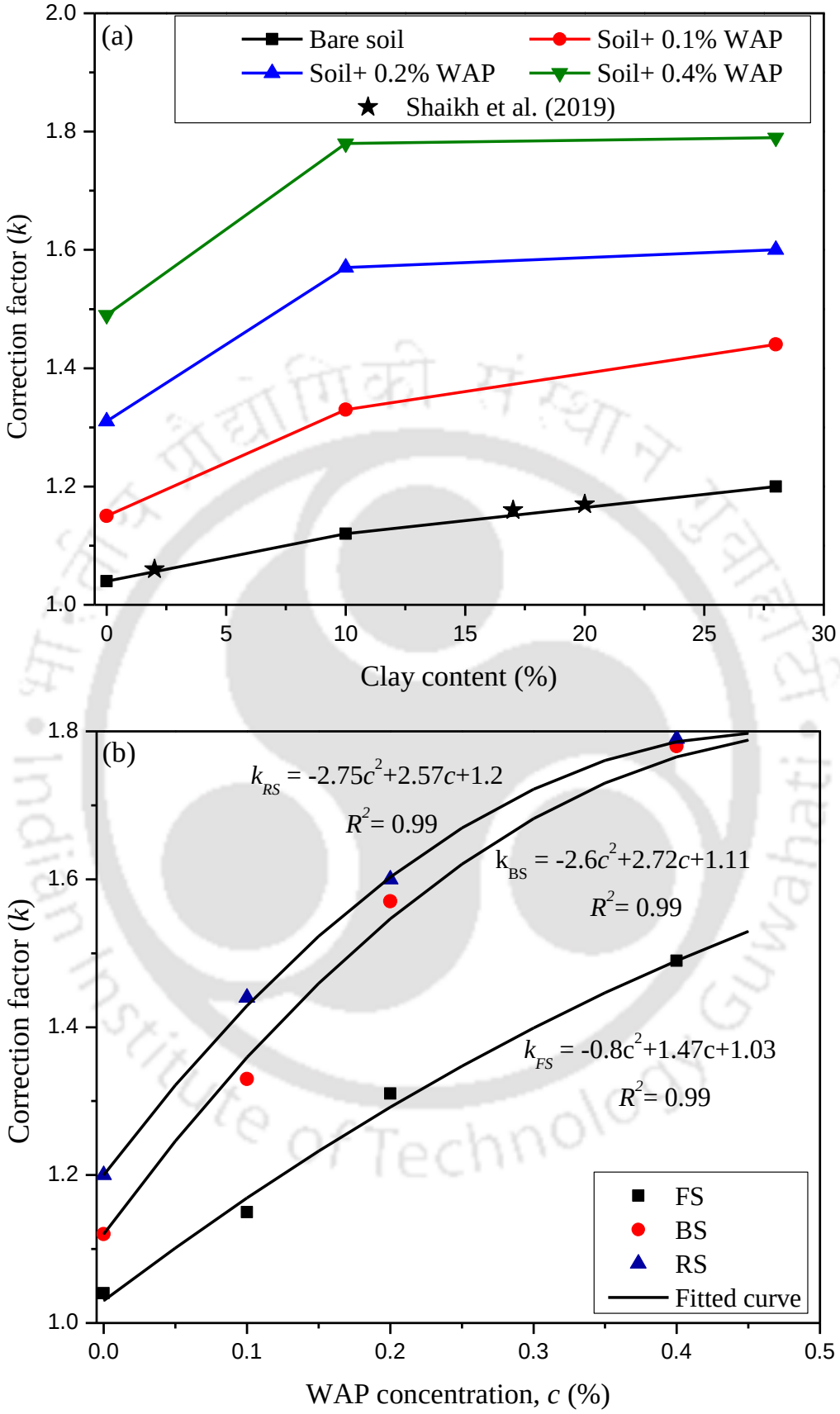

Fig. 6.12 Correlation of correction factor (k) with (a) clay content and (b) WAP concentrations

TH-2777_166104034

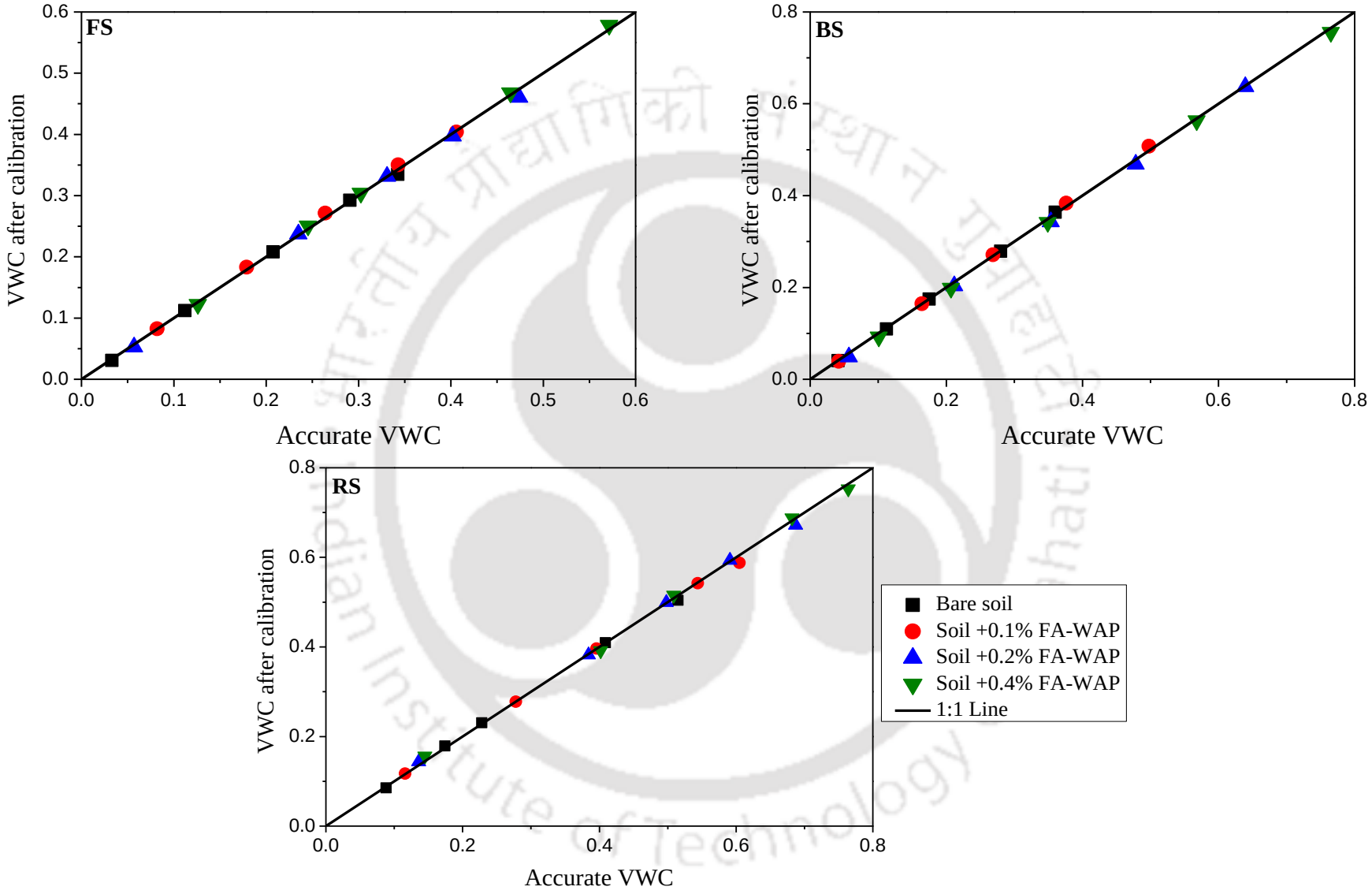

Fig. 6.13 Comparison between corrected VWC (using LC) and accurate VWC at different concentrations of FA-WAP

TH-2777_166104034

6.4 Summary

This chapter summarizes the performance evaluation of two different capacitance-based sensors used for suction (TEROS21) and moisture (ECH_2O 5TM) measurement. The suction sensor (TEROS21) was calibrated up to 100 kPa with a miniature tensiometer, and the accuracy of TEROS21 was not verified by manufacturer, beyond this suction range. In the present study, the accuracy of TEROS21 up to 80 kPa was established by comparing the measurements with well-established T5 miniature tensiometer, whereas for suction greater than 80 kPa, the TEROS21 measurements were compared with the relative humidity (RH) based dew point potentiameter (WP4C) in two different soils. It was found that TEROS21 can measure matric suction accurately up to 1850 kPa for the soils used in this study. The accuracy limit can vary between 1550 kPa to 2000 kPa, depending on the type of soil, which is conclusive from this study. The inaccuracy of the sensor beyond 1550 kPa may be the result of the insensitive response of ceramic disc at low water content and exponential calibration equation. Therefore, the TEROS21 was used to measure suction up to 2000 kPa for WRCC determination of WAP amended soils.

The present chapter also evaluates the performance of capacitance moisture sensor (ECH_2O 5TM) for continuous real-time monitoring of volumetric water content (VWC) in water absorbing polymer (WAP) amended soils. The effectiveness of the factory calibration equation for θ measurement was thoroughly investigated in three different textured soils with four different WAP concentrations (0, 0.1%, 0.2%, and 0.4% on w/w basis). It was observed that adopting the factory calibration equation would underestimate the VWC measurement for WAP amended soils. At the maximum WAP concentrations (i.e., 0.4%), the accurate VWC value was found to be varying from 1.5 times to 2 times (depending on the soil texture) higher than the sensor measured VWC value. The error in θ measurement was relatively higher in the wet side (close to saturation) as compared to the dry side. An increase in error in θ measurement with increasing water content can be attributed to the dielectric loss due to the presence of bound water in clay particles (adsorbed on the particle surface) and WAP particles (absorbed within the polymer network). The bound water in WAP amended soils inhibits its response to an external electromagnetic field, resulting in a lower dielectric permittivity as compared to free water. A corrective procedure was proposed to minimize the error in θ measurement using 5TM sensor in WAP amended soils. Two different calibration approaches, including polynomial calibration (PC) and linear calibration (LC), were demonstrated to obtain accurate VWC value from the sensor measured permittivity (ε_a) and VWC value, respectively. The

TH-2777_166104034

results showed that the LC is a simple and robust corrective procedure, which can be used to obtain the correction factor (k) for a wide range of soils and WAP concentrations. Moreover, it was found that the k value obtained with commercial WAP can be used for FA-WAP as the difference in water absorbency of FA-WAP and Com-WAP is not very high. Based on these observations, it is conclusive that the factory calibration equation of the 5TM sensor is not accurate for θ measurement in WAP amended soils. Therefore, the present study proposed material-specific calibration equations and correction factors for an accurate determination of θ before employing the 5TM for laboratory monitoring in WAP amended soils.

TH-2777_166104034

Chapter 7

Water retention characteristics of WAP amended soil

7.1 General

Water absorbing polymer (WAP) is being used in agricultural and horticultural applications for a very long time as it can absorb and retain large quantities of water. However, the use of WAP as soil amendment under drought stress condition is not very popular till now because of the various complexities associated with the chemical structure of the polymer and its sensitivity to the different environmental stimuli of either chemical or physical nature, such as changes in pH, ionic strength of the surrounding solution. The complexities increased to a greater extent when WAP particles were mixed with different types of soil. It was observed from the literature that most of the reported studies have considered only cohesionless sandy soils. Few studies that discussed the effect of texture on WAP performance in soil has not focused on the water retention characteristic curve (WRCC) (continuous drying and wetting) of WAP amended soil under drought condition (Agaba et al. 2010; Narjary et al. 2012). The water retention studies reported in the literature (Narjary et al. 2012) using conventional pressure plate apparatus are valid for a small sample size. Also, the applied air pressure in the pressure plate apparatus can have an undesirable effect on the swelling of WAP, which is not studied in detail. This necessitates to study the WRCC of WAP amended soil under zero stress ambient drying conditions. The appropriate application rate of WAP and its effect on the irrigation frequency related to different soil texture was not quantified in the literature. Therefore, the present study investigates the influence of commercial WAP as well as synthesized FA-WAP on the water retention behavior of three different textured natural soils.

7.2 Measurement methodology of WRCC

The matric suction of the bare soil, as well as the WAP amended soils, were measured using a miniature T5 tensiometer (UMS GmbH, Munich, Germany) and a capacitance senor TEROS21 (METER Group, Inc., USA). The tensiometer was used in this study for the lower range of suction measurement (ψ_m < 80 kPa), and the TEROS21 was used to measure the suction up to a range of 1500 to 2000 kPa. Beyond this suction value, the factory calibration curve of TEROS21 may become sensitive and can lead to inaccurate measurement of suction.

The PVC column test setup, as shown in Fig. 7.1, was developed to measure the drying water retention characteristic curve (DWRCC) and wetting water retention characteristic curve

TH-2777_166104034

(WWRCC) of the WAP amended soils. The test setup consists of a PVC column of diameter 250 mm and height 300 mm connected to the PVC water reservoir (with an effective head of 1m) via a flow valve. A porous stone was used at the bottom of the column to facilitate uniform entry of water into the soil. A filter paper was placed on the porous stone to avoid the escape of soil grains that can block the pores of the porous stone. The air-dried soil sample passing through 2 mm sieve was uniformly mixed with the dry WAP particles at three different concentrations, including 0.1% (C1), 0.2% (C2), and 0.4% (C3) on weight by weight (w/w) basis. These three concentrations of WAP were selected based on the previously reported literature (Dorraji et al., 2010; El- Asmar et al. 2017). A control sample without any WAP amendment (C0) was kept as a reference to understand the influence of WAP on the water retention properties of different textured soils.

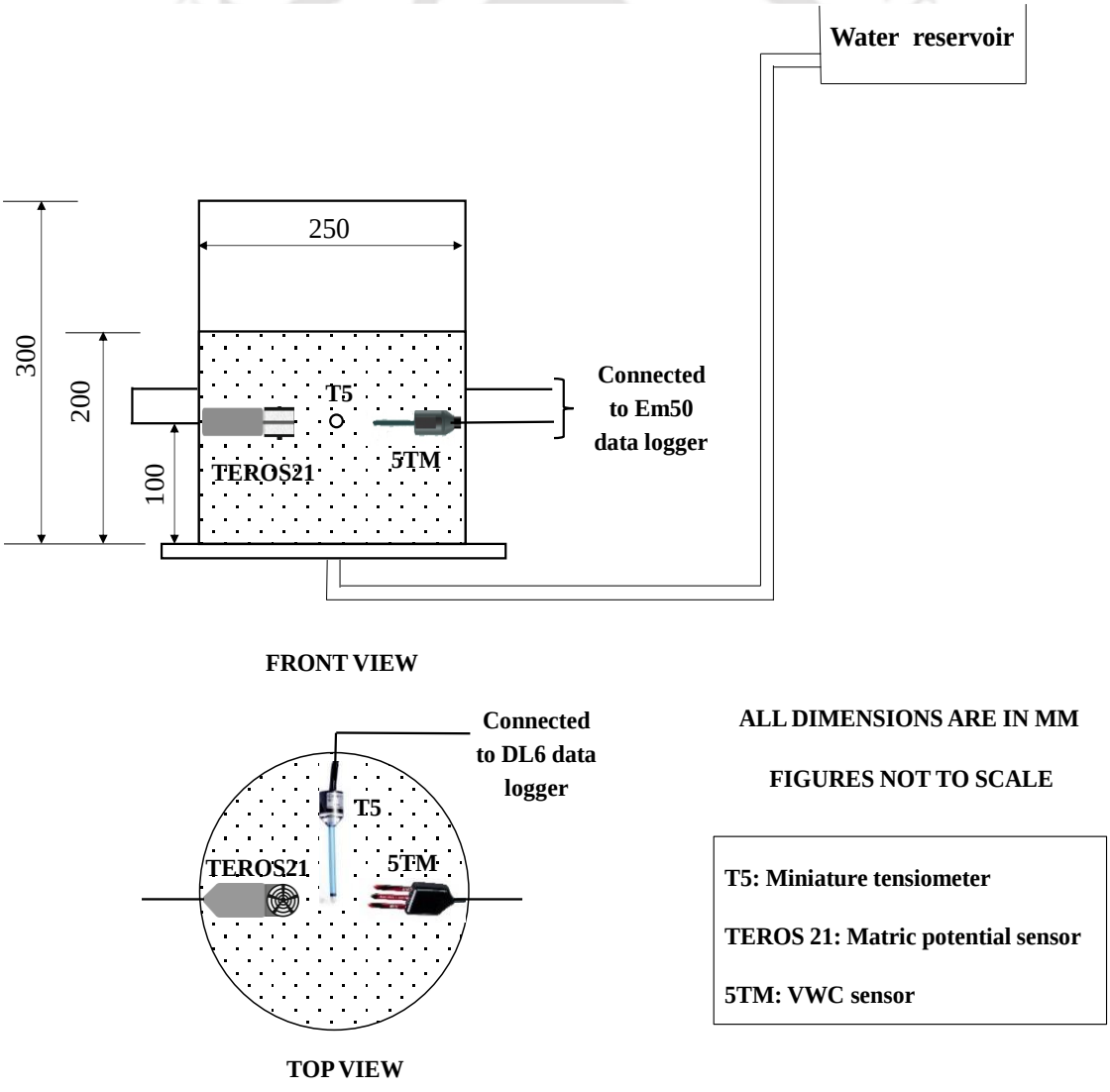

Fig. 7.1 Methodology adopted for measurement of drying-wetting WRCC of the WAP amended soil

TH-2777_166104034

The soil samples with different amounts of WAP were mixed with a sufficient quantity of demineralized water to obtain water content close to the liquid limit for ensuring the initial state close to saturation. The wet samples were poured in polyethylene bags and stored in an airtight container for 24 hours to ensure uniform distribution of water. The soil samples were then placed in the PVC column (at slurry state) with TEROS21, 5TM sensor, and T5 tensiometer placed horizontally at a depth of 10 cm from the top. It was ensured that the tip of T5 tensiometer, TEROS21, and 5TM remain at the same horizontal level. The DWRCC of the WAP amended soil was first determined before the wetting process to ensure continuity between measured DWRCC and WWRCC. For this purpose, the column setup was subjected to ambient drying conditions [average temp 25°C, and average relative humidity (RH) =70%], and the suction-water content variation was continuously monitored using T5, TEROS21, and 5TM sensors. At the end of the drying experiment, a flexible hose was connected between the water reservoir and the PVC column to allow the water to flow into the specimen in a controlled manner. The water flow was controlled using the flow valve to ensure the slow wetting process so that the variation in suction-water content can be captured reasonably well. During the wetting process, the suction-water content variation was continuously monitored using TEROS21 and 5TM sensors until the suction value of the specimen reached close to 100 kPa. After this point, a freshly refilled T5 tensiometer was placed, removing the previous one, and the measurements were carried out until the sample reaches the near-saturated state. The same procedure was repeated one more time to measure the 2nd drying-wetting WRCC of the WAP amended soils.

7.3 Drying WRCC of commercial WAP (Com-WAP) amended soil

The measured WRCCs of the three different textured soils with varying concentrations of Com-WAP amendment (0, 0.1%, 0.2%, and 0.4%) were presented in Fig. 7.2 for FS, BS, and RS, respectively. The results clearly indicate that the suction measurement using T5 and TEROS21 complements each other very well. The combined measurement facilitates a wide range of continuous suction measurements during drying (imposing drought condition) in WAP amended soil. While the measurements of T5 and TEROS21 are established for soils, their utility was not explored and demonstrated for determining the WRCC of WAP amended soils. Both the sensors gave identical measurements from the saturated state to the suction value of 80 kPa (maximum range of T5). The observations imply that these sensors can be used with confidence for long-term field monitoring of suction and drought management studies in WAP amended soils.

TH-2777_166104034

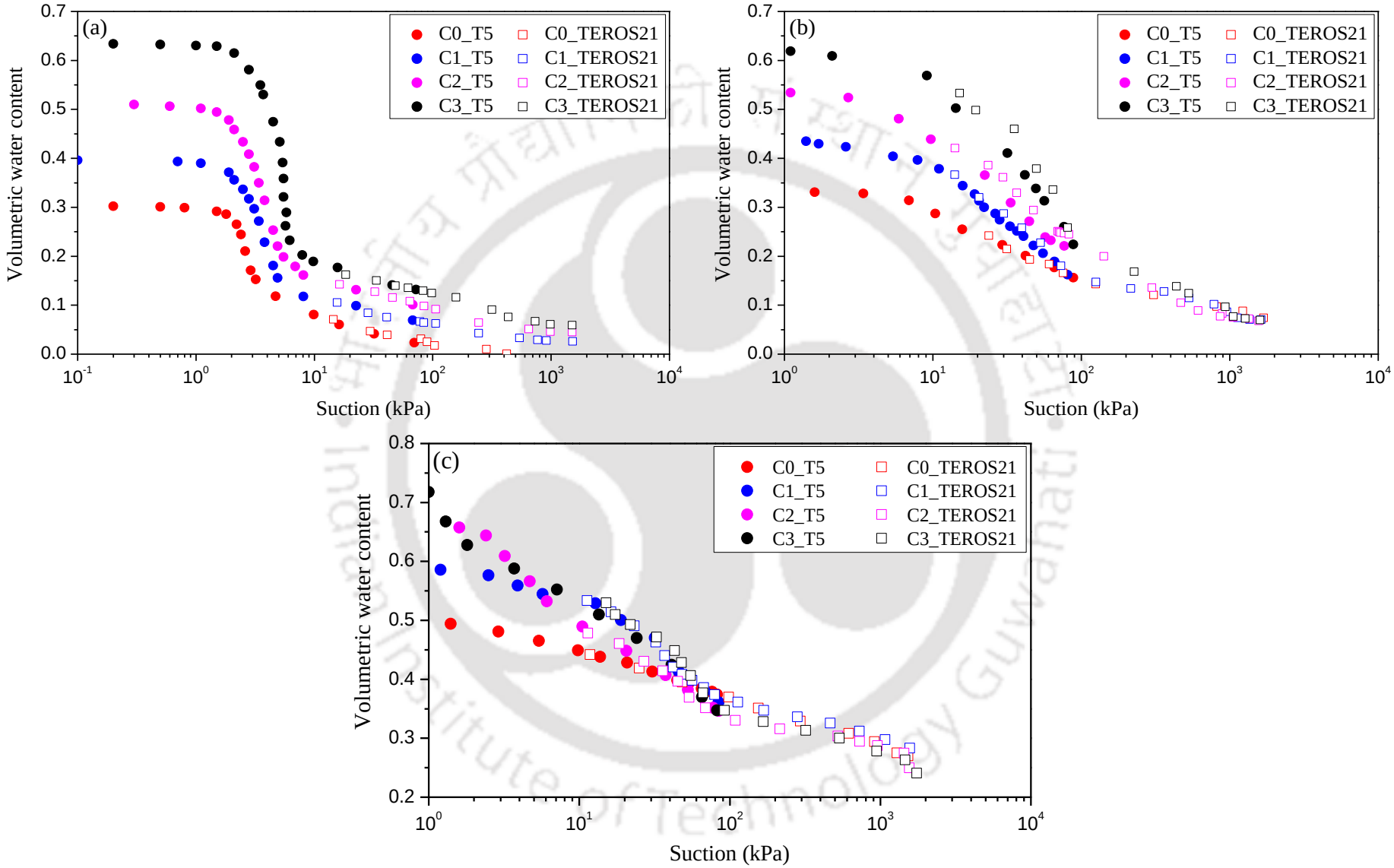

Fig. 7.2 Measured DWRCC of (a) Fine sand (FS), (b) Brahmaputra silt (BS) and (c) Red soil (RS) with different Com-WAP concentration

TH-2777_166104034

Figure 7.2 further indicates that the polymer amendment has increased the water retention of all the soils, specifically in the low suction range (ψ_m < 100 kPa). Presence of WAP altered the microstructure of soil pores (reduction in macro and mesopores), which predominantly affects the water retention at low matric suction (Agaba et al. 2010; Narjary et al. 2012). It is a well-known fact that water retention at low suction is primarily dominated by capillary pore water, which in turn is dependent on soil particle and pore size diameter (Lu and Likos 2004). With the addition of WAP, the empty pore spaces in the soil are occupied by the polymer with water absorbed in it (Rahmati et al. 2019). This is visible in the form of increasing saturated volumetric water content (θs) with an increase in WAP content in soil. As the soil texture becomes finer, the difference in θs of amended and bare soil gradually decreases. For sand, the improvement can be visualized for the entire range of WRCC, whereas for silt loam and clay loam, the improvement in WRCC was found to be minimal beyond 100 kPa. Wei and Durian (2013) have reported that the total fraction of water-accessible pore space in the soil for a particular packing density decreases exponentially with the increase in polymer concentration. Therefore, for the same suction, the amount of water in the pores drastically increases due to the high storage of water in the three-dimensional (3D) network of WAP as compared to water-filled pores of bare soil. To prove this point, FESEM analysis was performed for the soils with different concentrations of WAP amendment.

Figures 7.3-7.5 depict the FESEM images that represent the surface morphologies of Com-WAP amended FS, BS, and RS, respectively. It may be noted that different scales and magnification of images were selected depending on the type of soil (different particle size range) for visualizing the pore structure. However, for the same soil, these properties of images were kept constant for an unambiguous comparison of bare and WAP amended soils. Bare FS and BS showed lots of water-accessible pores as compared to RS. With increasing concentration of WAP, the pore spaces were progressively occupied by the water-swollen WAP, leading to a more compact and denser pore structure at 0.4% WAP amendment. However, the pore structure of WAP amended RS was found to be similar to the bare soil (Fig. 7.5). This is attributed to the fine texture and less inter pore sizes of RS, and the effect of WAP amendment is not visibly explicit. Due to the restricted interpore space of a fine-textured soil (Nimmo 2004) like clay loam, WAP particles are incapable of swelling to their full capacity in RS. This observation matches well with the improvement in WRCC depicted in Fig. 7.2. The combined WRCC and morphological observations of bare and WAP amended soils add to the experimental reasoning for the low improvement of water retention in fine-textured soil.

TH-2777_166104034

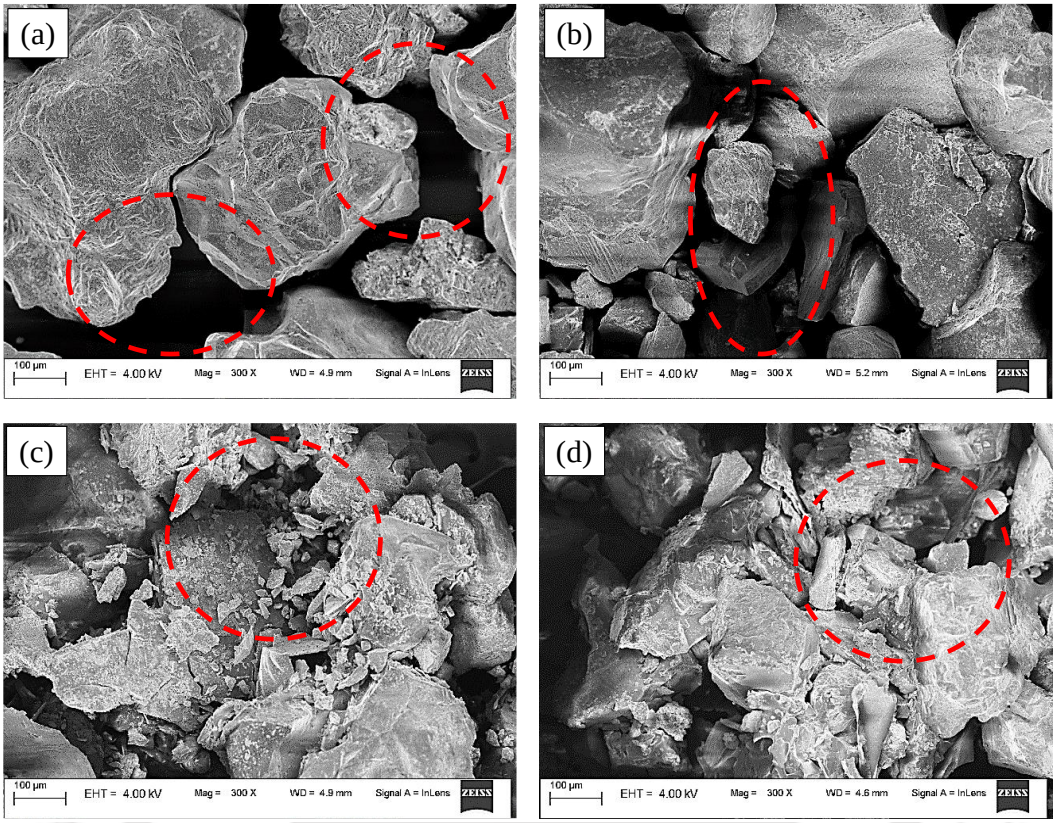

Fig. 7.3 FESEM images of FS with (a) C0, (b) C1, (c) C2, (d) C3 WAP concentrations

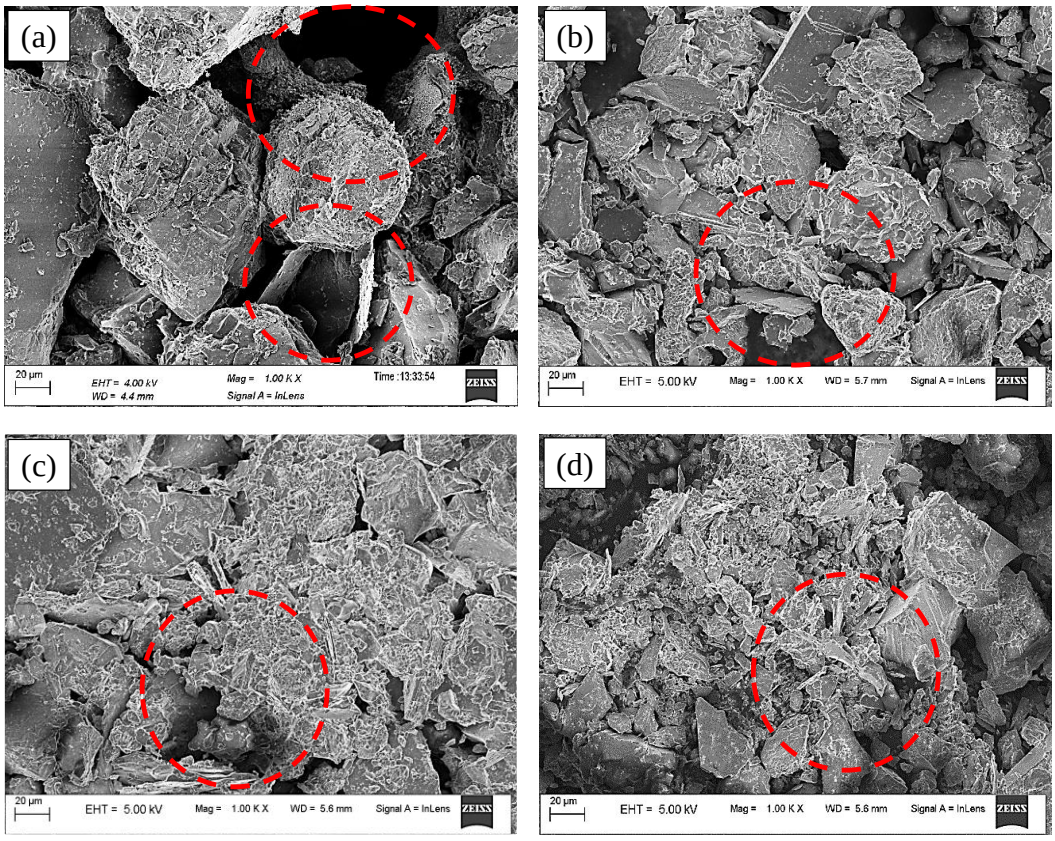

Fig. 7.4 FESEM images of BS with (a) C0, (b) C1, (c) C2, (d) C3 WAP concentrations

TH-2777_166104034

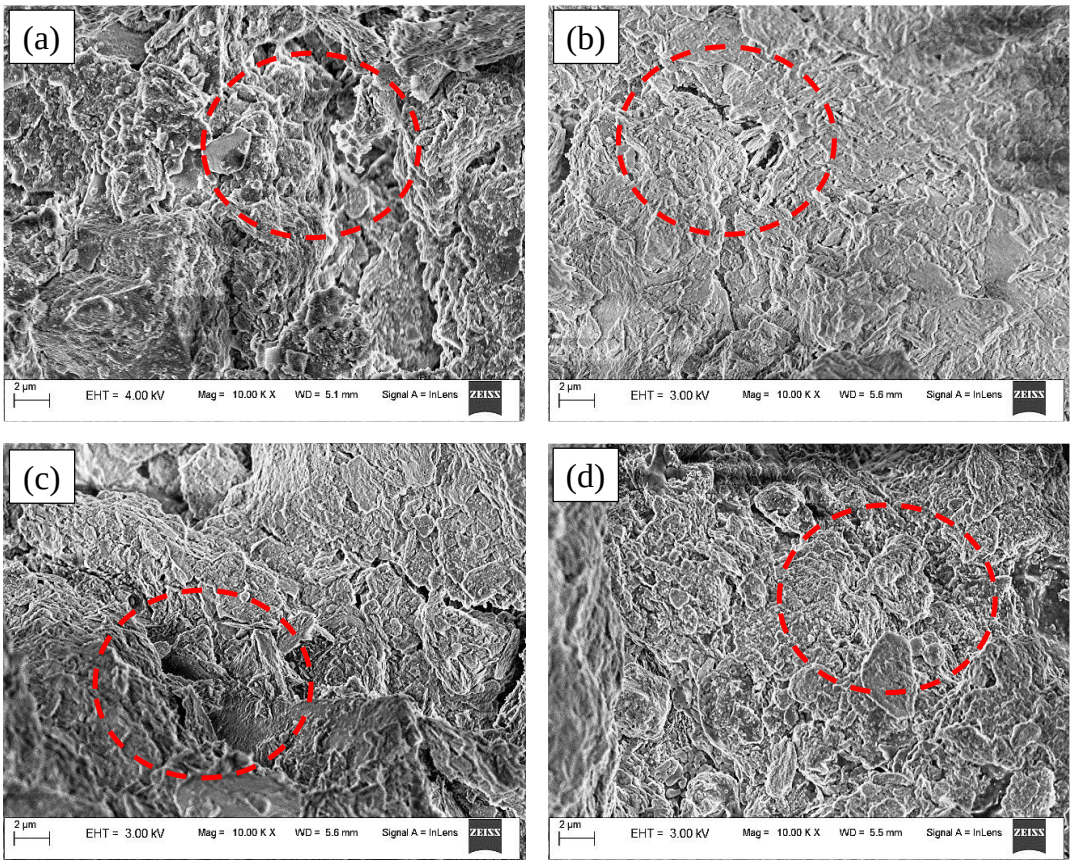

Fig. 7.5 FESEM images of RS with (a) C0, (b) C1, (c) C2, (d) C3 WAP concentrations

The hypothesis of restricted swelling on water absorbency of Com-WAP in different soil texture was further investigated. This was accomplished by determining the difference in equilibrium swelling capacity of bare soil and 0.4% WAP amended soil. The respective soil was placed in a small container with a perforated bottom and submerged in distilled water. After allowing sufficient time to swell (24 hrs), the excess water from the container was drained off, and the weight of the sample was taken. The equilibrium swelling capacity of WAP in different soil texture was determined as the difference in WAC between WAP amended soil and bare soil. It was found that the equilibrium swelling capacity of WAP progressively decreased from 260 g/g in FS to 211 g/g in BS and 168 g/g in RS. It may be noted that the WAC of Com-WAP in only distilled water (absence of soil) was 279 g/g. The reduction in equilibrium swelling capacity associated with the physicochemical factors of the soil matrix is minimal for FS (0.93 times) and maximum for RS (0.61 times). This restriction in equilibrium swelling is one of the main reasons for the lower improvement in water retention behavior of WAP amended RS as compared to the other two soils (Fig. 7.2).

TH-2777_166104034

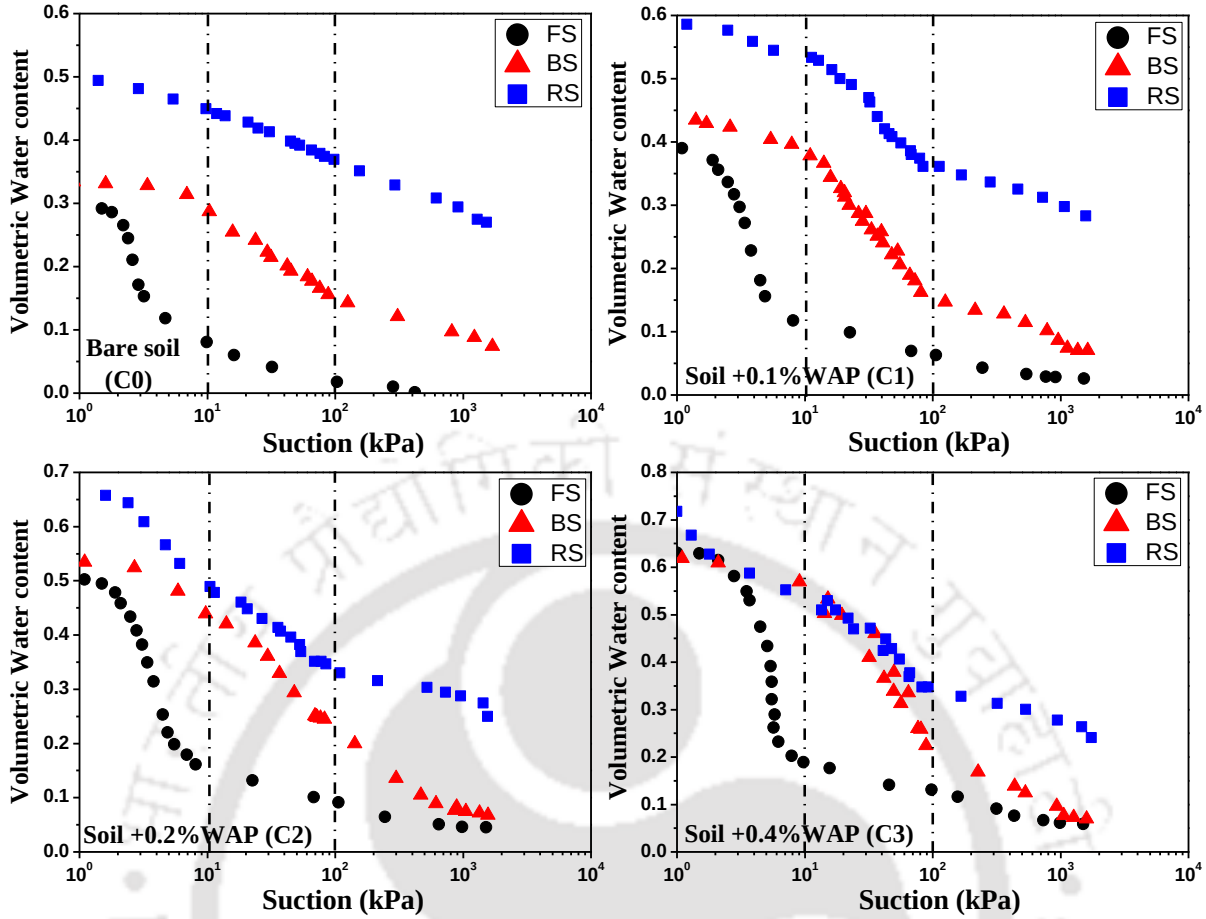

Fig. 7.6 Comparison of WRCC of the different texture soils with varying WAP concentration

A comparative study of water retention behavior of the three different textured soils at a particular concentration of polymer was presented in Fig. 7.6. The results showed that the WRCC is distinct for FS, and the difference between WRCC of BS and RS reduces with the increasing concentration of polymer. For the maximum concentration of WAP (C4), the WRCC of all soil textures coincide at the low suction range (ψ_m < 10 kPa). The WRCC of BS and RS was found to be same for ψ_m < 100 kPa. For all the cases, the WRCC of all soil textures showed a significant difference for ψ_m > 100 kPa. This is mainly due to the difference in the inherent residual suction characteristic of the bare soils and not necessarily due to the effect of WAP. For example, the soil FS approach residual state in the range of 10 kPa < ψ_m < 100 kPa, whereas RS is still in the desaturation zone of WRCC for suction close to 1000 kPa. Another important observation is the alteration of the shape of the WRCC of WAP amended RS. With the addition of WAP, the WRCC of RS closely resembles a dual-porosity model (Burger and Shackelford, 2001; Zhang and Chen, 2005) as compared to the bare soil. With an addition of 0.4% WAP, the water retention of the FS approach that of clay loam soil (RS). The FS exhibited progressive improvement in water retention up to 0.4% WAP addition, whereas there was no

TH-2777_166104034

improvement for RS beyond 0.2%. This clearly demonstrates that the choice of percentage WAP addition is soil texture dependent, and a comprehensive investigation is needed to understand the optimal percentage of WAP for different soil texture.

7.4 Drying WRCC of FA-WAP amended soil

The drying WRCC of the used soils with FA-WAP amendment was measured using the same methodology as discussed above and presented in Fig. 7.7. A similar improvement in water retention behavior of the used soils with FA-WAP amendment was observed. For a better comparison of the improvement in water retention characteristics, some of the important parameters of the WRCC were calculated and compared in the following section.

7.4.1 Saturated VWC of Com-WAP and FA-WAP amended soil

At fully saturated state, volumetric water content (θ_s) was observed to be highest in RS (49.4%), followed by BS (33.4%) and FS (30.2%) without polymer amendment. Addition of FA-WAP and Com-WAP has increased the θ_s value for each soil texture, as presented in Fig. 7.8. It can be seen from the figure that the increase in θ_s is proportional to the concentration of WAP. At maximum concentration of FA-WAP amendment (0.4%), the increase in θ_s for RS is 50%, whereas for BS and FS, the increase is about 92% and 120%, respectively. The higher improvement in θ_s for FS is attributed to the low cationic exchange capacity (CEC) of coarse-textured soil (FS) compared to the other two soils (BS and RS). As the used hydrophilic polymer is ionic in nature, the equilibrium swelling capacity of the polymer decreases with the increase in CEC of soil resulting in less improvement in θ_s for fine-textured soil (Agaba et al. 2010). The improvement in θ_s value with FA-WAP amendment is very similar to that of the com-WAP amendment in each soil texture. It should be noted that θs is a representation of soil-water storage, and it increases with WAP addition. For a known volume of soil, the increase in soil-water storage can be calculated by Eq. (7.1).

$$\Delta S = V_G \times (\theta_{SA} - \theta_{SB}) \qquad 7.1$$

where ΔS = increase in soil-water storage; V_G = geometric volume of the soil; θ_{SA} = saturated volumetric water of WAP amended soil; θ_{SB} = saturated volumetric water of bare soil. From Fig. 7.8, it can be understood that the soil-water storage increases with WAP amendment and found to be highest in the case of FS at 0.4% WAP concentration (C3). It is worth noting that irrespective of texture, all soils considered in this study exhibit reasonably high soil-water storage at 0.4% WAP addition.

TH-2777_166104034

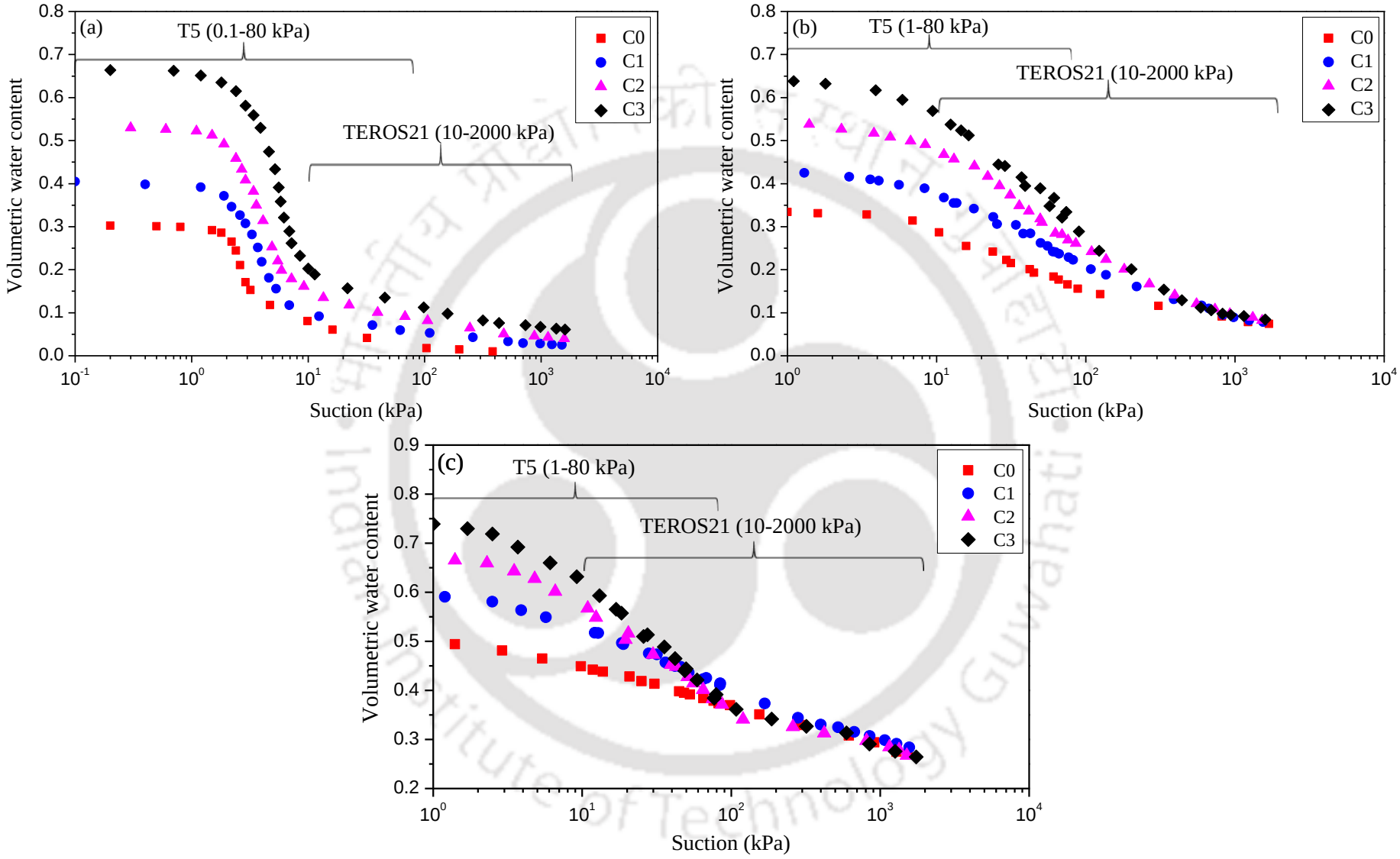

Fig. 7.7 Measured DWRCC of (a) Fine sand (FS), (b) Brahmaputra silt (BS) and (c) Red soil (RS) with different FA-WAP concentration

TH-2777_166104034

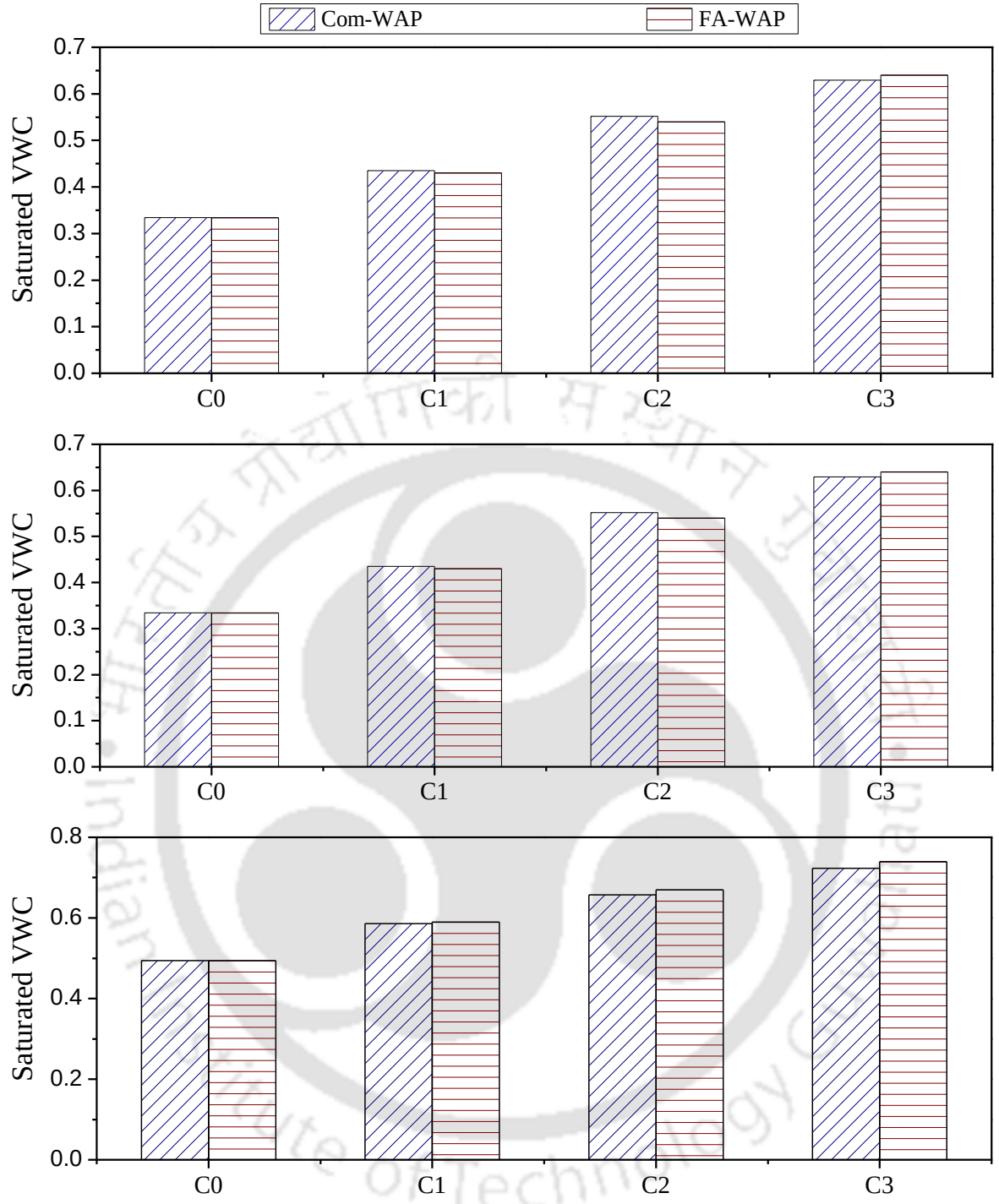

Fig. 7.8 Comparison of saturated VWC of the used soils with different WAP concentrations

7.4.2 Plant available water content (PAWC) in Com-WAP and FA-WAP amended soil

For agronomic applications and water stress conditions, one of the important parameters is to quantify the amount of water held in soil pores that can be used by the flora. Hence, it is necessary to estimate the efficiency of WAP for increasing the plant available water content (PAWC) in different soil texture. In general, PAWC is quantified as the difference between field capacity (FC) and the permanent wilting point (PWP). As the exact quantification

TH-2777_166104034

of FC through laboratory experimentation for a given soil type is rarely possible, the lower positive pressures applied to the pressure chamber (5 kPa and 10 kPa) were used for coarse-textured soils in the previous studies (Coleman 1947; Jamison and Kroth 1958; Rivers and Shipp 1977; Cassel and Nielsen 1986). Therefore, in the present study, a matric suction value of 5 kPa was selected for estimating FC of FS, while 33 kPa suction value was selected for BS and RS. The main reason for selecting such a low value of suction in coarser textured soil is that the water held at suction 5 kPa is equivalent to the pores sizes finer than 60 μm, which is the maximum limit of drainage pores as suggested by Greenland (1981). On the other hand, the water content corresponding to 1500 kPa is considered as PWP because the plant permanently wilts beyond this suction and fails to recover even after irrigation.

Figure 7.9 represents the variation of FC, PWP for the used soils at four different concentrations of Com-WAP and FA-WAP amendment. It can be observed that both the FC and PAWC were increased with the incorporation of WAP for FS and BS. At the maximum concentration of FA-WAP, the increase in PAWC for FS and BS were 3.3 times and 2.5 times, respectively, as compared to bare soil. This clearly indicated that WAP absorbs and retains a huge quantity of water during irrigation or rainfall and acts as an additional reservoir. As the soil dries during the drought period, the absorbed water in WAP is released to the soil, which the plant roots can uptake. However, the improvement in FC and PAWC for RS was found to be only 1.4 times even after 0.4% FA-WAP amendment. Moreover, water content at PWP of bare RS, as well as FA-WAP amended RS, was found within a range of 26-28%, which denotes that a significant amount of water stored by RS was not available for plant roots. As a result, the WAP amendment was found less effective for RS for increasing the PAWC during water stress period. A comparison in the performance of FA-WAP with the commercial WAP showed slightly higher improvement in the FC and PAWC with the former one. These results indicate the improved efficiency of synthesized FA-WAP over the commercial WAP.

7.4.3 Plant wilting time in Com-WAP and FA-WAP amended soil

The plant wilting time (Johnson 1984; Koupai et al. 2008) was determined from the measured matric suction versus time response (measured using T5 and TEROS21) during continuous drying, as depicted in Fig. 7.10 and 7.11. Generally, the time required to reach PWP is denoted as the wilting time of the plant under water stress conditions since plant roots cannot extract water beyond this (Koupai et al. 2008). It may be noted that wilting time is calculated from the measured WRCC of soil without considering the plant physiology, which is widely adopted method in the literature (Koupai et al. 2008; Banedjschafie and Durner 2015).

TH-2777_166104034

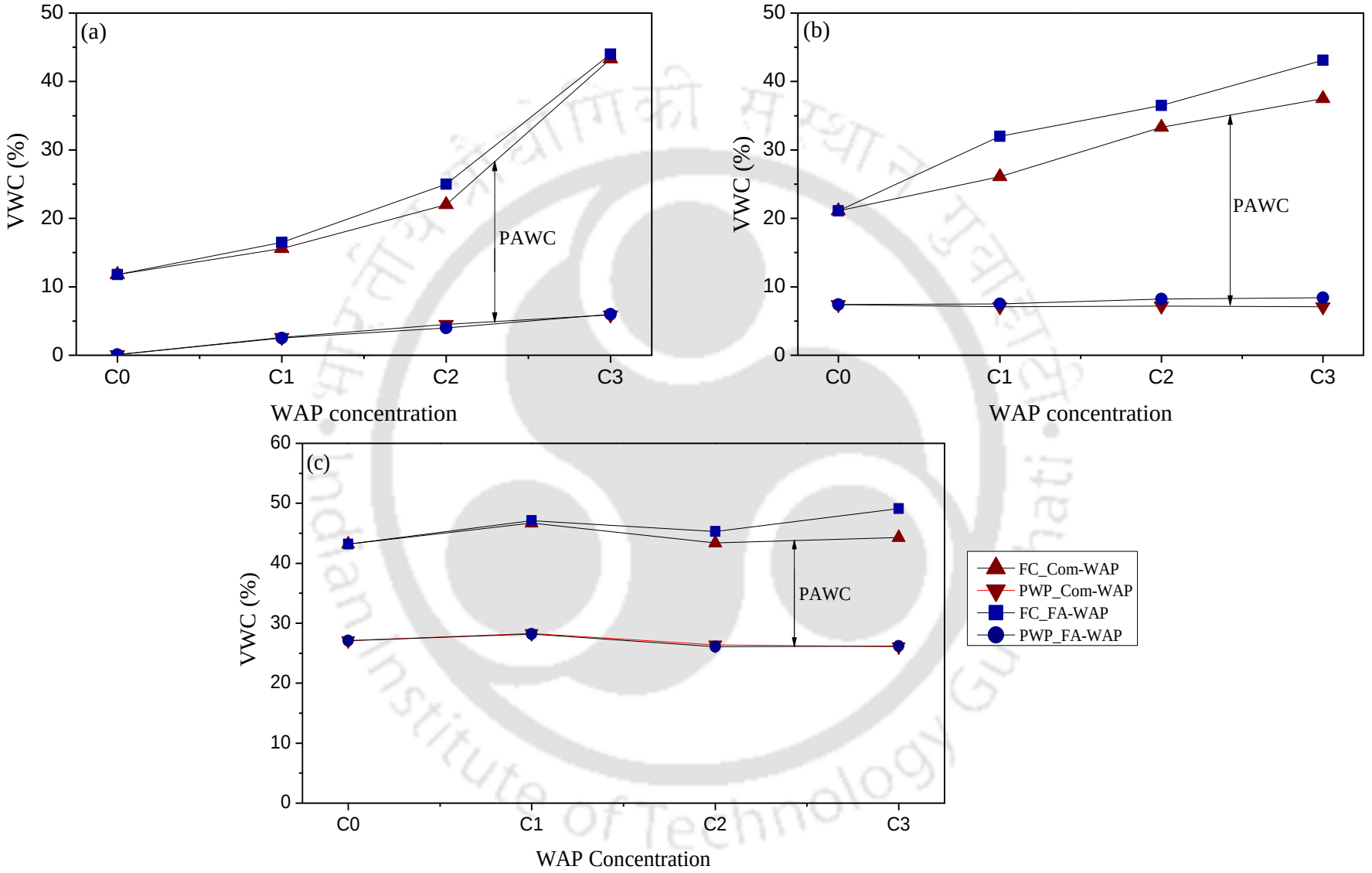

Fig. 7.9 FC, PWP of (a) Fine sand (FS), (b) Brahmaputra silt (BS) and (c) Red soil (RS) with different WAP concentrations

TH-2777_166104034

As it can be observed in Fig. 7.10 and Fig. 7.11, the application of WAP has significantly increased the time to reach the PWP. The bare FS has reached the wilting point within 8 days, whereas the maximum concentration of FA-WAP (C3) has prolonged the wilting time to 32 days. The increase in the wilting time can be directly related to the increase in the PAWC. A similar trend was noted for BS, where the maximum concentration of Com-WAP has prolonged the wilting time by 2.6 times. In the case of RS, though the PAWC was not significantly improved with the WAP amendment, the witling time was also increased by a factor of 2.6 times as compared to bare soil due to the increase in water storage with WAP addition. On the other hand, the addition of Com-WAP increased the wilting time by 4 times, 2.8 times, and 2.4 times FS, BS, and RS, respectively.

For the assessment of irrigation water requirement, the irrigation frequency was calculated based on the suction-time variation. Irrigation frequency (IF) can be denoted by the time difference between FC and PWP. The obtained IF for the used soils with four different concentrations of FA-WAP and Com-WAP were presented in Table 7.1. It can be observed that incorporation of both the WAP has increased the IF, irrespective of soil texture. The results showed that the IF was increased by 4 times, 3.3 times, and 3.5 times with maximum FA-WAP concentrations in FS, BS, and RS, respectively. This indirectly restricts excess leaching of nutrients by subsurface water flow and saves a considerable amount of irrigation water under drought conditions. However, this study was conducted under laboratory conditions, and its application in field condition needs to be assessed.

A comparative study was presented in Fig. 7.12 based on the obtained results to estimate the amount of irrigation water saved due to the WAP addition for establishing the effectiveness of WAP in drought conditions. The amount of irrigation water required (per annum) for agricultural land of 1 ha was evaluated with different WAP concentrations (using Eq. 7.2). It may be noted that the above quantification is proposed for an ideal condition without considering any water loss due to downward infiltration and surface runoff.

$$\text{Water requirement per irrigation, V} = (\theta_{FC} - \theta_{PWP}) \times A \times h$$

$$\text{Total water requirement (per annum)} = \text{V} \times \frac{365}{IF} \qquad 7.2$$

Here, A is the area of land, and h is the depth of WAP amended soil, which is equal to the root zone of crop species (taken as 15 cm).

TH-2777_166104034

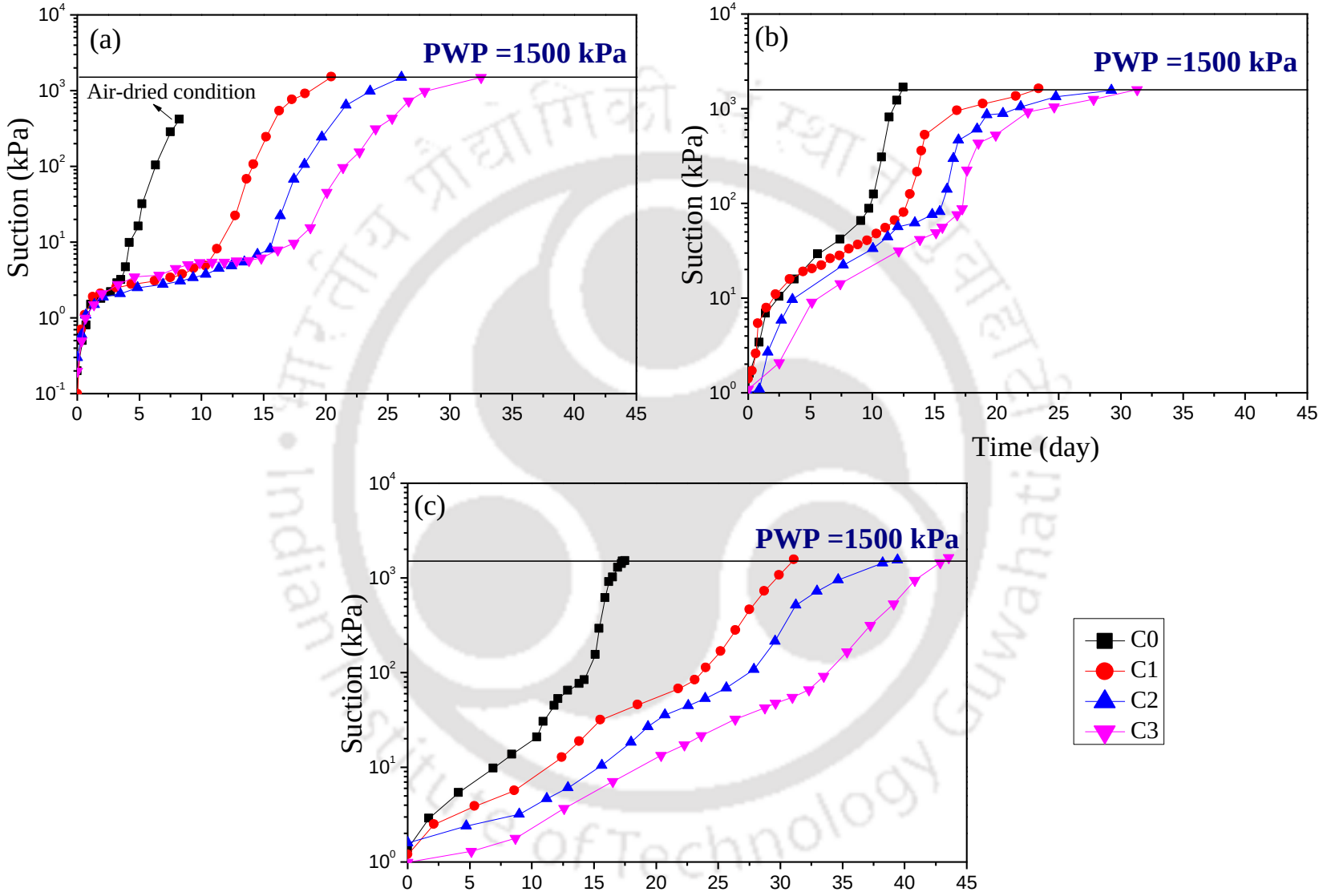

Fig. 7.10 Suction-time variation time for (a) FS, (b) BS, and (c) RS with varying Com-WAP concentration

TH-2777_166104034

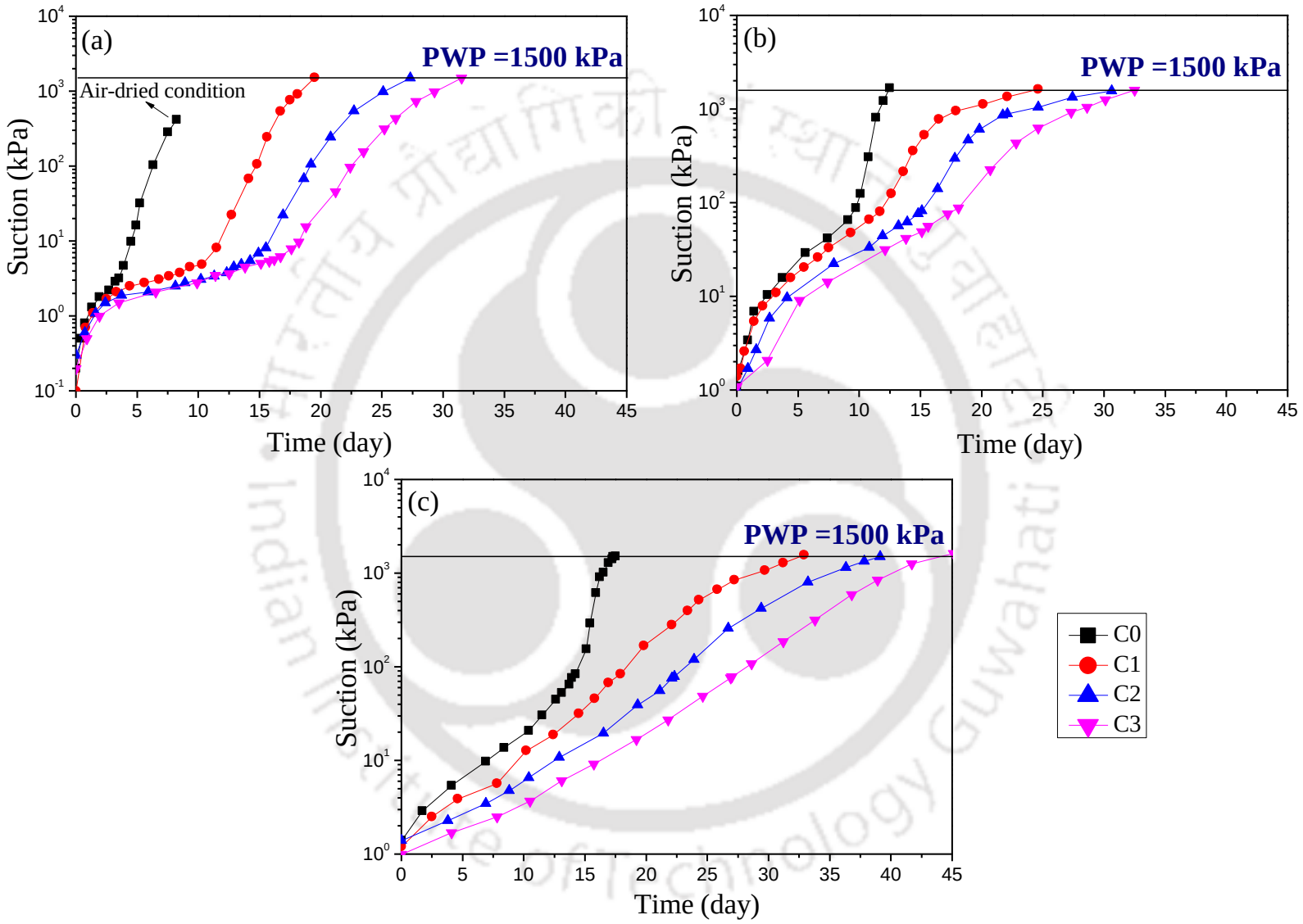

Fig. 7.11 Suction-time variation time for (a) FS, (b) BS, and (c) RS with varying FA-WAP concentration

TH-2777_166104034

Table 7.1 Calculated irrigation frequency (IF) for the used soils

Used soils	WAP concentrations (%)	IF (days)	
		Com-WAP	FA-WAP
FS	C0	4	4
	C1	8	9
	C2	10	13
	C3	15	16
BS	C0	6	6
	C1	14	17
	C2	18	19
	C3	18	20
RS	C0	6	6
	C1	15	18
	C2	17	20
	C3	16	21

It can be observed from Fig. 7.12 that the WAP amendment has significantly reduced the irrigation water requirement for all soil texture. A maximum reduction of 52%, 40%, and 62% in irrigation water was noticed with FA-WAP amendment in FS, BS, and RS, respectively, as compared to bare soil. Based on the irrigation water requirement, it can be concluded that the optimum WAP application rate (both FA-WAP and Com-WAP) for coarse-textured soils (sand, silt loam) is 0.1% while for fine-textured soil (clay loam) the application rate is 0.2%. However, it is worth noting that the present study was conducted in a pot experiment under controlled laboratory conditions and its application in field condition needs to be assessed. Moreover, the recommendation needs to be further verified based on the crop yield observed in the field for a wide variety of soil texture.

7.5 Prediction of drying WRCC of WAP amended soil

To overcome tedious suction measurement procedures, the present study tries to develop a simple WRCC model that can predict water retention behavior of WAP amended soils based on individual WRCC parameters of bare soil and WAP. Previous researchers have proposed predictive WRCC models for soil amended with biochar, natural fibre, and plant roots (Ng et al. 2016; Ni et al. 2019; Yi et al. 2020). It may be noted that the properties of WAP are

TH-2777_166104034

quite different than those materials because WAP can store huge amounts of water within its polymer structure and induce volume change after swelling. Therefore, the existing models may not be suitable for WAP amended soil, and there is a need to develop predictive model for WRCC of WAP amended soils.

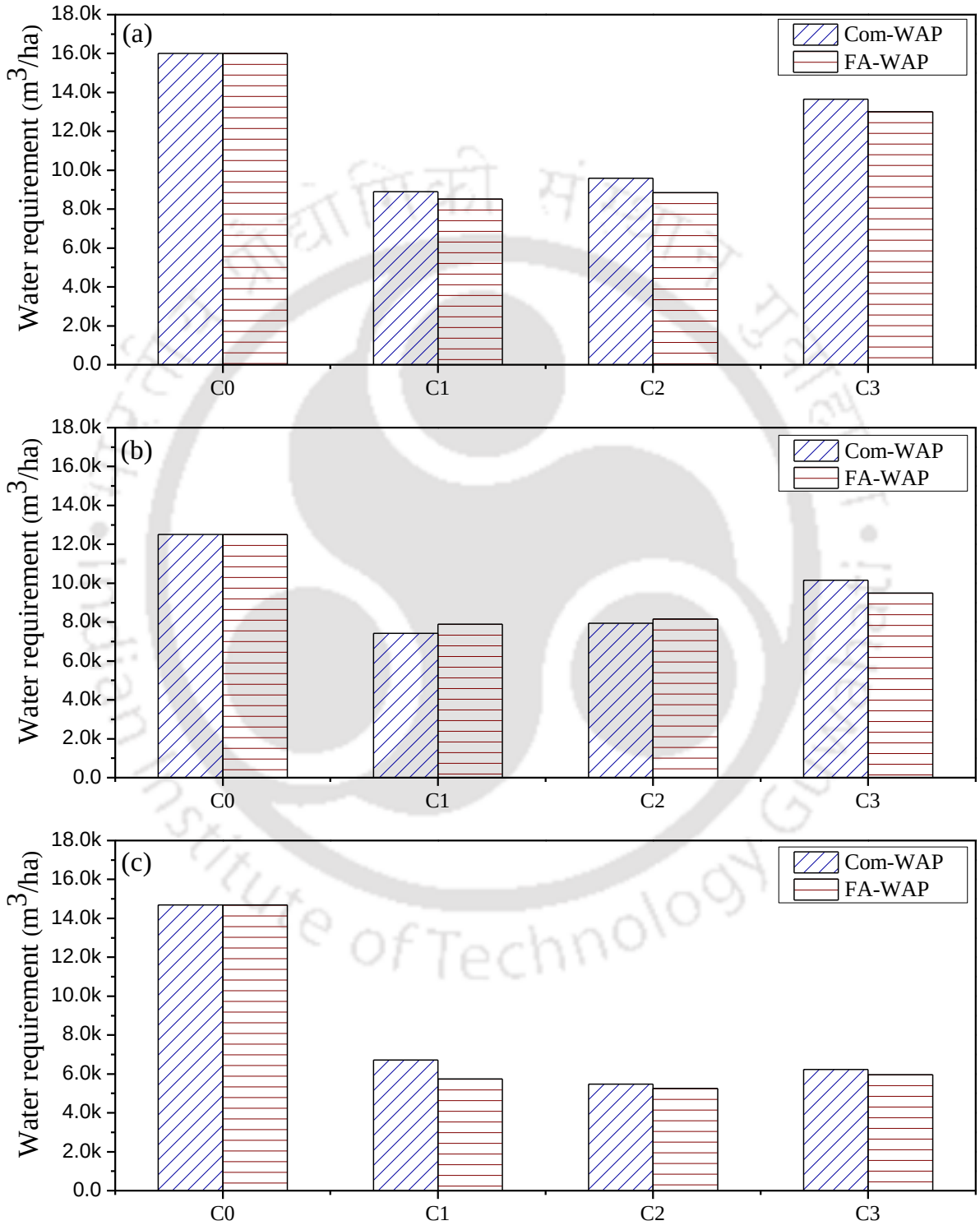

Fig. 7.12 Requirement of irrigation water in different textured soils

TH-2777_166104034

There are few theoretical WRCC models present in the literature for biopolymer amended soil. Rosenzweig et al. (2012) reported a WRCC model of biopolymer amended soil based on the linear superposition of retention curves for bare soil and pure xanthan gum. The model did not consider the influence of biopolymer on the volumetric behavior of amended soil and hence can predict only gravimetric water content. Zhou et al. (2020) developed a theoretical model to describe the WRCC of biopolymer amended soil by considering soil-biopolymer interaction. However, the model requires knowledge of seven parameters, out of which one parameter needs the knowledge of swelling-suction characteristic curve of biopolymer amended soils.

7.5.1 Development of WRCC model

The degree of saturation (S_r) of bare soil at particular suction, ψ can be obtained from the void ratio-dependent WRCC equation proposed by Gallipoli et al. (2003),

$$S_r = \left[1 + \left(\frac{\psi \times e_s^{m_4}}{m_3}\right)^{m_2}\right]^{-m_1} \qquad 7.3$$

Here, e_s is the void ratio of bare soil; m_1 (dimensionless), m_2 (dimensionless), m_3 (kPa), and m_4 (dimensionless) are WRCC model parameters, where m_1, and m_2 control the shape of WRCC, and m_3 and m_4 are related to the air-entry value of soil (Ng et al. 2016). These model parameters can be obtained by fitting Eq. (7.3) to the measured WRCC of bare soil.

2.2 Void ratio of the WAP amended soil

The void ratio of WAP amended soil was calculated based on the phase diagram, as presented in Fig. 7.13. A typical WAP amended soil consists of soil particles, WAP particles, pore water, and air. The pore water can be divided into two categories, i.e., water retained by the WAP particles within its polymer network and water retained by the soil-pores. There are two important assumptions and simplifications for the estimation of void ratio for WAP amended soil. Firstly, it was assumed that the WAP swells after water absorption, and the swelling of WAP induce volume change in the amended soil. The volume expansion in amended soil is assumed to be same as the incremental volume of swollen WAP. Secondly, the density of absorbed water within the WAP particle is assumed to be same as the density of water retained in soil-pores.

Void ratio of bare soil can be expressed as,

TH-2777_166104034

$$e_s = \frac{V_{vs}}{V_{ss}} \tag{7.4}$$

Void ratio of the WAP can be expressed as,

$$e_p = \frac{V_{wp}}{V_{sp}} = \frac{\frac{M_{wp}}{\gamma_w}}{\frac{M_{sp}}{G_p \gamma_w}} = \frac{M_{wp}}{M_{sp}} \times G_p$$

$$e_p = w_{p(\psi)} \times G_p \tag{7.5}$$

Here, V_{vs} and V_{ss} represent the volume of voids and solids in bare soil, V_{wp} is the volume of water absorbed by WAP, V_{sp} is the volume of solid in WAP, M_{wp} is the mass of water absorbed by WAP, M_{sp} is the mass of WAP, G_p is the specific gravity of WAP, and $w_{p(\psi)}$ is the gravimetric water content (GWC) of WAP at any suction, ψ.

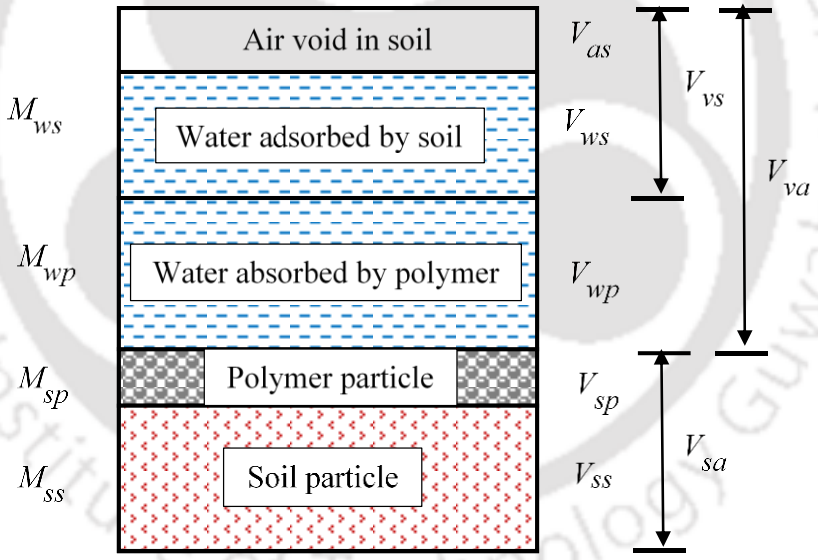

Fig. 7.13 Phase diagram of unsaturated soil amended with WAP

The gravimetric WRCC of hydrophilic polymer can be described by Eq. (7.6) [Zhou et al. 2020]

$$w_{p(\psi)} = \frac{p_1}{1 + \psi^{p_2}} \tag{7.6}$$

Here, p_1 and p_2 are the polymer-based parameters, which can be obtained from the measured WRCC of WAP.

TH-2777_166104034

Volume ratio of WAP-soil solid is given by

$$v = \frac{V_{sp}}{V_{ss}} = \frac{\frac{M_{sp}}{G_p \gamma_w}}{\frac{M_{ss}}{G_s \gamma_w}} = \frac{M_{sp} \times G_s}{M_{ss} \times G_p} = m \times \frac{G_s}{G_p} \quad 7.7$$

Here, m $(= \frac{M_{sp}}{M_{ss}})$ is dry mass ratio of WAP and soil, G_s represent specific gravity of bare soil.

Now, void ratio of the amended soil can be expressed as,

$$e_a = \frac{V_{va}}{V_{sa}} = \frac{V_{vs} + V_{wp}}{V_{ss} + V_{sp}} = \frac{\frac{V_{vs}}{V_{ss}} + \frac{V_{wp}}{V_{ss}}}{1 + \frac{V_{sp}}{V_{ss}}} = \frac{e_s + \frac{V_{wp}}{V_{sp}} \times \frac{V_{sp}}{V_{ss}}}{1 + \frac{V_{sp}}{V_{ss}}}$$

$$e_a = \frac{e_s + e_p \times v}{1 + v} = \frac{e_s + \left(\frac{p_1}{1 + \psi^{p_2}}\right) \times m \times G_s}{1 + \left(m \times \frac{G_s}{G_p}\right)} \quad 7.8$$

The WRCC of WAP amended soil in term of S_r–ψ can be expressed as,

$$S_r = \left[1 + \left(\frac{\psi \times e_a^{m_4}}{m_3}\right)^{m_2}\right]^{-m_1} \quad 7.9$$

The WRCC in term of volumetric water content (VWC), θ–ψ can be expressed as,

$$\theta = (\theta_s - \theta_r) \times \left[1 + \left(\frac{\psi \times e_a^{m_4}}{m_3}\right)^{m_2}\right]^{-m_1} + \theta_r \quad 7.10$$

Here, θ_s and θ_r are saturated and residual VWC, respectively.

7.5.2 Validation of the proposed WRCC model

To validate the proposed model, laboratory test was conducted to measure the WRCC of a commercial-grade WAP and synthesized FA-WAP. The WRCC of both the WAPs were measured using a miniature tensiometer, T5 (UMS GmbH, Munich, Germany) connected to a data logger (DL6) and a high accuracy weighing balance (accuracy= 0.001 g), as shown in Fig. 7.14. Prior to the measurement, the dry WAP particles were immersed in the deionized water until it reaches the equilibrium condition. The water-swollen WAP was placed in a PVC

TH-2777_166104034

column (with a diameter of 150 mm and height of 200 mm) after filtering out the excess water. The tensiometer was placed inside the column vertically for continuous measurement of suction, while the GWC of WAP was monitored using the weighing balance. The whole setup was subjected to ambient drying conditions, with an average temperature =25 ℃ and average relative humidity =70%.

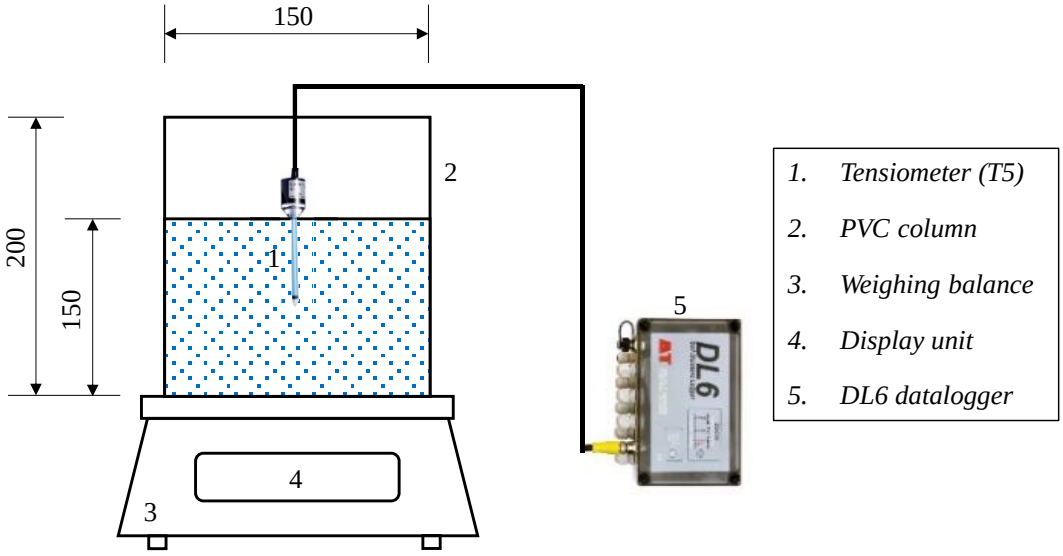

Figure not to scale

All dimensions are in mm

Fig. 7.14 Experimental methodology to measure WRCC of WAP

The measured gravimetric WRCC of WAPs, as presented in Fig. 7.15, showed very high-water retention capacity in near-saturated state. With the progressive drying in ambient condition, the GWC of Com-WAP and FA-WAP were reduced to 30 (g/g), and 12 (g/g) at ψ value close to 10 kPa. A similar trend of WRCC was observed in Rosenzweig et al. (2012) for WRCC of pure xanthan gum biopolymer. Equation 7.6 was fitted to the measured data using nonlinear regression analysis, and the obtained values of polymer-based parameters (p_1 and p_2) were presented in Table 7.2 along with the regression coefficient (R^2) value. These values were further used for validation of the proposed model for different textured soils.

Table 7.2 Polymer based parameters for the used WAPs

Used WAP	p_1	p_2	R^2
Com-WAP	280	1	0.99
FA-WAP	310	1.5	0.99

TH-2777_166104034

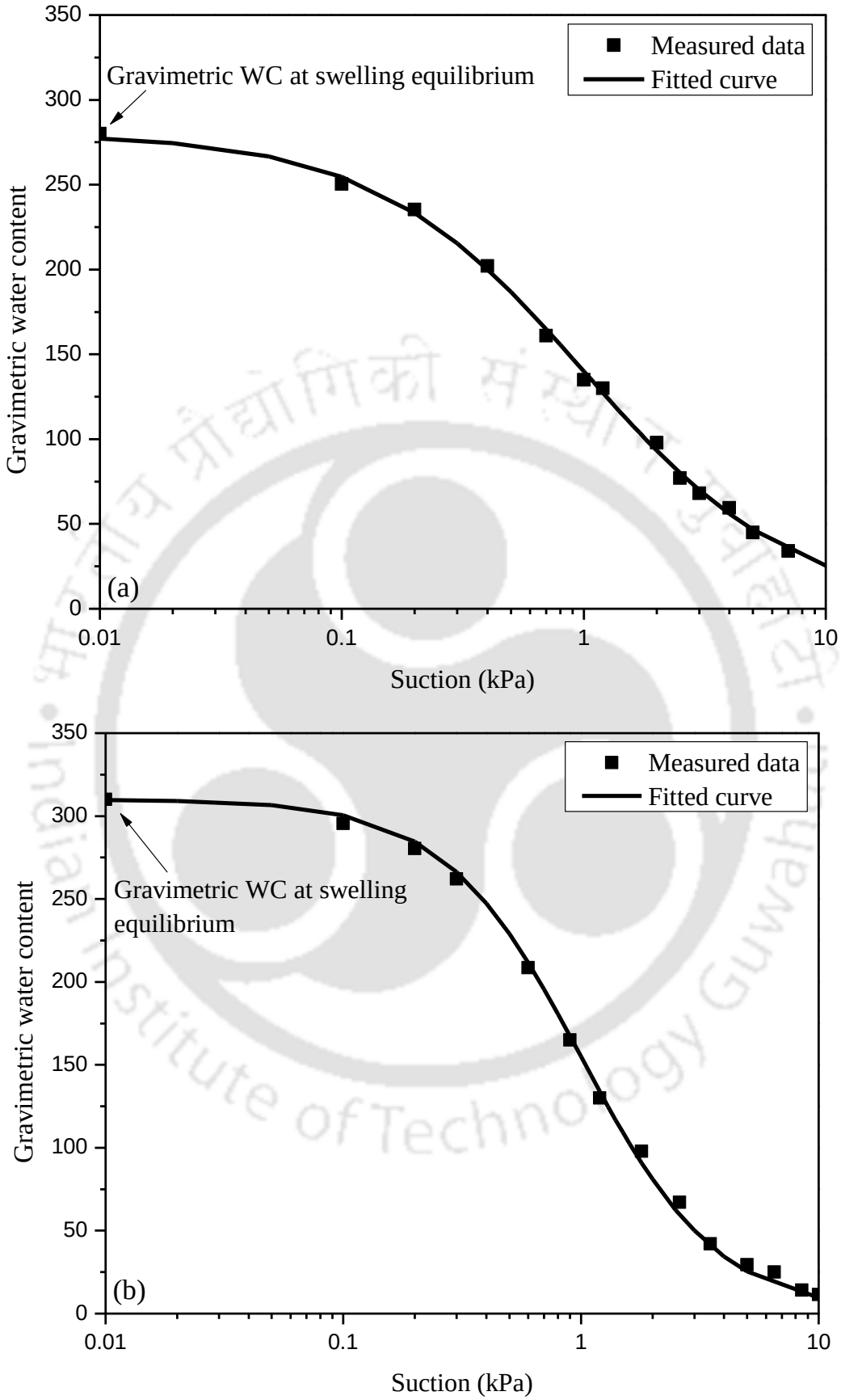

Fig. 7.15 Measured gravimetric-WRCC of (a) Com-WAP and (b) FA-WAP using T5 tensiometer

TH-2777_166104034

Figures 7.16-7.17 present the measured WRCC of bare soil and WAP amended soils reported in the previous section. Each of the WRCC for bare soil was fitted to Eq. (7.3) to obtain m_1, m_2, m_3, and m_4 parameters for different textured soils (Table 7.3). It can be observed from Eq. (7.10) that the prediction of volumetric WRCC requires the value of θ_s and θ_r for WAP amended soils. The θ_s and θ_r values can be theoretically computed by measuring the GWC at the saturated state and air-dried state, respectively. It was observed from the measured WRCC data that the average θ_r value of WAP amended soils could be approximated as 0.03 for the amendment rate considered in this study. However, the prediction of WRCC, in terms of S_r-ψ, does not require these additional parameters.

Table 7.3 Summary of the WRCC parameters [Eq. (7.3)] for different textured bare soil

Used soil	e_s	m_1	m_2	m_3 (kPa)	m_4
FS	0.44	0.1	8	1.7	0.1
BS	0.5	0.14	2.8	7	0.4

The WRCC of the WAP amended soils were predicted based on the individual WRCC model parameters of bare soil and WAP and compared with the measured data. The proposed model was also validated with the literature reported WRCC of Com-WAP amended loamy sand (Leciejewski 2009). The R^2 value and root mean square error (RMSE) for each WAP concentration were calculated and presented in Figs. 7.16-7.18, which showed a good agreement between the reported and predicted WRCC for all the soil texture. It was further observed that the addition of WAP has significantly improved the saturated VWC as well as water retention behavior of soil in the low suction range (ψ <100 kPa). The reason for less improvement in the water retention of the amended soil in the higher suction range is attributed to the release of water from WAP and subsequent volume reduction at higher suction. The pore-blocking effect in the lower suction range and volume reduction of WAP in the higher suction range were well captured by the proposed model for different textured soils (FS, and BS). It can be noted that the proposed model is valid for cohesionless and low plastic soils, as it does not consider the complex interaction between WAP and negatively charged clay particles. Therefore, the proposed model cannot be applicable for fine-textured RS, where the clay percentage is close to 30%. However, the model can be used for any WAP type, and the polymer-based parameters (p_1 and p_2) need to be calculated for different types of WAP.

TH-2777_166104034

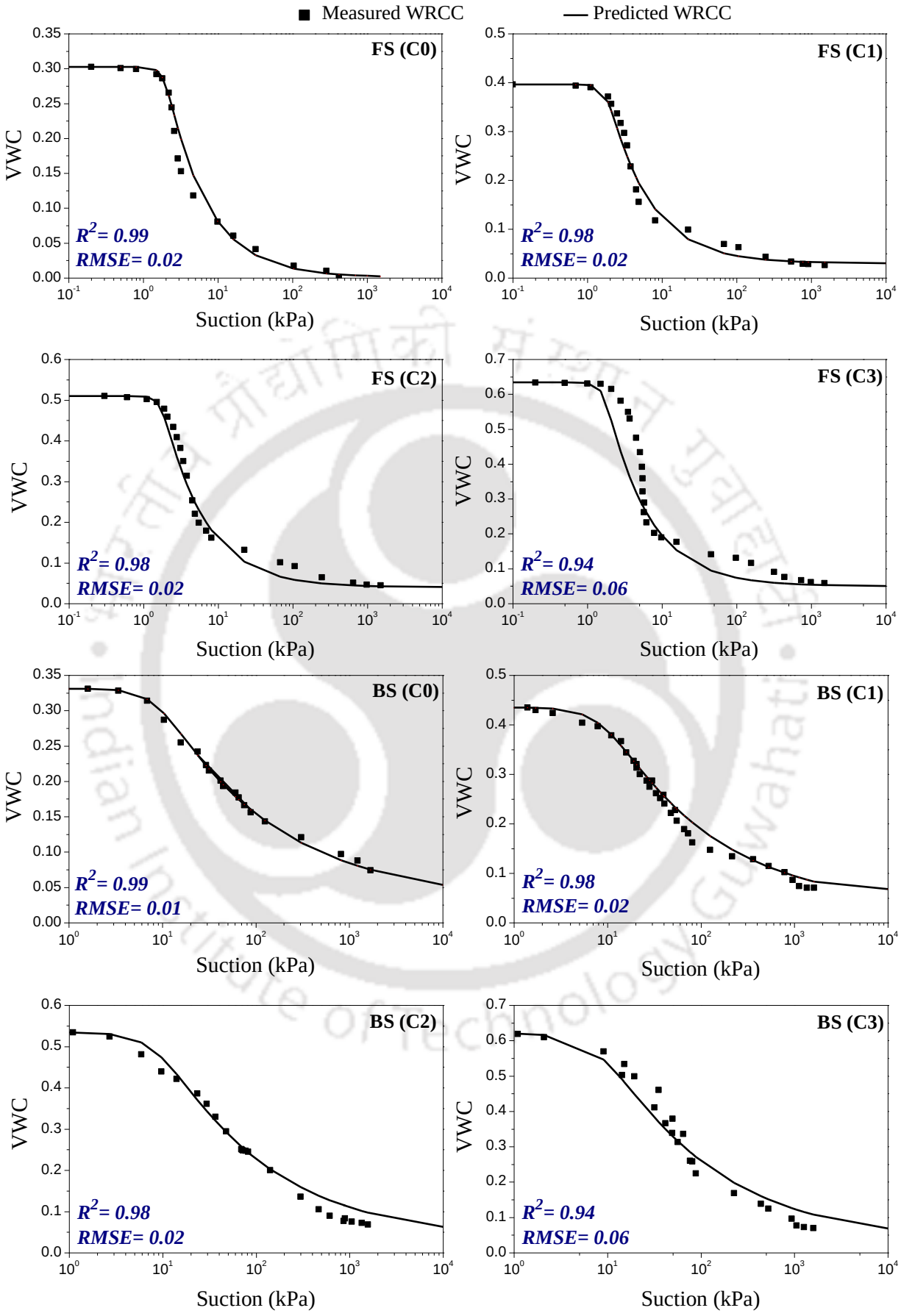

Fig. 7.16 Measured and predicted WRCC of Com-WAP amended soils

TH-2777_166104034

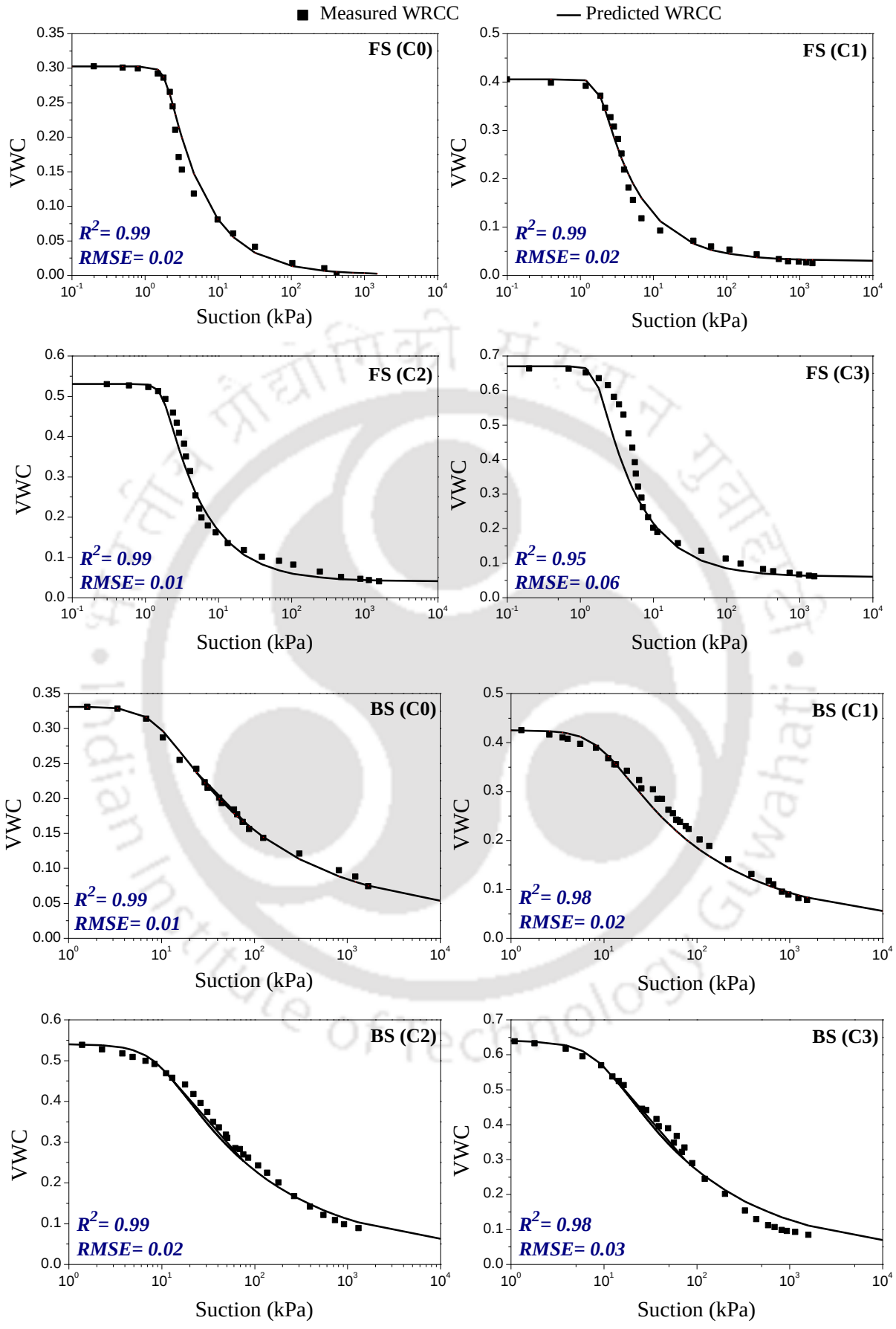

Fig. 7.17 Measured and predicted WRCC of FA-WAP amended soils

TH-2777_166104034

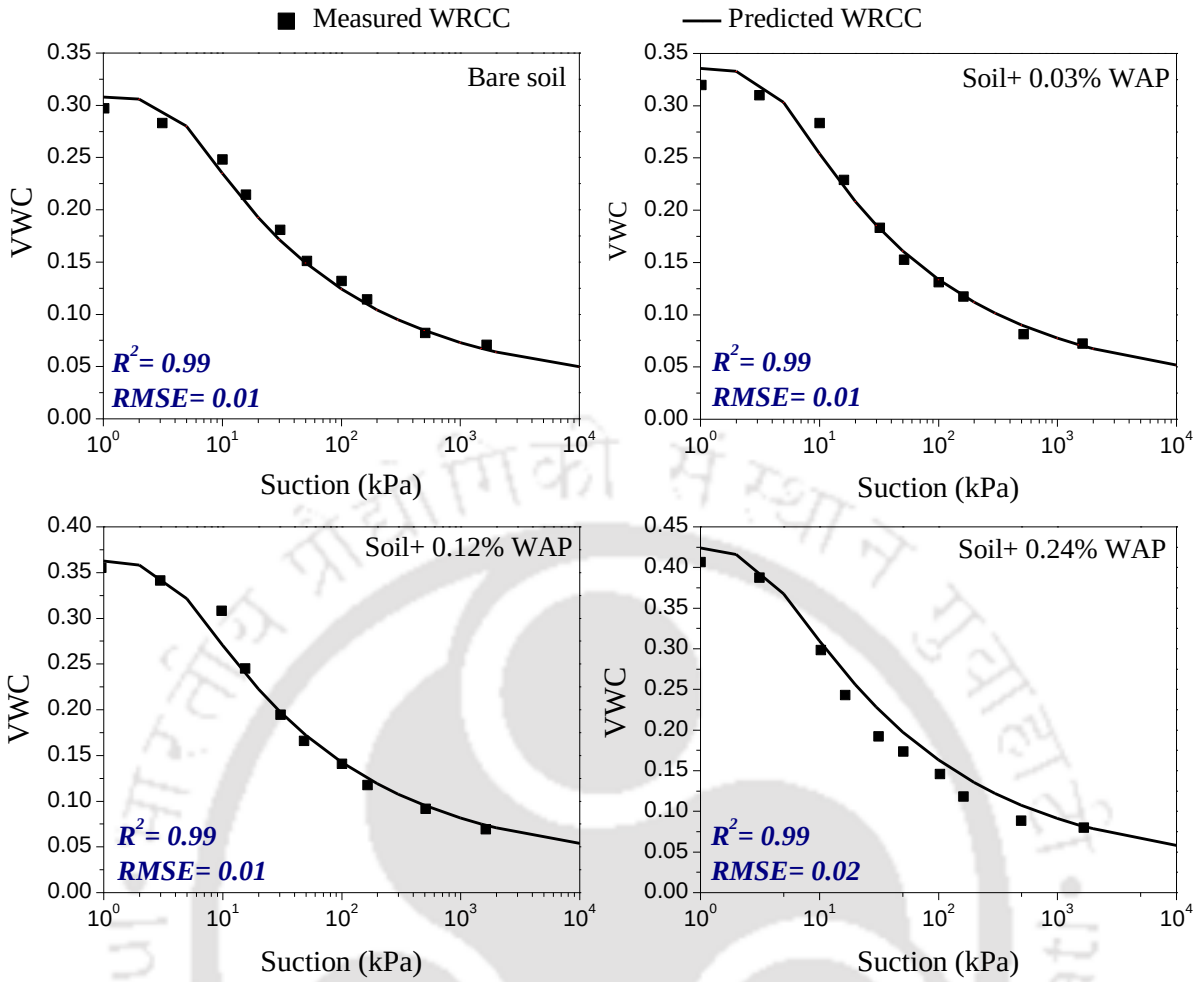

Fig. 7.18 Measured (Leciejewski, 2009) and predicted WRCC of WAP amended soil (Loamy sand)

7.6 Hysteresis in WRCC of WAP amended soil

The WRCC of soil can be obtained by progressively drying and wetting the sample. Continuous measurement of WRCC from a high-water content (suction corresponding to saturated state) to low-water content termed as drying water retention characteristic soil (DWRCC), whereas the WRCC obtained through continuous wetting of the same sample starting from a very low water content termed as wetting water retention characteristic soil (WWRCC). These WRCCs are often observed to exhibit hysteresis, which results in higher soil-water content along the drying path than the wetting path at the same suction (Lu and Khorsidi 2015; Chetia and Sekharan 2016). The hysteretic behavior of soil can be influenced by soil type, compaction state, stress history, and required to be accurately measured to evaluate the variation in hydraulic characteristics of soil with time (Likos et al. 2014). Determining the hysteresis in WRCC of WAP amended soils is extremely important as it is often exposed to the

TH-2777_166104034

changing weather and undergoes multiple wetting-drying cycles. Moreover, the existing theoretical models to predict the wetting WRCC from the drying WRCC need to be modified for WAP amended soils to avoid the direct measurement of wetting WRCC. There are not many studies reported in this direction.

The soil samples with different amounts of WAP were mixed with a sufficient quantity of tap water (EC= 0.11 mS/cm) to obtain water content close to the liquid limit prior to DWRCC measurement. The purpose of using tap water instead of distilled water is that the influence of WAP degradation on the hysteresis of WAP amended soils can be well understood. The measured DWRCC of the used soils amended with different WAPs were presented in Fig. 7.19 and 7.20, along with the WWRCC. It can be observed that the saturated VWC of the WAP amended soils were decreased in tap water due to the lower water absorbency of WAP in tap water. For the establishment of WWRCC, the TEROS21 data was not considered as it may give erroneous value due to the inherent hysteresis of the ceramic disk. Figures 7.19 and 7.20 clearly indicated that only T5 data was well enough to establish the WWRCC of the soil. Moreover, the initial portion of the wetting curve (i.e., ψ_m close to 80 kPa) for all the WAP concentrations was nearly the same. Afterward, the water content of the samples increased to its final value depending on the soil type and the application rate of WAP. The specific moisture capacity, represented by the slope of the curve ($d\theta/d\psi$), was found to be higher for higher concentrations of WAP and followed the trend C0 < C1 < C2 < C3 for all the soils. This was attributed to the fact that soil with a higher WAP percentage retained more water in comparison to the others, resulting in a higher specific moisture capacity.

It can be further observed from the wetting curve that the final VWC, achieved after the 1st wetting phenomenon, is lower than the initial saturated VWC due to the presence of entrapped air in the soil matrix. Hence, the next drying WRCC starts from a point lower than the initial drying WRCC (or boundary drying WRCC). It can be observed that the amount of water retained by the soil during the drying phase is higher than the water absorbed during the wetting phase at the same suction value. The hysteretic behavior in WRCC of soil is generally governed by the ink-bottle effect, resulting from the nonuniformity in the soil pore size distribution, contact angle hysteresis, and presence of entrapped air during wetting. These mechanisms are most common and predominant for the hysteretic behavior in bare soil, especially for cohesionless soil (FS) and low plastic clays (BS, RS).

TH-2777_166104034

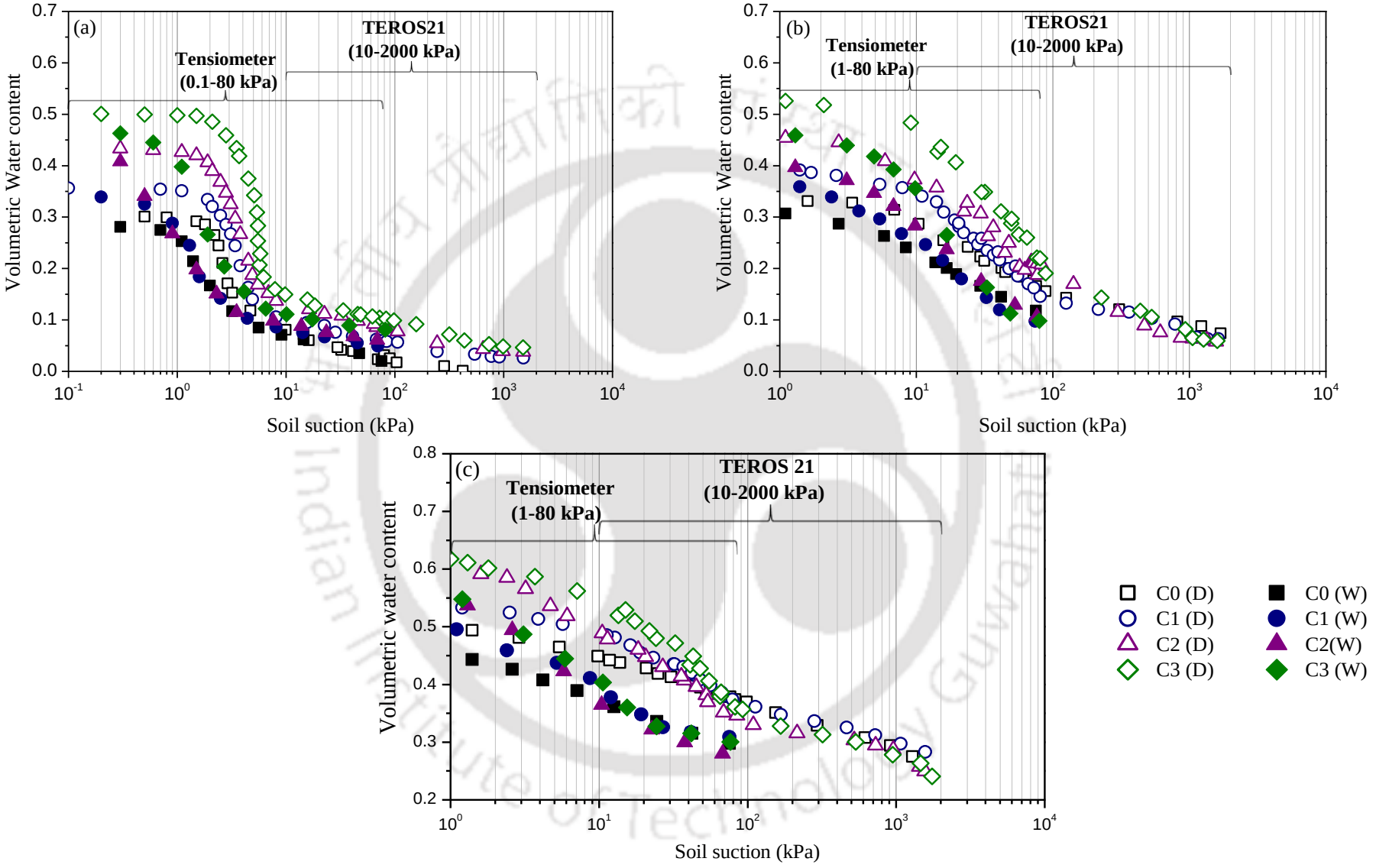

Fig. 7.19 Measured 1st drying-wetting WRCC of Com-WAP amended (a) FS, (b) BS and (c) RS

TH-2777_166104034

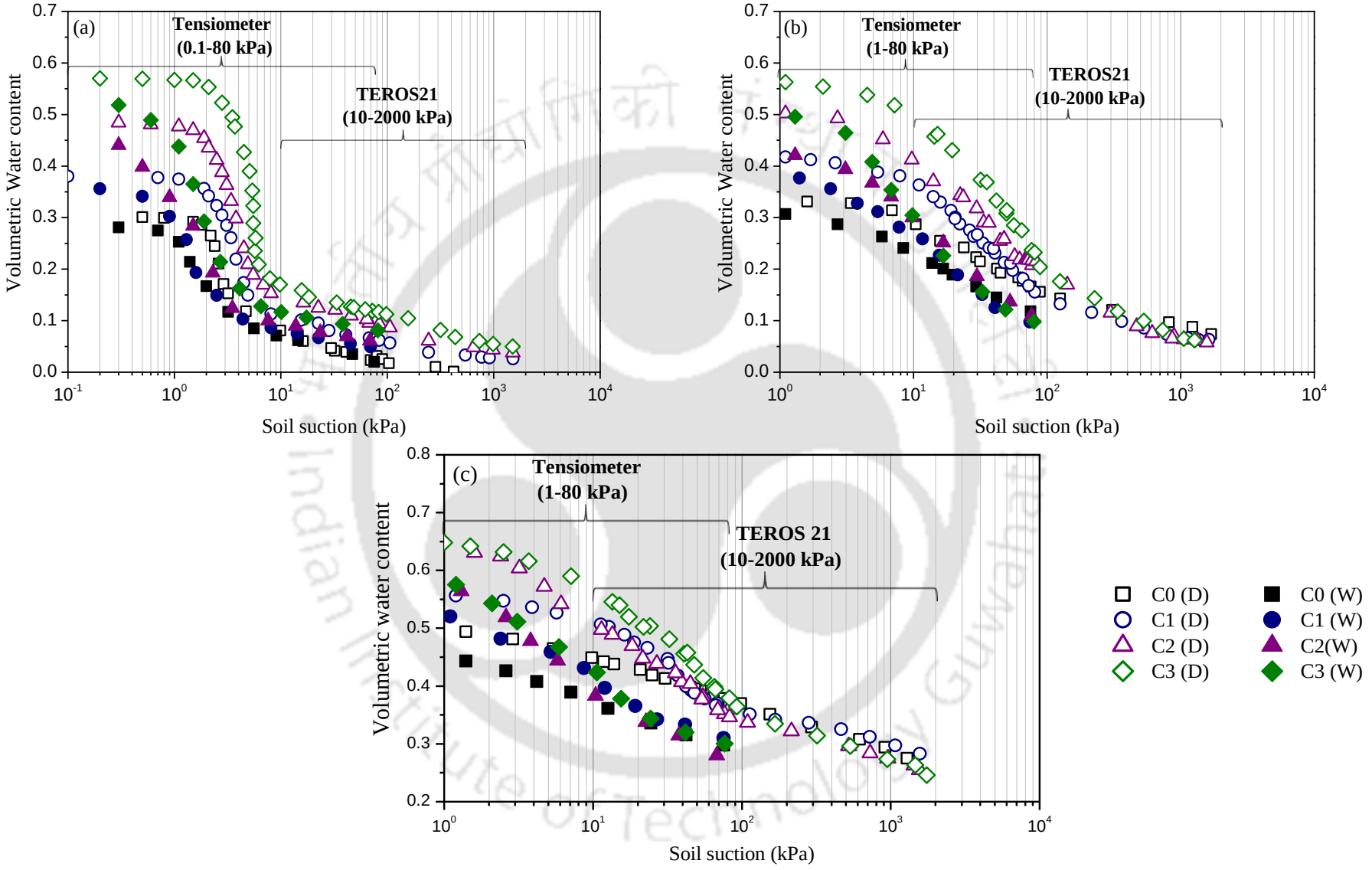

Fig. 7.20 Measured 1st drying-wetting WRCC of FA-WAP amended (a) FS, (b) BS and (c) RS

TH-2777_166104034

For WAP amended soils, along with the aforementioned mechanisms, there are additional mechanisms that also influence the hysteresis in WRCC. During the saturated state, with the increase in soil suction, water escapes from the largest pore in the soil matrix. This creates a pressure difference between soil particles and WAP particles and leads to the movement of water from the swollen WAP to soil-pores to maintain the degree of saturation close to 100%. As the soil continues to dry, the WAP particles shrink further to attain almost constant volume at the end of the saturation zone. The desaturation zone starts with the extraction of water from the largest pores of the soil matrix only at higher suction. In contrast, water enters into the WAP network at higher suction during the wetting phenomenon due to its higher water affinity, resulting in the swelling of WAP amended soil. Therefore, saturation of the largest soil-pore possible at lower suction value, creating a difference in the WRCC during the drying and wetting. During this process, the excess swelling and de-swelling of WAP also change the soil fabric and particle orientation differently between the drying and wetting cycles. Moreover, the swollen WAP traps water inside its polymer structure by strong attractive forces and hydrogen bond mechanism (ref. Fig. 7.21). Because of the existing attractive forces, more energy is required to expel water (during drying) from the polymer network as compared to water absorption (during wetting), resulting in a difference in WRCC. Apart from these, the aging of WAP plays a significant part in the hysteretic behavior of WAP amended soils, depending on the history of drying-wetting cycles. As the duration of the drying process is much higher as compared to the wetting process, the degradation of WAP is more pronounced during the drying phenomenon. This also leads to a difference in water absorbency of WAP between the drying and wetting cycles.

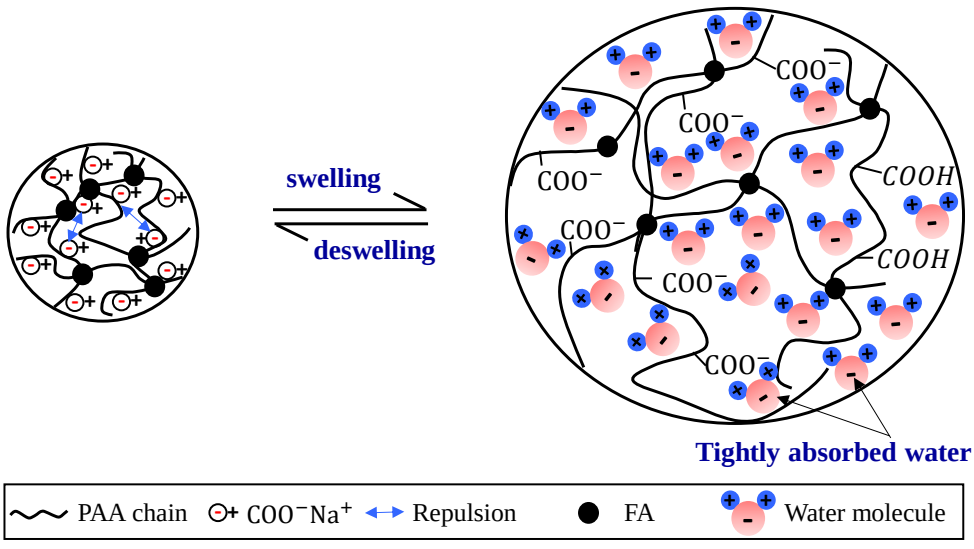

Fig. 7.21 Illustration of swelling mechanism and water molecule attraction inside FA-WAP

TH-2777_166104034

7.7 Hysteresis model for WAP amended soil

7.7.1 Theoretical background of hysteresis model

Figure 7.22 illustrates a typical representation of hysteretic behavior in WRCC of soil. The WRCC initiating from a completely saturated state ($\psi \approx 0$; θ_s) to a residual saturated state (due to progressive drying) is termed as initial drying WRCC. The WRCC starting from residual saturated state to saturated state (due to progressive wetting) is known as the main wetting WRCC. Upon further drying, The WRCC follows completely different path from the initial drying WRCC, which is termed as the main drying WRCC. The main drying WRCC and main wetting WRCC forms the hysteresis loop, and there can be infinite numbers of drying-wetting curves (known as scanning curve) within the hysteresis loop. Therefore, the main drying and wetting WRCC are also termed as boundary drying-wetting WRCC.

The measurement of hysteresis in WRCC is a time-consuming process and requires careful experimentation to measure the suction and water content during the drying-wetting process. To avoid the measurement of both drying and wetting WRCC, past researchers (Pham et al. 2003; Pham et al. 2005) have presented predictive models to obtain boundary wetting WRCC from boundary wetting WRCC. The boundary drying WRCC can be represented by the following equation (Eq. 7.11) proposed by Feng and Fredlund (1999),

$$\theta(\psi) = \frac{(\theta_u b_d + c\psi^{d_d})}{(b_d + \psi^{d_d})} \qquad 7.11$$

where, θ_u represents the volumetric water content (VWC) at zero suction on boundary drying WRCC; c parameter represents the VWC at the residual state and therefore same for both drying and wetting WRCC; b_d and d_d parameters are curve fitting parameters (boundary drying WRCC), which control to the air entry suction value.

For the prediction of wetting WRCC, Pham et al. (2003) provided the locations of two additional points on the wetting WRCC. The suction value (ψ_{1w}) of the first point on wetting WRCC can be calculated using,

$$\psi_{1w} = \left(\frac{b_d}{10}\right)^{\frac{1}{d_d}} \qquad 7.12$$

The suction value (ψ_{2w}) of second point on wetting WRCC can be calculated using,

TH-2777_166104034

$$\psi_{2w} = \psi_{1w} - 2\left[\left\{\frac{b_d(\theta_u - \theta_{1w})}{\theta_{1w} - c}\right\}^{\frac{1}{d_d}} - b_d{}^{\frac{1}{d_d}}\right] \quad 7.13$$

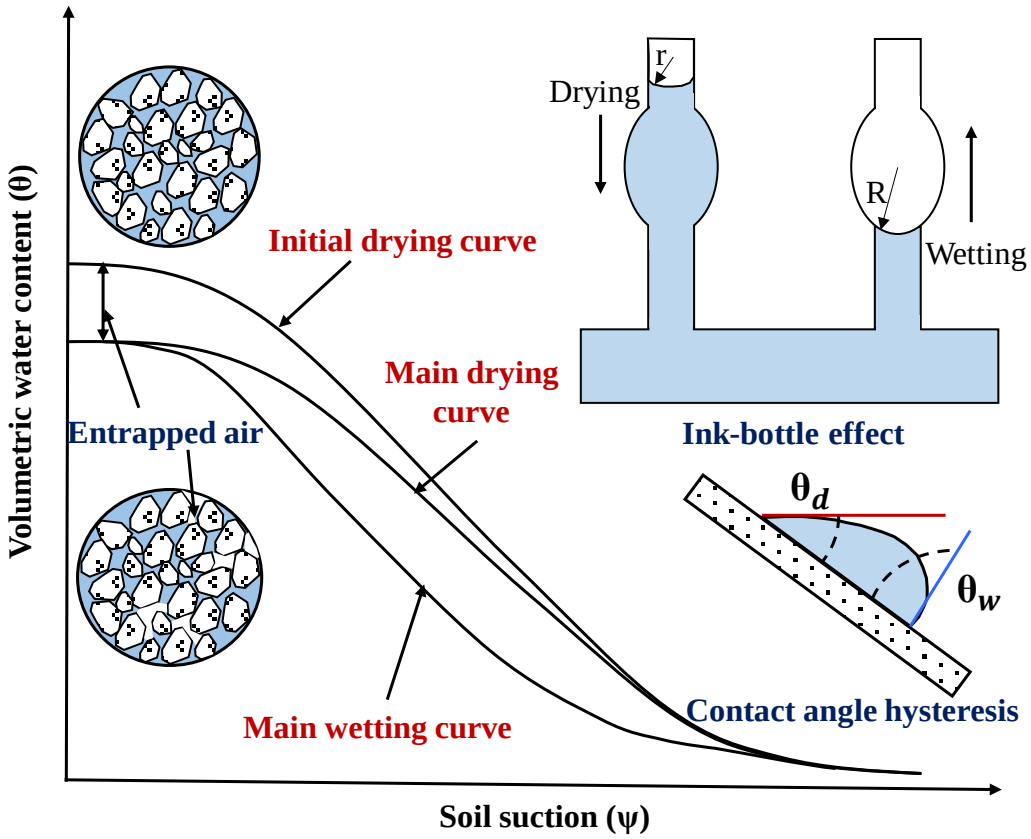

Fig. 7.22 Hysteresis in WRCC for bare soil

Where, θ_{1w} is the known VWC value corresponding to the first additional suction (ψ_{1w}) along wetting WRCC. The fitting parameters for wetting WRCC (b_w, and d_w) can be estimated from the location of these two additional points [(ψ_{1w}, θ_{1w}) and (ψ_{2w}, θ_{2w})] using the following equation,

$$d_w = \frac{\log\left[\frac{(\theta_{1w} - c)(\theta_u - \theta_{2w})}{(\theta_u - \theta_{1w})(\theta_{2w} - c)}\right]}{\log[\frac{\psi_{2w}}{\psi_{1w}}]} \quad 7.14$$

$$b_w = \frac{(\theta_{1w} - c)\psi_{1w}^{d_w}}{\theta_u - \theta_{1w}} \quad 7.15$$

TH-2777_166104034

The estimated fitting parameters (b_w, d_w, and c) can be used to predict the main wetting WRCC using,

$$\theta(\psi) = \frac{(\theta_u b_w + c\psi^{d_w})}{(b_w + \psi^{d_w})} \quad 7.16$$

Several past studies have highlighted the improved accuracy of the aforementioned hysteresis model for the prediction of boundary wetting WRCC from the boundary drying WRCC as compared to other existing models. Later, Pham et al. (2005) developed a scaling method (slope ratio and distance between boundary curves on semi-logarithm scale of soil suction) to predict the main wetting WRCC from initial drying WRCC. Pham and Fredlund (2011) proposed a volume–mass constitutive model to predict the main wetting WRCC from the initial drying WRCC under isotropic loading-unloading conditions. Gallipoli et al. (2015) proposed boundary hysteretic model based on a modified form of the van Genuchten equation (Galipoli et al. 2003) by taking void ratio into consideration, which can be used for expansive soils or high swelling clays. From these studies, it is quite evident that the prediction of main wetting WRCC from initial drying WRCC requires measured data of both initial drying WRCC and main drying WRCC.

7.7.2 Proposed model

The concept of boundary drying-wetting WRCC may not be valid for WAP amended soil. This is mainly due to the fact that the WAP particles interact with soil and water present in the pores, leading to degradation of the polymer chain as well as the water absorbency of WAP. This would influence the hysteresis in WRCC for WAP amended soils with repeated wetting-drying cycles. Hence, the modified representation of drying-wetting WRCC was proposed as shown in Fig. 7.23 based on the phase relationship, considering the following points,

i) The addition of WAP result in swelling due to water absorption, and therefore pore volume increases. This is represented by the increase in saturated volumetric water content [θ_u] of WAP amended soil.

ii) Due to the degradation of WAP network after alternate drying-wetting cycles, the swelling capacity of WAP reduces. Hence, θ_u of WAP amended soils reduce after every cycle.

iii) The *c* parameter (i.e., water content at high suction value) of WAP amended soil can change after repeated cycles (depending on soil minerology) due to the degradation of WAP network.

TH-2777_166104034

iv) After complete WAP degradation, the swelling ceases and the WRCC becomes similar to the bare soil.

v) The model fitting parameters, b_w and d_w are related to the water entry value and slope of the desaturation portion (or rate of water sorption), respectively.

As it is shown in Fig. 7.23, the 1st drying WRCC initiates from a fully saturated state and reaches to residual state with progressive drying, while the 1st wetting WRCC starts from the residual state to saturated state due to progressive wetting. Upon further drying, the 2nd drying WRCC starts from the endpoint of 1st wetting WRCC.

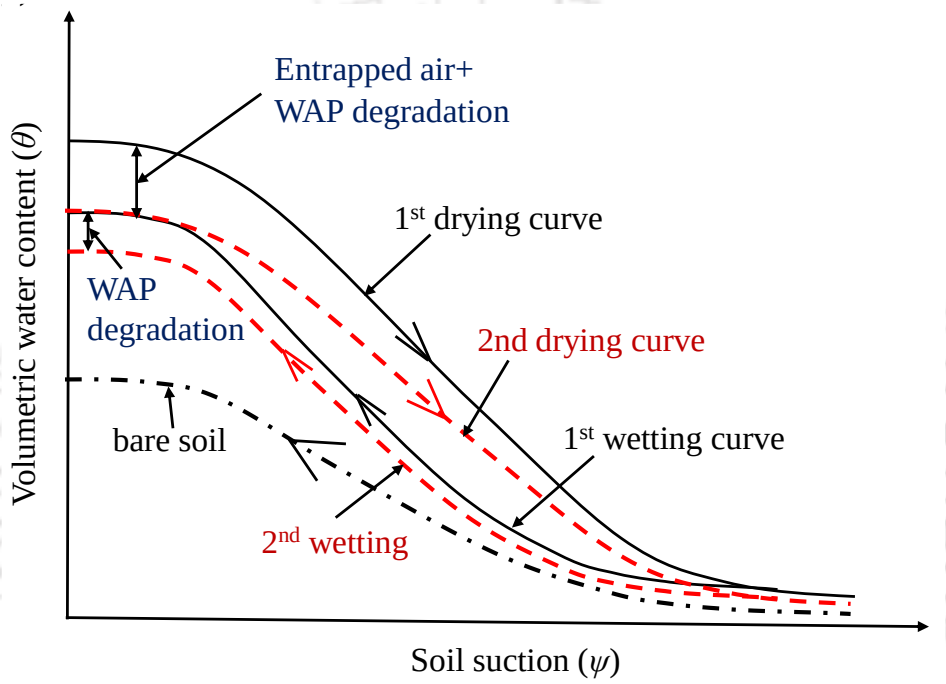

Fig. 7.23 Hysteresis in WRCC for WAP amended soil

Now, the 1st drying WRCC can be represented by Eq. (7.17) [similar to Eq. (7.11)],

$$\theta(\psi) = \frac{(\theta_{1u} b_{1d} + c\psi^{d_{1d}})}{(b_{1d} + \psi^{d_{1d}})} \qquad 7.17$$

where, θ_{1u} represents the saturated VWC (θ_s); b_{1d} and d_{1d} parameters are curve fitting parameters for 1st drying WRCC. The additional two points on 1st wetting can be calculated using the following equation,

$$\psi_{1(1w)} = \left(\frac{b_{1d}}{10}\right)^{\frac{1}{d_{1d}}} \qquad 7.18$$

TH-2777_166104034

$$\psi_{2(1w)} = \psi_{1(1w)} - 2\left[\left\{\frac{b_{1d}\left(\theta_{1u} - \theta_{1(1w)}\right)}{\theta_{1(1w)} - c}\right\}^{\frac{1}{d_{1d}}} - b_{1d}{}^{\frac{1}{d_{1d}}}\right] \quad 7.19$$

Where, $\theta_{1(1w)}$ and $\theta_{2(1w)}$ are known VWC values corresponding to suction values $\psi_{1(1w)}$ and $\psi_{2(1w)}$ along 1st wetting WRCC. It may be noted that Eq. (7.18) and (7.19), proposed for WAP amended soil, remain similar to the bare soil.

The known VWC on the wetting path can be presented based on Eq. (7.11), as

$$\theta_{1(1w)} = \frac{\left[\theta_{2u} b_{1w} + c\psi_{1(1w)}^{d_{1w}}\right]}{\left[b_{1w} + \psi_{1(1w)}^{d_{1w}}\right]} \quad 7.20$$

$$\theta_{2(1w)} = \frac{\left[\theta_{2u} b_{1w} + c\psi_{2(1w)}^{d_{1w}}\right]}{\left[b_{1w} + \psi_{2(1w)}^{d_{1w}}\right]} \quad 7.21$$

Here, θ_{2u} denotes the VWC at zero suction for 1st wetting WRCC (or 2nd drying WRCC). Solving Eq. (7.20) and (7.21), the fitting parameters for 1st wetting WRCC (b_{1w}, and d_{1w}) can be estimated as,

$$d_{1w} = \frac{\log\left[\frac{\left(\theta_{1(1w)} - c\right)\left(\theta_{2u} - \theta_{2(1w)}\right)}{\left(\theta_{2u} - \theta_{1(1w)}\right)\left(\theta_{2(1w)} - c\right)}\right]}{\log\left[\frac{\psi_{2(1w)}}{\psi_{1(1w)}}\right]} \quad 7.22$$

$$b_{1w} = \frac{\left[\theta_{1(1w)} - c\right]\psi_{1(1w)}^{d_{1w}}}{\theta_{2u} - \theta_{1(1w)}} \quad 7.23$$

For, prediction of nth wetting WRCC from nth drying WRCC, Eq. (7.20) and (7.21) becomes,

$$d_{nw} = \frac{\log\left[\frac{\left(\theta_{1(nw)} - c\right)\left(\theta_{(n+1)u} - \theta_{2(nw)}\right)}{\left(\theta_{(n+1)u} - \theta_{1(nw)}\right)\left(\theta_{2(nw)} - c\right)}\right]}{\log\left[\frac{\psi_{2(nw)}}{\psi_{1(nw)}}\right]} \quad 7.24$$

TH-2777_166104034

$$b_{nw} = \frac{[\theta_{1(nw)} - c]\psi_{1(nw)}^{d_{nw}}}{\theta_{(n+1)u} - \theta_{1(nw)}} \quad 7.25$$

In the present study, the wetting WRCC of WAP amended soils for two alternate drying-wetting cycles were predicted from the drying WRCC and the two additional points on wetting WRCC using the proposed equations [Eq. (7.17) to Eq. (7.25)]. The VWC corresponding to the lowest measured suction (close to 0.1 kPa for sand and 1 kPa for fine-grained soil) in the drying WRCC was considered as the VWC at zero suction, and the predicted wetting WRCC was compared with the measured wetting WRCC of WAP amended soils.

7.7.3 Validation of the proposed model

The experimentally measured drying WRCC (both 1st and 2nd) of bare soil and WAP amended soils (both Com-WAP and FA-WAP) were fitted to Eq. (7.17) using nonlinear regression analysis to obtain the curve fitting parameters (b_{1d}, d_{1d}, b_{2d}, d_{2d}). It may be noted that the VWC at saturated state (θ_{1u} and θ_{2u}) was taken as the VWC at the lowest measured suction of drying WRCC while the parameters *c* was fixed at the VWC at the highest measured suction (or starting point of wetting WRCC) to maintain continuity between drying and wetting WRCC. Table 7.2-7.4 summarizes the obtained curve fitting parameters [along with the coefficient of determination (R^2) and root mean square error (RMSE) value] for the 1st and 2nd drying WRCC of FS, BS, and RS, respectively. It can be observed that fitting parameter *d*, which depends on the slope of the desaturation portion, remains almost constant with the WAP amendment. On the other hand, the fitting parameter *b* increases with the WAP amendment in FS and BS, which is an indication of an increase in air entry value (AEV) with the addition of WAP. The AEV can be defined as the suction value at which air enters into the largest pore of the soil matrix. It can be observed that the value of *b* increases with the increasing WAP concentration for FS and BS, whereas for RS, the value of *b* parameter followed a reverse trend with the WAP addition. This is due to the fact that the average pore diameter of coarse-textured to medium-textured soil (FS and BS) is relatively larger than the fine-textured soil (RS). In the case of FS and BS, the water-swollen WAP particle can occupy the large-sized pore (macro-pores) in the soil matrix, leading to a more compact pore structure in the amended soil. With the reduction in the pore diameter, the AEV increases with the increasing WAP concentration, and subsequently, the *b* parameter increases. A comparison between the curve fitting parameters obtained for Com-WAP and FA-WAP indicated better improvement in *b* parameter with the FA-WAP amendment for FS. Moreover, the saturated VWC of FA-WAP amended

TH-2777_166104034

soil were found to be higher than Com-WAP after two consecutive cycles for the used soil textures.

The fitting parameters (b_{1w}, d_{1w}, b_{2w}, d_{2w}) of the wetting WRCC of the used soils with different WAP concentrations were predicted using two measured points on the wetting curve and the curve fitting parameters of drying WRCC using Eq. (7.24) and (7.25). The obtained parameters, along with the coefficient of determination (R^2) and root mean square error (RMSE) value, were reported in Table 7.2-7.4 for FS, BS, and RS, respectively. The predicted wetting curves for the two consecutive cycles were presented along with the measured data in Fig. 7.24 to 7.29. It can be observed that the predicted wetting curves using the proposed model are in good agreement with the measured wetting WRCC for the used soil textures. The coefficient of determination (R^2) and root mean square error (RMSE) between the measured and predicted WRCC varies between 0.95 to 0.99 and 0.01 to 0.05, respectively, indicating the effectiveness of the proposed model for WAP amended soils.

7.8 Degree of hysteresis in WAP amended soil

For the quantification of hysteresis in WRCC of bare soil and WAP amended soils, the degree of hysteresis value was calculated from the following equation (Eq. 7.26 and Eq. 7.27), as proposed by Lu and Khorsidi (2015). The degree of hysteresis can be expressed in terms of the local degree of hysteresis (D_{hi}) and the average degree of hysteresis (D_h). The D_{hi} indicates the water content difference between the drying and wetting WRCC at any suction value, Ψ_i, whereas the D_h indicates the average degree of hysteresis over a suction range between data points Ψ_1 and Ψ_n. Figure 7.30 illustrates the procedure, which was followed to quantify the D_{hi} as well as D_h values of the bare soil and WAP amended soils in the present study.

$$D_{hi} = \frac{\theta_{di} - \theta_{wi}}{\theta_{mi}} \tag{7.26}$$

$$D_h = \frac{\sum_{i=1}^{i=n} \frac{\theta_{di} - \theta_{wi}}{\theta_{mi}}}{n} \tag{7.27}$$

Here, θ_{di} and θ_{wi} represent the VWC at any suction value, ψ_i on the drying and wetting WRCC, respectively; θ_{mi} represents the average VWC of drying and wetting WRCC at point Ψ_i.

TH-2777_166104034

Table 7.4 Predicted curve-fitting parameters for wetting WRCC of WAP amended FS

Drying/ wetting	Fitting parameters	Bare soil	Soil+0.1% WAP		Soil+0.2% WAP		Soil+0.4% WAP	
			Com-WAP	FA-WAP	Com-WAP	FA-WAP	Com-WAP	FA-WAP
1st drying WRCC (fitted)	θ_{1u}	0.31	0.36	0.38	0.44	0.49	0.51	0.57
	c	0.005	0.03	0.04	0.04	0.05	0.04	0.05
	b_{1d}	9	14	20	15	20	18	20
	d_{1d}	1.4	1.4	1.6	1.4	1.6	1.4	1.6
	R^2	0.96	0.94	0.94	0.91	0.92	0.92	0.93
	RMSE	0.02	0.03	0.03	0.05	0.05	0.05	0.05
1st wetting WRCC (predicted)	$\psi_{1(2w)}^*$	0.9	1.3	1.5	1.3	1.5	1.5	1.5
	$\psi_{2(2w)}^*$	7	5	5.1	2.8	2.9	6.5	4.9
	$\theta_{1(2w)}^*$	0.25	0.235	0.25	0.26	0.29	0.34	0.37
	$\theta_{2(2w)}^*$	0.06	0.1	0.09	0.15	0.16	0.125	0.15
	θ_{2u}	0.28	0.34	0.36	0.39	0.44	0.46	0.52
	b_{1w}	3.9	2.3	2.6	1.4	1.6	3.3	2.8
	d_{1w}	1.72	1.42	1.91	1.66	1.98	1.63	1.8
	R^2	0.96	0.97	0.99	0.98	0.98	0.98	0.99
	RMSE	0.03	0.02	0.02	0.03	0.04	0.03	0.04
2nd drying WRCC (fitted)	c	0.005	0.03	0.03	0.04	0.04	0.05	0.05
	b_{2d}	6	8	12	9	10	14	15
	d_{2d}	1.2	1.4	1.6	1.4	1.6	1.4	1.4
	R^2	0.91	0.93	0.92	0.91	0.93	0.92	0.94
	RMSE	0.03	0.03	0.03	0.04	0.04	0.04	0.04
2nd wetting WRCC (predicted)	$\psi_{1(2w)}^*$	0.7	0.9	1.1	0.93	1	1.3	1.3
	$\psi_{2(2w)}^*$	8.5	6.5	6.9	4.9	3.1	5.6	5.3
	$\theta_{1(2w)}^*$	0.26	0.28	0.3	0.28	0.29	0.31	0.34
	$\theta_{2(2w)}^*$	0.07	0.08	0.08	0.105	0.13	0.11	0.12
	θ_{3u}	0.28	0.32	0.34	0.37	0.4	0.41	0.47
	b_{2w}	8.9	3.7	4.8	2.4	2.2	3.1	2.7
	d_{2w}	1.44	1.67	1.96	1.51	1.74	1.74	1.74
	R^2	0.95	0.98	0.99	0.97	0.98	0.98	0.98
	RMSE	0.03	0.01	0.02	0.02	0.02	0.02	0.02

*additional data along wetting WRCC

TH-2777_166104034

Table 7.5 Predicted curve-fitting parameters for wetting WRCC of WAP amended BS

Drying/ wetting	Fitting parameters	Bare soil	Soil+0.1% WAP		Soil+0.2% WAP		Soil+0.4% WAP	
			Com-WAP	FA-WAP	Com-WAP	FA-WAP	Com-WAP	FA-WAP
1st drying WRCC (fitted)	θ_{1u}	0.34	0.4	0.42	0.46	0.51	0.53	0.57
	c	0.06	0.06	0.06	0.06	0.06	0.06	0.06
	b_{1d}	55	70	70	80	75	80	75
	d_{1d}	1	1.15	1.15	1.15	1.15	1.15	1.15
	R^2	0.98	0.98	0.99	0.99	0.99	0.99	0.99
	RMSE	0.01	0.01	0.01	0.01	0.02	0.01	0.01
1st wetting WRCC (predicted)	$\psi_{1(2w)}^*$	5.5	5.4	5.4	6.1	5.8	6.1	5.8
	$\psi_{2(2w)}^*$	71.5	48.3	46.7	53.2	44.4	60.8	44.4
	$\theta_{1(2w)}^*$	0.26	0.3	0.32	0.34	0.36	0.41	0.4
	$\theta_{2(2w)}^*$	0.12	0.12	0.13	0.13	0.17	0.13	0.15
	θ_{2u}	0.32	0.38	0.39	0.42	0.43	0.47	0.5
	b_{1w}	13.8	13.1	14.8	16.9	19.7	28.1	15.6
	d_{1w}	0.86	1.17	1.15	1.23	1.13	1.45	1.26
	R^2	0.99	0.98	0.98	0.99	0.99	0.98	0.99
	RMSE	0.01	0.01	0.03	0.01	0.02	0.02	0.02
2nd drying WRCC (fitted)	c	0.06	0.06	0.06	0.06	0.06	0.06	0.06
	b_{2d}	45	50	60	40	55	70	70
	d_{2d}	1	1.15	1.15	1.15	1.15	1.15	1.15
	R^2	0.98	0.98	0.99	0.99	0.99	0.99	0.99
	RMSE	0.01	0.01	0.01	0.01	0.01	0.01	0.01
2nd wetting WRCC (predicted)	$\psi_{1(2w)}^*$	4.5	4.1	4.8	3.3	4.4	5.4	5.4
	$\psi_{2(2w)}^*$	80.5	44.2	48.9	36.1	45.3	59.2	48.1
	$\theta_{1(2w)}^*$	0.285	0.31	0.31	0.34	0.34	0.38	0.37
	$\theta_{2(2w)}^*$	0.12	0.13	0.14	0.16	0.16	0.145	0.16
	θ_{3u}	0.32	0.36	0.37	0.38	0.4	0.44	0.47
	b_{2w}	28.9	16.9	16.2	20	16.9	23.2	13.5
	d_{2w}	1.05	1.17	1.06	1.15	1.04	1.22	1.04
	R^2	0.99	0.98	0.99	0.99	0.99	0.99	0.99
	RMSE	0.003	0.01	0.01	0.01	0.01	0.01	0.02

*additional data along wetting WRCC

TH-2777_166104034

Table 7.6 Predicted curve-fitting parameters for wetting WRCC of WAP amended RS

Drying/ wetting	Fitting parameters	Bare soil	Soil+0.1% WAP		Soil+0.2% WAP		Soil+0.4% WAP	
			Com-WAP	FA-WAP	Com-WAP	FA-WAP	Com-WAP	FA-WAP
1st drying WRCC (fitted)	θ_{1u}	0.5	0.55	0.56	0.61	0.64	0.63	0.65
	c	0.27	0.28	0.28	0.25	0.26	0.25	0.24
	b_{1d}	40	30	35	20	20	25	30
	d_{1d}	0.9	0.9	0.9	0.9	0.9	0.9	0.9
	R^2	0.98	0.99	0.96	0.99	0.99	0.99	0.99
	RMSE	0.01	0.01	0.02	0.01	0.02	0.01	0.01
1st wetting WRCC (predicted)	$\psi_{1(2w)}^*$	4.7	3.4	4	2.2	2.2	2.8	3.9
	$\psi_{2(2w)}^*$	51.4	38	62.6	38.7	37.4	40	53.6
	$\theta_{1(2w)}^*$	0.41	0.445	0.47	0.51	0.53	0.5	0.52
	$\theta_{2(2w)}^*$	0.31	0.32	0.31	0.3	0.31	0.315	0.31
	θ_{2u}	0.45	0.5	0.52	0.55	0.57	0.55	0.58
	b_{1w}	19.4	11.6	17.8	15.3	15.9	15.5	18.1
	d_{1w}	1.04	1.08	1.19	1.21	1.25	1.09	1.05
	R^2	0.99	0.98	0.99	0.99	0.98	0.99	0.97
	RMSE	0.01	0.01	0.01	0.01	0.01	0.02	0.02
2nd drying WRCC (fitted)	c	0.27	0.28	0.27	0.25	0.25	0.25	0.25
	b_{2d}	35	35	40	20	20	30	30
	d_{2d}	0.9	0.9	0.9	0.9	0.9	0.9	0.9
	R^2	0.98	0.97	0.98	0.98	0.98	0.99	0.99
	RMSE	0.01	0.01	0.01	0.01	0.02	0.01	0.01
2nd wetting WRCC (predicted)	$\psi_{1(2w)}^*$	4	4	4.7	2.2	2.2	3.4	3.4
	$\psi_{2(2w)}^*$	82.1	82.9	99.4	39.8	41.5	56.8	66.3
	$\theta_{1(2w)}^*$	0.41	0.45	0.47	0.47	0.49	0.46	0.5
	$\theta_{2(2w)}^*$	0.305	0.31	0.31	0.295	0.31	0.31	0.31
	θ_{3u}	0.45	0.47	0.49	0.5	0.55	0.51	0.53
	b_{2w}	16.4	42.3	55.4	17.3	9.4	16.3	32.3
	d_{2w}	0.89	1.18	1.24	1.2	0.94	0.94	1.15
	R^2	0.99	0.98	0.99	0.99	0.99	0.99	0.99
	RMSE	0.01	0.01	0.01	0.01	0.01	0.01	0.01

*additional data along wetting WRCC

TH-2777_166104034

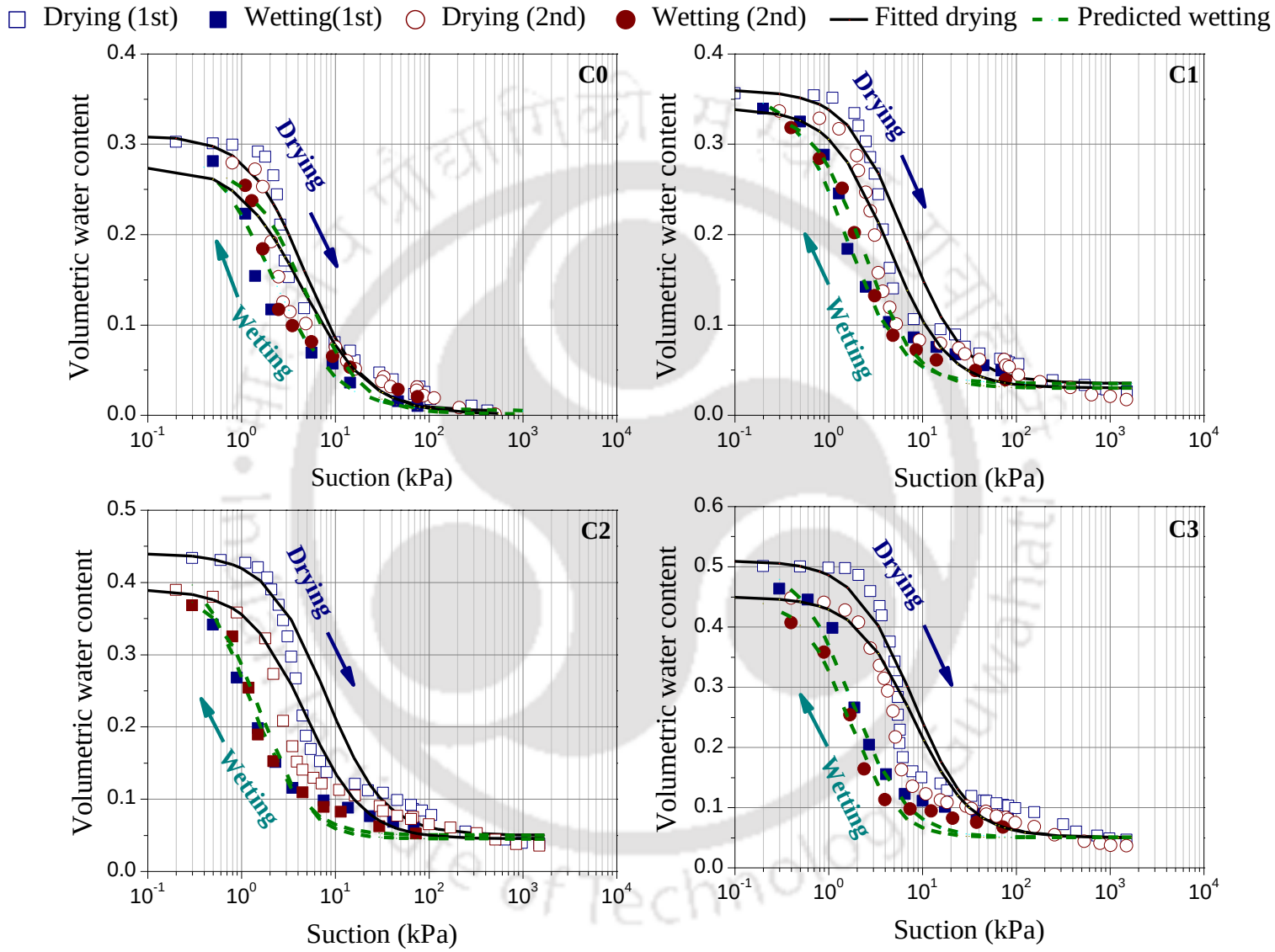

Fig. 7.24 Measured and predicted hysteresis in WRCC for two alternate cycles for Com-WAP amended FS

TH-2777_166104034

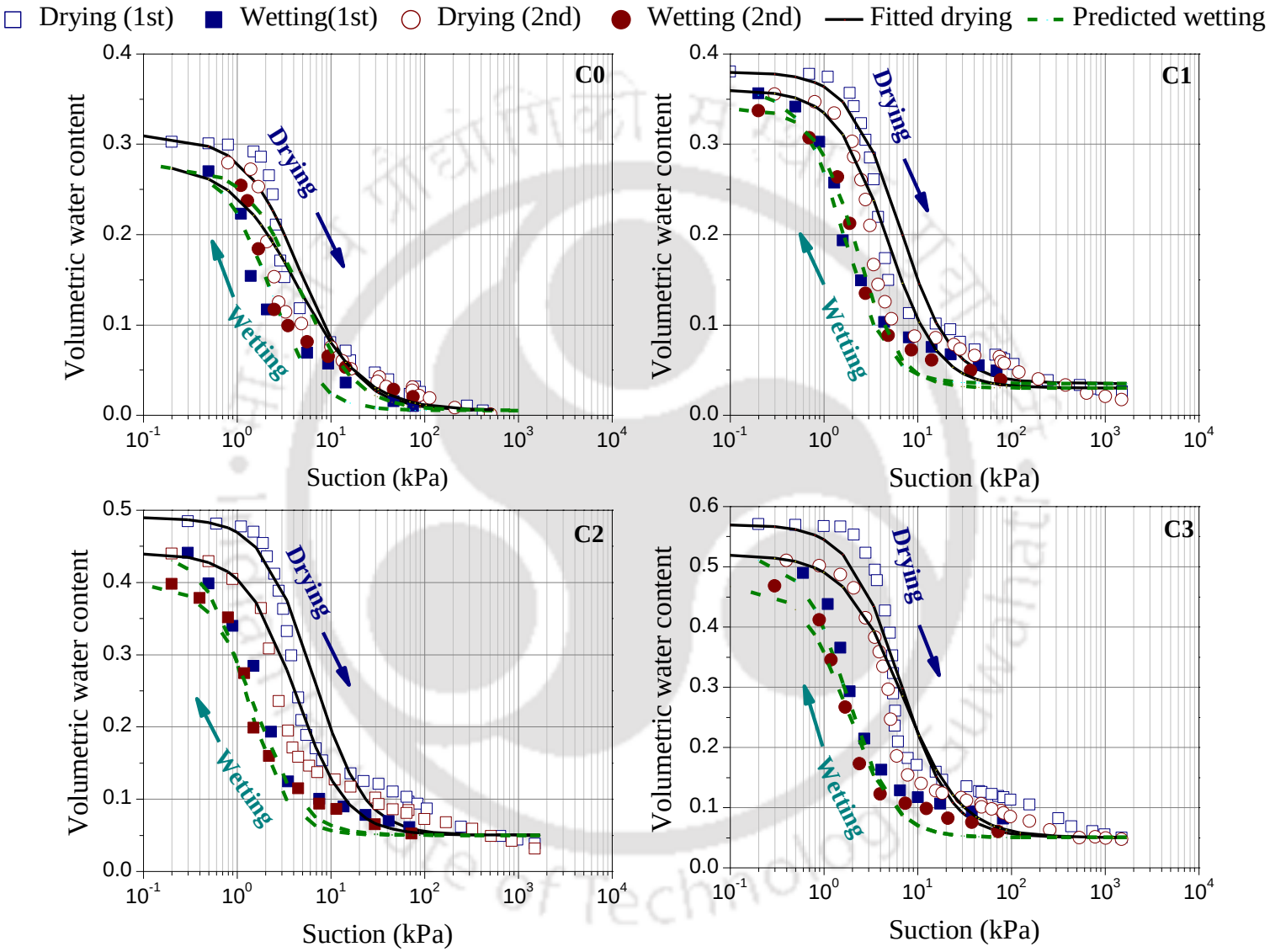

Fig. 7.25 Measured and predicted hysteresis in WRCC for two alternate cycles for FA-WAP amended FS

TH-2777_166104034

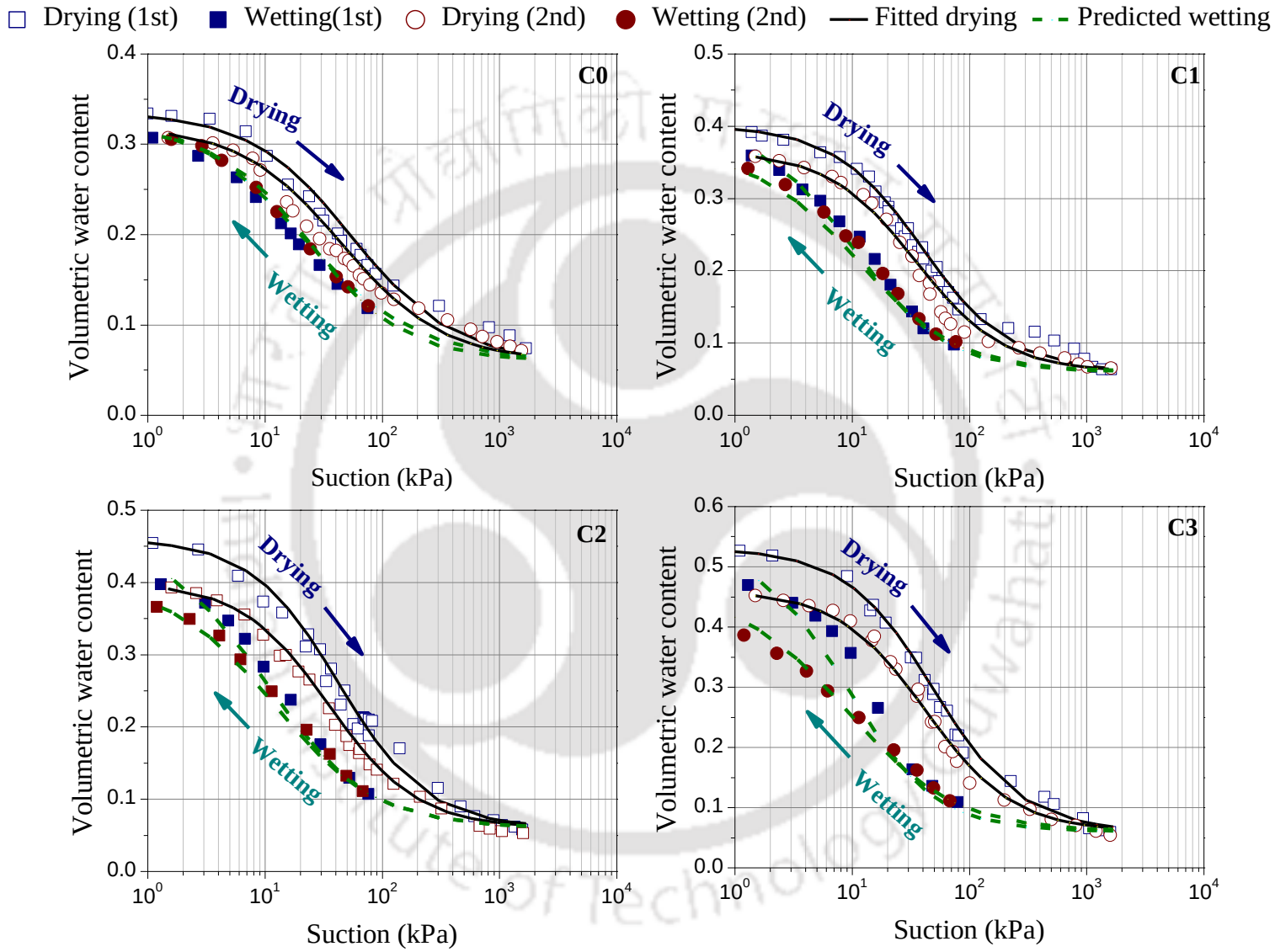

Fig. 7.26 Measured and predicted hysteresis in WRCC for two alternate cycles for Com-WAP amended BS

TH-2777_166104034

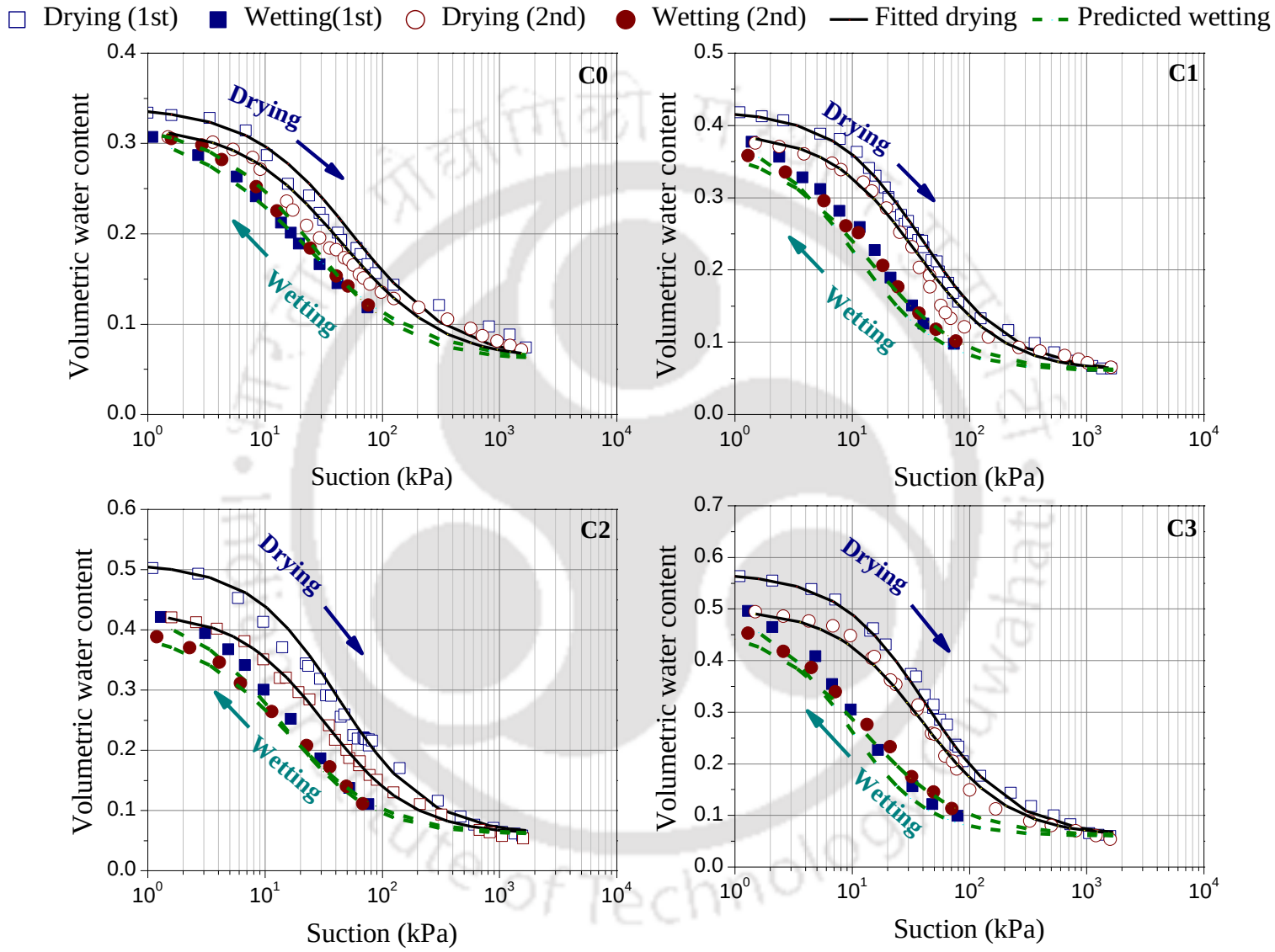

Fig. 7.27 Measured and predicted hysteresis in WRCC for two alternate cycles for FA-WAP amended BS

TH-2777_166104034

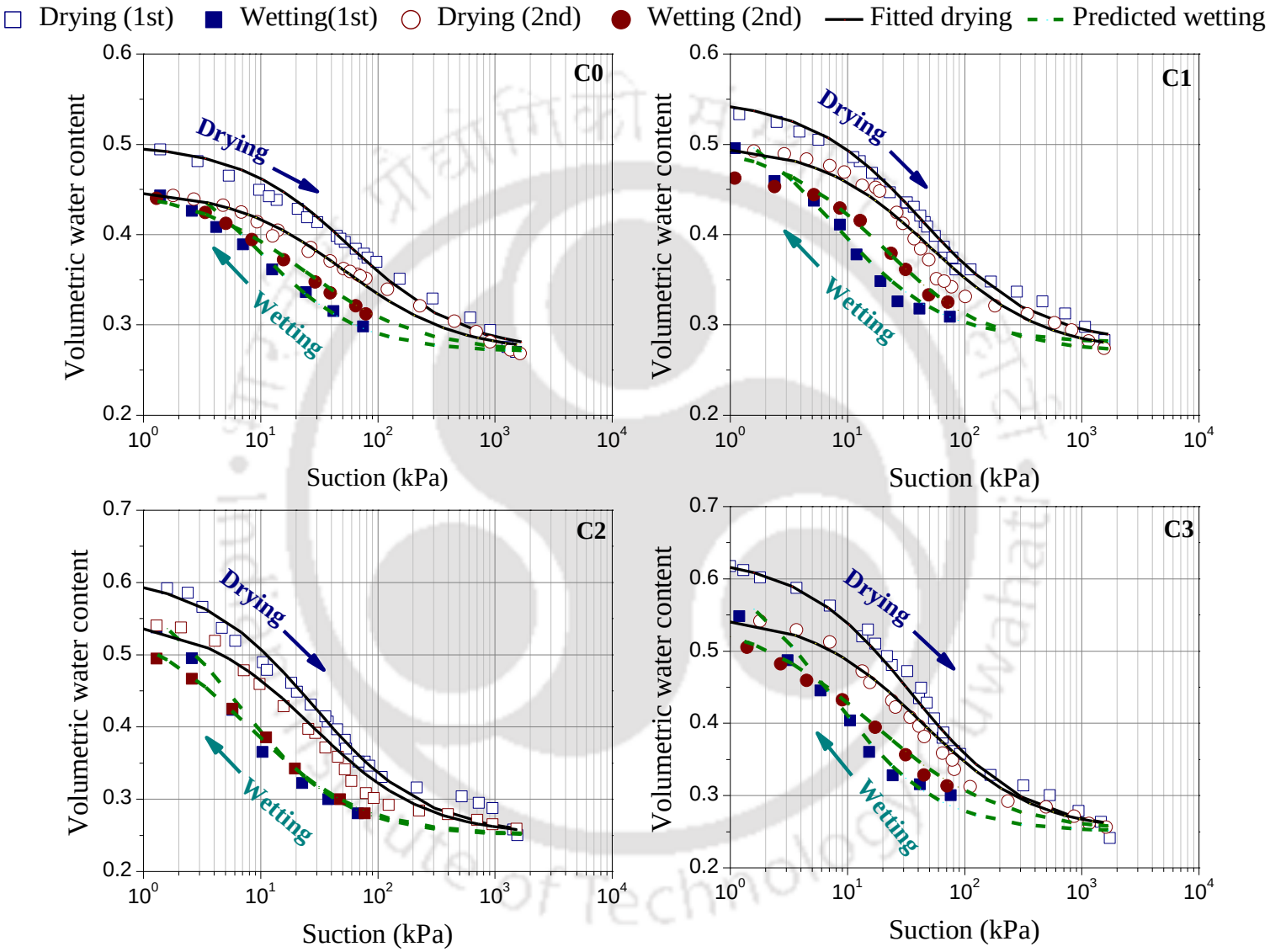

Fig. 7.28 Measured and predicted hysteresis in WRCC for two alternate cycles for Com-WAP amended RS

TH-2777_166104034

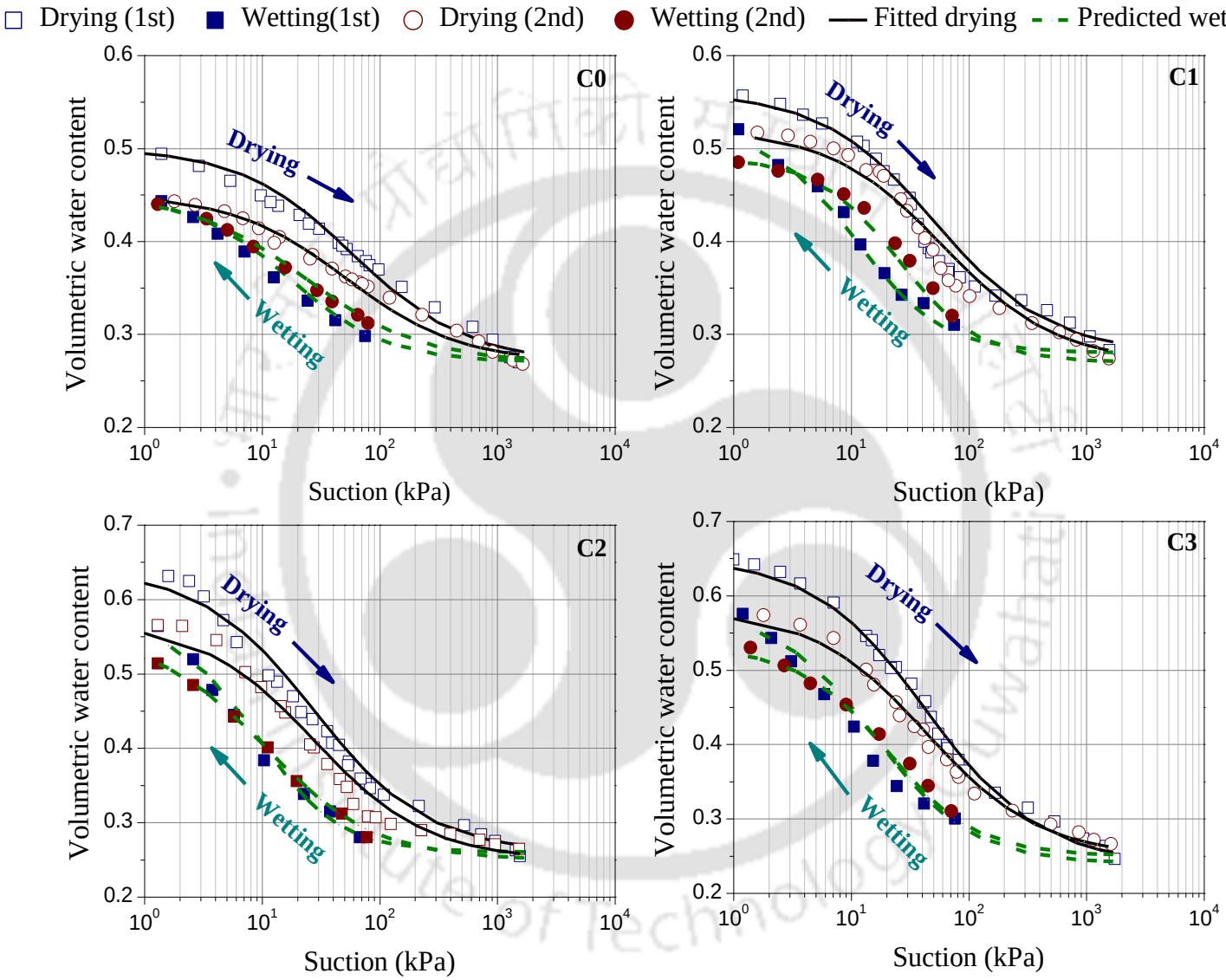

Fig. 7.29 Measured and predicted hysteresis in WRCC for two alternate cycles for FA-WAP amended RS

TH-2777_166104034

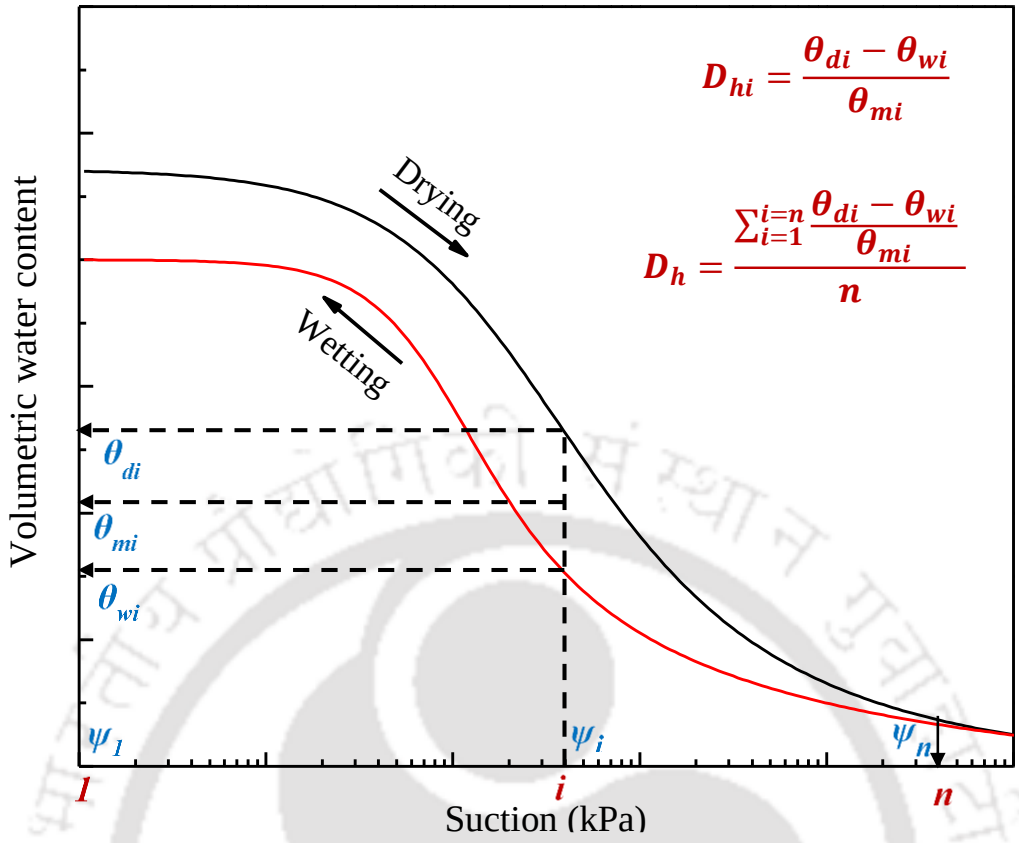

Fig. 7.30 Quantification of degree of hysteresis (modified after Lu and Khorsidi 2015)

The average degree of hysteresis (D_h value) was quantified using Eq. (7.27) for the multiple drying-wetting cycles of bare soils and WAP amended soils and reported in Table 7.7. It may be noted that a D_h value of 0.1 indicates a water content difference of 10% of the mean water content for DWRCC and WWRCC. The obtained D_h value for bare FS, BS, and RS was found to be 0.29, 0.21, and 0.14, respectively, for the 1st drying-wetting cycles. A similar observation of decreasing degree of hysteresis for soils with higher fines content (silt +clay content) was reported in the literature (Raghuram et al. 2020). In the 2nd drying-wetting cycle, the order of D_h values for bare FS, BS, and RS followed the same trend with some reduction in the value as compared to the 1st cycle. This was due to the rearrangement of soil particles and the modification of soil-pore structure after the initial drying-wetting curve.

The addition of WAP in soil has increased the D_h value for coarse to fine-textured soils for both the 1st and 2nd drying-wetting cycles. The D_h value after two consecutive cycles was also increased by 250%, 105%, and 67% (maximum) in FS, BS, and RS, respectively, due to the incorporation of Com-WAP. On the other hand, the D_h value after two consecutive cycles was increased by 225%, 95%, and 58% (maximum) in FA-WAP amended FS, BS, and RS, respectively. These results clearly indicate that the consideration of hysteresis in WRCC for

TH-2777_166104034

WAP amended soil is essential to evaluate its hydraulic performance with time. It may be noted that there is no direct correlation found between the re-swelling ability of WAP and the measured hysteresis in WRCC as the degradation of WAP in soil are dependent on various soil-specific properties, such as soil texture, quality of pore water, presence of exchangeable cations.

Table 7.7 Obtained degree of hysteresis in WAP amended soils

Soil type	WAP concentrations		D_h value		
			1st drying-wetting	2nd drying-wetting	1st drying-2nd wetting
FS	C0		0.29	0.12	0.12
	C1	Com-WAP	0.31	0.22	0.4
		FA-WAP	0.34	0.23	0.39
	C2	Com-WAP	0.4	0.22	0.35
		FA-WAP	0.39	0.25	0.39
	C3	Com-WAP	0.35	0.33	0.42
		FA-WAP	0.34	0.36	0.37
BS	C0		0.21	0.13	0.21
	C1	Com-WAP	0.37	0.25	0.35
		FA-WAP	0.35	0.22	0.3
	C2	Com-WAP	0.42	0.19	0.39
		FA-WAP	0.38	0.19	0.37
	C3	Com-WAP	0.49	0.32	0.43
		FA-WAP	0.5	0.31	0.41
RS	C0		0.14	0.05	0.12
	C1	Com-WAP	0.16	0.09	0.15
		FA-WAP	0.16	0.11	0.15
	C2	Com-WAP	0.17	0.14	0.2
		FA-WAP	0.18	0.11	0.19
	C3	Com-WAP	0.18	0.11	0.17
		FA-WAP	0.18	0.13	0.18

TH-2777_166104034

7.9 Degradation of WAP in soil

The degradation kinetics of WAP is one of the important factors to consider before using it as a soil amendment under drought conditions. Past studies have highlighted that purely synthetic WAPs are non-biodegradable and remain in the soil for a long time (degradability less than 5% after 3 months) [Sharmah and Karak 2020]. Therefore, most of the recent studies are focused on the development of biodegradable polymer, prepared from natural materials like starch, cellulose, chitosan, yeast, and clay. The degradation test of these laboratory-made WAPs was generally conducted using soil burial method (Phang et al. 2011; Jin et al. 2013; Zhao et al. 2019) and enzyme/bacterial buffer solution (Xie et al. 2012; Sharmah and Karak 2020). In soil burial methods, a certain quantity of WAP was buried in soil, and the weight of the remaining WAP was measured after different time intervals to measure its degradation kinetics. The disadvantage of the soil burial method is that the extraction of swollen WAP from soil and the washing process becomes very difficult in case of fine-textured soils. Moreover, the influence of WAP concentrations on the degradation kinetics cannot be well understood from the soil burial method. The other method includes preparation of enzyme buffer solution or bacterial culture medium and measurement of weight loss of WAP in the solution, which is not an actual representation of WAP degradation in soil. The present study proposed a simple method to evaluate the degradation of WAP indirectly by measuring the water holding capacity of WAP amended soil, subjected to multiple drying-wetting cycles.

7.9.1 Test plan and procedure

Three different textured air-dried soils (50 g) were first mixed with dry WAP (both Com-WAP and FA-WAP) at three different concentrations, including 0.1% (C1), 0.2% (C2), and 0.4% (C3) on weight by weight (w/w) basis (ref. Fig. 7.31). The respective soil samples mixed with different proportions of WAP along with the control sample (C0) were placed in small containers with perforated bottom and submerged in tap water. A filter paper was placed at the bottom of the containers to restrict the escape of fine particles present in soil samples. After allowing sufficient time to swell (24 hrs), the excess water from the container was drained off, and the weight of the sample was taken. The water holding capacity of the WAP amended soil is defined as the gravimetric water content (GWC) after draining out the excess water. The wet samples were allowed to dry in the ambient conditions until the weight loss from the samples become negligible. The dry samples were again submerged in tap water, and the corresponding GWC was measured. The procedure was repeated until the water holding capacity of WAP amended soil was reduced to the water holding capacity of bare soil.

TH-2777_166104034

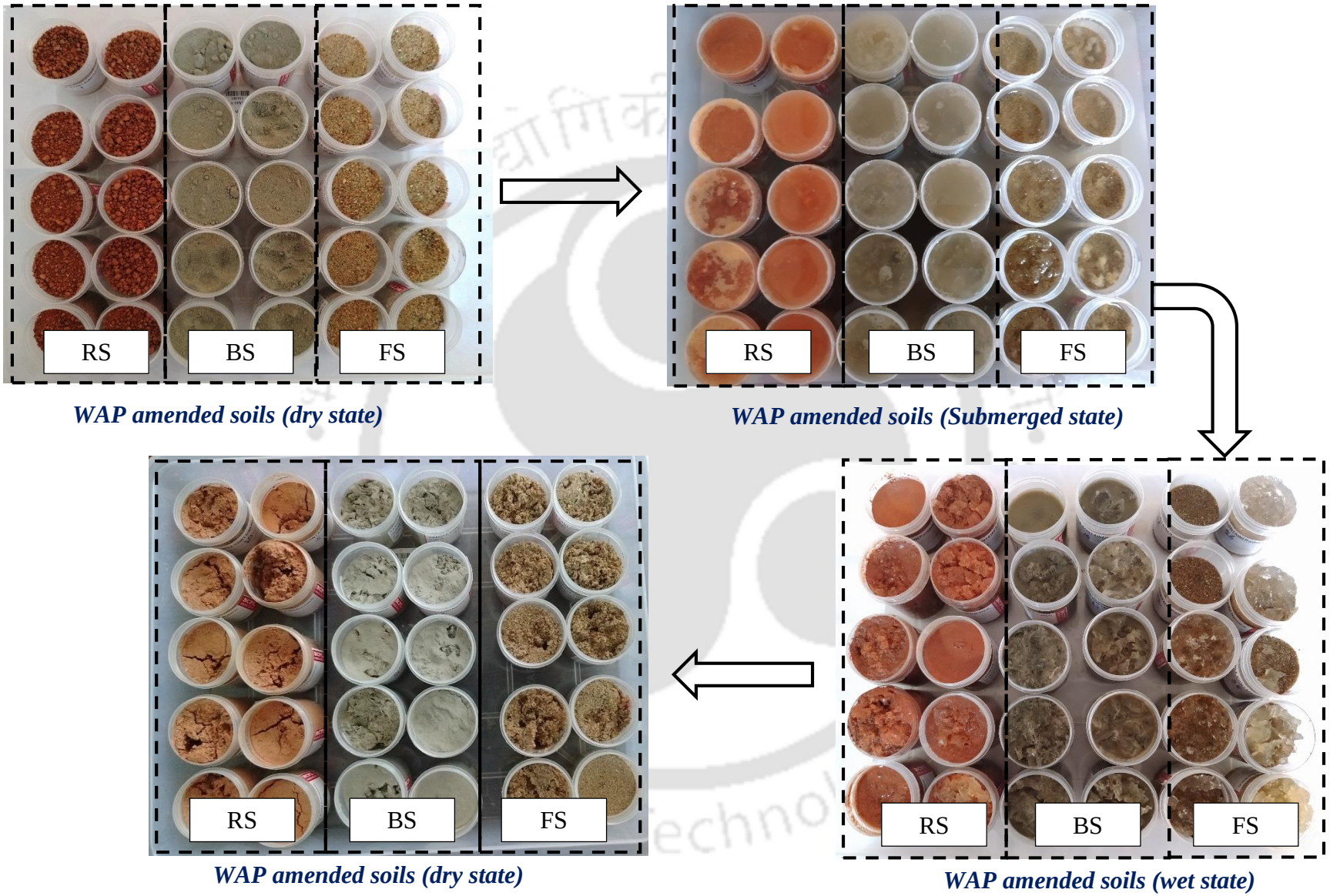

Fig. 7.31 Pictorial view of the dry and water-swollen FA-WAP amended soils

TH-2777_166104034

7.9.2 Observations and discussion

Figures 7.32-7.34 represent the variation of GWC of WAP amended soils subjected to multiple alternate drying-wetting cycles for FS, BS, and RS. It may be noted that the variation of GWC of WAP amended soils was plotted against the number of alternate cycles instead of time duration as the drying time of WAP amended soil for alternate cycles depends on the various external factors such as ambient temperature, relative humidity, sample diameter. As it can be observed in Figs. 7.32-7.34, the GWC of WAP amended soils were higher in FA-WAP amended soils as compared to Com-WAP amended soils at the initial stage due to the higher water absorbency of FA-WAP. However, the decrement rate of GWC with the alternate drying-wetting cycles was found to be lower in Com-WAP than FA-WAP. This indicates that the degradation rate of FA-WAP in soil is higher than Com-WAP due to the incorporation of FA in the polymeric structure of PAA.

For better understanding, the influence of alternate drying-wetting cycles on the water absorbency of WAP was evaluated from the measured data. The specific amount of water absorbed by a unit mass of WAP in soil was evaluated by Eq. (7.28) for this purpose.

$$Water\ absorbency\ in\ soil\ (g/g) = \frac{W_{w(as)} - W_{w(bs)} - W_{d(p)}}{W_{d(p)}} \qquad 7.28$$

Here, $W_{w(as)}$ represents the wet weight of WAP amended soil; $W_{w(bs)}$ represents the wet weight of bare soil, and $W_{d(p)}$ represents the dry weight of WAP.

The variation of water absorbency of both WAPs in different textured soils were also presented in Figs. 7.32-7.34. These figures give a clear indication of WAP degradation and subsequent reduction in water absorbency of WAP with alternate drying-wetting cycles. The water absorbency of Com-WAP becomes zero after 9th, 13th, and 21st cycles in FS for WAP concentrations of 0.1%, 0.2%, and 0.4%, respectively. On the other hand, the water absorbency of FA-WAP becomes zero after the 8th, 11th, and 17th cycles in FS for WAP concentrations of 0.1%, 0.2%, and 0.4%, respectively. At the maximum concentration of FA- WAP (0.4%), the water absorbency of WAP becomes zero after the 17th, 15th, and 11th cycles in FS, BS, and RS, respectively. Therefore, the degradation and reduction in water absorbency of WAP are mainly governed by three parameters, including (a) ionic nature of the soil pore-water and surrounding particles and (b) WAP composition (monomer, backbone material), and (c) WAP concentrations.

TH-2777_166104034

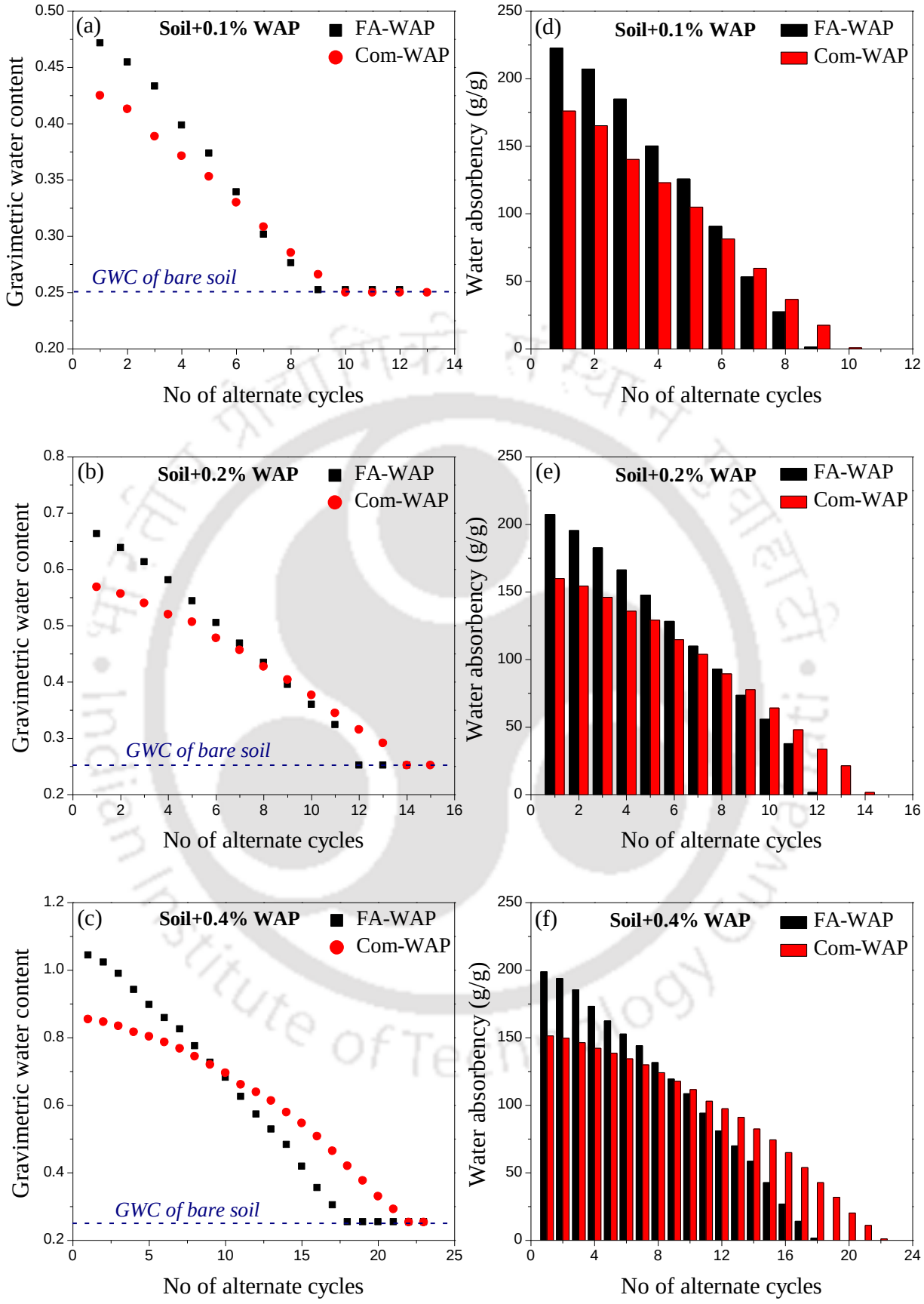

Fig. 7.32 Variation of gravimetric water content (GWC) of WAP amended FS and water absorbency of WAP in FS with the number of alternate cycle

TH-2777_166104034

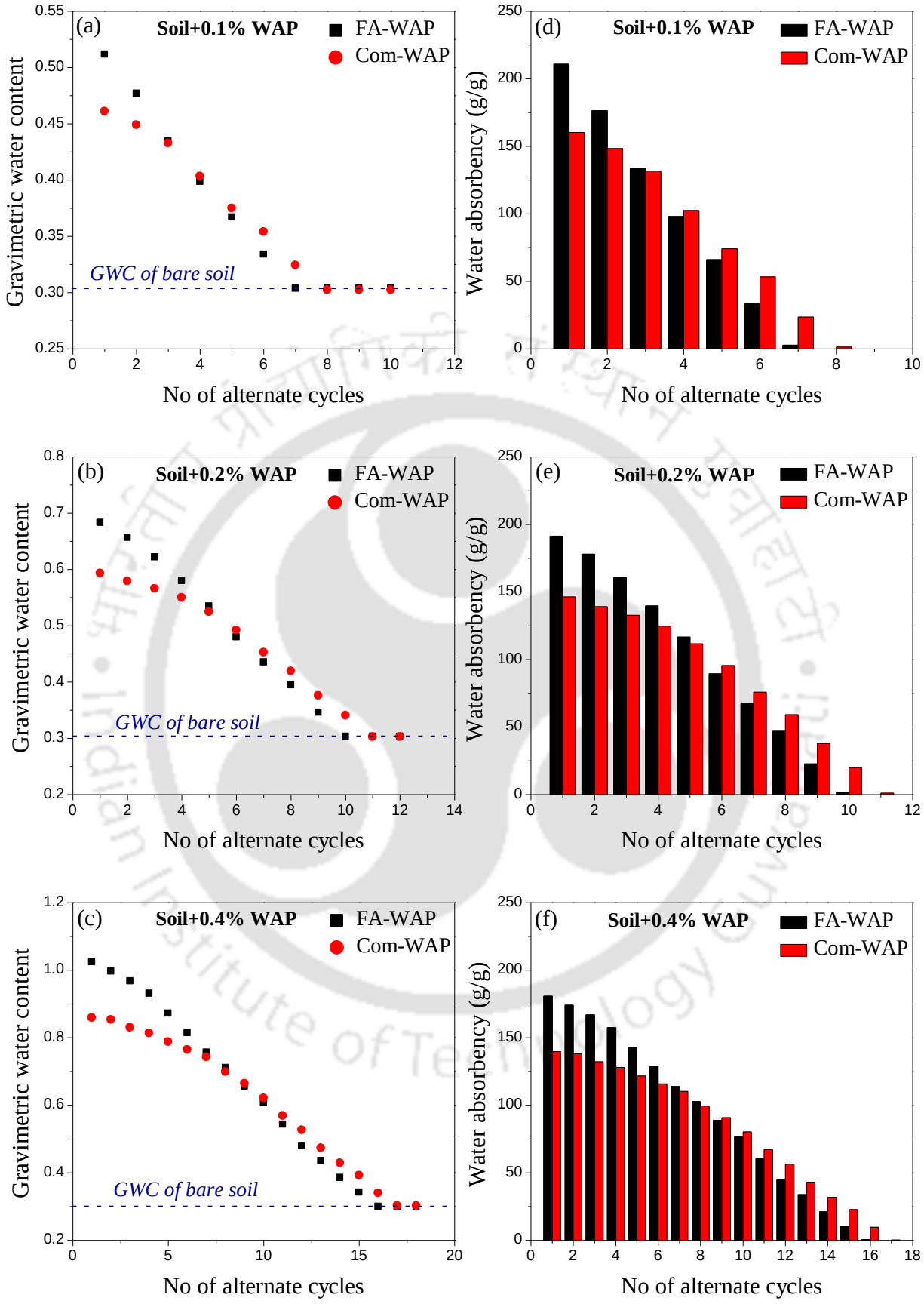

Fig. 7.33 Variation of gravimetric water content (GWC) of WAP amended BS and water absorbency of WAP in BS with the number of alternate cycle

TH-2777_166104034

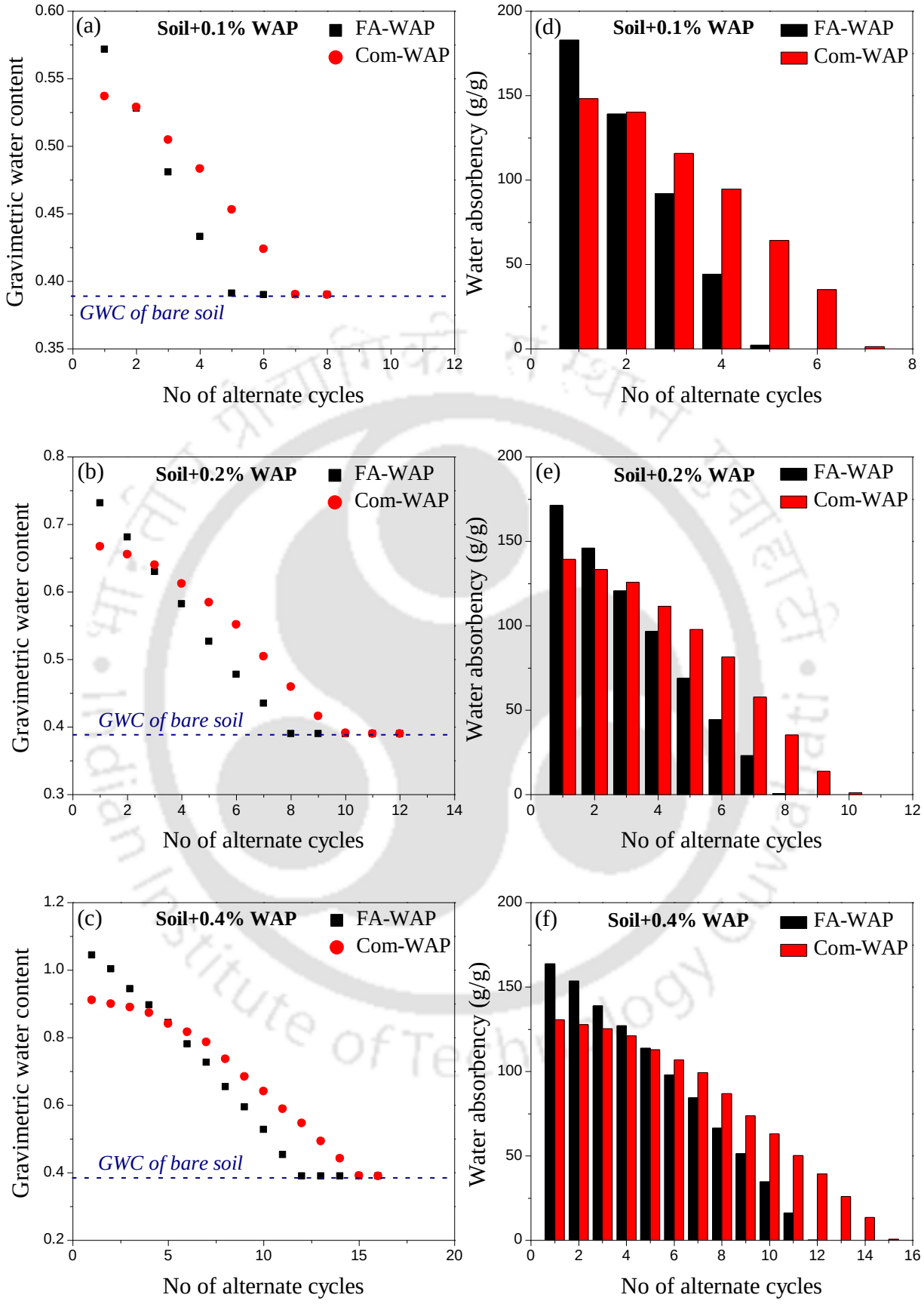

Fig. 7.34 Variation of gravimetric water content (GWC) of WAP amended RS and water absorbency of WAP in RS with the number of alternate cycle

TH-2777_166104034

The percentage degradation of WAP after any drying-wetting cycle was evaluated indirectly from the ratio of water absorbency of WAP after that cycle and 1st cycle (Eq. 7.29).

$$\%degradation = \left[1 - \frac{water\ absorbency\ after\ n^{th}\ cycle}{water\ absorbency\ at\ 1^{st}\ cycle}\right] \times 100 \qquad 7.29$$

The percentage degradation of both WAPs in three different textured soils was presented in Fig. 7.35. The same procedure can be adopted for the evaluation of WAP degradation in field conditions. For field experiments, a fixed quantity of soil sample needs to be extruded at field capacity (3 days after irrigation). From the measured gravimetric water content (GWC) of the extruded sample, the degradation kinetics can be obtained as a function of number of alternate cycles or time duration. It can be expected that the degradation rate in the experimental laboratory setup may be less than the field soil as microbial activities will be more intense and controlled by the type of crops.

7.10 Summary

The present chapter quantifies the interaction between water absorbing polymer (WAP) and different soil texture (Sand FS; silt loam BS; clay loam RS) and utilizes this understanding to evaluate its impact on water retention of soil, saturated volumetric water content (θ_s), plant available water content, wilting time and irrigation frequency. The usefulness of T5 and TEROS21 sensors for establishing WRCC of WAP amended soils was demonstrated in this study. This observation implies their utility for long-term field monitoring of suction and drought management studies in WAP amended soils. The FESEM images proved the alteration in the microstructure of soil pores (reduction in macro and mesopores) in the presence of WAP, which predominantly affects the water retention at low matric suction. With increasing concentration of WAP, the pore spaces were progressively occupied by the water-swollen WAP, resulting in a more compact and denser pore structure. The study proved that the inter-pore space of fine-textured soil restricted the swelling of WAP to its full capacity. At maximum concentration of FA-WAP amendment (0.4%), the increase in saturated VWC (θ_s) for RS is 50%, whereas for BS and FS, the increase is about 92% and 120%, respectively. Further, the plant available water content (PAWC) was obtained from the WRCC as the difference between field capacity (FC) and the permanent wilting point (PWP). At the maximum concentration of FA-WAP, the increase in PAWC for FS, BS, and RS was found to be 3.3, 2.5, and 1.4 times, respectively, as compared to bare soil. The study, therefore, indicates that higher moisture retention of fine texture soil need not necessarily translate to a higher PAWC.

TH-2777_166104034

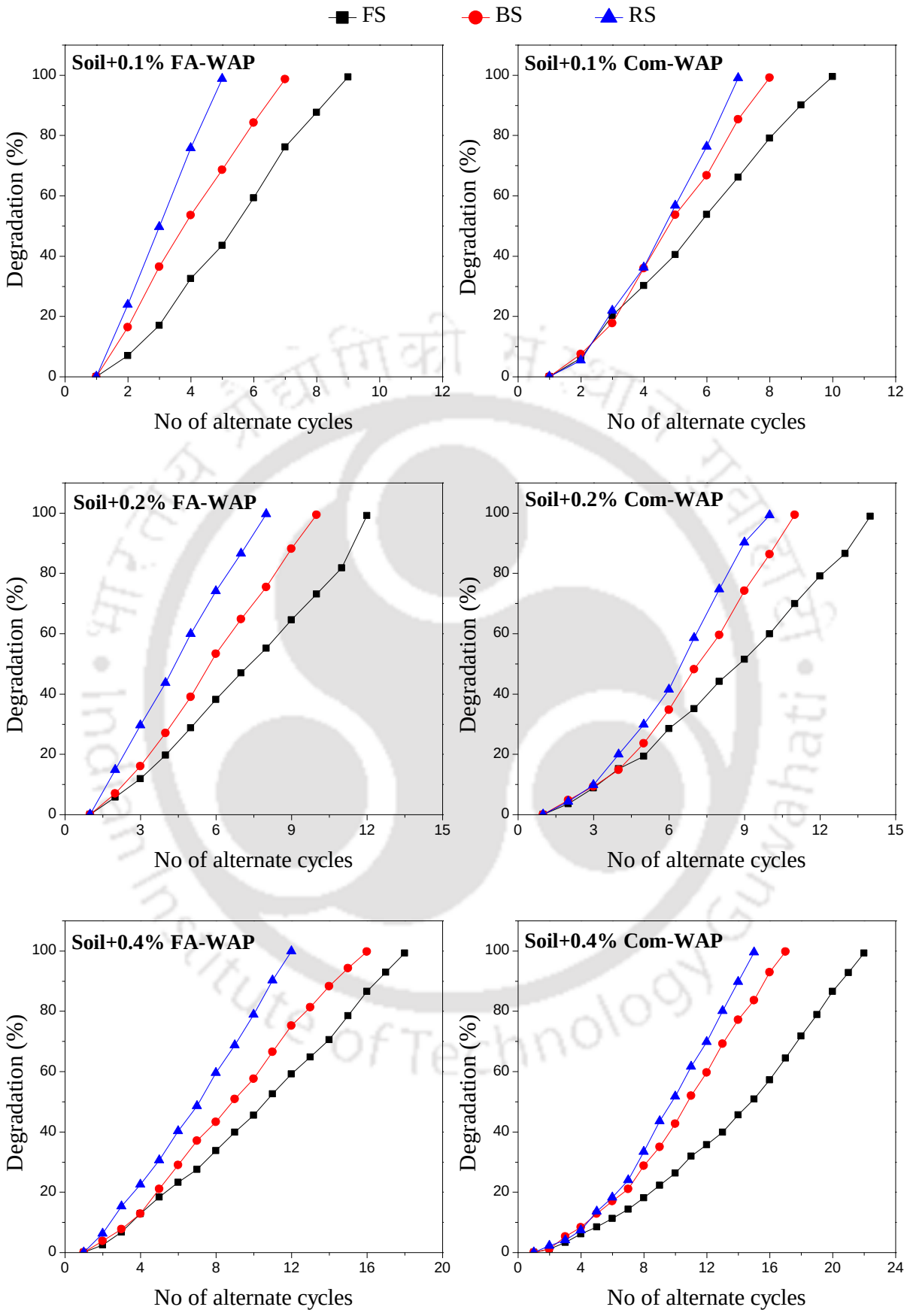

Fig. 7.35 Degradation kinetics of the used WAPs in different textured soils

TH-2777_166104034

Irrespective of the soil texture, the wilting time was found to increase for all WAP amended soils, and the improvement factor varied between 4 times to 2.4 times for coarse and fine textured soil, respectively. A maximum reduction of 52%, 40%, and 62% in irrigation water requirement was noticed in WAP amended FS, BS, and RS, respectively, as compared to bare soil. Based on the irrigation water requirement, it was recommended that the optimum WAP application rate for coarse-textured soils (sand, silt loam) is 0.1%, while for fine-textured soil (clay loam), the application rate is 0.2%. This recommendation needs to be further validated based on the crop yield observed in the field for a wide variety of soil texture.

The present study developed a simple predictive model to describe the water retention characteristic of water absorbing polymer (WAP) amended soil. The model can capture the changes in the void ratio of soil due to the addition of different WAP concentrations based on a modified phase relationship of WAP amended soil. There are six parameters in the proposed model, out of which four parameters can be obtained from the WRCC of bare soil, and the remaining two parameters can be obtained from WRCC of pure WAP. The performance of the new model was validated based on the laboratory-measured data. The model demonstrates its ability to predict the WRCC of WAP amended soil in two different textured soils (sand, silt loam) with varying WAP concentrations.

The present study further proposed a methodology to measure the hysteresis in water retention characteristic curve (WRCC) of WAP amended soils subjected to alternate drying-wetting cycles. For this purpose, the multiple cycles of drying and wetting WRCC of used soils were determined for varying WAP concentrations (0.1%, 0.2%, and 0.4% on w/w basis) using tap water. A predictive model was proposed to estimate the wetting WRCC from the drying WRCC for WAP amended soils, valid till the complete degradation of WAP. The proposed model was validated for two consecutive drying-wetting cycles for the selected soils with varying WAP concentrations, which showed its effectiveness for predicting hysteresis in WRCC of WAP amended soils. Further, the degree of hysteresis in WRCC of WAP amended soil was quantified after each drying-wetting cycle. The experimental results revealed that the presence of WAP and its degradation with time significantly increased the degree of hysteresis in WRCC. To quantify the degradation kinetics of WAP in soil, the water holding capacity of WAP amended soils was measured after multiple drying-wetting cycles. The degradation rate of FA-WAP was found to higher than Com-WAP due to the incorporation of FA in the polymer structure.

TH-2777_166104034

Chapter 8

Conclusions and Future scope

8.1 General

The conclusions derived from this study are summarized in this chapter followed by major contributions of this study and future scope of work.

8.2 Conclusions from this study

- A novel and eco-friendly fly ash-based water absorbing polymer (FA-WAP) was synthesized by grafting the partially neutralized polyacrylic acid (PAA) chain onto the surface of fly ash (FA) using graft polymerization technique.
- The optimization of various parent materials for FA-WAP synthesis (includes FA content, cross-linker content, initiator content, and neutralization degree of monomer) resulted in a water-absorbing capacity (WAC) of 310 g/g in distilled water, and 230 g/g in tap water.
- The synthesized FA-WAP was found to be sensitive to various salt solutions, and the sensitivity value for various cations was found to be in the order of NH_4^+<Na^+<K^+<Ca^{2+}, while for anions, it was found to be NO_3^-<Cl^-<CO_3^{2-}<SO_4^{2-}.
- The FA-WAP showed a better WAC of 80 g/g (for monovalent ions) as compared to Com-WAP at salt concentrations of 0.1 M, which is the limiting value for plant survival under ion toxicity.
- The effect of solution pH on the WAC of FA-WAP was negligible for the pH range of 5.5 to 7.5, which is the recommended pH range of soil for plant growth.
- The toxicity characteristic leaching procedure (TCLP) results showed that the leaching potential of various trace elements (such as Pb, Cd, Cr, Ni, Cu, Zn, Mn, Fe) from the parent FA, synthesized FA-WAP, and 0.4% WAP amended soil was well below the regulatory values.
- The moisture sorption mechanism of WAP was characterized from the measured swelling kinetics of both the WAP (FA-WAP and Com-WAP) in distilled, and tap water, which showed the moisture transport into the polymer network is governed by non-Fickian diffusion mechanism.
- The water transfer mechanism from swollen WAP to dry soil was characterized by conducting a horizontal absorption experiment in a diffusion cell, which showed the

TH-2777_166104034

movement of moisture is primarily governed by two soil properties, including hydraulic conductivity and potential energy gradient between soil and swollen WAP.

- The moisture diffusivity value was found to be similar for a particular soil texture, in contact with both the WAP (synthesized and commercial), indicating the fact that moisture diffusivity function is independent of WAP type.
- The moisture release rate from the synthesized FA-WAP was found to be higher as compared to Com-WAP. This quick release of moisture in FA-WAP could be an added advantage during water stress conditions.
- Performance evaluation of the capacitance sensor (TEROS21) indicated that the sensor could measure matric suction accurately up to the suction value of 1550 kPa to 2000 kPa, depending on the type of soil due to the exponential trend of the manufacturer calibration equation.
- The capacitance-based moisture senor (5TM) showed an error in volumetric water content (VWC) measurement for WAP amended soils, attributed to the dielectric loss associated with the presence of bound water inside WAP particles.
- The error associated with the VWC measurement in WAP amended soils was removed by conducting material-specific calibration using an in-house laboratory fabricated setup, which enhanced the accuracy (measurement error less than ±5%) of the sensor.
- Addition of WAP has improved the water retention characteristic of different textured soils in the low suction range (ψ < 100 kPa). The FESEM images proved the alteration in the microstructure of soil pores (reduction in pores) in the presence of WAP, which predominantly affects the water retention at low matric suction.
- At the maximum concentration of FA-WAP amendment (0.4%), the increase in saturated VWC (θ_s) for clay loam (RS) was 50%, whereas, for silt loam (BS) and sand (FS), the increase was about 92% and 120% respectively.
- A maximum reduction of 52%, 40%, and 62% in irrigation water requirement was noticed in FA-WAP amended FS, BS, and RS, respectively, as compared to bare soil.
- The optimum WAP application rate for coarse-textured soils (sand, silt loam) is 0.1%, while for fine-textured soil (clay loam), the application rate is 0.2%.
- The incorporation of WAP significantly influences the hysteresis in WRCC, depending on the soil texture. Hence, it is essential to consider the hysteresis in WRCC for WAP amended soils with multiple drying-wetting cycles for evaluation of hydraulic characteristics of WAP amended soils.

TH-2777_166104034

- The degradation kinetics of both the WAP showed that the degradation rate of FA-WAP was higher than the Com-WAP due to the incorporation of FA in the polymer matrix. Moreover, the degradation kinetics of WAP also depends on the soil texture and WAP concentration.
- Assimilating all the results from this study, it is quite evident that WAP can serve as an environment-friendly material for promoting grass covers in various geotechnical and geoenvironmental projects, such as vegetated landfill cover systems, green infrastructures, urban green space, bioengineered slopes under semi-arid climates.
- The increase in global temperature and erratic change in rainfall pattern has a significant impact on soil infrastructures and soil ecosystem. Drought-induced long-term water scarcity results in land degradation, desertification, salinization and soil erosion. FA-WAP, transformed from an industrial waste, is one of the sustainable ways to provide enhanced water holding capacity and act as a barrier layer that absorbs (during rain) and releases (during evaporation) water for supporting vegetation growth. This would have positive contribution towards achieving food security and water conservation under the changing climate scenarios resulting in frequent droughts.

8.3 Statement of novelty

The present study proposed a method to develop a novel WAP through recycling an industrial solid waste, FA. The effort aims at mass utilization of FA-WAP for sustainable management of irrigation water in semi-arid regions by increasing the soil-water retention capacity of soil and minimizing long-term effect of drought on soil ecosystem (such as soil degradation and desertification). Huge quantities of FA are produced in India, out of which about 40% remained unutilized. Recycling FA to a value-added product (such as WAP) alleviates the negative impact of water stress conditions on soil infrastructure and improves vegetation growth, along with the nutritional enhancement of soil.

8.4 Major contributions from the study

- Developed a low-cost, eco-friendly WAP by transforming an industrial waste material, FA, to alleviate the negative influence of drought stress on plant growth.
- Characterized the moisture transport mechanism from swollen WAP to soil by conducting the horizontal absorption test in a diffusion cell.
- Demonstrated the utility of soil-specific calibration in improving the accuracy of volumetric water content sensor (ECH_2O 5TM) used in this study.

TH-2777_166104034

- Explored the optimum application rate of WAP for different soil types considering the complex soil-water-WAP interaction.
- Developed a predictive model to estimate the water retention characteristic curve (WRCC) of WAP amended soils, valid for soils with low clay content.
- Demonstrated the influence of WAP application on the hysteresis in WRCC of soil.
- Proposed a new hysteresis model that can predict the entire wetting curve of WAP amended soils from the measured drying curve and two additional points on wetting curve.
- Presented the degradation kinetics of WAP in soil with multiple alternate drying-wetting cycles.

8.5 Limitations and future scope

- The FA-WAP was synthesized using a single FA sample obtained from one thermal power plant (NTPC, Farakka, West Bengal). The influence of FA compositions (obtained from different thermal power plants) on the water absorption properties of FA-WAP needs to be studied further.
- The influence of chemical and organic fertilizers on the water retention characteristics of WAP amended soil needs to be investigated in detail.
- The volume change behavior of WAP amended soils subjected to alternate drying-wetting cycles is not measured and needs to be studied in detail.
- The influence of synthesized FA-WAP on the plant parameters, such as root growth, leaf area index, leaf chlorophyll index, and plant yield, need to be investigated with varying WAP content for different plant species and soil type.
- The performance of the synthesized FA-WAP needs to be monitored in the field under real climatic conditions as the present study is limited to laboratory environments.

TH-2777_166104034

References

Abdallah, A.M., 2019. The effect of hydrogel particle size on water retention properties and availability under water stress. Int. Soil Water Conserv. Res. 7, 275–285.

Abdollahi, L., Schjønning, P., Elmholt, S., Munkholm, L.J., 2014. The effects of organic matter application and intensive tillage and traffic on soil structure formation and stability. Soil Till. Res. 136, 28–37.

Abedi-Koupai, J., Asadkazemi, J., 2006. Effects of a hydrophilic polymer on the field performance of an ornamental plant (Cupressus arizonica) under reduced irrigation regimes. Iran. Polym. J. 15, 715.

Abhijit, D., Sreedeep, S., 2015. Evaluation of measurement methodologies used for establishing water retention characteristic curve of fly ash. J. Test. Eval. 43(5), 1066-1077.

Abrisham, E.S., Jafari, M., Tavili, A., Rabii, A., Zare Chahoki, M.A., Zare, S., Egan, T., Yazdanshenas, H., Ghasemian, D., Tahmoures, M., 2018. Effects of a super absorbent polymer on soil properties and plant growth for use in land reclamation. Arid Land Res. Manag. 32, 407–420.

Abrol, I.P., Yadav, J.S.P., Massoud, F.I., 1988. Salt-affected soils and their management (No. 39). Food & Agriculture Organization.

Acosta-Motos, J.R., Ortuño, M.F., Bernal-Vicente, A., Diaz-Vivancos, P., Sanchez-Blanco, M. J., Hernandez, J.A., 2017. Plant responses to salt stress: adaptive mechanisms. Agronomy 7(1), 18.

Agaba, H., Baguma Orikiriza, L.J., Esegu, O., Francis, J., Obua, J., Kabasa, J.D., Hüttermann, A., 2010. Effects of hydrogel amendment to different soils on plant available water and survival of trees under drought conditions. Clean–Soil, Air, Water 38, 328–335.

Agegnehu, G., Nelson, P.N., Bird, M.I., 2016. Crop yield, plant nutrient uptake and soil physicochemical properties under organic soil amendments and nitrogen fertilization on Nitisols. Soil Till. Res. 160, 1–13.

Ahmed, E.M., 2015. Hydrogel: preparation, characterization, and applications: a review. J. Adv. Res. 6, 105–121.

TH-2777_166104034

Akar, G., Polat, M., Galecki, G., Ipekoglu, U., 2012. Leaching behavior of selected trace elements in coal fly ash samples from Yenikoy coal-fired power plants. Fuel Process. Technol. 104, 50-56.

Akhter, J., Mahmood, K., Malik, K.A., Mardan, A., Ahmad, M., Iqbal, M.M., 2004. Effects of hydrogel amendment on water storage of sandy loam and loam soils and seedling growth of barley, wheat and chickpea. Plant Soil Environ. 50, 463–469.

Al Jabri, S.A., Abdel Rahman, H.A., Ibrahim, A.M., 2015. Agricultural polymers revisited: salinity interactions and soil-water conservation. Commun. Soil Sci. Plant Anal. 46, 2661–2674.

Al-Darby, A.M., 1996. The hydraulic properties of a sandy soil treated with gel-forming soil conditioner. Soil Technol. 9, 15–28.

Al-Humaid, A.I., Moftah, A.E., 2007. Effects of hydrophilic polymer on the survival of buttonwood seedlings grown under drought stress. J. Plant Nutr. 30 (1), 53–66.

Almeida, F.C., Klemm, A.J., 2018. Effect of GGBS on water absorption capacity and stability of superabsorbent polymers partially crosslinked with alkalis. J. Mater. Civil. Eng. 30, 04018315.

Andry, H., Yamamoto, T., Irie, T., Moritani, S., Inoue, M., Fujiyama, H., 2009. Water retention, hydraulic conductivity of hydrophilic polymers in sandy soil as affected by temperature and water quality. J. Hydrol. 373, 177–183.

Arbona, V., Iglesias, D.J., Jacas, J., Primo-Millo, E., Talon, M., Gómez-Cadenas, A., 2005. Hydrogel substrate amendment alleviates drought effects on young citrus plants. Plant Soil 270, 73–82.

Arrowood, T.J., 2008. Determining the Fate and Transport of the Acrylamide Monomer (AMD) in Soil and Groundwater Systems. University of Nevada, Las Vegas.

ASTM, 2004. Test method for shrinkage factors of soils by the mercury method. ASTM D427-04. West Conshohocken, PA: ASTM.

ASTM, 2005. Standard specification for coal fly ash and raw or calcined natural pozzolan for use in concrete. ASTM C618-05. West Conshohocken, PA: ASTM.

ASTM, 2007. Standard test method for particle-size analysis of soils. ASTM D422-63. West Conshohocken, PA: ASTM.

TH-2777_166104034

ASTM, 2014a. Standard test method for specific gravity of soil solids by water pycnometer. ASTM D854-14. West Conshohocken, PA: ASTM.

ASTM, 2014b. Standard test methods for one-dimensional swell or settlement potential of cohesive soils. ASTM D4546-14e1. West Conshohocken, PA: ASTM.

ASTM, 2016a. Standard test method for determination of water content of soil by direct heating. ASTM D4959-16. West Conshohocken, PA: ASTM.

ASTM, 2016b. Standard test methods for determination of the soil water characteristic curve for desorption using hanging column, pressure extractor, chilled mirror hygrometer, or centrifuge. ASTM D6836-16. West Conshohocken, PA: ASTM.

ASTM, 2017a. Standard practice for classification of soils for engineering purposes (Unified Soil Classification System). ASTM D2487-17. West Conshohocken, PA: ASTM.

ASTM, 2017b. Standard test methods for liquid limit, plastic limit, and plasticity index of soils. ASTM D4318-17e1. West Conshohocken, PA: ASTM.

ASTM, 2018. Standard test method for measuring the exchange complex and cation exchange capacity of inorganic fine-grained soils. ASTM D7503-18. West Conshohocken, PA: ASTM.

ASTM, 2019a. Standard test method for pH of soils. ASTM D4972-19. West Conshohocken, PA: ASTM.

ASTM, 2019b. Standard Specification for Coal Fly Ash and Raw or Calcined Natural Pozzolan for Use in Concrete. ASTM C618-19. West Conshohocken, PA: ASTM.

Ataka, M., Kominami, Y., Miyama, T., Yoshimura, K., Jomura, M., Tani, M., 2014. Using capacitance sensors for the continuous measurement of the water content in the litter layer of forest soil. Appl. Environ. Soil. Sci. 1-5, https://doi.org/10.1155/2014/627129

Bagheri, H., Afrasiab, P., 2013. The effects of superabsorbent, vermicompost and different levels of irrigation water salinity on soil saturated hydraulic conductivity and porosity and bulk density. Int. Res. J. Basic. Appl. Sci. 4, 2381–2388.

Bai, M., Wilske, B., Buegger, F., Esperschütz, J., Bach, M., Frede, H.G., Breuer, L., 2015. Relevance of nonfunctional linear polyacrylic acid for the biodegradation of superabsorbent polymer in soils. Environ. Sci. Pollut. Res. 22, 5444–5452.

TH-2777_166104034

Bai, W., Zhang, H., Liu, B., Wu, Y., Song, J., 2010. Effects of superabsorbent polymers on the physical and chemical properties of soil following different wetting and drying cycles. Soil Use Manag. 26, 253–260.

Bajpai, S.K., Johnson, S., 2005. Superabsorbent hydrogels for removal of divalent toxic ions. Parts I: Synthesis and swelling characterization. React. Funct. Polym. 62: 271–283.

Bakass, M., Mokhlisse, A., Lallemant, M., 2002. Absorption and desorption of liquid water by a superabsorbent polymer: effect of polymer in the drying of the soil and the quality of certain plants. J. Appl. Polym. Sci. 83 (2), 234–243.

Banedjschafie, S., Durner, W., 2015. Water retention properties of a sandy soil with superabsorbent polymers as affected by aging and water quality. J. Plant Nutr. Soil Sci. 178, 798–806.

Bao, Y., Ma, J., Li, N., 2011. Synthesis and swelling behaviors of sodium carboxymethyl cellulose-g-poly (AA-co-AM-co-AMPS)/MMT superabsorbent hydrogel. Carbohydr. Polym. 84, 76–82.

Basu, M., Pande, M., Bhadoria, P.B.S., Mahapatra, S.C., 2009. Potential fly-ash utilization in agriculture: a global review. Prog. Nat. Sci. 19(10), 1173-1186.

Bhandari, G., Panthi, B.B., 2014. Analysis of agricultural drought and its effects on productivity at different district of Nepal. J. Inst. Sci. Technol. 19, 106–110.

Bhangare, R.C., Tiwari, M., Ajmal, P.Y., Sahu, S.K., Pandit, G.G., 2014. Distribution of natural radioactivity in coal and combustion residues of thermal power plants. J. Radioanal. Nucl. Chem. 300(1), 17-22.

Bhardwaj, A.K., McLaughlin, R.A., Shainberg, I., Levy, G.J., 2009. Hydraulic characteristics of depositional seals as affected by exchangeable cations, clay mineralogy, and polyacrylamide. Soil Sci. Soc. Am. J. 73, 910–918.

Bhardwaj, A.K., Shainberg, I., Goldstein, D., Warrington, D.N., Levy, G.J., 2007. Water retention and hydraulic conductivity of crosslinked polyacrylamides in sandy soils. Soil Sci. Soc. Am. J. 71, 406–412.

Bhattacharya, A., Misra, B.N., 2004. Grafting: a versatile means to modify polymers: techniques, factors and applications. Prog. Polym. Sci. 29(8), 767-814.

TH-2777_166104034

Bhattacharyya, S., Donahoe, R.J., Patel, D., 2009. Experimental study of chemical treatment of coal fly ash to reduce the mobility of priority trace elements. Fuel 88(7):1173-1184.

Birle, E., Heyer, D., Vogt, N., 2008. Influence of the initial water content and dry density on the soil–water retention curve and the shrinkage behavior of a compacted clay. Acta Geotech. 3(3), 191-200.

Bogena, H.R., Huisman, J.A., Oberdörster, C., Vereecken, H., 2007. Evaluation of a low-cost soil water content sensor for wireless network applications. J. Hydrol. 344(1-2), 32-42.

Bowman, D.C., Evans, R.Y., 1991. Calcium inhibition of polyacrylamide gel hydration is partially reversible by potassium. HortScience 26, 1063–1065.

Boyarskii, D.A., Tikhonov, V.V., Komarova, N.Y., 2002. Model of dielectric constant of bound water in soil for applications of microwave remote sensing-abstract. J. Electromagn. Waves Appl. 16(3), 411-412.

Brooks, R.H., Corey, A.T., 1964. Hydraulic properties of porous media (Doctoral dissertation, Colorado State University).

Bruce, R.R., Klute, A., 1956. The measurement of soil-water diffusivity. Soil Sci. Soc. Amer. J. 20(4), 458-462.

Buchmann, C., Bentz, J., Schaumann, G.E., 2015. Intrinsic and model polymer hydrogel induced soil structural stability of a silty sand soil as affected by soil moisture dynamics. Soil Till. Res. 154, 22–33.

Bulut, R., Leong, E.C., 2008. Indirect measurement of suction. In: Tarantino et al. (eds) Laboratory and field testing of unsaturated soils. Springer, pp. 21–32.

Burger, C.A., Shackelford, C.D., 2001. Evaluating dual porosity of pelletized diatomaceous earth using bimodal soil-water characteristic curve functions. Can. Geotech. J. 38(1), 53–66.

Busscher, W.J., Bjorneberg, D.L., Sojka, R.E., 2009. Field application of PAM as an amendment in deep-tilled US southeastern coastal plain soils. Soil Till. Res. 104 (2), 215–220.

Cameron, M.D., Post, Z.D., Stahl, J.D., Haselbach, J., Aust, S.D., 2000. Cellobiose dehydrogenase- dependent biodegradation of polyacrylate polymers by Phanerochaete chrysosporium. Environ. Sci Pollut. Res. 7, 130–134.

TH-2777_166104034

Cannazza, G., Cataldo, A., De Benedetto, E., Demitri, C., Madaghiele, M., Sannino, A., 2014. Experimental assessment of the use of a novel superabsorbent polymer (SAP) for the optimization of water consumption in agricultural irrigation process. Water 6 (7), 2056–2069.

Carles Brangari, A., Sanchez- Vila, X., Freixa, A., M. Romaní, A., Rubol, S., Fernàndez-Garcia, D., 2017. A mechanistic model (BCC- PSSICO) to predict changes in the hydraulic properties for bio- amended variably saturated soils. Water Resour. Res. 53(1), 93-109.

Cassel, D. K., Nielsen, D.R., 1986. Field capacity and available water capacity. Methods of soil analysis: Part 1—Physical and mineralogical methods, 901-926.

Caulfield, M.J., Qiao, G.G., Solomon, D.H., 2002. Some aspects of the properties and degradation of polyacrylamides. Chem. Rev. 102, 3067–3084.

Central Authority of Electricity, 2015. Report on fly ash generation at coal/lignite based thermal power stations and its utilization in the country for the year 2014-15, New Delhi, India.

Central Authority of Electricity, 2018a. National Electricity Plan (Volume I - Generation and Volume II - Distribution).

Central Authority of Electricity, 2018b. Report on fly ash generation at coal/lignite based thermal power stations and its utilization in the country for the year 2017-18, New Delhi, India.

Chandler, D.G., Seyfried, M., Murdock, M., McNamara, J.P., 2004. Field calibration of water content reflectometers. Soil Sci. Soc. Amer. J. 68(5), 1501-1507.

Chang, A.C., Lund, L.J., Page, A.L., Warneke, J.E., 1977. Physical Properties of Fly Ash-Amended Soils 1. J. Environ. Qual. 6(3), 267-270.

Chen, R., Chen, Y., Chen, W., Chen, Y., 2012. Time domain reflectometry for water content measurement of municipal solid waste. Environ. Eng. Sci. 29(6), 486-493.

Cheng, B., Pei, B., Wang, Z., Hu, Q., 2017. Advances in chitosan-based superabsorbent hydrogels. RSC Adv. 7, 42036–42046.

Chetia, M., Sekharan, S., 2016. Evaluation of different laboratory procedures for determining suction–water content relationship of cohesionless geomaterials. J. Mater. Civil Eng. 28(2), 04015123.

Chirino, E., Vilagrosa, A., Vallejo, V.R., 2011. Using hydrogel and clay to improve the water status of seedlings for dryland restoration. Plant Soil 344, 99–110.

TH-2777_166104034

Choudhary, M.I., AI-Omran, A.M., Shalaby, A.A., 1998. Physical properties of sandy soil affected by soil conditioner under wetting and drying cycles. J. Agric. Mar. Sci. 3(2), 69–74.

Clothier, B.E., Scotter, R.D., Green, E.A., 1983. Diffusivity and one dimensional absorption experiments. Soil Sci. Soc. Amer. J. 47(4), 641-644.

Coelho, J.F., Ferreira, P.C., Alves, P., Cordeiro, R., Fonseca, A.C., Góis, J.R., Gil, M.H., 2010. Drug delivery systems: advanced technologies potentially applicable in personalized treatments. EPMA J. 1, 164–209.

Colman, E.A., 1947. A laboratory procedure for determining the field capacity of soils. Soil Sci. 63(4), 277–284.

Cowie, J.M.G., Arrighi, V., 2007. Polymers: Chemistry and Physics of Modern Materials (CRC Press, Boca Raton).

Crank, J., 1975. The mathematics of diffusion. Oxford, Clarendon.

Darini, A.K., Naderi, R., Khalighi, A., Taheri, M., 2015. Effect of superabsorbent polymer on lawn under drought stress condition. Agric. Sci. Dev. 4, 22–26.

De Kee, D., Liu, Q., Hinestroza, J., 2005. Viscoelastic (non-Fickian) diffusion. Can. J. Chem. Eng. 83(6), 913–929.

de Vasconcelos, M.C., Gomes, R.F., Sousa, A.A., Moreira, F.J., Rodrigues, F.H., Fajardo, A.R., Neto, L.G.P., 2020. Superabsorbent hydrogel composite based on Starch/Rice husk ash as a soil conditioner in melon (Cucumis melo L.) seedling culture. J. Polym. Environ. 28 (1), 131–140.

Dehkordi, D.K., 2015. Evaluation of superabsorbent application on corn yield under deficit irrigation. Int. J. Agric. Biosyst. Eng. 9, 811–815.

Dehkordi, D.K., 2017. Effect of superabsorbent polymer on salt and drought resistance of eucalyptus globulus. Appl. Ecol. Environ. Res. 15 (4), 1791–1802.

Deka, A., Sekharan, S., 2017. Contaminant retention characteristics of fly ash–bentonite mixes. Waste Manage. Res. 35(1):40-46.

Demitri, C., Scalera, F., Madaghiele, M., Sannino, A., Maffezzoli, A., 2013. Potential of cellulose-based superabsorbent hydrogels as water reservoir in agriculture. Int. J. Polym. Sci. https://doi.org/10.1155/2013/435073.

TH-2777_166104034

Dorraji, S.S., Golchin, A., Ahmadi, S., 2010. The effects of hydrophilic polymer and soil salinity on corn growth in sandy and loamy soils. Clean–Soil, Air, Water 38, 584–591.

Dwivedi, S., Tripathi, R.D., Srivastava, S., Mishra, S., Shukla, M.K., Tiwari, K.K., Singh, R., Rai, U.N., 2007. Growth performance and biochemical responses of three rice (Oryza sativa L.) cultivars grown in fly-ash amendment soil. Chemosphere 67, 140–151.

Ekebafe, L.O., Ogbeifun, D.E., Okieimen, F.E., 2011. Polymer applications in agriculture. Biokemistri 23, 81–89.

Ekebafe, M.O., Ekebafe, L.O., Maliki, M., 2013. Utilisation of biochar and superabsorbent polymers for soil amendment. Sci. Prog. 96, 85–94.

El-Asmar, J., Jaafar, H., Bashour, I., Farran, M.T., Saoud, I.P., 2017. Hydrogel banding improves plant growth, survival, and water use efficiency in two calcareous soils. CLEAN–Soil, Air, Water 45, 1700251.

El-Rehim, H.A., Hegazy, E.S.A., El-Mohdy, H.L., 2006. Effect of various environmental conditions on the swelling property of PAAm/PAAcK superabsorbent hydrogel prepared by ionizing radiation. J. Appl. Polym. Sci. 101, 3955–3962.

El-Tohamy, W.A., El-Abagy, H.M., Ahmed, E.M., Aggor, F.S., Hawash, S.I., 2014. Application of super absorbent hydrogel poly (acrylate/acrylic acid) for Water conservation in Sandy soil. Trans. Egypt Soc. Chem. Eng. 40, 1–8.

Entry, J.A., Sojka, R.E., Hicks, B.J., 2008. Carbon and nitrogen stable isotope ratios can estimate anionic polyacrylamide degradation in soil. Geoderma 145, 8–16.

Espejo, A., Giráldez, J.V., Vanderlinden, K., Taguas, E.V., Pedrera, A., 2014. A method for estimating soil water diffusivity from moisture profiles and its application across an experimental catchment. J. Hydrol. 516, 161-168.

Evangelides, C., Arampatzis, G., Tzimopoulos, C., 2010. Estimation of soil moisture profile and diffusivity using simple laboratory procedures. Soil Sci. 175(3), 118–127.

Evangelides, C., Tzimopoulos, C., Arampatzis, G., 2005. Flux-saturation relationship for unsaturated horizontal flow. Soil Sci. 170(9), 671-679.

Evett, S.R., Steiner, J.L., 1995 Precision of neutron scattering and capacitance type soil water content gauges from field calibration. Soil Sci. Soc. Amer. J. 59(4), 961-968.

TH-2777_166104034

Fallahi, H.R., Kalantari, R.T., Aghhavani-Shajari, M., Soltanzadeh, M.G., 2015. Effect of super absorbent polymer and irrigation deficit on water use efficiency, growth and yield of cotton. Not. Sci. Biol. 7, 338–344.

Fan, Y., Zhang, M., Shangguan, L., 2018. Synthesis of a novel and salt sensitive superabsorbent hydrogel using soybean dregs by UV-irradiation. Materials 11, 2198.

Fares, A., Alva, A.K., 2000. Evaluation of capacitance probes for optimal irrigation of citrus through soil moisture monitoring in an entisol profile. Irrig. Sci. 19(2), 57-64.

Farrell, C., Ang, X.Q., Rayner, J.P., 2013. Water-retention additives increase plant available water in green roof substrates. Ecol. Eng. 52, 112–118.

Feng, D., Bai, B., Ding, C., Wang, H., Suo, Y., 2014. Synthesis and swelling behaviors of yeast-g-poly (acrylic acid) superabsorbent co-polymer. Ind. Eng. Chem. Res. 53, 12760–12769.

Feng, M., Fredlund, D.G., 1999. Hysteretic influence associated with thermal conductivity sensor measurements. Proceedings of 52nd Canadian Geotechnical Conference, Regina, SK, Canada, 651–657.

Food and Agriculture Organization, 2006. FAO Fertilizer and Plant Nutrition Bulletin. 17, Rome.

Fredlund, D.G., Rahardjo, H., 1993. Soil Mechanics for Unsaturated Soils. John Wiley & Sons.

Frisch, H.L., 1980. Sorption and transport in glassy polymers – A review. Polym. Eng. Sci. 20(1), 2–13.

Gallipoli, D., Bruno, A.W., D'Onza, F., Mancuso, C., 2015. A bounding surface hysteretic water retention model for deformable soils. Géotechnique 65(10), 793–804.

Gallipoli, D., Wheeler, S.J., Karstunen, M., 2003. Modelling the variation of degree of saturation in a deformable unsaturated soil. Géotechnique 53(1), 105-112.

Gao, D., Heimann, R.B., Lerchner, J., Seidel, J., Wolf, G., 2001. Development of a novel moisture sensor based on superabsorbent poly (acrylamide)-montmorilloniteand Luquasorb polymers on salt and drought tolerance of Populus popularis. Sci. Hort. 124, 268–273.

Gardner, W.R., 1956. Calculation of capillary conductivity from pressure plate outflow data. Soil Sci. Soc. Amer. J. 20(3), 317-320.

TH-2777_166104034

Gatima, E., Mwinyihija, M., Killham, K., 2005. Assessment of Pulverised Fly Ash (PFA) as an Ameliorant of Lead Contaminated Soils. Am. J. Environ. Sci. 1(3), 230-238.

Gollakota, A.R., Volli, V., Shu, C.M., 2019. Progressive utilisation prospects of coal fly ash: A review. Sci. Total Environ. 672, 951-989.

Gong, Y., Cao, Q., Sun, Z., 2003. The effects of soil bulk density, clay content and temperature on soil water content measurement using time-domain reflectometry. Hydrol. Process. 17(18), 3601-3614.

Gong. X., Wu, T., Qiao, Y., Xu, M., 2009. In situ leaching of trace elements in a coal ash dump and time dependence laboratory evaluation. Energ. Fuel. 24(1):84-90.

Greenland, D.J., 1981. Soil management and soil degradation. J. Soil Sci. 32(3), 301–322.

Han, Y., Yu, X., Yang, P., Li, B., Xu, L., Wang, C., 2013. Dynamic study on water diffusivity of soil with super-absorbent polymer application. Environ. Earth Sci. 69(1), 289-296.

Hansen, V.E., Israelsen, O.W., Stringham, G.E., (eds.) 1980. Irrigation Principles and Practices (fourth edition). Wiley, New York.

He, Y., Pei, M., Xue, N., Wang, L., Guo, W., 2016. Synthesis of sodium polyacrylate–bentonite using in situ polymerization for Pb^{2+} removal from aqueous solutions. RSC Adv. 6(53), 48145-48154.

Hermans, J.J., 1953. Flow Properties of Disperse System 61 (Wiley-Inter-science, New York).

Huang, Q., Akinremi, O.O., Rajan, R., Bullock, P., 2004. Laboratory and field evaluation of five soil water sensors. Can. J. Soil Sci. 84(4), 431-438.

Hosney, M., Rowe, R. K., 2017. Polymer-618 enhanced bentonite–sand to cover calcium-rich soil. Environ. Geotech. 6(3), 155-161.

Hüttermann, A., Orikiriza, L.J., Agaba, H., 2009. Application of superabsorbent polymers for improving the ecological chemistry of degraded or polluted lands. Clean-Soil Air Water 37(7), 517-526.

Hüttermann, A., Zommorodi, M., Reise, K., 1999. Addition of hydrogels to soil for prolonging the survival of Pinus halepensis seedlings subjected to drought. Soil Till. Res. 50, 295–304.

Inbar, A., Ben-Hur, M., Sternberg, M., Lado, M., 2015. Using polyacrylamide to mitigate post-fire soil erosion. Geoderma 239, 107–114.

TH-2777_166104034

Islam, M.R., Hu, Y., Mao, S., Mao, J., Eneji, A.E., Xue, X., 2011. Effectiveness of a watersaving super-absorbent polymer in soil water conservation for corn (Zea mays L.) based on eco-physiological parameters. J. Sci. Food Agric. 91 (11), 1998–2005.

Ismail, H., Irani, M., Ahmad, Z., 2013. Starch-based hydrogels: present status and applications. International Journal of Polymeric Mater. Polym. Biomater. 62(7), 411-420.

Jala, S., Goyal, D., 2006. Fly ash as a soil ameliorant for improving crop production—a review. Bioresour. Technol. 97(9), 1136-1147.

Jamison, V.C., 1956. Pertinent factors governing the availability of soil moisture to plants. Soil Sci. 81(6), 459–472.

Jamison, V.C., Kroth, E.M., 1958. Available Moisture Storage Capacity in Relation to Textural Composition and Organic Matter Content of Several Missouri Soils 1. Soil Sci. Soc. Am. J. 22(3), 189–192.

Johnson, S.J., 1984. The effects of gel-forming polyacrylamides on moisture storage in sandy soils. J. Sci. Food Agric. 35, 1196–1200.

Kalhapure, A., Kumar, R., Singh, V.P., Pandey, D.S., 2016. Hydrogels: a boon for increasing agricultural productivity in water-stressed environment. Curr. Sci. 111 (11), 1773–1779.

Kalra, N., Harit, R.C., Sharma, S.K., 2000. Effect of flyash incorporation on soil properties of texturally variant soils. Bioresour. Technol. 75(1), 91-93.

Laegdsmand, M., Moldrup, P., Schjønning, P., 2010. Multitracer and filter-separated half-cell method for measuring solute diffusion in undisturbed soil. Soil Sci. Soc. Amer. J. 74(4), 1084-1091.

Leciejewski, P., 2009. The effect of hydrogel additives on the water retention curve of sandy soil from forest nursery in Julinek. J. Water Land Dev. 13(1), 239–247.

Lee, H.C., Wray, W.K., 1995. Techniques to evaluate soil suction: a vital unsaturated soil water variable. In: Proceedings of the first international conference on unsaturated soils, vol 2. Paris, France, pp 615–622.

Lee, S.S., Chang, S.X., Chang, Y.Y., Ok, Y.S., 2013. Commercial versus synthesized polymers for soil erosion control and growth of Chinese cabbage. SpringerPlus 2(1), 1-10.

Lentz, R.D., 2015. Polyacrylamide and biopolymer effects on flocculation, aggregate stability, and water seepage in a silt loam. Geoderma 241, 289–294.

TH-2777_166104034

Li, A., Wang, A., 2005. Synthesis and properties of clay-based superabsorbent composite. Eur. Polym. J. 41, 1630-1637.

Li, A., Wang, A., Chen, J., 2004. Studies on poly (acrylic acid)/attapulgite superabsorbent composite. I. Synthesis and characterization. J. Appl. Polym. Sci. 92(3), 1596-1603.

Li, Y. B., Fan, Y. W., Liu, Y., Ma, X.Y., 2017. Influencing factors and simplified model of film hole irrigation. Water 9(7), 543.

Likos, W.J., Lu, N., Godt, J.W. 2014. Hysteresis and uncertainty in soil water-retention curve parameters. J. Geotech. Geoenviron. Eng. 140(4), 04013050.

Liu, X., Zhao, H., He, Y., Zhao, X., Zhang, T., Li, Y., 2009. Water diffusivity of sandy soil of different particle sizes in typical sandy cropland. In: Environmental Science and Information Application Technology 2, 335–338.

Lu, N., and Likos, W.J. 2004. Unsaturated soil mechanics. Wiley, New York.

Lu, N., Khorshidi, M., 2015. Mechanisms for soil-water retention and hysteresis at high suction range. J. Geotech. Geoenviron. Eng. 141(8), 04015032.

Lu, N., Likos, W., 2004. Unsaturated Soil Mechanics. New York.

Ma, D., Zhang, J., Lai, J., Wang, Q., 2016. An improved method for determining Brooks–Corey model parameters from horizontal absorption. Geoderma 263, 122-131.

Mahdavinia, G.R., Pourjavadi, A., Hosseinzadeh, H., Zohuriaan, M.J., 2004. Modified chitosan 4. Superabsorbent hydrogels from poly (acrylic acid-co-acrylamide) grafted chitosan with salt- and pH-responsiveness properties. Eur. Polym. J. 40(7), 1399-1407.

Mahur, A.K., Kumar, R., Sengupta, D., Prasad, R., 2008. Estimation of radon exhalation rate, natural radioactivity and radiation doses in fly ash samples from Durgapur thermal power plant, West Bengal, India. J. Environ. Radioact. 99(8), 1289-1293.

Maitra, J., Shukla, V.K., 2014. Cross-linking in hydrogels-a review. Am. J. Polym. Sci. 4(2), 25-31.

Malaya, C., Sreedeep, S., 2016. Effect of fertilizers and fly ash addition on suction–water content relationship of a sandy soil. Indian Geotech. J. 46(3), 327-333.

Malik, A., Thapliyal, A., 2009. Eco-friendly fly ash utilization: potential for land application. Crit. Rev. Environ. Sci. Technol. 39(4), 333-366.

TH-2777_166104034

Manoharan, V., Yunusa, I.A.M., Loganathan, P., Lawrie, R., Skilbeck, C.G., Burchett, M.D., Eamus, D., 2010. Assessments of Class F fly ashes for amelioration of soil acidity and their influence on growth and uptake of Mo and Se by canola. Fuel 89(11), 3498-3504.

Matsi, T., Keramidas, V.Z., 1999. Fly ash application on two acid soils and its effect on soil salinity, pH, B, P and on ryegrass growth and composition. Environ. Pollut. 104(1), 107-112.

METER Group Inc., 2017. Operator's manual, 5TM ECH$_2$O Water content and temperature sensor. Pullman, WA.

METER Group Inc., 2019a. Operator's manual, TEROS21. Pullman, WA.

METER Group Inc., 2019b. Operator's manual, WP4C Dew point potentiameter. Pullman, WA.

Mishra, M., Sahu, R.K., Padhy, R.N., 2007. Growth, yield and elemental status of rice (Oryza sativa) grown in fly ash amended soils. Ecotoxicology 16, 271–278

Misiewicz, J., Lejcuś, K., Dąbrowska, J., Marczak, D., 2019. The characteristics of absorbency under load (AUL) for superabsorbent and soil mixtures. Sci. Rep. 9(1), 1-9.

Mittra, B.N., Karmakar, S., Swain, D.K., Ghosh, B.C., 2005. Fly ash—a potential source of soil amendment and a component of integrated plant nutrient supply system. Fuel 84(11), 1447-1451.

Mohamed, A.M.O., Paleologos, E.K., 2017. Fundamentals of geoenvironmental engineering: understanding soil, water, and pollutant interaction and transport. Butterworth-Heinemann, https://doi.org/10.1016/C2015-0-01982-7

Mohawesh, O., Durner, W., 2019. Effect of bentonite, hydrogel and biochar amendments on soil hydraulic properties from saturation to oven dryness. Pedosphere 29(5), 598-607.

Montesano, F.F., Parente, A., Santamaria, P., Sannino, A., Serio, F., 2015. Biodegradable superabsorbent hydrogel increases water retention properties of growing media and plant growth. Agric. Agric. Sci. Procedia 4, 451–458.

Munns, R., Termaat, A., 1986. Whole-plant responses to salinity. Aust. J. Plant Physiol. 13, 143–160.

Munns, R., Tester, M., 2008. Mechanisms of salinity tolerance. Annu. Rev. Plant Biol. 59, 651–681.

TH-2777_166104034

Nawaz, I., 2013 Disposal and utilization of fly ash to protect the environment. Int. J. Innov. Res. Sci. Eng. Technol. 2(10), 5259-5266.

Ng, C.W.W., Ni, J.J., Leung, A.K., Wang, Z.J., 2016. A new and simple water retention model for root-permeated soils. Geotech. Lett. 6(1), 106-111.

Ni, J., Sanandam, B., Garg, A., Shao, W., Sreedeep, S., 2019. Simple Model on Water Retention and Permeability in Soil Mixed with Lignocellulose Fibres. KSCE J. Civ. Eng. 23(1), 138-146.

Nimmo, J.R., 2004. Porosity and pore size distribution. Encyclopedia of Soils in the Environment 3(1), 295–303.

Orts, W.J., Roa-Espinosa, A., Sojka, R.E., Glenn, G.M., Imam, S.H., Erlacher, K., Pedersen, J.S., 2007. Use of synthetic polymers and biopolymers for soil stabilization in agricultural, construction, and military applications. J. Mater. Civil Eng. 19(1), 58-66.

Page, A.L., Elseewi, A.A., Straughan, I.R., 1979. Physical and chemical properties of fly ash from coal-fired power plants with reference to environmental impacts. In: Residue Reviews, Springer, New York, pp. 83-120.

Pan, H., Qing, Y., Young, L.P., 2010. Direct and indirect measurement of soil suction in the laboratory. Electron. J. Geotech. Eng. 15, 1–14.

Pandey, V.C., Abhilash, P.C., Upadhyay, R.N., Tewari, D.D., 2009. Application of fly ash on the growth performance and translocation of toxic heavy metals within Cajanus cajan L.: implication for safe utilization of fly ash for agricultural production. J. Hazard. Mater. 166, 255–259.

Pandey, V.C., Singh, N., 2010. Impact of fly ash incorporation in soil systems. Agric. Ecosyst. Environ. 136(1-2), 16-27.

Parvin, N., Degré, A., 2016. Soil-specific calibration of capacitance sensors considering clay content and bulk density. Soil Res. 54(1), 111-119.

Pathan, S.M., Aylmore, L.A.G., Colmer, T.D., 2003. Properties of several fly ash materials in relation to use as soil amendments. J. Environ. Qual. 32, 687–693.

Patra, K.C., Rautray, T.R., Nayak, P., 2012. Analysis of grains grown on fly ash treated soils. Appl. Radiat. Isotopes 70(8), 1797-1802.

TH-2777_166104034

Peleg, M., 1988. An empirical model for the description of moisture sorption curves. J. Food Sci. 53(4), 1216-1217.

Pham, H.Q., Fredlund, D.G. 2011. Volume–mass unsaturated soil constitutive model for drying–wetting under isotropic loading–unloading conditions. Can. Geotech. J. 48(2), 280-313.

Pham, H.Q., Fredlund, D.G., Barbour, S.L., 2003. A practical hysteresis model for the soil–water characteristic curve for soils with negligible volume change. Géotechnique 53(2), 293-298.

Pham, H.Q., Fredlund, D.G., Barbour, S.L., 2005. A study of hysteresis models for soil-water characteristic curves. Can. Geotech. J. 42(6), 1548-1568.

Phang, Y.N., Chee, S.Y., Lee, C.O., Teh, Y.L., 2011. Thermal and microbial degradation of alginate-based superabsorbent polymer. Polym. Degrad. Stabil. 96(9), 1653-1661.

Piqué, T. M., Manzanal, D., Codevilla, M., Orlandi, S., 2019. Polymer-enhanced soil mixtures for potential use as covers or liners in landfill systems. Environ. Geotech. https://doi.org/10.1680/jenge.18.00174

Polyakov, V., Fares, A., Ryder, M.H., 2005. Calibration of a capacitance system for measuring water content of tropical soil. Vadose Zone J. 4(4), 1004-1010.

Prakash, K., Sridharan, A., 2009. Beneficial properties of coal ashes and effective solid waste management. Practice periodical of hazardous, toxic, and radioactive waste management 13(4), 239-248.

Puri, P., Liu, Q., De Kee, D., 2008. Diffusion through swelling membranes with a Robin boundary condition. J. Appl. Polym. Sci. 108(1), 47–51.

Queensland Department of Environment and Heritage Protection, 2013. Soil pH. www.qld.gov.au

Raghuram, A.S.S., Basha, B.M., Moghal, A.A.B., 2020. Effect of Fines Content on the Hysteretic Behavior of Water-Retention Characteristic Curves of Reconstituted Soils. J. Mater. Civil Eng. 32(4), 04020057.

Rahmati, M., Pohlmeier, A., Abasiyan, S.M.A., Weihermüller, L., Vereecken, H., 2019. Water retention and pore size distribution of a biopolymeric-amended loam soil. Vadose Zone J. 18(1), 1-13.

TH-2777_166104034

Ritger, P.L., Peppas, N.A., 1987. A simple equation for description of solute release I. Fickian and non-Fickian release from non-swellable devices in the form of slabs, spheres, cylinders or discs. J. Controll. Release 5, 23–36.

Rivas, B.L., Urbano, B.F., Sánchez, J., 2018. Water-soluble and insoluble polymers, nanoparticles, nanocomposites and hybrids with ability to remove hazardous inorganic pollutants in water. Front. Chem. 6, 320.

Rivers, E.D., Shipp, R.F., 1977. Soil water retention as related to particle size in selected sands and loamy sands. Soil Sci. 126, 94–100.

Rodrigues, F.H., Fajardo, A.R., Pereira, A.G., Ricardo, N.M., Feitosa, J.P., Muniz, E.C., 2012. Chitosan-graft-poly (acrylic acid)/rice husk ash based superabsorbent hydrogel composite: preparation and characterization. J. Polym. Res. 19(12), 1-10.

Rogers, C.E., 1985. Sorption and diffusion in multicomponent polymers. J. Polym. Sci.: Polym. Symp. 72(1), 301.

Rosenzweig, R., Shavit, U., Furman, A., 2012. Water retention curves of biofilm- affected soils using xanthan as an analogue. Soil Sci. Soc. Amer. J. 76(1), 61-69.

Saikia, N., Kato, S., Kojima, T., 2006. Compositions and leaching behaviours of combustion residues. Fuel 85(2), 264-271.

Scalia, J., Benson, C. H., 2017. Polymer fouling and hydraulic conductivity of mixtures of sodium bentonite and a bentonite-polymer composite. J. Geotech. Geoenviron. Eng. 143(4), 04016112.

Selim, H.M., Kirkham, D., Amemiya, M.A., 1970. A comparision of two methods for determining soil water diffusivity. Soil Sci. Soc. Amer. J. 34(1), 14–18.

Sepaskhah, A.R., Shahabizad, V., 2010. Effects of water quality and PAM application rate on the control of soil erosion, water infiltration and runoff for different soil textures measured in a rainfall simulator. Biosyst. Eng. 106 (4), 513–520.

Serrano, R., Culiañz-Maciá, F.A., Moreno, V., 1998. Genetic engineering of salt and drought tolerance with yeast regulatory genes. Sci. Hortic. 78(1-4), 261-269.

Shackelford, C.D., 1991. Laboratory diffusion testing for waste disposal—A review. J. Contam. Hydrol. 7(3), 177-217.

TH-2777_166104034

Shaikh, J., Yamsani, S.K., Sekharan, S., Rakesh, R.R., 2019. Performance evaluation of 5TM sensor for real-time monitoring of volumetric water content in landfill cover system. Adv. Civil Eng. Mater. 8(1), 322-335.

Shao, M., Horton, R., 1998. Integral method for estimating soil hydraulic properties. Soil Sci. Soc. Amer. J. 62(3), 585-592.

Shi, Y., Li, J., Shao, J., Deng, S., Wang, R., Li, N., Sun, J., Zhang, H., Zhu, H., Zhang, Y., Zheng, X., 2010. Effects of Stockosorb and Luquasorb polymers on salt and drought tolerance of Populus popularis. Scientia horticulturae 124 (2), 268–273.

Sillers, W.S., Fredlund, D.G., Zakerzadeh, N., 2001. Mathematical attributes of some soil—water characteristic curve models. In: Unsaturated soil concepts and their application in geotechnical practice, Springer, pp. 243-283.

Sime, G., Aune, J.B., Mohammed, H., 2015. Agronomic and economic response of tillage and water conservation management in maize, central rift valley in Ethiopia. Soil Till. Res. 148, 20–30.

Siriwatwechakul, W., Siramanont, J., Vichit-Vadakan, W., 2012. Behavior of superabsorbent polymers in calcium-and sodium-rich solutions. J. Mater. Civil Eng. 24, 976–980.

Sojka, R.E., Bjorneberg, D.L., Entry, J.A., Lentz, R.D., Orts, W.J., 2007. Polyacrylamide in agriculture and environmental land management. Adv. Agron. 92, 75–162.

Spagnol, C., Rodrigues, F.H., Neto, A.G., Pereira, A.G., Fajardo, A.R., Radovanovic, E., Rubira, A.F., Muniz, E.C., 2012a. Nanocomposites based on poly (acrylamide-co-acrylate) and cellulose nanowhiskers. Eur. Polym. J. 48 (3), 454–463.

Spagnol, C., Rodrigues, F.H., Pereira, A.G., Fajardo, A.R., Rubira, A.F., Muniz, E.C., 2012b. Superabsorbent hydrogel composite made of cellulose nanofibrils and chitosan-graft-poly (acrylic acid). Carbohydr. Polym. 87 (3), 2038–2045.

Śpitalniak, M., Lejcuś, K., Dąbrowska, 686 J., Garlikowski, D., Bogacz, A., 2019. The Influence of a Water Absorbing Geocomposite on Soil Water Retention and Soil Matric Potential. Water 11(8), 1731.

Sreedeep, S., Singh, D.N., 2006. Methodology for determination of osmotic suction of soils. Geotech. Geol. Eng. 24(5), 1469–1479.

TH-2777_166104034

Sreedeep, S., Singh, D.N., 2008. A novel technique for studying diffusion of contaminants in fine-grained soils. Geomech. Geoeng. 3(3), 199-209.

Sreedeep, S., Singh, D.N., 2011. Critical review of the methodologies employed for soil suction measurement. Int. J. Geomech. 11(2), 99-104.

Stahl, J.D., Cameron, M.D., Haselbach, J., Aust, S.D., 2000. Biodegradation of superabsorbent polymers in soil. Environ. Sci. Pollut. Res. Int. 7, 83–88.

Sudhir, P., Murthy, S.D.S., 2004. Effects of salt stress on basic processes of photosynthesis. Photosynthetica 42 (2), 481–486.

Swain, S.K., Prusty, K., 2018. Biomedical applications of acrylic-based nanohydrogels. J. Mater. Sci. 53, 2303–2325.

Tavakkoli, E., Rengasamy, P., McDonald, G.K., 2010. High concentrations of Na^+ and Cl^- ions in soil solution have simultaneous detrimental effects on growth of faba bean under salinity stress. J. Exp. Bot. 61(15), 4449-4459.

Tongo, A., Mahdavi, A., Sayad, E., 2014. Effect of superabsorbent polymer aquasorb on chlorophyll, antioxidant enzymes and some growth characteristics of Acacia victoriae seedlings under drought stress. Ecopersia 2, 571–583.

Topp, G.C., Davis, J.L., Annan, A.P., 1980. Electromagnetic determination of soil water content: Measurements in coaxial transmission lines. Water Resour. Res. 16(3), 574-582.

Tuli, A., Hopmans, J.W., Rolston, D.E., Moldrup, P., 2005. Comparison of air and water permeability between disturbed and undisturbed soils. Soil Sci. Soc. Am. J. 69, 1361–1371.

Ukwattage, N.L., Ranjith, P.G., Bouazza, M., (2013). The use of coal combustion fly ash as a soil amendment in agricultural lands (with comments on its potential to improve food security and sequester carbon). Fuel 109, 400–408.

Ullah, F., Othman, M.B.H., Javed, F., Ahmad, Z., Akil, H.M., 2015. Classification, processing and application of hydrogels: a review. Mater Sci. Eng. C 57, 414–433.

UMS GmbH (Umwelt-Monitoring-Systeme), 2001. T5 user manual, Munich, Germany.

United States Dept. of Agriculture (USDA), 1993. Soil Survey Division, & United States. Division of Soil Survey. Soil survey manual (No. 18).

TH-2777_166104034

United States Environmental Protection Agency (USEPA), 1990. Test Methods for Evaluating Solid Waste, SW-846. https://www.epa.gov/hw-sw846/sw-846-test-method-1311-toxicity-characteristic-leaching-procedure

United States Environmental Protection Agency (USEPA), 2002. Hazardous Waste Management System; Definition of Solid Waste; Toxicity Characteristic; Final Rule. Fed Regist. https://www.govinfo.gov/content/pkg/FR-2002-03-13/html/02-6063.htm

USDA, 2010. Keys to soil taxonomy. USDA, Washington DC, 197-240.

Van Loon, A.F., 2015. Hydrological drought explained. Wiley Interdiscip. Rev. Water 2, 359–392.

Van Loon, A.F., Van Lanen, H.A., 2012. A process-based typology of hydrological drought. Hydrol. Earth Syst. Sci. 16, 1915.

Vassilev, S.V., Vassileva, C.G., 2005. Methods for characterization of composition of fly ashes from coal-fired power stations: a critical overview. Energ. Fuel. 19(3), 1084-1098.

Vaz, C.M., Jones, S., Meding, M., Tuller, M., 2013. Evaluation of standard calibration functions for eight electromagnetic soil moisture sensors. Vadose Zone J. 12(2), 1-16.

Veihmeyer, F.J., Hendrickson, A.H., 1931. The moisture equivalent as a measure of the field capacity of soils. Soil Sci. 32(3), 181–194.

Villarreal, R., Lozano, L.A., Melani, E.M., Salazar, M.P., Otero, M.F., Soracco, C.G., 2019. Diffusivity and sorptivity determination at different soil water contents from horizontal infiltration. Geoderma 338, 88-96.

Visconti, F., de Paz, J.M., Martínez, D., Molina, M.J., 2014. Laboratory and field assessment of the capacitance sensors Decagon 10HS and 5TE for estimating the water content of irrigated soils. Agric. Water Manag. 132, 111-119.

Vundavalli, R., Vundavalli, S., Nakka, M., Rao, D.S., 2015. Biodegradable nano-hydrogels in agricultural farming-alternative source for water resources. Procedia Mater. Sci. 10, 548–554.

Wan, T., Huang, R., Zhao, Q., Xiong, L., Luo, L., Tan, X., Cai, G., 2013. Synthesis and swelling properties of corn stalk-composite superabsorbent. J. Appl. Polym. Sci. 130(1), 698-703.

TH-2777_166104034

Wan, T., Wang, X., Yuan, Y., He, W., 2006. Preparation of a kaolinite–poly (acrylic acid acrylamide) water superabsorbent by photopolymerization. J. Appl. Polym. Sci. 102, 2875–2881.

Wang, D., Song, Z.Q., Shang, S.B., 2008. Characterization and biodegradability of amphoteric superabsorbent polymers. J. Appl. Polym. Sci. 107 (6), 4116–4120.

Wang, W., Qin, Y., Song, D., Wang, K., 2008. Column leaching of coal and its combustion residues, Shizuishan, China. Int. J. Coal Geol. 75(2), 81-87.

Wang, W., Wang, A., 2010. Utilization of plant ash for the fabrication of novel superabsorbent composites with potassium-release characteristics. J. Appl. Polym. Sci. 115 (3), 1814-1822.

Wei, Y., Durian, D.J., 2013. Effect of hydrogel particle additives on water-accessible pore structure of sandy soils: a custom pressure plate apparatus and capillary bundle model. Phys. Rev. E 87, 053013.

Weston, D.P., Lentz, R.D., Cahn, M.D., Ogle, R.S., Rothert, A.K., Lydy, M.J., 2009. Toxicity of anionic polyacrylamide formulations when used for erosion control in agriculture. J. Environ. Qual. 38, 238–247.

Whisler, F.D., Klute, A., Peters, B.D., 1968. Soil water diffusivity from horizontal infiltration. Soil Sci. Soc. Amer. J. 32(1), 6–11.

Wilhelmi, O.V., Wilhite, D.A., 2002. Assessing vulnerability to agricultural drought: a Nebraska case study. Nat. Hazards 25, 37–58.

Wilhite, D.A., Glantz, M.H., 1985. Understanding: the drought phenomenon: the role of definitions. Water Int. 10, 111–120.

Wilhite, D.A., Sivakumar, M.V., Pulwarty, R., 2014. Managing drought risk in a changing climate: the role of national drought policy. Weather. Clim. Extremes 3, 4–13.

Wilske, B., Bai, M., Lindenstruth, B., Bach, M., Rezaie, Z., Frede, H.G., Breuer, L., 2014. Biodegradability of a polyacrylate superabsorbent in agricultural soil. Environ. Sci. Pollut. Res. Int. 21, 9453–9460.

Witono, J.R., Noordergraaf, I., Heeres, H.J., Janssen, L.P.B.M., 2014. Water absorption, retention and the swelling characteristics of cassava starch grafted with polyacrylic acid. Carbohydr. Polym. 103, 325-332.

TH-2777_166104034

World Health Organization (WHO), 1996. Permissible limits of heavy metals in soil and plants, Geneva, Switzerland.

World Health Organization, 1985. Acrylamide. Environmental Health Criteria 49, Geneva.

Wu, F., Zhang, Y., Liu, L., Yao, J., 2012. Synthesis and characterization of a novel cellulose-g-poly (acrylic acid-co-acrylamide) superabsorbent composite based on flax yarn waste. Carbohydr. Polym. 87, 2519–2525.

Xiao, X., Yu, L., Xie, F., Bao, X., Liu, H., Ji, Z., Chen, L., 2017. One-step method to prepare starch-based superabsorbent polymer for slow release of fertilizer. Chem. Eng. J. 309, 607–616.

Xie, L., Liu, M., Ni, B., Wang, Y., 2012. New environment-friendly use of wheat straw in slow-release fertilizer formulations with the function of superabsorbent. Ind. Eng. Chem. Res. 51 (10), 3855–3862.

Xu, J., Liu, X., Ren, X., Gao, G., 2018. The role of chemical and physical crosslinking in different deformation stages of hybrid hydrogels. Eur. Polym. J. 100, 86–95.

Xu, S., Zhang, L., McLaughlin, N.B., Mi, J., Chen, Q., Liu, J., 2015. Effect of synthetic and natural water absorbing soil amendment soil physical properties under potato production in a semi-arid region. Soil Till. Res. 148, 31–39.

Xue, S., Pei, D., Jiang, W., Mu, Y., Wan, X., 2016. A simple and fast formation of biodegradable poly (urethane-urea) hydrogel with high water content and good mechanical property. Polym. 99, 340–348.

Yang, H., Rahardjo, H., Leong, E.C., Fredlund, D.G., 2004. Factors affecting drying and wetting soil-water characteristic curves of sandy soils. Canadian Geotech. J. 41(5), 908-920.

Yang, L., Han, Y., Yang, P., Wang, C., Yang, S., Kuang, S., Yuan, H., Xiao, C., 2015. Effects of superabsorbent polymers on infiltration and evaporation of soil moisture under point source drip irrigation. Irrig. Drain. 64, 275–282.

Yang, L., Yang, Y., Chen, Z., Guo, C., Li, S., 2014. Influence of super absorbent polymer on soil water retention, seed germination and plant survivals for rocky slopes eco-engineering. Ecol. Eng. 62, 27–32.

Yao, Z.T., Ji, X.S., Sarker, P.K., Tang, J.H., Ge, L.Q., Xia, M.S., Xi, Y.Q., 2015. A comprehensive review on the applications of coal fly ash. Earth-Sci. Rev. 141, 105-121.

TH-2777_166104034

Yazdani, F., Allahdadi, I., Akbari, G.A., 2007. Impact of superabsorbent polymer on yield and growth analysis of soybean (Glycine max L.) under drought stress condition. Pak. J. Biol. Sci. 10 (23), 4190–4196.

Ye, H., Zhao, J.Q., Zhang, Y.H., 2004. Novel degradable superabsorbent materials of silicate/ acrylic-based polymer hybrids. J. Appl. Polym. Sci. 91 (2), 936–940.

Yi, S., Chang, N.Y., Imhoff, P.T., 2020. Predicting water retention of biochar-amended soil from independent measurements of biochar and soil properties. Adv. Water Resour. 142, 103638.

Young, M.H., Tappen, J.J., Miller, G.C., Carroll, S., Susfalk, R.B., 2007. Risk characterization: Using linear anionic polyacrylamide (LA-PAM) to reduce water seepage from unlined water delivery canal systems. Desert Research Institute, Las Vegas, NV.

Yu, C., Huang, X., Chen, H., Huang, G., Ni, S., Wright, J.S., Hall, J., Ciais, P., Zhang, J., Xiao, Y., Sun, Z., 2018. Assessing the impacts of extreme agricultural droughts in China under climate and socioeconomic changes. Earths Future 6, 689–703.

Yu, J., Shi, J.G., Ma, X., Dang, P.F., Yan, Y.L., Mamedov, A.I., Levy, G.J., 2017. Superabsorbent polymer properties and concentration effects on water retention under drying conditions. Soil Sci. Soc. Am. J. 81, 889–901.

Yunusa, I.A., Loganathan, P., Nissanka, S.P., Manoharan, V., Burchett, M.D., Skilbeck, C.G., Eamus, D., 2012. Application of coal fly ash in agriculture: a strategic perspective. Crit. Rev. Environ. Sci. Technol. 42(6), 559-600.

Zhang, J., Li, A., Wang, A., 2006c. Synthesis and characterization of multifunctional poly (acrylic acid-co-acrylamide)/sodium humate superabsorbent composite. React. Funct. Polym. 66 (7), 747–756.

Zhang, J., Liu, R., Li, A., Wang, A., 2006b. Preparation, swelling behaviors and application of polyacrylamide/attapulgite superabsorbent composites. Polym. Adv. Technol. 17(1), 12-19.

Zhang, J., Wang, L., Wang, A., 2006a. Preparation and swelling behavior of fast-swelling superabsorbent hydrogels based on starch-g-poly (acrylic acid-co-sodium acrylate). Macromol. Mater. Eng. 291(6), 612-620.

Zhang, J., Wang, Q., Wang, A., 2007a. Synthesis and characterization of chitosan-g-poly (acrylic acid)/attapulgite superabsorbent composites. Carbohydr. Polym. 68, 367–374.

TH-2777_166104034

Zhang, J., Yuan, K., Wang, Y.P., Gu, S.J., Zhang, S.T., 2007b. Preparation and properties of polyacrylate/bentonite superabsorbent hybrid via intercalated polymerization. Mater. Lett. 61 (2), 316–320.

Zhang, J.P., Li, A., Wang, A.Q., 2005. Study on superabsorbent composite. V. Synthesis, swelling behaviors and application of poly (acrylic acid- co- acrylamide)/sodium humate/attapulgite superabsorbent composite. Polym. Adv. Technol. 16, 813-820.

Zhang, M., Cheng, Z., Zhao, T., Liu, M., Hu, M., Li, J., 2014. Synthesis, characterization, and swelling behaviors of salt-sensitive maize bran–poly (acrylic acid) superabsorbent hydrogel. J. Agric. Food Chem. 62, 8867–8874.

Zhang, X., Obringer, R., Wei, C., Chen, N., Niyogi, D., 2017. Droughts in India from 1981 to 2013 and Implications to Wheat Production. Sci. Rep. 7, 44552.

Zhang, X.C., Miller, W.P., 1996. Polyacrylamide effect on infiltration and erosion in furrows. Soil Sci. Soc. Am. J. 60, 866–872.

Zhang, Y., Fan, L., Cheng, L., Zhang, L., Chen, H., 2009. Preparation and morphology of high-performance exfoliated poly (sodium acrylate)/hydrotalcite nanocomposite superabsorbents. Polym. Eng. Sci. 49 (2), 264–271.

Zhang, Y., Gao, P., Zhao, L., Chen, Y., 2016. Preparation and swelling properties of a starch-g-poly (acrylic acid)/organo-mordenite hydrogel composite. Front. Chem. Sci. Eng. 10(1), 147-161.

Zhang, Y., Zhao, L., Chen, Y., 2015. Synthesis and characterization of starch-g-Poly (acrylic acid)/Organo-Zeolite 4A superabsorbent composites with respect to their water-holding capacities and nutrient-release behavior. Polym. Compos. 38, 1838–1848.

Zhao, H., Song, J., Zhao, G., Xiang, Y., Liu, Y., 2019. Novel semi-IPN nanocomposites with functions of both nutrient slow-release and water retention. 2. Effects on soil fertility and tomato quality. J. Agric. Food Chem. 67(27), 7598-7608.

Zhao, Y., Li, Y., Wang, J., Pang, H., Li, Y., 2016. Buried straw layer plus plastic mulching reduces soil salinity and increases sunflower yield in saline soils. Soil Till. Res. 155, 363–370.

Zheng, Y., Li, P., Zhang, J., Wang, A., 2007. Study on superabsorbent composite XVI. Synthesis, characterization and swelling behaviors of poly (sodium acrylate)/vermiculite superabsorbent composites. Eur. Polym. J. 43 (5), 1691–1698.

TH-2777_166104034

Zhou, C., So, P.S., Chen, X.W., 2020. A water retention model considering biopolymer soil interactions. J. Hydrol. 586, 124874.

Zhou, M., Zhao, J., Zhou, L., 2011. Utilization of starch and montmorrilonite for the preparation of superabsorbent nanocomposite. J. Appl. Polym. Sci. 121, 2406–2412.

Zhu, J.K., 2007. Plant salt stress. In: Encyclopedia of Life Sciences. Wiley. https ://www.els.net

Zhuang, W., Li, L., Liu, C., 2013. Effects of Sodium Polyacrylate on Water Retention and Infiltration Capacity of a Sandy Soil. SpringerPlus 2, Springer International Publishing.

Zohuriaan-Mehr, M.J., Kabiri, K., 2008. Superabsorbent polymer materials: a review. Iran. Polym. J. 17, 451.

Zupanc, V., Justin, M.Z., 2010. Changes in soil characteristics during landfill leachate irrigation of Populus deltoides. Waste Manag. 30(11), 2130-2136.

TH-2777_166104034

List of publications from this study

Patent

- **Saha, A.**, Sreedeep, S. and Manna, U. Transformation of fly ash into non-toxic, high water absorbing polymer for drought management. Indian Patent filed on November 21, 2019, Application no. 201931047641.

Journals

- **Saha, A.**, Rattan, B., Sreedeep, S. and Manna, U. (2021). Quantifying the effect of soil pH and salinity on the performance of water absorbing polymer used for drought management. Journal of Polymer Research 28(11), 428. Springer. (Impact factor: 3.097; H-Index: 54) [https://doi.org/10.1007/s10965-021-02795-5]
- **Saha, A.**, Sreedeep, S. and Manna, U. (2021). Predictive model for water retention curve of water-absorbing polymer amended soil. Géotechnique Letters 11(3), 164-170. ICE. (Impact factor: 2.462; H-Index: 28) [https://doi.org/10.1680/jgele.21.00015]
- **Saha, A.**, Sreedeep, S., Manna, U. and Sahoo, L. (2020). Transformation of non-water sorbing fly ash to a water sorbing material for drought management. Scientific Reports 10(1), 1-16. Nature. (Impact factor: 4.011; H-Index: 179) [https://doi.org/10.1038/s41598-020-75674-6]
- **Saha, A.**, Sreedeep, S. and Manna, U. (2020). Superabsorbent hydrogel (SAH) as a Soil Amendment for Drought Management: A Review. Soil & Tillage Research 204, 104736. Elsevier. (Impact factor: 4.601; H-Index: 128) [https://doi.org/10.1016/j.still.2020.104736]
- **Saha, A.**, Sreedeep, S. and Manna, U. (2020). Evaluation of Capacitance Sensor for Suction Measurement in Silty Clay Loam. Geotechnical and Geological Engineering 38(4), 4319-4331. Springer. (H-Index: 51) [https://doi.org/10.1007/s10706-020-01297-3]
- **Saha, A.**, Rattan, B., Sreedeep, S. and Manna, U. (2020). Quantifying the interactive effect of water absorbing polymer (WAP)-soil texture on plant available water content and irrigation frequency. Geoderma 368, 114310. Elsevier. (Impact factor: 4.848; H-Index: 154) [https://doi.org/10.1016/j.geoderma.2020.114310]

Manuscripts under revision/ review

- **Saha, A.**, Sreedeep, S. and Manna, U. Characterization of Moisture Movement in Water Absorbing Polymer-Soil System: A Horizontal Absorption Method. Journal of Materials in Civil Engineering, ASCE. (***under revision***)

TH-2777_166104034

➢ **Saha, A.**, Sreedeep, S. and Manna, U. Hysteresis model for water retention characteristics of water absorbing polymer amended soils. Journal of Geotechnical and Geoenvironmental Engineering, ASCE. (***under revision***)

➢ **Saha, A.**, Sreedeep, S. and Manna, U. Capacitance soil moisture sensor for field monitoring of soil-water retention curve of water absorbing polymer amended soils. Geotechnical and Geological Engineering, Springer. (***under review***)

Book Chapters

➢ **Saha, A.**, Sreedeep, S. and Manna, U. Role of biopolymers and their composites in sustainable agriculture: recent developments and future perspectives. Wiley. (***under review***)

➢ **Saha, A.**, Sreedeep, S. and Manna, U. (2021). Performance of an Electromagnetic Sensor for Field Monitoring of Volumetric Water Content in Water-Absorbing Polymer Amended Soil. In: Transportation, Water and Environmental Geotechnics. Lecture Notes in Civil Engineering, Vol 159. Springer, Singapore.

➢ **Saha, A.**, Rattan, B., Sreedeep, S. and Manna, U. (2020). Effect of Water Absorbing Polymer Amendment on Water Retention Properties of Cohesionless Soil. In: Advances in Computer Methods and Geomechanics (pp. 185-195). Springer, Singapore.

➢ Sreedeep, S., Gadi, V. K., Bordoloi, S., **Saha, A.**, Kumar, H., Hazra, B. and Garg, A. (2019). Sustainable geotechnics: a bio-geotechnical perspective. In: Frontiers in Geotechnical Engineering (pp. 313-331). Springer, Singapore.

Conference Proceedings

➢ **Saha, A.**, Sreedeep, S. and Manna, U. (2020). Performance of an Electromagnetic Sensor for Field Monitoring of Volumetric Water Content in Water Absorbing Polymer Amended Soil. Proceedings of Indian Geotechnical Conference, Andhra University, Visakhapatnam, India.

➢ **Saha, A.**, Rattan, B., Sreedeep, S. and Manna, U. (2020). Characterization and reutilization prospective of an industrial solid waste fly ash: A state of the art review. Proceedings of 3rd International Conference on Waste Management-Recycle 2020, Indian Institute of Technology Guwahati, India.

TH-2777_166104034